



UNIVERSITÀ DELLA CALABRIA



UNIVERSITÀ DELLA CALABRIA

Dipartimento di Ingegneria per l'Ambiente e il Territorio e Ingegneria Chimica

Dottorato di Ricerca in Ingegneria Chimica e dei Materiali

(Scuola di Dottorato "Pitagora" in Scienze Ingegneristiche)

Tesi in co-tutela con Universitat Politècnica de València

Con il contributo di

POR CALABRIA FSE 2007/2013

CICLO XXVI

GRAPHENE AND TITANIUM BASED SEMICONDUCTORS IN PHOTOCATALYTIC HYDROGEN AND OXYGEN GENERATION AND HYDROGENATION OF ORGANICS ALSO IN MEMBRANE REACTORS

Settore Scientifico Disciplinare CHIM07 - Fondamenti chimici delle tecnologie

Coordinatore: Ch.mo Prof. Raffaele Molinari

Supervisor: Ch.mo Prof. Raffaele Molinari

Ch.mo Prof. Hermenegildo Garcia

Ing. PhD Pietro Argurio

Dottoranda: Dott.ssa Cristina Lavorato

A.A. 2012-2013

La presente tesi è cofinanziata con il sostegno della Commissione Europea, Fondo Sociale Europeo e della Regione Calabria. L'autore è il solo responsabile di questa tesi e la Commissione Europea e la Regione Calabria declinano ogni responsabilità sull'uso che potrà essere fatto delle informazioni in essa contenute.

Index

ABSTRACT	p.	V
RIASSUNTO	»	IX
RESUMEN	»	XV
Introduction	»	1
References.....	»	6
Chapter 1. Photocatalysis and Photocatalysts		
1.1. Introduction.....	»	7
1.2. Photocatalytic mechanism.....	»	8
1.3. Solid semiconducors	»	10
1.4. Limits of photocatalytic processes	»	12
1.5. Electron donors	»	13
1.6. Sensitizers	»	14
1.7. Noble metal.....	»	16
1.7.1.Preparation methods for noble metal doped catalyst	»	17
1.7.1.1. Impregnation	»	18
1.7.1.2. Deposition-precipitation.....	»	21
1.8. Water splitting.....	»	24
1.9. Graphene based semiconductor.....	»	29
1.9.1.Graphene	»	29
1.9.2.Graphene oxide	»	31
1.9.2.1. Graphene and graphene oxide as co-catalysts	»	33
1.9.3.N-doped graphene	»	37
1.9.4.Graphene quantum dots.....	»	41
1.10 References	»	45
SECTION I Graphene based semiconductors in photocatalytic hydrogen and oxygen generation.....		
	»	55
Chapter 2. Visible-Light Photocatalytic Hydrogen Generation by Using Dye Sensitized Graphene Oxide as a Photocatalyst		
2.1. Introduction.....	»	57
2.2. Experimental section.....	»	59
2.2.1.Photocatalytic hydrogen production tests	»	59
2.2.2.Quantum yield calculation.....	»	61
2.2.3.preparation of graphene oxides (GOs)	»	61

2.2.4. Preparation of GO with dyes	»	63
2.2.5. Characterization techniques	»	64
2.3. Results and discussion	»	65
2.3.1. Hydrogen generation using laser irradiation	»	65
2.3.2. Dyes as GO photosensitizers	»	70
2.3.3. Photocatalytic hydrogen generation using solar simulator	»	80
2.3.4. Stability of the $[\text{Ru}(\text{bipy})_3]^{2+}$ @GO photocatalyst.....	»	82
2.3.5. Oxygen evolution.....	»	85
2.4. Conclusions	»	86
2.5. References	»	87
 Chapter 3. N-doped graphene derived from biomass as visible light photocatalyst for hydrogen generation from water-methanol mixtures		
3.1. Introduction	»	91
3.2. Experimental section	»	93
3.2.1. Synthesis of (N)G	»	93
3.2.2. Photocatalytic hydrogen production tests.....	»	94
3.2.3. Characterization techniques	»	95
3.3. Results and discussions.....	»	96
3.3.1. Preparation of (N)G	»	96
3.3.2. UV light photocatalytic activity	»	102
3.3.3. Visible light photocatalytic activity	»	106
3.3.4. Power dependency and influence of (N)G amount on photocatalytic H_2 evolution	»	107
3.3.5. Failure of water oxidation	»	109
3.3.6. Photocatalytic hydrogen generation by (N)G under simulated solar light irradiation.....	»	109
3.4. Conclusions	»	110
3.5. References	»	111
 Chapter 4. Natural alginate as graphene precursor and template in the synthesis of nanoparticulate ceria-graphene water oxidation photocatalyst		
4.1. Introduction	»	115
4.2. Experimental	»	117
4.2.1. Photocatalytic oxygen production tests	»	117
4.2.2. Synthesis of CeO_x /graphene	»	117
4.2.3. Textural and analytical properties measurements.....	»	117
4.3. Results and discussion	»	118
4.3.1. Photocatalytic activity.....	»	126

4.3.2. Oxygen generation by photocatalytic water oxidation.....	»	127
4.4. Conclusions.....	»	129
4.5. References.....	»	130
Chapter 5. Preparation of graphene quantum dots from pyrolyzed alginate		
5.1. Introduction.....	»	133
5.2. Experimental section.....	»	134
5.2.1. Synthesis of graphene (G) quantum dots	»	134
5.2.2. Textural and analytical properties measurements	»	135
5.3. Results and discussion	»	136
5.4. Conclusions.....	»	148
5.5. References.....	»	148
SECTION II Titanium based semiconductors in photocatalytic hydrogenation of organics also in membrane reactors		
Chapter 6. Overview on photocatalytic reduction of organics		
6.1. Introduction.....	»	155
6.2. Hydrogenation	»	159
6.2.1. Catalytic hydrogenation and transfer hydrogenation	»	159
6.2.2. Photocatalytic transfer hydrogenation	»	161
6.2.3. Photocatalytic hydrogenation of ketones	»	163
6.2.4. Photocatalytic hydrogenation of ketones with visible light ..	»	167
6.2.5. Photocatalytic hydrogenation of nitrocompounds	»	169
6.2.6. Photocatalytic hydrogenation of nitrocompounds with visible light.....	»	173
6.2.7. Photocatalytic hydrogenation of unsaturated compounds.....	»	175
6.2.8. Photocatalytic partial hydrogenation of unsaturated compounds	»	177
6.3. Studies on photo-conversions in PMRs.....	»	180
6.3.1. Outline on photocatalytic membrane reactors	»	180
6.3.2. Partial hydrogenation in PMRs.....	»	182
6.4. Conclusions	»	186
6.5. References	»	187
Chapter 7. TiO₂ and Pd/TiO₂ as photocatalysts for hydrogenation of acetophenone in ethanol and aqueous solution under UV and visible light in batch and membrane reactors		
7.1. Introduction.....	»	205

7.2. Experimental section	» 209
7.2.1.Apparatus and Methods	» 209
7.2.2.Synthesis of Pd/TiO ₂	» 217
7.3. Results and discussion	» 219
7.3.1.Pd/TiO ₂ characterization	» 219
7.3.2.Photocatalytic hydrogenation of acetophenone in ethanol in batch reactor.....	» 220
7.3.2.1. Amount of titanium dioxide.....	» 221
7.3.2.2. Acetophenone photolysis	» 222
7.3.2.3. Pd/TiO ₂ photocatalytic activity	» 225
7.3.2.4. Influence of the intensity and distribution of irradiation source	» 228
7.3.2.5. Influence of solvent	» 230
7.3.3. Photocatalytic hydrogenation of acetophenone in aqueous solution in batch reactor	» 231
7.3.3.1. Different substrate concentrations.....	» 232
7.3.3.2. Addition of methanol in the solution.....	» 233
7.3.3.3. Tests at different pH	» 234
7.3.3.4. Amount of titanium dioxide.....	» 236
7.3.3.5. Amount of formic acid.....	» 238
7.3.4.Photocatalytic hydrogenation of acetophenone in aqueous solution in membrane reactors	» 239
7.3.4.1. Substrate feeding with a syringe pump	» 239
7.3.4.2. Acetophenone in heptane	» 242
7.3.4.3. Acetophenone as organic phase	» 244
7.3.4.4. Formic acid / triethylamine	» 248
7.3.4.5. Visible light activity.....	» 251
7.4 Conclusions.....	» 254
7.5 References.....	» 256
Conclusions.....	» 261
Appendix	» 265

Abstract

The development of graphene (G)-based materials as photocatalysts has become in the last years of high interest due to their sustainability and flexibility in the modification and design, particularly in the field of photocatalytic generation of hydrogen. Carbon based materials are sustainable when they are derived from renewable biomass feedstocks. G is a versatile material allowing different modification strategies to improve its activity. Thus, the present thesis reports that inserting heteroatoms, adding semiconductors or changing the layers size, the activity of the materials prepared can be improved for different applications.

Sun light is one of major renewable energy resource. The use of light as driving force for chemical reactions has attracted much attention of organic chemists. Heterogeneous photocatalysis is a discipline which includes a large variety of reactions, in particular hydrogen (considered the perfect renewable energy source in the future) and oxygen generation from water and hydrogenation of multiple bonds are the target of this PhD thesis. Photocatalytic reductions represent an alternative to conventional catalytic hydrogenation and it represent a more sustainable method to synthesize organic compounds under mild conditions in the presence of affordable photocatalysts. Photocatalytic processes in membrane reactors represent a technology of great scientific interest because it allows chemical reactions and separation processes to be accomplished in one step, which in turn results in lower processing cost and minimum environmental impact.

The preparation and characterization of G-based semiconductors has been carried out in the first part of the Thesis and their photocatalytic

activity for hydrogen and oxygen generation from water was determined in the second part.

Graphite was oxidized to graphene oxide (GO) and its photocatalytic activity for hydrogen generation from water/methanol mixtures with visible or solar light was enhanced by the presence of dyes, in the absence of any noble metal. The most efficient tested photocatalyst was the one containing a tris(2,2-bipyridyl) ruthenium(II) complex incorporated in the interlayer spaces of a few layers of GO platelets with a moderate degree of oxidation. This photocatalyst was two orders of magnitude more efficient than a titania based photocatalyst containing Au, when the reaction is performed under 532 nm laser as excitation light.

Doping G with nitrogen by pyrolysis of chitosan leads to a material that behaves as a semiconductor and exhibits high efficiency for the photocatalytic generation of hydrogen from water-methanol mixtures with similar efficiency using UV or visible light. This similar photocatalytic activity was due to the fact that, in contrast to GO, N-doped G exhibits an almost “neutral” absorption spectrum. The main parameter controlling the residual amount of nitrogen and the resulting photocatalytic activity is the pyrolysis temperature that produces an optimal material when the thermal treatment is carried out at 900 °C. Furthermore, N-doped G was able to generate hydrogen also upon illumination of simulated sunlight.

The use of G as co-catalyst of metal oxides semiconductors to enhance their photocatalytic activity has been extensively reported. Using alginate, a natural polysaccharide from algae, simultaneously as G precursor and as ceria nanoparticles template agent, a series of materials consisting of highly crystalline ceria nanoparticles embedded on a few layers G matrix has been prepared. Varying the weight percentage of

ceria/alginate and the pyrolysis temperature, it was possible to prepare a ceria/G photocatalyst that exhibits about three times higher photocatalytic activity for water oxidation to oxygen than commercial ceria.

Pyrolysis at 900 °C under inert atmosphere of alginate renders a graphitic carbon that upon ablation by exposure to a pulsed 532 nm laser (7 ns, 50 mJ pulse⁻¹) in acetonitrile, water, and other solvents leads to the formation of multilayer graphitic quantum dots. The dimensions and the number of layers of these graphitic nanoparticles decrease along the number of laser pulses leading to G quantum dots (GQDs). Accordingly, the emission intensity of these GQDs increases along the number of laser shots, the maximum emission intensity appearing at about 500 nm in the visible region increasing in intensity along the reduction of the particle size. Transient absorption spectroscopy has allowed detection of a transient signal decaying in the microsecond time scale that has been attributed to the charge separation state.

During the second part of the present thesis the photocatalytic hydrogenation of acetophenone by using titanium based semiconductors in batch and membrane reactors under UV and visible light has been studied. Different photocatalytic tests have been performed using ethanol or water and formic acid in a batch reactor in order to optimize the reaction parameters before to be applied in membrane reactors with different substrate addition mode. The use of a membrane reactor system for the photocatalytic hydrogenation of acetophenone in water solution with formic acid as hydrogen and electron donor was found to improve the efficiency of the photocatalytic system with respect to the use of batch reactor. The most efficient system for photocatalytic hydrogenation of acetophenone in terms of productivity, amount of phenylethanol produced

and extraction of desired product was found to be the membrane reactor in which acetophenone was used as both organic phase and substrate. The presence of palladium enhances the visible light photocatalytic activity of TiO₂ photocatalyst, that is not active alone. The productivity by using Pd/TiO₂ photocatalyst under visible light increases five times more than using TiO₂ under UV light.

Riassunto

Negli ultimi anni lo sviluppo di materiali semiconduttori a base di grafene (G) sta diventando di grande interesse per la loro sostenibilità e flessibilità nella modifica e progettazione di fotocatalizzatori, in particolare nel campo della generazione fotocatalitica di idrogeno dall'acqua. L'uso di materiali a base di carbonio risulta essere sostenibile quando questi materiali sono sintetizzati utilizzando materie prime derivate della biomassa. Il grafene è un materiale versatile che consente di attuare diverse strategie di modificazione permettendo di migliorarne l'attività. Pertanto, parte di questo lavoro di tesi è stata incentrata sulla sintesi di nuovi semiconduttori a base di grafene ottenuti tramite l'inserimento di eteroatomi, l'aggiunta di ossidi metallici o la modifica della dimensione degli strati di grafene, in modo da migliorarne l'efficienza in svariate applicazioni.

L'utilizzo di fonti energetiche pulite, rinnovabili e a basso costo è di ampio interesse per un approccio nello svolgimento di processi industriali. Un processo 'verde', come la fotocatalisi, è una buona alternativa all'utilizzo delle energie convenzionali poichè permette di sfruttare un'energia rinnovabile come quella solare. La fotocatalisi eterogenea è una disciplina che include una grande varietà di reazioni. In particolare, la generazione di idrogeno e di ossigeno dall'acqua e le reazioni di idrogenazione di composti organici sono le reazioni effettuate durante questa tesi di dottorato. Le reazioni di riduzione fotocatalitiche stanno offrendo metodi alternativi più sostenibili per sintetizzare composti organici in condizioni blande e utilizzando catalizzatori più economici. Inoltre, l'applicazione di reattori fotocatalitici a membrana è di grande interesse scientifico perché permette di accoppiare la reazione

fotocatalitica con processi di separazione a membrana in un'unica fase, consentendo una diminuzione dell'impatto ambientale e dei costi di produzione.

La prima parte di questo lavoro di tesi è stata incentrata sulla sintesi di nuovi semiconduttori a base di grafene con lo scopo di modificarli in modo da migliorarne l'efficienza fotocatalitica principalmente in reazioni di riduzione e ossidazione dell'acqua.

L'inserzione di eteroatomi come l'ossigeno nella matrice del grafene, tramite reazione di ossidazione, ha permesso di ottenere ossido di grafene (GO) che è un semiconduttore. L'attività fotocatalitica del GO nella generazione di idrogeno da una miscela di acqua e metanolo, è stata migliorata grazie alla presenza di coloranti, supportati sulla sua superficie o inseriti all'interno delle lamine di GO, la cui presenza ha permesso l'utilizzo della luce visibile e solare per effettuare la reazione oggetto di studio, in assenza di metalli nobili. Il fotocatalizzatore che è risultato più efficiente è stato l'ossido di grafene con un moderato grado di ossidazione contenente il complesso tris(2,2-bipiridile)rutenio(II) complesso incorporato negli spazi inter-lamina. I risultati ottenuti durante la prova fotocatalitica, effettuata utilizzando un laser come sorgente luminosa con lunghezza d'onda di 532 nm, hanno dimostrato che questo fotocatalizzatore è di due ordini di grandezza più efficiente di un fotocatalizzatore a base di biossido di titanio dopato con oro.

La sintesi di graphene dopato con azoto, tramite pirolisi di un polimero naturale qual è il chitosano, ha permesso di ottenere un semiconduttore (N-grafene) che presenta un'elevata efficienza nella generazione fotocatalitica di idrogeno da miscele di acqua e metanolo mostrando un'attività equivalente sia se è irradiato con luce UV che con quella

visibile. Questi risultati sono determinati dallo spettro di assorbimento del N-grafene che è quasi costante in tutto lo spettro della luce visibile e ultravioletta, al contrario di ciò che avviene per l'ossido di graphene che presenta un maggiore assorbimento nello spettro della luce ultravioletta. Il parametro principale che permette di controllare la percentuale di azoto presente nei campioni sintetizzati e di conseguenza l'attività fotocatalitica dei fotocatalizzatori ottenuti è la temperatura di pirolisi, che è risultata ottimale quando il trattamento termico è stato condotto a 900°C. Inoltre, è dimostrato che N-graphene possiede attività fotocatalitica nella produzione di idrogeno dall'acqua anche adoperando la luce solare come sorgente luminosa.

Una delle principali applicazioni del grafene è quella di fungere da co-catalizzatore di ossidi metallici permettendo di migliorarne l'attività fotocatalitica. Al fine di preparare una serie di materiali cristallini costituiti da nanoparticelle di cerio supportate su lamine di grafene, è stato utilizzato l'alginato, un polimero naturale derivato dall'alga bruna, che, pirolizzato ad elevate temperature in atmosfera inerte, funge contemporaneamente da agente templante e precursore di grafene. Variando la temperatura di pirolisi e la percentuale di precursore di ossido di cerio, è stato possibile preparare vari fotocatalizzatori; ottimizzando il metodo di preparazione è stato ottenuto un fotocatalizzatore che ha mostrato un'attività fotocatalitica, nella reazione di ossidazione dell'acqua, tre volte maggiore di quella dell'ossido di cerio commerciale.

Il presente lavoro comprende, inoltre, un metodo di preparazione per ottenere la grafite da un polimero naturale ampiamente disponibile, come l'alginato, tramite trattamento termico a 900°C in atmosfera inerte. La grafite ottenuta, sospesa in vari solventi, è stata deslaminata e le

dimensioni delle lamine sono state ridotte notevolmente dopo essere state irradiate con un laser a lunghezza d'onda di 532nm, fino ad assumere le dimensioni nanometriche tipiche dei punti quantici (GQDs). Diminuendo la dimensione delle particelle aumenta l'intensità dell'emissione dei GQDs nella regione del visibile a circa 500 nm. "Transient absorption spectroscopy" ha permesso il rilevamento di un segnale transiente di decomposizione nella scala di tempo di un microsecondo che è stato attribuito allo stato di separazione di carica.

Durante la seconda parte del lavoro di tesi di dottorato è stata considerata la riduzione fotocatalitica di composti organici, in particolare dell'acetofenone il cui prodotto di reazione è anche una materia prima utilizzata nella sintesi di composti farmaceutici. Le reazioni fotocatalitiche sono state condotte in reattori batch e a membrana utilizzando come sorgenti luminose la luce ultravioletta e quella visibile.

Il lavoro comprende una prima fase di analisi dell'influenza di diverse condizioni operative sull'efficienza delle reazioni fotocatalitiche di riduzione dell'acetofenone in reattori "batch" utilizzando etanolo o acqua e acido formico, e la successiva applicazione in reattori fotocatalitici a membrana variando la modalità di somministrazione del substrato. Lo scopo principale di questa parte di lavoro è stato quello di preparare un sistema fotocatalitico a membrana, utilizzando acqua come solvente e acido formico come donatore di idrogeno e di elettroni, che ha permesso di effettuare la reazione di riduzione dell'acetofenone e l'estrazione del prodotto di reazione in unico step ottenendo un miglioramento in termini di conversione, resa e selettività rispetto alle prove condotte nel reattore batch.

Il sistema più efficiente, in termini di estrazione del prodotto desiderato, di produttività e quantità di feniletanolo prodotto, nella reazione d'idrogenazione fotocatalitica dell'acetofenone, è risultato essere il reattore a membrana in cui l'acetofenone è stato utilizzato sia come fase organica che come substrato.

Infine durante questo lavoro è stato dimostrato che l'uso di TiO_2 dopato con palladio aumenta l'attività fotocatalitica rispetto al TiO_2 che, in assenza di palladio, non è risultato essere attivo nelle prove condotte con la luce visibile. Le prove effettuate utilizzando Pd/TiO_2 , irradiato con luce visibile, hanno mostrato un incremento della produttività che è risultata cinque volte migliore rispetto a quella ottenuta utilizzando TiO_2 irradiato con la luce UV.

Resumen

En los últimos años el desarrollo de materiales de grafeno (G) como fotocatalizadores ha atraído un gran interés debido a que estos materiales son considerados sostenibles y a la flexibilidad en su modificación y diseño, que podría permitir su adaptación al campo de la generación fotocatalítica de hidrógeno. En contraste con los metales o los óxidos metálicos, los materiales basados en carbono son un ejemplo de sostenibilidad cuando derivan de la biomasa renovable. G es un material versátil que permite diferentes estrategias de modificación para mejorar su actividad. En este contexto, en la presente tesis doctoral se describen formas para mejorar la actividad de materiales fotocatalíticos basadas en: la inserción de heteroátomos en G, y la combinación de semiconductores inorgánicos y G o el cambio en el tamaño de las capas.

Una de las principales fuentes de energía renovable es la luz del sol. El uso de la luz como fuerza motriz de las reacciones químicas ha llamado mucho la atención de los investigadores en áreas de ciencia de materiales y química orgánica. La fotocatálisis heterogénea es una disciplina que incluye una gran variedad de reacciones. En particular, en esta tesis doctoral, se llevaron a cabo reacciones que incluyen la generación de hidrógeno (considerada la fuente de energía renovable ideal en el futuro) y de oxígeno a partir del agua, así como también reacciones de hidrogenación. Las reacciones fotocatalíticas representan rutas alternativas y métodos más sostenibles para sintetizar compuestos orgánicos con condiciones moderadas y siendo necesario desarrollar catalizadores más asequibles. Los procesos fotocatalíticos en reactores de membrana representan una tecnología de gran interés científico debido a que permiten efectuar reacciones químicas y procesos de separación en un solo

paso. Esto a su vez se traduce en un menor costo de procesamiento y mínimo impacto ambiental.

Durante la primera parte de la presente tesis doctoral se llevó a cabo la preparación y caracterización de semiconductores basados en grafeno y su actividad fotocatalítica para la generación de hidrógeno y de oxígeno a partir de agua.

El grafeno es oxidado a óxido de grafeno (GO) y su actividad fotocatalítica para la generación de hidrógeno a partir de mezclas de agua/metanol con luz visible o solar, fue incrementada por la presencia de colorantes sine el empleo de cualquier metal noble. El fotocatalizador probado más eficiente fue el que contenía un tris (2,2 - bipyridilo) rutenio (II) incorporado en los espacios interlaminares de un numero limitado de capas de óxido de grafeno con un grado moderado de oxidación. Se encontró que este fotocatalizador era dos órdenes de magnitud más eficiente que un fotocatalizador basado en óxido de titanio conteniendo Au cuando se irradian las muestras con un laser de 532 nm como luz de excitación.

El dopaje grafeno con nitrógeno mediante pirólisis de quitosano da lugar a un material que se comporta como un semiconductor y exhibe una alta eficiencia para la generación fotocatalítica de hidrógeno a partir de mezclas de metanol/agua con una productividad similar utilizando luz UV o visible, debido al hecho de que, en contraste con el óxido de grafeno, N-grafeno exhibe un espectro de absorción casi "neutro". El principal parámetro que controla la cantidad residual de nitrógeno y la actividad fotocatalítica resultante es la temperatura de pirólisis que produce un material óptimo cuando se lleva a cabo el tratamiento térmico a 900 °C.

Por otra parte, el grafeno dopado con nitrógeno fue capaz de generar hidrógeno también con irradiación por luz solar simulada.

El principal uso del grafeno es como co-catalizador de óxidos metálicos semiconductores para mejorar su actividad fotocatalítica. Utilizando alginato, un polisacárido natural de las algas, al mismo tiempo como precursor de grafeno y como agente de plantilla en la preparación de nanopartículas de ceria, se han preparado una serie de materiales que consisten en nanopartículas de óxido de cerio altamente cristalinas fijadas en una matriz de varias capas de grafeno. Variando el porcentaje en peso de óxido de cerio/alginato y la temperatura de pirólisis, es posible preparar un fotocatalizador de óxido de cerio/grafeno que exhibe una actividad fotocatalítica para la oxidación del agua a oxígeno que es alrededor de tres veces más alta comparada con la actividad del óxido de cerio comercial.

La pirólisis de alginato (un biopolímero natural ampliamente disponible) efectuada a 900 °C, bajo atmósfera inerte, produce un carbono grafitico el cual conduce a la formación de puntos cuánticos de grafito de capas múltiples mediante la ablación por exposición a un láser pulsado de 532 nm (7 ns, 50 mJ pulso⁻¹) en acetonitrilo, agua, y otros disolventes. Las dimensiones y el número de capas de estas nanopartículas de grafito disminuyen con el número de pulsos de láser al que se somete la muestra de alginato pirolizador para producir los puntos cuánticos de grafeno (GQDs). En consecuencia, la intensidad de emisión de estos GQDs, que aparecen a aproximadamente 500 nm en la región visible, aumenta con la reducción del tamaño de partícula. Espectroscopía de absorción con resolución temporal ha permitido la detección de una señal transitoria que decae en la escala de tiempo de microsegundos que se ha atribuido al estado de separación de cargas.

Durante la segunda parte de la presente tesis doctoral se llevó a cabo la hidrogenación catalítica de acetofenona utilizando semiconductores basados en titanio en reactores por cargas y de membrana utilizando luz ultravioleta (UV) y visible. Se realizaron diferentes pruebas fotocatalíticas utilizando etanol o agua y ácido fórmico en un reactor por cargas con el fin de optimizar los parámetros de la reacción antes de su aplicación en reactores de membrana en el que se pueden adicionar diferentes sustratos. Se encontró que el uso de sistema de reactor de membrana para la hidrogenación de acetofenona fotocatalítica en solución de agua con ácido fórmico como donante de hidrógeno y de electrones, mejora la eficiencia del sistema fotocatalítico con respecto al reactor por cargas. Se encontró que el sistema más eficaz para la hidrogenación fotocatalítica de acetofenona en términos de productividad, de la cantidad de feniletanol producido y de la extracción de producto deseado fue el reactor de membrana en el que se utilizó acetofenona tanto como fase orgánica y como de sustrato. La presencia de paladio aumenta la actividad fotocatalítica del fotocatalizador (TiO_2) bajo luz visible, el cual no es activo cuando está puro en estas condiciones. La productividad utilizando el fotocatalizador Pd/TiO_2 bajo luz visible aumenta cinco veces más que el uso de TiO_2 bajo luz ultravioleta.

Introduction

In the last decades chemical reactions have been widely achieved by green processes. Traditional industrial processes, today, are considered unsustainable in terms of resources and environmental impact. Chemical industries need to improve the efficiency of their processes by minimizing or avoiding the use of toxic and hazardous substances such as catalysts and solvents. To solve these problems the use of light, particularly visible light, as driving force for chemical reactions has attracted much attention of organic chemists. [1,2]

The advantages associated to reactions conducted in photocatalytic systems are:

- Mild experimental conditions.
- Wide range of application to substrates in liquid, solid and gaseous phase.
- Compatibility with other physical and chemical technologies (e.g. membrane reactors).
- Potential use of renewable solar energy as an alternative to energy intensive conventional treatment methods.

In this context photocatalytic processes in membrane reactors represent a technology of great scientific interest because they allow chemical reactions and separation processes to be accomplished in one step, which in turn results in lower processing cost and minimum environmental impact [3].

Initial interest in these photoinduced redox reactions has been shown by Fujishima and Honda. They discovered that water could be simultaneously

oxidized and reduced by light to produce oxygen and hydrogen [4]. This observation promoted extensive work focusing on the production of hydrogen (as a combustible fuel) from water as a means of solar energy conversion. It can be considered the perfect renewable energy source [5], because hydrogen can generate not only thermal energy but also electricity (using fuel cells) and mechanical energy (using hydrogen engines), before ultimately be converted back to water. Therefore, photocatalytic hydrogen production could potentially form the basis of a clean, renewable energy cycle.

Heterogeneous photocatalysis is a discipline which includes a large variety of reactions: partial or total oxidations, dehydrogenation, hydrogen transfer, metal deposition, water detoxification, gaseous pollutant removal, bactericidal action etc.[6]. Photocatalytic reduction has been studied extensively because it is generally safer than the conventional methods employing dangerous reducing agents such as hydrogen and carbon monoxide. Despite this, photocatalytic reductions are less frequent than oxidations most probably because the reducing ability of a conduction band electron is considerably lower than the oxidizing one of a valence band hole. The first study reported on photocatalytic hydrogenation was on acetylene reduction using TiO_2 as photocatalyst [7]. Some photocatalytic studies recently reported include: the transfer hydrogenation of ketones using titanium dioxide as photocatalyst and alcohol as hydrogen donor [8,9], the reduction of nitro groups in a photocatalytic system using TiO_2 [10], in water solution, using formic acid or oxalic acid as hydrogen donor, [11] and the selective photocatalytic reduction of cyclooctadiene using $(\text{Rh}_4(\text{CO})_{12})$ as catalyst [12].

Among various photocatalysts used in the photocatalytic processes the most employed is titanium dioxide (TiO₂) for its strong catalytic activity, high chemical stability in aqueous solution and in a wide pH range, relatively low cost, and high availability. The applicability of semiconductors depends on their possible sun light activity. Noble metals, such as Pd, have been reported to be very effective for enhancement of semiconductors efficiency in photocatalysis improving also their visible light response.

In the last years the development of graphene (G)-based materials as photocatalysts is becoming of high interest for their sustainability and flexibility in the modification and design of photocatalysts. The use of carbon based materials is still more sustainable since they can be derived from renewable biomass feedstocks. The synthesis of semiconductors such as N-doped graphene and quantum dots graphene, using natural biopolymers such as chitosan or alginate, and the application of alginate as templates for the synthesis of photocatalysts and graphene as co-catalyst having activity for water splitting, are example of biomass waste valorization.

The overall objective of this PhD thesis is the synthesis of graphene based semiconductors and their application on photocatalytic hydrogen and oxygen generation and the photocatalytic hydrogenation of acetophenone in batch and membrane reactors using titanium based photocatalysts.

This work is divided in two main sections and seven chapters having the following content:

Chapter 1 describes the basics of photocatalysis and in particular of water splitting, a summary of the preparation methods of metal doped catalysts

and an overview on the recent development of new semiconductors based on graphene.

The first section (Chapters 2 - 5) of this thesis describes the preparation and characterization of semiconductors based on graphene and their photocatalytic activity for hydrogen and oxygen generation from water.

Chapter 2 presents a study on the influence of the degree of graphene oxide oxidation on the photocatalytic activity as well as the possibility of using dyes as photosensitizers of G-like materials to reach high quantum yield efficiencies for visible-light hydrogen evolution from water.

Chapter 3 reports a novel preparation method using natural chitosan, a biomass waste, to obtain N-doped graphene and a study on the optimization of photocatalytic activity based on the preparation conditions for enhanced hydrogen generation from water-methanol mixtures under UV and visible light.

Chapter 4 reports a novel synthetic method to prepare ceria nanoparticles supported on graphene by using alginate, a natural polysaccharide, as graphene precursor and ceria nanoparticles template agent, varying the weight percentage of ceria/alginate and the pyrolysis temperature, obtaining three times higher photocatalytic activity for water oxidation to oxygen than commercial ceria.

Chapter 5 presents an innovative and efficient preparation of Graphene quantum dots (GQDs) by 532 nm laser pulse of graphitic carbon obtained by pyrolysis at 900°C of alginate, a natural widely available biopolymer, and describes the unique photophysical properties of GQD suspensions.

The second section (Chapters 6 - 7) of this thesis, reports an overview on photocatalytic reduction of organics and the photocatalytic hydrogenation

of acetophenone in batch and in membrane reactors using titanium based semiconductors.

Chapter 6 gives a presentation on photocatalytic reduction of organics with a wide overview on the recent progresses in this field, the latest developments of semiconductors, and some possible application in photocatalytic membrane reactors.

Chapter 7 reports the photocatalytic hydrogenation of acetophenone under visible light using palladium doped titanium dioxide conducted in photocatalytic membrane reactor using a green solvent such as water and a pollutant as formic acid as electron donor. This chapter describes also a different system for the optimization of the substrate addition in a membrane reactor subsequently to the optimization of reaction parameters in a batch reactor with different solvent.

References

- [1] Molinari R., Caruso A, Palmisano L., *Academic Press: Oxford*, **2010**, 3, 165-193.
- [2] Li J., Yang J., Wen F. and Li C. *Chem. Commun.*, **2011**, 47, 7080-7082
- [3] Molinari R., A. Caruso, T. Poerio. *Catalysis Today*, **2009**, 144, 81–86.
- [4] Fujishima A. and Honda K. *Nature*, **1972**, 238, 37 - 38
- [5] J. A. Turner, M. C. Williams, and K. Rajeshwar, 2004, 13, 3, 24–30.
- [6] J.-M. Herrmann. *Topics in Catalysis*, **2005**, 34, 1–4, 49
- [7] Al-Thabaiti S. and. R. R Kuntz. *American Chemical Society*, **1990**, 6, 782-786.
- [8] Kohtani S., E. Yoshioka, K. Saito, A. Kudo, H. Miyab. *Catalysis Communications*, **2010**, 11, 1049–1053.
- [9] Escobar E.A., M. Á. V. Zapata, S.A. Hernández, S. O. Flores Valle, O. R. Berny, V. J. G.Ángeles, I. C. Reyes. *J. Mex. Chem. Soc.*, **2010**, 54, 3, 133-138
- [10] Imamura K., S. Iwasaki, T. Maeda, K. Hashimoto, B. Ohtani and H. Kominami. *Phys. Chem. Chem. Phys.*, **2011**, 13, 5114–5119
- [11] Hanaoka T., T. Matsuzaki, Y. Sugi. *Journal of Molecular Catalysis A: Chemical*, **1999**, 149, 161–167.
- [12] Hanaoka T., Y. Kubota, K. Takeuchi, T. Matsuzaki, Y. Sugi. *Journal of Molecular Catalysis A: Chemical*, **1995**, 98, 157-160.

1

Photocatalysis and photocatalysts

1.1 Introduction

The primary source of life on earth is the sun. Most of the living systems, plant, algae, some bacteria, on earth depend on photosynthesis for producing nutrients, oxygen. etc. In nature, photosynthesis has been efficacy in synthesizing starch from water and CO₂, to combine molecules to produce macromolecules, etc. carrying out all reactions with high efficiency [1]. The possibility of using sun light as energy source for chemical reactions can solve many energy and environmental problems. Petroleum and natural gas have been widely used as fuels, as primary source for chemicals, and in various applications. The dependence on fossil fuel source should be reduced employing alternative strategies such as photocatalytic process.

Solar is one of major sources of renewable energy, use of light as driving force for chemical reactions has attracted much attention of organic chemists, in particular the use of visible light as energy source allows to develop environmentally benign synthetic processes [2].

The use of a photocatalytic system allows to obtain the following advantages : i) the reactions can be carried out under mild conditions running them closer to room temperature and pressure; ii) it avoids the use of environmentally and unhealthy dangerous heavy metal catalysts and

strong chemical oxidant/reducing agents by using safer photocatalysts (TiO₂ is the most used); iii) it uses mild oxidants (molecular oxygen, in some cases from the air); iv) it requests very few auxiliary additives; v) it does not produce harmful chemicals; vi) it can be applied to a wide range of substrates in liquid, solid and gaseous phase; vii) it offers a good alternative to the energy-intensive conventional treatments methods with the possibility to use renewable solar energy; viii) it can be combined with other physical and chemical technologies (e.g. membrane separations) [1]. The heterogeneous photocatalysis is a discipline that includes a wide range of reactions that can be conducted in the gas or liquid phase: total or partial oxidation, dehydrogenation, hydrogenation, water purification, pollutants removal, hydrogen and oxygen generation from water etc. [3].

1.2 Photocatalytic mechanism

Regarding the heterogeneous photocatalysis in liquid phase the entire process can be decomposed in the five independent steps [3]:

1. Transfer of reagents from the liquid phase to the catalyst surface;
2. Adsorption of reactants;
3. Reaction in the adsorbed phase;
4. Desorption of the products;
5. Removal of the products from the interface solid/liquid.

The difference compared to the conventional catalysis is the mode of thermal activation of the catalyst replaced by photon using UV or visible light irradiation.

In particular the photocatalytic process can be divided in four steps [4]:

- Light absorption followed by the separation of the electron–hole couple;

- Adsorption of Reagents;
- Redox reaction;
- Desorption of products.

The electronic structure of a semiconductor is characterized by a conduction band (CB) and a valence band (VB) separated by a band gap of energy (E_g).

When semiconductors are excited by photons with energy equal or higher than their band gap energy level ($h\nu \geq E_g$), electrons receive energy from the photons and are thus promoted from VB to CB.

Electrons and holes that migrate to the surface of the semiconductor can, respectively, reduce and oxidize the reactants adsorbed on the semiconductor surface which depends on the redox potential (or energy level) of the substrate (Figure 1.1).

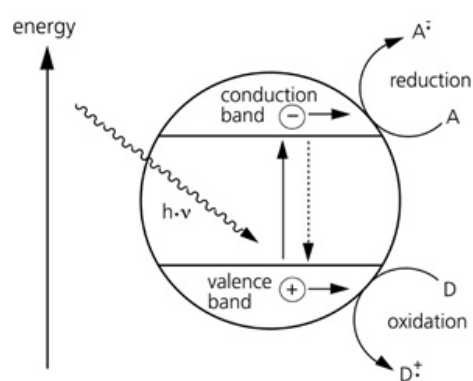


Figure 1.1. Process involved in semiconductor photocatalysis [1].

The photocatalyst ability to carry out a particular reaction depends on the energy levels position of the catalyst and the substrate. The adsorbed molecule can be reduced if its reduction potential is higher than that of the

photoelectrons or it can be oxidized if its potential is lower than that of the photohole [5].

1.3. Solids Semiconductors

The most widely used semiconductors are oxides (TiO_2 , ZnO , ZrO_2 , CeO_2 , WO_2 , etc.) or sulphides (CdS , ZnS , WS_2 , etc.) [3].

Among various catalysts used in the photocatalytic processes the most employed is titanium dioxide (TiO_2) for its strong catalytic activity, high chemical stability in aqueous solution and in a wide range of pH, low cost due to the abundance of titanium on the Earth. It exists in nature in three crystalline forms (rutile, anatase, and brookite) and amorphous phase. The rutile form is the thermodynamically most stable, while anatase, that is metastable, is the most active as photocatalyst among them. The most widely used commercial form is P-25 produced by the German company Degussa and consists of 80% anatase and 20% rutile.

In the last years tin oxide (SnO_2) has been largely used for its chemical and mechanical stability, it crystallizes in the tetragonal rutile [6]. It finds application in the construction of gas sensors, transparent electrodes, lithium batteries, and as a photocatalyst [7, 8, 9]. The tungsten oxide (WO_3), which shows cubic crystal structure, has been extensively studied, since the 80s, especially for oxygen and hydrogen generation from water and for amino-acids synthesis [10, 11]. Only very recently graphene based materials, which will be described in paragraph 1.9, are developing in photocatalysis.

Each photocatalyst is characterized by a band-gap energy as showed in Figure 1.2.

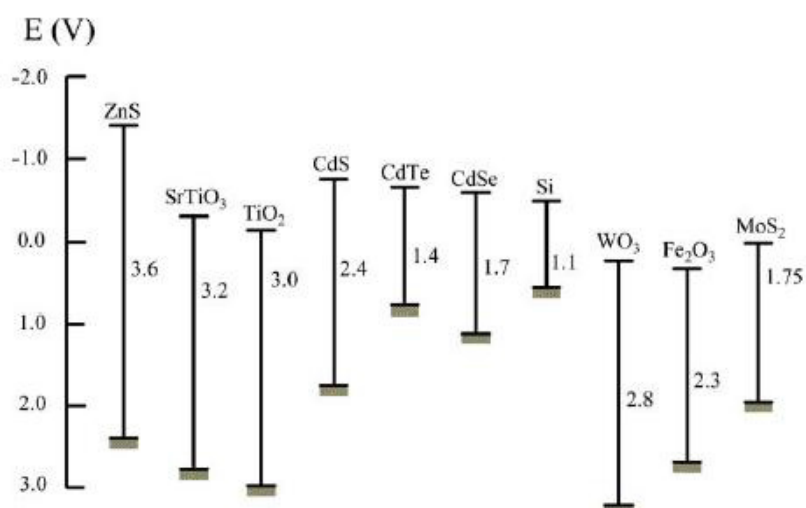


Figure 1.2. Band-gap energy and redox potentials at pH=1 of some semiconductors [4].

The photocatalysts band-gap energy position allows knowing what type of reactions can be conducted with each semiconductor and what their absorption spectrum is.

Among them WO₃ and Fe₂O₃ cannot perform water photo splitting for hydrogen generation because their conduction band potentials are less negative than the hydrogen evolution potential. However, all the catalysts shown in Figure 1.2, can carry out the oxygen evolution reaction because they have the potential of the valence band greater than that of oxygen [1]. TiO₂ P-25 has an energy band-gap of 3.2 eV, the conduction band and the valence band potential values at pH 0 are: -0.05 V and +3.15 V, respectively [12, 13, 14]. Tin oxide (SnO₂), has an energy band-gap equal to 3.6 eV, at pH values of 0 it has a potential equal to +0.5 V for the conduction band, and +4.1 V for the valence band, [9,15]. TiO₂ has a

band-gap wider than SnO₂, but both are able to absorb light only in the UV range.

The most used semiconductor active under visible light irradiation is tungsten oxide (WO₃) which presents cubic crystal structure, energy band gap equal to 2.8 eV, and the potential of the conduction band and the valence band values equal to +0.4 V and +3.2 V at pH 0, respectively [16]. Another important parameter to choose the photocatalyst is the percentage of ionic character of the cation-anion bond. A system which has higher percentage of ionic character (> 40%) will have higher band gap and will not be able to absorb light in the visible region. A catalyst which has a percentage of ionic character between 20-30% with appropriate positions of the valence and conduction band potentials with respect to the considerate reaction could be used in photocatalysis under visible light illumination [9].

1.4 Limits of photocatalytic processes

Despite the wide range of applications of the photocatalytic process, the use of photocatalysts at industrial level is still limited for three reasons [5, 17]:

1. Recombination electron/hole pairs: excited electrons and holes photo-generated are unstable species that can recombine quickly, during the recombination they can release energy in a non-productive form as heat or photons.
2. Generation of undesirable by-products caused by secondary reactions or fast backward reactions.
3. The absorption of light in the visible region is still too low. The commercial success of photo catalysts also depends on its ability to

operate using visible light because sunlight is composed by 46% of visible radiation, 47 % IR and only 7% by UV radiation. For example, TiO₂ that is one of the most efficient and stable photocatalysts highly available has the defect of work mostly using the UV light, it absorbs only 7 % of visible light [1].

In order to solve the above listed problems continuous efforts have been made to promote the photocatalytic activity and enhancing the visible light response such as: addition of electron donors, noble metal loading, dye sensitization, etc.[5].

1.5 Electron donors

To enhance the photocatalytic electron/hole separation several authors proposed the addition of electron donor compounds (sacrificial reagents or scavengers of hole) that react with the photo-generated VB holes resulting in higher quantum efficiency. The remaining strong reducing CB electrons can reduce the substrate. However, high amount of electron donor are needed to improve the photocatalytic performance of semiconductors because they are consumed during the photocatalytic process [17].

Nada et al., studied the effects of different electron donors on water splitting [18]. The hydrogen production is incremented according to the donor used in the following order: EDTA > methanol > ethanol > lactic acid. However, it must be taken into account the fact that the yield of hydrogen can be also favoured by their decomposition. Kohtani et al. and Escobar et al., reported that methanol, ethanol and 2-propanol were used as both hydrogen donor and hole scavengers in the photocatalytic reductions of aromatic ketones, using TiO₂ as catalyst [19, 20]. Formic

acid and oxalic acid were used as hole scavengers and hydrogen donor in the photocatalytic reduction of nitrobenzenes and nitrites [21, 22].

For green photocatalytic process the use of pollutants as electron donor was also investigated. Li et al., reported enhanced photocatalytic hydrogen production using a mixture of pollutants (oxalic acid, formic acid and formaldehyde) acting as electron donors. The authors reported that photocatalytic decomposition of pollutants and photocatalytic production of hydrogen can take place simultaneously when the pollutants are acted as electron donors [23].

1.6. Sensitizers

To enhance the visible light absorption of semiconductors the use of sensitizers is widely reported. Some dyes, excited under visible light, can transfer electrons to the conduction band of semiconductors, thus promoting the photocatalytic reaction (Figure 1.3).

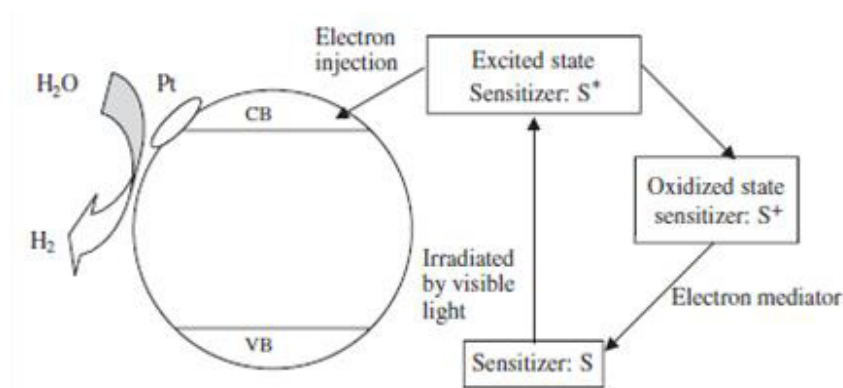


Figure 1.3. Mechanism of dye-sensitized photocatalytic hydrogen production under visible light irradiation [17].

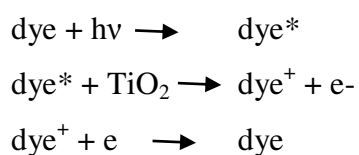
Dhanalakshmi et al. studied the effect of using $\text{Ru}[(\text{dcby})_2(\text{dpq})]^{2+}$ as a sensitizer on photocatalytic hydrogen generation from water, under visible light irradiation. Adsorbing dye molecules on TiO_2 surface the hydrogen production rate was enhanced [24].

Gurunathan et al. investigated the effects of different dyes on photocatalytic hydrogen production using SnO_2 that has a band gap of 3.5 eV and that is not active under visible light, but after sensitization with dyes, hydrogen production was observed also under visible light illumination [25]. The hydrogen production rate was improved by using the following dyes in the order: Eosin Blue > Rose Bengal > $\text{Ru}(\text{bipy})_3^{2+}$ > Rhodamine B \approx Acriflavin > Fluorescein. Table 1.1 shows the maximum absorption wavelengths of some dyes.

Table 1.1. Maximum absorption wavelength of some dyes.

Dyes	λ_{max} (nm)
Thionine	596
Toluidine blue	630
Methylene blue (MB)	665
New methylene blue	650
Azure A	635
Azure B	647
Azure C	620
Phenosafranin (PSF)	520
Safranin-O (Saf-O/SO)	520
Safranin-T (Saf-T/ST)	520
Neutral red (NR)	534
Fluorescein	490
Erythrosin	530
Erythrosin B	525
Rhodamin B (Rh. B)	551
Acridine orange (AO)	492
Proflavin (PF)	444
Acridine yellow (AY)	442
Fusion	545
Crystal violet	578
Malachite green	625
Methyl violet	580
tris(2,2-bipyridyl) ruthenium(II)	450

The reacted dyes molecules can be regenerated in solution with the addition of sacrificial reagents, such as EDTA [25] and IO_3^-/I^- [26]. The mechanism of dye excitation and regeneration can be expressed as follows [27]:



1.7 Noble Metals

Noble metals, such as Pt, Au, Pd, Rh, Ni, Cu and Ag, have been reported to be very effective to enhance efficiency of semiconductors in photocatalysis [5].

Photo-excited electrons can be transferred from CB to metal particles deposited on the surface of a semiconductor, if the Fermi levels of these noble metals are lower than that of the semiconductor; while photo-generated VB holes remain on the photocatalyst. Anpo et al. [28] employed Electron Spin Resonance (ESR) signals to investigate electron transfer from TiO_2 to Pt particles. It was found that Ti^{3+} signals increased with irradiation time and the loading of Pt reduced the amount of Ti^{3+} . This observation indicates the occurrence of electron transfer from TiO_2 to Pt particles. As electrons accumulate on the noble metal particles, their Fermi levels shift closer to the conduction band of TiO_2 [29,30,31], these activities greatly reduce the possibility of electron-hole recombination, resulting in efficient separation, and stronger photocatalytic reactions improving also the visible light absorption.

1.7.1 Preparation methods for noble metals doped catalyst

A wide range of techniques has been employed for the incorporation of a catalytically active species onto a support material. The most widely used and simple techniques are impregnation and deposition-precipitation or co-precipitation. The main catalyst-preparation techniques involve two stages [32]. First, rendering a metal-salt component into a finely divided form on a support and secondly conversion of the supported metal salt to a metallic or oxide state. The first stage is known as dispersion and is achieved by impregnation, adsorption from solution, co-precipitation, or

deposition, while the second stage consists of calcination or reduction that consists of a thermal treatment in an inert atmosphere or an active atmosphere of oxygen or hydrogen. When the active atmosphere is hydrogen the process is known as reduction.

1.7.1.1 Impregnation

Impregnation consists in dipping of porous support into a solution containing a desired catalytic agent [33]. It must be applied uniformly in a predetermined quantity especially for catalysts based on noble metals. The liquid penetration into the support is hindered by air trapped in the pores. Various expensive techniques like pressurizing, vacuum treatment, acoustic activation etc. are used to facilitate the impregnation process. A simple, method to eliminate vacuum is a three-step treatment of the catalyst support before impregnation. The pre-treatment removes all air trapped in the open pores and involves the following steps:

- heating the catalyst;
- introduction of non-reactive gas;
- desorption of gas.

The impregnation method [34] involves in three steps:

1. contacting the support with the impregnating solution;
2. drying the support to remove solvent;
3. catalyst activation by calcination, reduction etc.

Calcination is a further heat-treatment beyond drying. In general calcination is conducted in air at higher temperature. Others thermal treatments as activation operations, such as reductions, are performed in special atmospheres.

The active species are introduced into a porous support not in their final form but as a precursor. The first step is influenced by of the solution amount:

- *Impregnation with excess of solution.*

The support dipped in a high amount of solution for the time required for the total impregnation. Subsequently the solid is drained and dried. During this operation the solution can release debris forming a mud that makes difficult to completely utilize the solution.

- *Support impregnation with repeated application of solution.*

This technique is more precise and it is termed dry impregnation or impregnation to incipient wetness. In this case the amount of the solution used to impregnate the support corresponds to the total known pore volume. The support is kept in motion in a rotating cylinder and is sprinkled with the solution by sprayers.

For both techniques the interaction of the support with the active species, usually, is not only physical but also chemical. The impregnation with chemical interaction allows obtaining a better dispersion of the active species with particles size of metal supported in the order of 10 \AA , while using impregnation method without interaction the particles size is about 50 \AA .

In order to perform an impregnation with an effective interaction it must be considered that the surface of the support changes its polarization according to the pH value of the solution and to the isoelectric point of the solid (the isoelectric point of TiO_2 is 6). For simple electrostatic reason, if the pH of the solution is below the isoelectric point the supported surface

will be surrounded by anion, while at pH above the isoelectric point the surface will be negatively charged and it will be surrounded by cations.

A high dispersion of the active species on the support is usually desired because it corresponds to a greater utilization of the active species.

Higher surface areas may be obtained by increasing the pore volume (V_p) and decreasing the mean pore width or pore radius (r_p) as shown in the following equation:

$$S = 2 V_p / r_p$$

Metal loading catalyst using impregnation method is widely reported. Neri et al., to prepare supported Pd catalyst for the hydrogenation of campholenic aldehyde used the wetness impregnation as preparation method [35]. They plunged the support in an acid solution of PdCl₂. The resulting samples were dried at 120 °C for about 10–12 h. After preparations, the catalyst was reduced under flowing H₂ at 200 °C for 2 h before their use for catalytic tests. The nominal Pd loading was 2 wt. %.

Hong et al., prepared the supported palladium catalysts for selective hydrogenation of acetylene by the conventional wet impregnation method with a Pd content of 0.5 wt% [36]. Three grams of novel titania support was impregnated with PdCl₂ solution for 45 min, dried at 80 °C in a water bath and at 110 °C in an oven, calcined in air at 450°C for 3 h and then reduced in hydrogen at 450 °C for 3 h before its use in the selective hydrogenation. It was reported that TiO₂ interacted strongly with the noble metal Pd, particularly after a reduction at high temperature like 500 °C. This phenomenon is referred to “the strong metal-support interaction” (SMSI) and has been observed on catalysts supported on reducible metal

oxides, including CeO_2 , V_2O_5 , and TiO_2 . This interaction can remarkably change some catalysts activity and selectivity. Moreover they reported that the catalyst prepared at high pH value has favoured the ethylene selectivity obtaining a maximum yield of ethylene at pH 8.

Wu et al., prepared Pd-modified TiO_2 photocatalysts for the photocatalytic oxidation of NO by thermal impregnation method [37]. The photocatalysts were prepared by dispersal of 8.0 g TiO_2 powder into 100 ml $\text{Pd}^{2+}/\text{HCl}$ solution (4–160 mg/100 ml) to obtain 0.02–1 wt. % Pd loading TiO_2 . The solution was stirred for 48 h, and then heated at 100 °C for 12 h and calcinated in air at 400 °C for 1 h. They reported that the optimum Pd dopant content was 0.05 wt. PL spectra identified that the doping of Pd on TiO_2 could inhibit the recombination of photogenerated electrons and holes.

Grams et al., prepared Pd- TiO_2 adding ZrO_2 to protect the catalyst surface avoiding the formation of PdCl_2 and the backwards reaction [38]. The support was prepared by the impregnation of TiO_2 by aqueous solution of $\text{ZrO}(\text{NO}_3)_2$. In the next step, the support was impregnated with aqueous solution of PdCl_2 . The obtained material was dried under atmospheric pressure at 110 °C for 2 h and calcinated in air at 500 °C for 4 h and then at 100 °C using CCl_4/H_2 (1:10) as a reactant mixture. Before the reaction the catalysts were reduced by a hydrogen flow at 500 °C for 4 h.

1.7.1.2 Deposition-precipitation

The precipitation occurs in three steps [34]:

- supersaturation;
- nucleation;
- growth.

The solubility curves are in functions of temperature and pH. To approach the supersaturation region (Figure 1.4), with formation of unstable system where the precipitation occurs with any small perturbation, the concentration can be increased through solvent evaporation (A to C), the temperature can be lowered (A to B) or the pH can be increased.

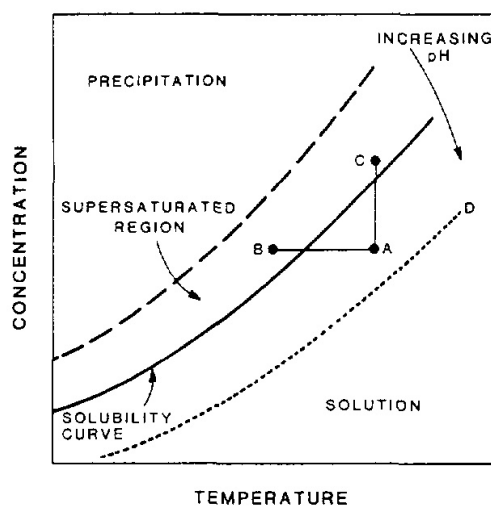


Figure 1.4. Supersaturation dependence on concentration, T and pH [34].

Particles within the supersaturation region develop a nucleation that may proceed spontaneously (homogeneous nucleation) or be initiated with seed materials (heterogeneous nucleation). The successive step is the growth process that depends on concentration, temperature, pH and ripening.

The reaction to achieve the precipitation consists of mixing a metal salt solution with the support at basic pH obtained using sodium hydroxide or potassium hydroxide etc.

Powders or particles are slurred with an amount of metal salt sufficient to give the required loading.

Two processes are involved in the deposition:

- 1) precipitation of solution in bulk and pore fluid;
- 2) interaction with support surface.

Rapid nucleation and growth must be avoided, since it produces a deposition only outside the support porosity. Using urea as alkali is obtained a uniform precipitation because it decomposes in water very slowly at 90 °C giving a uniform concentration of OH⁻. The precipitation is preferred for loading higher than 10-20%.

Xu et al. reported the effect of Pd/TiO₂ preparation methods as sol–gel (SG), impregnation (Imp) and deposition–precipitation (DP), on the hydrogenation of maleic anhydride [39]. For all catalysts prepared, 100% conversion of maleic anhydride was achieved after 2 h. The yield of butyric acid over three catalysts is found to be in the order: SG>DP>Imp and respectively 93.5, 86.6 and 81.3. The characteristics of Pd/TiO₂ catalyst are shown in table 1.2.

Table 1.2. Characteristics of Pd/TiO₂ catalyst prepared by different methods.

Catalyst code	BET surface area (m ² /g catalyst)	Pore diameter (Å)	Pd surface area (m ² /g catalyst)	Pd dispersity on surface (%) ^a	Pd particle size (nm) ^b
SG	103.3	81.5	0.68	0.91	7.5
DP	108.5	86.4	86.4	1.65	6.2
Imp	59.8	94.1	94.1	0.65	15.4

^a Defined by SPd/SBET

^b Evaluated from the FWHM using the Scherre equation

To prepare catalyst with DP method an aqueous solution of 0.25 M Na₂CO₃ was added drop-wise to an aqueous mixture of PdCl₂ and TiO₂ powder until the PH value reached 10. The resulting suspension was

stirred for 3h, and then was washed several times with distilled water until no chlorine anion was detected using AgNO_3 reagent. The resulting precipitate was filtered, dried at $120\text{ }^\circ\text{C}$, and calcined at $500\text{ }^\circ\text{C}$ for 2 h and reduced with pure hydrogen at $500\text{ }^\circ\text{C}$ before be used.

Bamwenda et al., prepared Pt-TiO₂ and Au-TiO₂ as catalysts, to use for photo assisted hydrogen production, by the followings preparation methods: photodeposition (FD), deposition-precipitation (DP), impregnation (IMP), physical mixing (MIX). The activity of Au catalyst for H₂ production strongly depends on the preparation method and decreases in the order $\text{FD} > \text{DP} > \text{IMP} > \text{MIX}$. The activity of platinum samples is less sensitive to the preparation methods and decreases in the order $\text{FD} > \text{DP} = \text{IMP} > \text{MIX}$ [40].

The deposition of the catalyst by DP was carried out as follows. Aqueous solution of the precursor was heated to $70\text{ }^\circ\text{C}$, NaOH was added to obtain the required pH. Subsequently was added TiO₂ (1-3 g) and aged for 1 h, after washed with distilled water for six times. The resulting material was vacuum dried at 0.4 Pa for 15 h and then calcined in air at $400\text{-}500\text{ }^\circ\text{C}$ for 4 h. The calcined samples were reduced with H₂ flow at $450\text{ }^\circ\text{C}$ for 10-20 h, and then cooled to room temperature under an argon flow.

1.8 Water splitting

Photocatalytic water splitting is a reaction in which hydrogen and oxygen are generated from water molecules that are reduced by photogenerated electrons and oxidized by photogenerated hole on a semiconductor surface.

In last years, a global energy crisis due to the depletion of resources and increased environmental problems is developing [41]. The extensive use

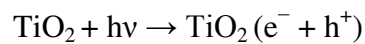
of fossil fuels and the consequently high production of carbon dioxide emissions are considered the major cause of global warming and climate change [42]

One of these alternative fuels, hydrogen, has the highest specific energy content of all conventional fuels and is the most abundant element in the universe [43]

Hydrogen is considered as an ideal fuel for the future because it may be produced in virtually unlimited quantities using renewable energy sources. Despite this, until now, [44] high hydrogen production is came from fossil fuels' conversion, such as natural gas reforming causing the co-production of carbon dioxide.

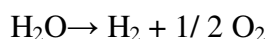
Solar is one of major sources of renewable energy and it is also the promising sources for renewable hydrogen production. Photocatalytic water-splitting using low cost semiconductors, such as TiO₂ or new photocatalysts such as graphene based semiconductors, for hydrogen production offers a promising way for a clean, low-cost and environmentally friendly production of hydrogen by solar energy [17]. The first work on water splitting using TiO₂ was reported by Fujishima et Honda in 1972 [45]. Subsequently the interest on this topic has grown significantly [5].

The general photocatalytic mechanism, described in paragraph 1.2, consists on excitation of semiconductors by photons with energy equal to or higher than their band gap energy level, thus promotion of electron from VB to CB, in particular for water splitting using semiconductor TiO₂, the reaction is expressed as:



The photo-generated electrons and holes can recombine in bulk or on surface of the semiconductor within a very short time, releasing energy in the form of heat or photons or electrons and holes that migrate to the surface of the semiconductor without recombination can, respectively, reduce and oxidize the reactants adsorbed by the semiconductor.

For hydrogen production, the CB level should be more negative than $E_{\text{red}}(\text{H}^+/\text{H}_2)$, 0 V vs. NHE at pH 0, while the VB should be more positive value than $E_{\text{ox}}(\text{H}_2\text{O}/\text{O}_2)$, 1.23 V vs. NHE at pH 0 the two electron process:



is endergonic, $\Delta G_1 = 238 \text{ kJ/mol} = 2.46 \text{ eV}$. Thus, the minimum energy required to drive the reaction corresponds to that of two photons of 1.23 eV, however, electron transfer (ET) involves an activation barrier, and photon energy greater than the above value is required for driving water splitting at a reasonable rate [45].

The photocatalytic hydrogen production by TiO_2 is shown in Fig. 1.5.

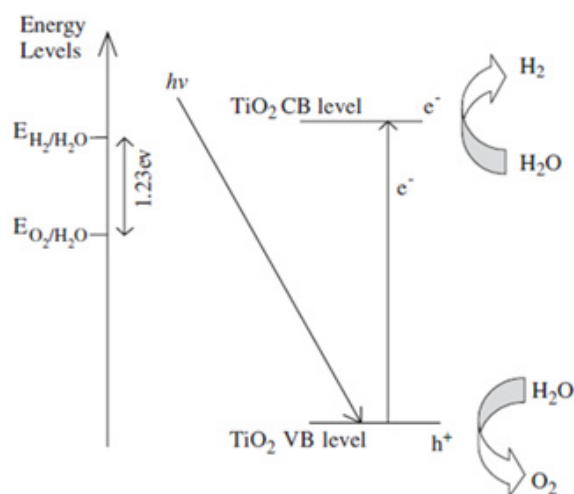


Figure 1.5. Mechanism of TiO_2 photocatalytic water-splitting for hydrogen production [17].

Suitable semiconductors for water splitting are mostly based on transition metal cations with d0 (Ti^{4+} , Zr^{4+} , Nb^{5+} , Ta^{5+} and W^{6+}) or d10 electronic configurations (Ga^{3+} , In^{3+} , Ge^{4+} , Sn^{4+} , and Sb^{5+}). Other metal oxides with empty/filled d orbitals, such as V^{5+} , Mo^{6+} , and Zn^{2+} , are also expected to be active provided that the band position is suitable. For example, WO_3 cannot reduce H^+ to H_2 because the CB is at a more positive potential than that of water reduction, but functions as a robust photocatalyst for O_2 evolution in the presence of an appropriate electron acceptor. Some semiconductor despite their potential application in water splitting are not stable under operative conditions, see figure 1.6.

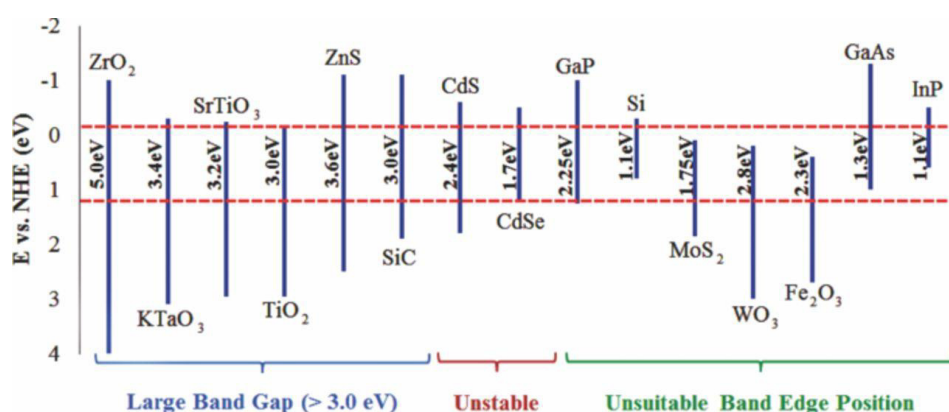


Figure 1.6. Band-gap structure of some semiconductors and their limitations for water splitting.

Thus, semiconductors based on Si, GaAs, InP and related materials, common in modern electronics and solar power engineering (photovoltaic), are not used in photocatalysis because, they are unstable in aqueous solutions. Moreover, this is the case for CdS and CdSe, photogenerated holes may cause the oxidation of the semiconductor

surface, resulting in corrosion of the material, because the S^{2-} and Se^{2-} anions are more susceptible to oxidation than water, and are degraded.

Another approach is using two-photon systems, mimicking the characteristic Z-scheme of photosynthesis [46]. Thus, an electron donor/acceptor (D/A) shuttle is added to two photocatalytic sites. On the H_2 evolution photocatalyst site, D is oxidized to A by h^+ and this is reduced back to D at the O_2 evolution site, while holes oxidize water to O_2 . However, at the H_2 evolution photocatalyst, reduction of H^+ to H_2 and oxidation of D to A may cease when the concentration of A becomes high enough that reduction of A to D (a thermodynamically favored reaction) competes. Likewise, the rate of O_2 evolution over the other photocatalyst may decrease when backward oxidation of D to A becomes competitive. A thoughtful choice of the photocatalytic components and a fine tuning of conditions are required. Suitable shuttles are the iodate/iodide (IO_3^-/I^-) and ferric/ferrous (Fe^{3+}/Fe^{2+}) redox pairs. Good results have been obtained by using Pt-ATaO₂N (A = Ca, Ba) and Pt-WO₃ for H_2 and O_2 evolution, respectively, and the iodate/iodide electron shuttle, with a spectral sensitivity extended to 660 nm (with Ba) [46, 47].

Finally, a convenient water splitting device requires that H_2 and O_2 are separated. Interestingly, a two-compartment plexiglas cell has been developed where the two gases are separately produced. The device worked at the same rate for more than 30 runs (ca. 180 h of work), although only under UV irradiation (efficiency = 2.1%; $\lambda > 300$ nm) [48].

1.9 Graphene based semiconductors

1.9.1 Graphene

Graphene (G) is a single layer of sp^2 - bonded carbon atoms, see figure 1.7, with a high thermal conductivity ($\approx 5000 \text{ W m}^{-1} \text{ K}^{-1}$), and a p-conjugation structure that exhibits excellent electronic mobility of charge carriers at room temperature ($200,000 \text{ cm}^2 \text{ V}^{-1} \text{ s}^{-1}$), and an extremely high theoretical specific surface area ($\approx 2600 \text{ m}^2 \text{ g}^{-1}$). For its mechanical, thermal, optical, and electrical properties has attracted a lot of attention since its discovery in 2004, it has emerged as one of the most active research fields. [49-54].

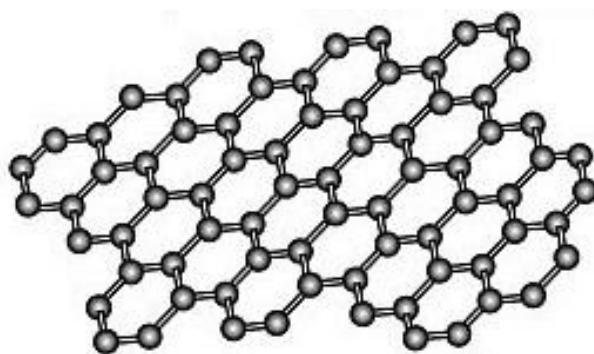


Figure 1.7. Graphene structure

The valence and conduction bands of graphene, consisting of bonding p and anti-bonding p (p^*) orbitals, respectively, touch at the Brillouin zone corners, which makes a single sheet of graphene a zero band-gap semiconductor [50, 55, 56], indicating that it is a conductor but not a semiconductor, furthermore it is hydrophobic and unsuitable for direct use in water splitting but its properties make graphene a possible co-catalyst for other semiconductors. Moreover introducing heteroatoms it is possible to extend the applications of graphene to photocatalytic processes [57, 50].

Graphene is a single atomic layer of graphite. Since the first report on graphene obtained by manual mechanical exfoliation of graphite with a Scotch tape [58] a wide range of techniques for the synthesis of this material have been reported [59], including micromechanical exfoliation, epitaxial growth, chemical and electrochemical reduction of graphite oxide and organic synthesis [59-65]. The most widely employed method used is the graphite oxidation using the Hummers' procedure followed by chemical reduction as shown in Figure 1.8

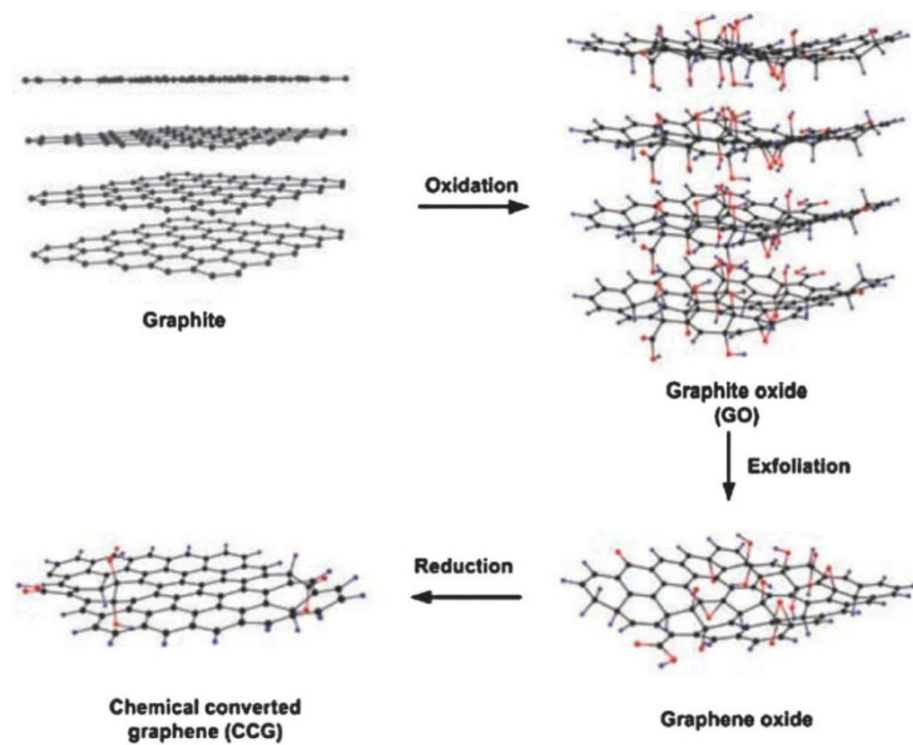


Figure 1.8. Preparation of graphene by chemical reduction of graphene oxide synthesized by Hummers' method. [65].

According to this method, graphite oxide is synthesized by a strong oxidation procedure that consists in mixing natural graphite powder with

strong chemical oxidants, such as HNO_3 , KMnO_4 and H_2SO_4 . The resulting graphite oxide after purification by washing is exfoliated by sonication to obtain graphene oxide sheets (GO). This methodology enjoys of high reproducibility and can produce highly concentrated aqueous suspensions of GO (about $0.1 \text{ mg}\times\text{L}^{-1}$) and the materials present in the suspensions are generally constituted by micrometric sheets of nanometric thickness [66, 67, 68]. The exfoliated GO sheets contain a high range of oxygen-containing groups, such as carboxylic, hydroxyl, and epoxide functional groups. Moreover, the functional GO can be reduced to graphene with partial restoration of the sp^2 - hybridized network by thermal [69] chemical [70], electrochemical [71], photothermal [72] photocatalytic [73] sonochemical [74] and microwave reduction methods [75].

1.9.2 Graphene oxide

Graphene oxide (GO) sheets, obtained by partial oxidation of graphene (Figure 1.9), are hydrophilic and exhibit notable performance in photocatalytic water splitting [76–79]. Oxygen adsorption forms C–O covalent bonds that damage the original carbon orbitals in graphene resulting in separation of damaged p and p* orbitals and creating a band gap in graphene [77].

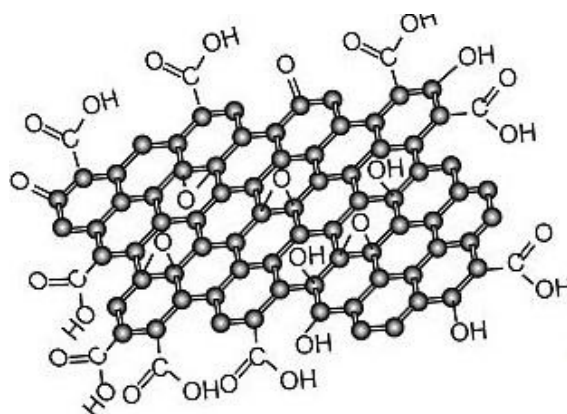


Figure 1.9. Possible structure of graphene oxide.

GO with a band gap of 2.4–4.3 eV can be used as a photocatalyst for H_2 generation under UV or visible light irradiation [80]. Yeh et al. reported the photocatalytic activity of various graphene oxide semiconductors synthesized by modified Hummers' procedure best performance in terms of photocatalytic hydrogen production was showed using as photocatalysts GO samples with lower oxygen content. Although all GOs tested by the authors generated H_2 from aqueous methanol solutions under UV and visible light illumination, they were not able to produce O_2 from water decomposition also in presence of electron-scavenger Ag^+ ions because the valence band minimum (VBM) of GO was insufficiently positive for water oxidation. Introducing more oxygen the charge transfer from the graphene sheet to oxygen atoms for the large electronegativity of oxygen enlarges the band gap. The valence band maximum (VBM) gradually changes from the p orbital of graphene to the 2p orbital of oxygen; the p^* orbital remains as the conduction band minimum (CBM). VBM value increases with increasing oxygen content which results from the increased dipoles in oxygenated graphene. The negatively charged oxygen ions

allocate their electrons into the vacuum to minimize the kinetic energy of the electrons, consequently increasing the energy barrier to removing an electron from the system [81].

Yeh et al. reported the photocatalytic mechanisms of GO sheets as a semiconductor under UV illumination. The absorption of UV light generates the formation of electron–hole pairs on GO sheets. The photogenerated electrons can reduce oxygen functional groups on GO sheets producing more defect carbon sites, which, the author reported, became active sites for water reduction to H₂. The photogenerated holes, instead, can modify the GO structure oxidizing defected carbon and producing CO₂. Probably, after long time of irradiation on GO this structure become stable and not more modification and CO₂ evolution occur [80].

1.9.2.1 Graphene and graphene oxide as co-catalysts

A wide range of semiconductors have been reported to catalyze the evolution of hydrogen from water (see paragraph 1.3). However, the rapid recombination of photogenerated electrons and holes limit the practical applications of these photocatalysts (see paragraph 1.4). Considering the superior electron mobility and high specific surface area of graphene it can be used as an efficient electron acceptor to enhance the photoinduced charge transfer and to inhibit the backward reaction (see Figure 1.10) improving photocatalytic activity of semiconductors [82].

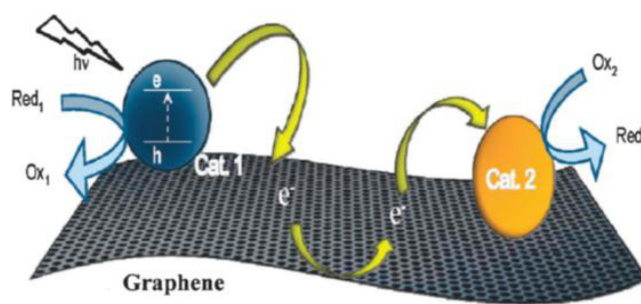


Figure 1.10. Schematic illustration of graphene used as a conducting support [82].

GO sheets are particularly effective in separating charges on TiO_2 because of their 2D profile. Additionally, the unpaired p electrons on GO can bond with Ti atoms of TiO_2 to form Ti–O–C bonding (see figure 3) and extending the light absorption range of TiO_2 to improve the photochemical responses under visible light ($\lambda > 400 \text{ nm}$) irradiation [83]. Zheng et al. reported a quantum efficiency of 8.2% for H_2 evolution from an aqueous triethanolamine solution under 420 nm monochromatic light irradiation using Pt-loaded GO- TiO_2 nanocomposites, synthesized by hydrothermal method [84].

Cui et al. studied the water splitting performance optimizing different loading contents of graphene in G/ TiO_2 composites using Na_2S and Na_2SO_3 as sacrificial agents under Xe lamp irradiation. The optimal graphene content was found to be 5.0 wt%, giving an H_2 -production rate of 8.6 mmol h^{-1} that was two times higher than pure P25 TiO_2 [85].

Very recently, Fan et al. reported the photocatalytic activity for H_2 evolution from methanol aqueous solution using the P25–graphene composite prepared with different methods: UV-assisted photocatalytic reduction, hydrazine reduction, and hydrothermal method. Although all

G/TiO₂ samples exhibited higher photocatalytic activity than P25 alone, the preparation method and the loading content of graphene greatly influence the efficiency of P25–graphene composite. The optimum mass ratio of P25/graphene, prepared by the hydrothermal method, has been found to be 1/0.2, giving a H₂-production rate of 74 mmol h⁻¹ that is ten times higher than obtained using pure P25 [86].

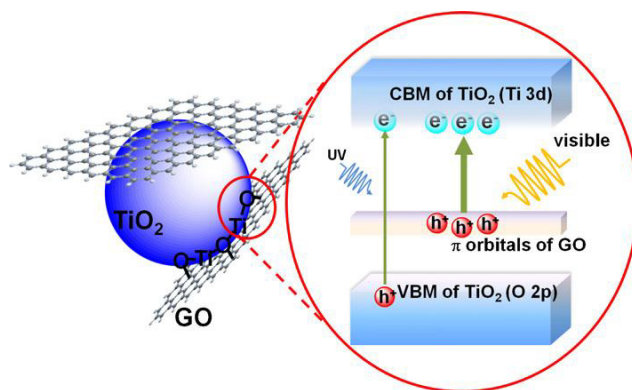


Figure 1.11. Interaction between unpaired p electrons on GO with surface Ti atoms of TiO₂ to form Ti–O–C bonding [50].

GO sheets for their flexibility, hydrophilicity, and higher surface area can be used also to disperse semiconductor particles avoiding their aggregation. For example CdS particles tend to aggregate, resulting in a reduced surface area and a higher possibility of recombination of photogenerated electron–hole pairs. Incorporating CdS in flexible GO sheets the residual oxygen-containing hydrophilic groups on GO sheets can facilitate the dispersion of the semiconductor in water [87], prevents particle aggregation and suppresses charge recombination [88]. The CdS particles were homogeneously deposited on GO sheets (Figure 1.12) using the solvothermal method with dimethyl sulfoxide to synthesize CdS/GO. To

enhance the H_2 evolution efficiency under visible light (420 nm) the GO-CdS nanocomposites with 1% of GO were loaded with Pt as co-catalyst exhibiting highest H_2 production rate with a quantum efficiency of 22.5% [87]. Using alginate, a natural polysaccharide from algae, simultaneously as graphene precursor and as ceria nanoparticles template agent, one step synthesis for preparation of ceria/graphene photocatalyst that exhibits about three times higher photocatalytic activity for water oxidation to oxygen than commercial ceria is presented in Chapter 4.

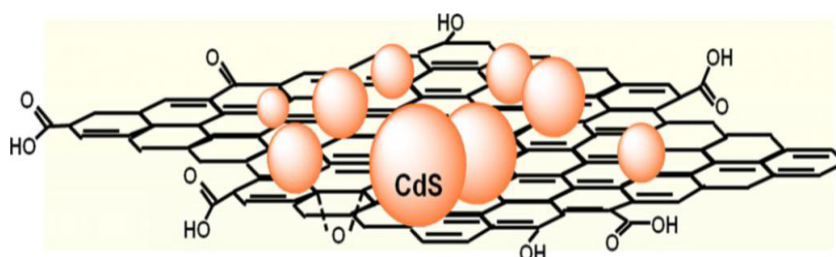


Figure 1.12. Homogeneous deposition of CdS nanoparticles on a GO sheet [50].

To improve the visible light absorption and then the photocatalytic activity of GO sheets they were used as a mediator between the photosensitizer and co-catalysts [89, 90]. The GO sheets were functionalized with dye Eosin Y (EY) through hydrogen bonding and p-p stacking. Under visible light irradiation, the H_2 evolution rate was negligible over the EY-GO photocatalyst. Because of the p-conjugated network, GO can accumulate the electrons injected from the photoexcited EY. The considerable charge recombination between EY and GO lowers the H_2 evolution efficiency. Metallic Pt nanoparticles, with a greater work function (5.65 eV) than that of GO (4.66 eV), were deposited on GO. The resulting Schottky barrier at the interface of GO and Pt particles promoted the transfer of trapped

electrons to Pt nanoparticles. The photocatalytic activity of EY-GO-Pt was considerably higher than that of EY-GO. The quantum efficiency of EY-GO-Pt was 4.15% at 420 nm. The higher H₂ evolution was attributed to the efficient charge transfer from GO to Pt particles. The enhancement of photocatalytic activity under visible light for hydrogen generation from water methanol mixture using graphene oxide contained a tris(2,2-bipyridyl) ruthenium(II) complex incorporated in the interlayer spaces of a few layers of GO sheets that was five times more than GO alone in absence of any expensive noble metal is presented in Chapter 2.

1.9.3 N-doped graphene

The electronic properties of graphene can be modulated introducing heteroatoms.

Graphene can be chemically doped by heteroatoms through: adsorption of gas [91], metal [92] or organic molecules [93] to the graphene surface and substitution doping, which introduces heteroatoms, such as nitrogen atoms and boron atoms, into the carbon lattice of graphene. N-graphene can be obtained through two different ways: direct synthesis and post treatment. Most post synthesis treatments may lead to surface doping only. Direct synthesis may have the potential to create a homogeneous doping, but not always this is confirmed by reported results.

Widely used as direct synthesis to prepare various carbon nanomaterials, such as graphene [94], carbon nanotubes (CNTs) [95], carbon nanofibers [96], N-doped CNTs [97] and recently, successfully applied to prepare N-graphene, consist of using a metal catalyst (Cu or Ni) as the substrate, then at high temperature, a carbon source gas mixed with a nitrogen-containing

gas is introduced [98,99,100]. These precursors dissociate and recombine into N-graphene by means of precipitation on the surface of the catalyst.

Besides the gas mixture, liquid organic precursors such as acetonitrile and pyridine have also been used to form N-graphene [102,103]. Theoretical study about different precursors shows that proper skeletal bonds of liquid precursors are crucial for the formation of N-graphene [104].

Widely used such as post treatment is the thermal treatment that consist in using high temperature to produce N-graphene, for example, largely reported is the synthesis of N-graphene heating graphene in NH_3 at high temperature (≥ 800 °C) [105-106]. The nitrogen content in the N-graphene synthesized by this method is relatively low. Guo et al. [105] obtained N-graphene with 1.1 wt. % doping level at 1100 °C; Geng et al. [106] reported that the highest nitrogen content equal to 2.8 wt. % heating at 800 and 900 °C.

Besides graphene, graphene oxide can also be used to synthesize N-graphene by thermal treatment in the presence of various nitrogen precursors. Sheng et al. [107] reported that annealing GO in the presence of melamine at high temperature (700–1000 °C) could be produce N-graphene.

When graphene is doped with nitrogen atoms (N), within the carbon lattice, nitrogen, typically, has three common bonding configurations that correspond to quaternary N (or graphitic N), pyridinic N, and pyrrolic N (Figure 1.13).

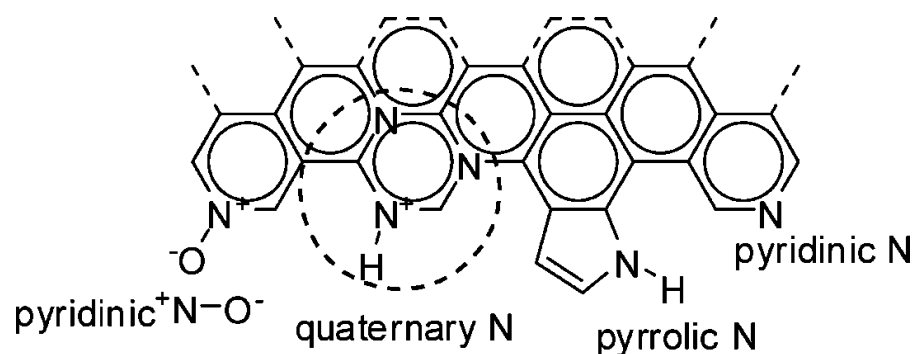


Figure 1.13. N-doped graphene structure [115].

Specifically, pyridinic N, sp² hybridized, bonds with two C atoms at the edges or defects of graphene and contributes one p electron to the π system. Nitrogen atoms of pyrrolic N that are sp³ hybridized contribute with two p electrons to the π system [108]. Quaternary N refers to N atoms with sp² hybridization, substitute C atoms in the hexagonal ring.

Among these three nitrogen types, N oxides of pyridinic N, nitrogen atom bonds with two carbon atoms and one oxygen atom, have been observed in both the N-graphene and N-carbon nanotube (N-CNT) studies [109-111]. N-graphene shows different properties compared with graphene, because the spin density and charge distribution of carbon atoms are influenced by the near nitrogen atoms dopants [112] which induce the “activation region” on the graphene surface that can participate in catalytic reactions directly or anchor the metal nanoparticles. Doping monolayer graphene with nitrogen atoms the Fermi level shifts above the Dirac point [113,114] and the density of state near the Fermi level is suppressed [115], thus, the band gap between the conduction band and the valence band will be opened. Instead doping graphene nanoribbons, the band gap is still kept after doping. The band gap in N-graphene makes it a candidate to be used

as a semiconductor; in fact the optimization of electronic properties of G surface modification is a promising technique for promoting water splitting.

Jia et. al. [117] reported a study on photocatalytic hydrogen production from water under visible light irradiation at $\lambda \geq 420$ nm using CdS nanoparticles on different supporting matrix such as N-graphene, graphene and graphene oxide. The relative order of reactivity for the synthesized catalysts was found to be N-graphene/CdS > graphene/CdS > GO/CdS > CdS.

The results show that N-graphene/CdS nanocomposites have a higher photocatalytic activity than pure CdS. The photocatalytic activity is significantly enhanced for the N-graphene/CdS photocatalysts for the inhibited electron-hole pairs recombination due to the photoinduced electrons in the CdS transferred to the N-doped graphene.

The amount of N-graphene is an important factor affecting photocatalytic activity of N-graphene/CdS nanocomposites. The authors reported that the optimum amount of N-graphene was found to be 2 wt. %, at which the N-graphene/CdS sample displays the highest reactivity that was five times higher than pure CdS. Therefore, N-graphene as a co-catalyst is promising candidate for development of high-performance photocatalysts in the photocatalytic H₂ production, instead, the authors reported that N-doped graphene alone was not able to produce detectable amount of hydrogen. Until now there are still not evidence in the use of N-doped graphene alone as a semiconductor, the first work on this field is presented in Chapter 3 prepared with a new synthetic method by using a biopolymer containing nitrogen (chitosan) as a precursor.

1.9.4 Graphene quantum dots

Properties of graphene can vary according to their size and morphologies. Graphene material includes two dimensional graphene nanosheets (GNSs), one-dimensional graphene nanoribbons (GNRs) [118-119] and zero-dimensional graphene quantum dots (GQDs) [120-121].

Graphene, as a perfect π -conjugated single sheet, have a zero bandgap. Various experimental techniques have been explored to introduce bandgaps in graphene sheets changing their size, edges or adding defects in the matrix [122]. To opens an energy gap and turns graphene into a semiconductor, a promising approach is to convert the 2D graphene sheets into 0D graphene quantum dots (GQDs), changing the band gap from zero to perhaps even the gap of the benzene ring by varying their sizes. GQDs, consisting of a single atomic layer of nano-sized graphite, have the excellent performances of graphene, such as high surface area, large diameter and better surface grafting using p-p conjugation and surface groups [123].

Semiconductor quantum dots are a natural step forward in allowing the control of material composition in three dimensions and at the nanoscale. Hence quantum dots are an example of nanoscience and nanotechnology in semiconductors [124]. A quantum dot is a semiconductor nanostructure that confines the motion of conduction band electrons, valence band holes, or excitons (bound pairs of conduction band electrons and valence band holes) in all three spatial directions [125].

Because of the structure of graphene, GQDs have some other special physical properties. Therefore, studies on GQDs in aspects of chemistry, physical, materials, biology and interdisciplinary science have been in full flow in the past decade.

During the past few years, fluorescent semiconductor quantum dots (QDs) have attracted much interest due to their unique optical and biochemical properties and their significant practical applications in many fields [126]. However, such QDs suffer from some serious health and environmental concerns due to the use of heavy metals as the essential elements, which limits their wide applications [127]. The above problems can be avoided by developing new nanomaterials with similar optical properties [128] such as carbon dots (CDs) and graphene quantum dots that have unique properties including low toxicity, easy labeling, and high stability [129]. GQDs can be also applied in catalysis due to their large surface area and accessibility of the active sites. Indeed, CNDs possess intrinsic peroxidase-like activity and have been successfully used as peroxidase mimetics for the colorimetric detection of H_2O_2 and glucose for the first time.

Zhuo et al. reported an easy ultrasonic route for the fabrication of graphene quantum dots (GQDs) with up converted emission [121]. The prepared GQDs exhibit an excitation-independent down conversion and up conversion photo luminescent (PL) behavior, and the complex photocatalysts (rutile TiO_2/GQD and anatase TiO_2/GQD systems) were designed to harness the visible spectrum of sunlight. It is interesting that the photocatalytic rate of the rutile TiO_2/GQD complex system is ca. nine times higher than that of the anatase TiO_2/GQD complex under visible light ($\lambda > 420 \text{ nm}$) irradiation in the degradation of methylene blue.

Approaches for synthesizing GQDs with tunable size can be generally classified into two main groups: top-down and bottom-up methods (Figure 1.14).

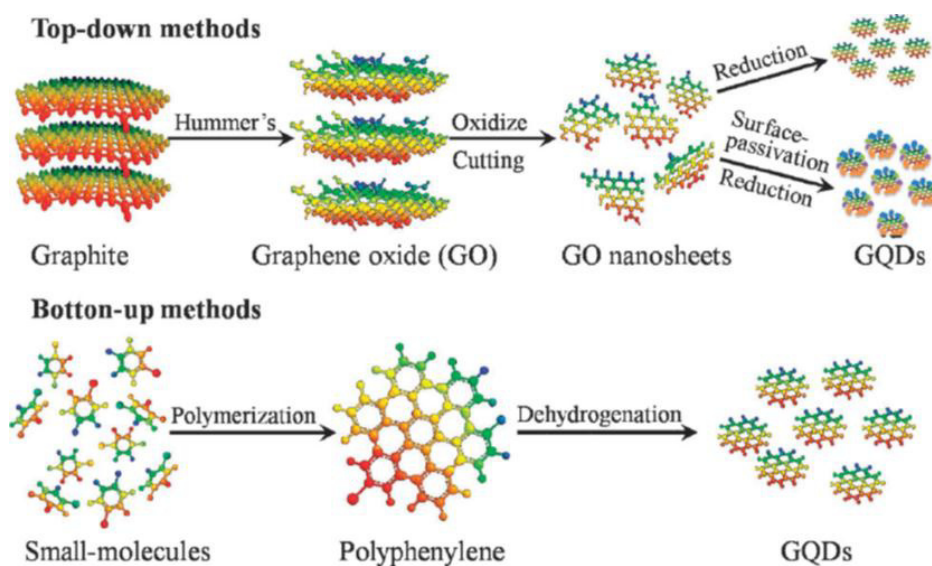


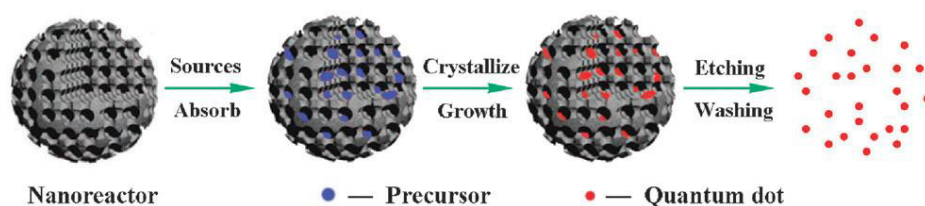
Figure 1.14. Schematic diagram of the top-down and bottom-up methods for synthesizing GQDs [123].

Top-down approaches refer to the cutting of graphene sheets into GQDs. The method consists of chemical ablation, electrochemical oxidation, and oxygen plasma treatment, where GQDs are formed or “broken off” from larger graphene sheets. Bottom-up methods involve the synthesis of graphene moieties containing a certain number of conjugated carbon atoms, for example, the approaches consist of the cage-opening of fullerene, or solution chemistry methods during which the GQDs are formed from molecular precursors. Typically, these GQDs have surfaces rich in carboxylic acid functionalities which can be used to bind surface-passivation reagents [121].

A top down approach to synthesize quantum dots by chemical ablation from graphene was described by Pan et al. that developed a hydrothermal route to cutting graphene sheets into GQDs, exhibiting blue luminescence [130]. The large graphene oxide sheets were cut into small sheets by

controlled oxidation in a mixture of sulfuric acid and nitric acid under mild ultra-sonication. The oxidized small graphene sheets were then reduced under hydrothermal conditions in Teflon lined autoclave at elevated temperature. The obtained GQDs had an average diameter of 9.6 nm consisting of 1–3 layers of graphene, and exhibited a quantum yield of 6.9% using quinine sulfate as a reference.

Very recently, Zhu et al. have reported a simple bottom-up synthesis method for C-dots by using a mesoporous silica microspheres template [131]. They proposed the concept of confined reaction in nanoreactors to prepare nanoparticles (Figure 1.15).



A bio-method to synthesize graphene by pyrolysis at 900 °C under an inert atmosphere of alginate, a natural widely available biopolymer, and the formation of graphitic quantum dots by exposure to a pulsed 532 nm laser in acetonitrile, water, and other solvents is presented in Chapter 5.

1.10 References

- [1] Magesh G., B. Viswanathan, R.P. Viswanath and T.K. Varadarajan. *Photo/Electrochemistry & Photobiology in the Environment, Energy and Fuel*. **2007**, Cap. 11
- [2] Gazi, S.; Ananthakrishnan, R. *Appl. Catal. B-Environ.*, **2011**, 105, 317–325.
- [3] Herrmann J.-M. *Topics in Catalysis*, **2005**, 34, 1–4.
- [4] Palmisano G., Augugliaro V., Pagliaro M. and Palmisano L. *Chem. Commun.*, **2007**, 3425–3437.
- [5] Molinari R., Caruso A., Palmisano L., Membrane operations- Innovative Separations and Transformations. Cap. 15, Wiley-VCH. **2009**, pp. 335-361.
- [6] Vayssieres L. Advanced semiconductor nanostructures. *C. R. Chimie*, **2006**, 6, 691-701.
- [7] Krishnakumar T., N. Pinna, K. P. Kumari, K. Perumal and R. Jayaprakash. *Materials Letters*, **2008**, 62, 3437-3440.
- [8] Deng H. and J. M. Hossenlopp. *Journal of Physical Chemistry. B*, **2005**, 109, 66-73.
- [9] Zhang H., N. Du, B. Chen, T. Cui and D. Yang. *Materials Research Bulletin*, **2008**, 43, 3164-3170.
- [10] Yang X. S., Y. Wang, L. Dong, M. Chen, F. Zhang and L. Z. Qi. *Materials Science and Engineering. B*, **2004**, 110, 6-10.
- [11] Granqvist C. G. *Solar Energy Materials & Solar Cells*, **2000**, 60, 201-262.
- [12] Chen D. and A. K. Ray. *Chemica Engineering Science*, **2001**, 56, 1561-1570.

- [13] Wang X., Pehkonen S.O. and A. K. Ray. *Electrochemical Acta*, **2004**, 49, 1435-1444.
- [14] Kabra K., C. Rubina and L. S. Rameshwar. *Ind. Eng. Chem. Res.*, **2004**, 43, 7683-7696.
- [15] Bedija I., S. Hotchandani and P. U. Kamat. *Journal of Physical Chemistry*, **1994**, 98, 15, 4133-4140.
- [16] Haamed A., M. A. Gondal and Z. H. Yamani. *Catalysis Communications*, **2004**, 5, 715-719.
- [17] Ni M., M. K. H. Leung, D. Y. C. Leung and K. Sumathy. *Renewable and Sustainable Energy Reviews*, **2007**, 11, 401-425.
- [18] Nada A. A., M. H. Barakat, H. A. Hamed, N. R. Mohamed and T. N. Veziroglu. *International Journal of Hydrogen Energy*, **2005**, 30, 687-691.
- [19] Kohtani S., E. Yoshioka, K. Saito, A. Kudo, H. Miyab. *Catalysis Communications*, **2010**, 11, 1049–1053.
- [20] Escobar E.A., M. Á. V. Zapata, S.A. Hernández, S. O. Flores Valle, O. R. Berny, V. J. G.Ángeles, I. C. Reyes. *J. Mex. Chem. Soc.*, **2010**, 54, 3, 133-138.
- [21] Imamura K., S. Iwasaki, T. Maeda, K. Hashimoto, B. Ohtani and H. Kominami. *Phys. Chem. Chem. Phys.*, **2011**, 13, 5114–5119.
- [22] Wehbe N., M. Jaafar, C. Guillard, J.-M. Herrmann, S. Miachon, E. Puzenat, N. Guilhaume. *Applied Catalysis A: General*. **2009**, 368, 1–8.
- [23] Li YX, Lu GX, Li SB. *Chemosphere*, **2003**, 52, 5, 843–50.
- [24] Dhanalakshmi KB, Latha S, Anandan S, Maruthamuthu P. *Int J Hydrogen Energy*. **2001**, 26, 669–74.

- [25] Gurutanathan K. *Journal of Molecular Catalysis A: Chemistry*. **2000**, 156, 59-67.
- [26] Abe R., K. Sayama and H. Arakawa. *Chemical Physics Letters*. **2002**, 362, 441-444.
- [27] Regan BO, Gratzel M. *Nature*. **1991**, 353, 737-40.
- [28] Anpo M, Takeuchi M. *J Catal*. **2003**, 216, 505-16.
- [29] Subramanian V, Wolf EE, Kamat P. *J Am Chem Soc*. **2004**, 126, 4943-50.
- [30] Subramanian V, Wolf E, Kamat P. *J Phys Chem B*. **2003**, 107, 7479-85.
- [31] Jakob M, Levanon H, Kamat PV. *Nano Lett*. **2003**, 3, 3, 353-8.
- [32] J. A. Schwarz , C. Contescu , A. Contescu. *Chem. Rev.*, **1995**, 95, 3, 477-510.
- [33] Zadorsky W.M.. Information supplied by author December 1998. Page last updated: July 03, 2005. http://www.ukrainebiz.com/technical/catalyst_impregnation.htm
- [34] Perego C., P. Villa. *Catalysis Today*. **1997**, 34, 281-305.
- [35] Neri G., G. Rizzo, L. De Luca, A. Donato, M.G. Musolino, R. Pietropaolo. *Applied Catalysis A: General*, **2009**, 356, 113-120.
- [36] Hong J., W. Chu, M. Chen, X. Wang, T. Zhang. *Catalysis Communications*. **2007**, 8, 593-597.
- [37] Wu Z., Z. Shenga, Y. Liu, H. Wang, N. Tanga and J. Wang. *Journal of Hazardous Materials*. **2009**, 164, 542-548.
- [38] Grams J., J. Góralski, J. Kleczewska, B. Szczepaniak, T. Paryjczak. *Polish Journal of Chemical Technology*, **2007**, 9, 3, 81-85.

- [39] Xu J., K. Sun, L. Zhang, Y. Ren, and X. Xu. *Catalysis Letters*. **2006**, 107, 1–2.
- [40] Bamwenda G.R., S. Tsubota, T. Nakamura, M. Haruta. *Journal of Photochemistry and photobiology A: Chemistry*. **1995**, 89, 177-189.
- [41] Ni M, Leung MKH, Sumathy K, Leung DYC. Proceedings of the International Hydrogen Energy forum, vol. 1, **2004**, Beijing, PRC. p. 475–480.
- [42] Fujishima A, Honda K. *Nature*. **1972**, 238, 37–8.
- [43] Asahi R, Morikawa T, Ohwaki T, Aoki K, Taga Y. *Science*, **2001**, 293, 269–71.
- [44] Khaselev O, Turner JA. *Science*, **1998**, 425–7.
- [45] Ravelli D., Dondi D., Fagnonia M. and Albini A. *Chem. Soc. Rev.*, **2009**, 38, 1999–2011.
- [46] R. Abe, K. Sayama and H. Sugihara, *J. Phys. Chem. B*, **2005**, 109, 16052.
- [47] M. Higashi, R. Abe, K. Teramura, T. Takata, B. Ohtani and K. Domen, *Chem. Phys. Lett.*, **2008**, 452, 120.
- [48] E. Selli, G. L. Chiarello, E. Quartarone, P. Mustarelli, I. Rossetti and L. Forni, *Chem. Commun.*, **2007**, 5022.
- [49] Quanjun Xiang, Jianguo Yu and Mietek Jaroniec. Graphene-based semiconductor photocatalysts. *Chem. Soc. Rev.*, **2012**, 41, 782–796
- [50] Te-Fu Yeh, Jaroslav Cihlar, Chih-Yung Chang, Ching Cheng and Hsisheng Teng. *Materials Today*, **2013**, 16, 3.

-
- [51] K. S. Novoselov, A. K. Geim, S. V. Morozov, D. Jiang, Y. Zhang, S. V. Dubonos, I. V. Grigorieva and A. A. Firsov, *Science*, **2004**, 306, 666.
- [52] A. K. Geim and K. S. Novoselov, *Nat. Mater.*, **2007**, 6, 183.
- [53] M. J. Allen, V. C. Tung and R. B. Kaner, *Chem. Rev.*, **2010**, 110, 132.
- [54] A. K. Geim, *Science*, **2009**, 324, 1530.
- [55] C. Berger, Z. Song, X. Li, X. Wu, N. Brown, C. Naud, D. Mayou, T. Li, J. Hass, A. N. Marchenkov, E. H. Conrad, P. N. First, and W. A. de Heer. *Science*, 312, **2006**, 1191.
- [56] J. Ito, J. Nakamura, and A. Natori. *J. Appl. Phys.* 103, **2008**, 113712
- [57] H. Liu, Y. Liu and D. Zhu. *J. Mater. Chem.*, **2011**, 21, 3335-3345. DOI: 10.1039/C0JM02922J
- [58] K. S. Novoselov, A. K. Geim, S. V. Morozov, D. Jiang, Y. Zhang, S. V. Dubonos, I. V. Grigorieva and A. A. Firsov, *Science*, **2004**, 306, 666.
- [59] M. J. Allen, V. C. Tung and R. B. Kaner, *Chem. Rev.*, **2010**, 110, 132.
- [60] A. K. Geim, *Science*, **2009**, 324, 1530.
- [61] X. S. Li, W. W. Cai, J. H. An, S. Kim, J. Nah, D. X. Yang, R. Piner, A. Velamakanni, I. Jung, E. Tutuc, S. K. Banerjee, L. Colombo and R. S. Ruoff, *Science*, **2009**, 324, 1312.
- [62] K. S. Kim, Y. Zhao, H. Jang, S. Y. Lee, J. M. Kim, K. S. Kim, J. H. Ahn, P. Kim, J. Y. Choi and B. H. Hong, *Nature*, **2009**, 457, 706.

- [63] C. N. R. Rao, A. K. Sood, K. S. Subrahmanyam and Govindaraj, *Angew. Chem., Int. Ed.*, **2009**, 48, 7752.
- [64] Y. Q. Sun, Q. O. Wu and G. Q. Shi, *Energy Environ. Sci.*, **2011**, 4, 1113.
- [65] H. Bai, C. Li and G. Q. Shi, *Adv. Mater.*, **2011**, 23, 1089.
- [66] W. S. Hummers and R. E. Offeman, *J. Am. Chem. Soc.*, **1958**, 80, 1339-1339.
- [67] D. C. Marcano, D. V. Kosynkin, J. M. Berlin, A. Sinitskii, Z. Sun, A. Slesarev, L. B. Alemany, W. Lu and J. M. Tour, *ACS Nano*, **2010**, 4, 4806-4814.
- [68] S. Park and R. S. Ruoff, *Nat. Nanotechnol.*, **2009**, 4, 217.
- [69] H. C. Schniepp, J. L. Li, M. J. McAllister, H. Sai, M. Herrera-Alonso, D. H. Adamson, R. K. Prud'homme, R. Car, D. A. Saville and I. A. Aksay, *J. Phys. Chem. B*, **2006**, 110, 8535.
- [70] X. F. Gao, J. Jang and S. Nagase, *J. Phys. Chem. C*, **2010**, 114, 832.
- [71] G. K. Ramesha and S. Sampath, *J. Phys. Chem. C*, **2009**, 113, 7985.
- [72] V. Abdelsayed, S. Moussa, H. M. Hassan, H. S. Aluri, M. M. Collinson and M. S. El-Shall, *J. Phys. Chem. Lett.*, **2010**, 1, 2804.
- [73] Y. H. Ng, I. V. Lightcap, K. Goodwin, M. Matsumura and P. V. Kamat, *J. Phys. Chem. Lett.*, **2010**, 1, 2222.
- [74] K. Vinodgopal, B. Neppolian, I. V. Lightcap, F. Grieser, M. Ashokkumar and P. V. Kamat, *J. Phys. Chem. Lett.*, **2010**, 1, 1987.
- [75] Jasuja, J. Linn, S. Melton and V. Berry, *J. Phys. Chem. Lett.*, **2010**, 1, 1853
- [76] X. An, J.C. Yu, *RSC Adv.* 1 (**2011**) 1426.

- [77] Q. Xiang, J. Yu and M. Jaroniec. *Chem. Soc. Rev.*, **2012**, 41, 782-796. DOI: 10.1039/C1CS15172J
- [78] N. Zhang, Y. Zhang and Y.-J. Xu. *Nanoscale*, **2012**, 4, 5792-5813. DOI: 10.1039/C2NR31480K.
- [79] L. Han, P. Wang and S. Dong. *Nanoscale*, **2012**, 4, 5814-5825. DOI: 10.1039/C2NR31699D
- [80] T.-F. Yeh, J.-M. Syu, C. Cheng, T.-H. Chang, and H. Teng. *Adv. Funct. Mater.* **2010**, 20, 2255–2262
- [81] J. Ito, J. Nakamura, and A. Natori. *Journal of Applied Physics* 103, 113712, **2008**; doi: 10.1063/1.2939270
- [82] I. V. Lightcap, T. H. Kosel and P. V. Kamat, *Nano Lett.*, **2010**, 10, 577.
- [83] H. Zhang , X. Lv , Y. Li , Y. Wang and J. Li. *ACS Nano*, **2010**, 4, 1, 380–386 DOI: 10.1021/nn901221k
- [84] J. S. Lee, K. H. You and C. B. Park, *Adv. Mater.*, **2012**, 24, 1084–1088.
- [85] X. Y. Zhang, H. P. Li, X. L. Cui and Y. H. Lin, *J. Mater. Chem.*, **2010**, 20, 2801.
- [86] W. Q. Fan, Q. H. Lai, Q. H. Zhang and Y. Wang, *J. Phys. Chem. C*, **2011**, 115, 10694.
- [87] Q. Li, et al. *J. Am. Chem. Soc.* 133, **2011**, 10878
- [88] A. Cao, Z. Liu, S. Chu, M. Wu, Z. Ye, Z. Cai, Y. Chang, S. Wang, Q. Gong, Y. Liu. *Adv. Mater.* **2010**, 22, 1, 103–106, DOI: 10.1002/adma.200901920
- [89] a) S. Min, G. Lu, *J. Phys. Chem. C*, **2011**, 115, 13938. b) P. Zeng, et al. *Phys. Chem. Chem. Phys.* 13, **2011**, 21496.
- [90] Z. Mou, et al. *Int. J. Hydrogen Energy* 36, **2011**, 8885.

- [91] Schedin, F.; Geim, A. K.; Morozov, S. V.; Hill, E. W.; Blake, P.; Katsnelson, M. I.; Novoselov, K. S. *Nat. Mater.* **2007**, 6, 652.
- [92] Giovannetti, G.; Khomyakov, P. A.; Brocks, G.; Karpan, V. M.; van den Brink, J.; Kelly, P. J. *Phys. Rev. Lett.* **2008**, 101, 026803.
- [93] Chen, W.; Chen, S.; Qi, D. C.; Gao, X. Y.; Wee, A. T. S. *J. Am. Chem. Soc.* **2007**, 129, 10418.
- [94] Liu, H.; Liu, Y.; Zhu, D. J. *Mater. Chem.* **2011**, 21, 3335.
- [95] Zhang, J.; Zou, H.; Qing, Q.; Yang, Y.; Li, Q.; Liu, Z.; Guo, X.; Du, Z. J. *Phys. Chem. B* **2003**, 107, 3712.
- [96] Che, G.; Lakshmi, B. B.; Martin, C. R.; Fisher, E. R.; Ruoff, R. S. *Chem. Mater.* **1998**, 10, 260.
- [97] Maldonado, S.; Morin, S.; Stevenson, K. J. *Carbon* **2006**, 44, 1429.
- [98] Wei, D.; Liu, Y.; Wang, Y.; Zhang, H.; Huang, L.; Yu, G. *Nano Lett.* **2009**, 9, 1752.
- [99] Luo, Z.; Lim, S.; Tian, Z.; Shang, J.; Lai, L.; MacDonald, B.; Fu, C.; Shen, Z.; Yu, T.; Lin, J. J. *Mater. Chem.* **2011**, 21, 8038.
- [100] Qu, L.; Liu, Y.; Baek, J. B.; Dai, L. *ACS Nano* **2010**, 4, 1321.
- [101] Di, C. A.; Wei, D.; Yu, G.; Liu, Y.; Guo, Y.; Zhu, D. *Adv. Mater.* **2008**, 20, 3289.
- [102] Reddy, A. L. M.; Srivastava, A.; Gowda, S. R.; Gullapalli, H.; Dubey, M.; Ajayan, P. M. *ACS Nano* **2010**, 4, 6337.
- [103] Jin, Z.; Yao, J.; Kittrell, C.; Tour, J. M. *ACS Nano* **2011**, 5, 4112.
- [104] Imamura, G.; Saiki, K. J. *Phys. Chem. C* **2011**, 115, 10000.
- [105] Guo, B.; Liu, Q.; Chen, E.; Zhu, H.; Fang, L.; Gong, J. R. *Nano Lett.* **2010**, 10, 4975.

- [106] Geng, D.; Chen, Y.; Chen, Y.; Li, Y.; Li, R.; Sun, X.; Ye, S.; Knights, S. *Energy Environ. Sci.* **2011**, 4, 760.
- [107] Sheng, Z. H.; Shao, L.; Chen, J. J.; Bao, W. J.; Wang, F. B.; Xia, X. H. *ACS Nano* **2011**, 5, 4350.
- [108] Casanovas, J.; Ricart, J. M.; Rubio, J.; Illas, F.; Jiménez-Mateos, J. M. *J. Am. Chem. Soc.* **1996**, 118, 8071.
- [109] Kundu, S.; Nagaiah, T. C.; Xia, W.; Wang, Y.; Dommele, S. V.; Bitter, J. H.; Santa, M.; Grundmeier, G.; Bron, M.; Schuhmann, W.; Muhler, M. *J. Phys. Chem. C* **2009**, 113, 14302.
- [110] Matter, P. H.; Zhang, L.; Ozkan, U. S. *J. Catal.* **2006**, 239, 83.
- [111] Shao, Y.; Zhang, S.; Engelhard, M. H.; Li, G.; Shao, G.; Wang, Y.; Liu, J.; Aksay, I. A.; Lin, Y. *J. Mater. Chem.* **2010**, 20, 7491.
- [112] Groves, M. N.; Chan, A. S. W.; Malardier-Jugroot, C.; Jugroot, M. *Chem. Phys. Lett.* **2009**, 481, 214.
- [113] Lherbier, A.; Blase, X.; Niquet, Y. M.; Triozon, F.; Roche, S. *Phys. Rev. Lett.* **2008**, 101, 036808.
- [114] Wu, M.; Cao, C.; Jiang, J. Z. *Nanotechnology* **2010**, 21, 505202.
- [115] H. Wang, T. Maiyalagan, and X. Wang. *ACS Catal.* **2012**, 2, 781–794
- [116] Wang, X.; Li, X.; Zhang, L.; Yoon, Y.; Weber, P. K.; Wang, H.; Guo, J.; Dai, H. *Science* **2009**, 324, 768.
- [117] L. Jia, D.-H. Wang, Y.-X. Huang, A.-W. Xu, and H.-Q. Yu. *J. Phys. Chem. C*, **2011**, 115, 23, 11466–11473
- [118] Barone, V.; Hod, O.; Scuseria, G. E. *Nano Lett.* **2006**, 6, 2748.
- [119] Kosynkin, D. V.; Higginbotham, A. L.; Sinitskii, A.; Lomeda, J. R.; Dimiev, A.; Price, B. K.; Tour, J. M. *Nature* **2009**, 458, 872.

- [120] Ponomarenko, L. A.; Schedin, F.; Katsnelson, M. I.; Yang, R.; Hill, E. W.; Novoselov, K. S.; Geim, A. K. *Science* **2008**, 320, 356.
- [121] Ritter, K. A.; Lyding, J. W. *Nat. Mater.* **2009**, 8, 235.
- [122] L. Cao, M. J. Mezziani, S. Sahu, and Y.-P. Sun. *Acc. Chem. Res.* **2013**, 46, 1,171–180.
- [123] J. Shen, Y. Zhu, X. Yang and C. Li. *Chem. Commun.*, **2012**, 48, 3686–3699.
- [124] W. Sheng, M. Korkusinski, A. Devrim G., M. Zielinski, P. Potasz, E.S. Kadantsev, O.Voznyy, P. Hawrylak. *Front. Phys.*, **2012**, 7, 3, 328–352. DOI 10.1007/s11467-011-0200-5
- [125] S. Liu, J. Tian, L. Wang, Y. Luo and X. Sun. *RSC Advances*, **2012**, 2, 411–413
- [126] X. Peng, L. Manna, W. Yang, J. Wickham, E. Scher, A. Kadavanich and A. P. Alivisatos, *Nature*, **2000**, 404, 59;
- [127] A. M. Derfus, W. C.W. Chan and S. N. Bhatia, *Nano Lett.*, **2004**, 4, 11.
- [128] M. Bottini, F. Cerignoli, D. M. Mills, F. D’Annibale, M. Leone, N. Rosato, A. Magrini, M. Pellicchia, A. Bergamaschi and T. Mustelin, *J. Am. Chem. Soc.*, **2007**, 129, 7814.
- [129] S. N. Baker and G. A. Baker, *Angew. Chem., Int. Ed.*, **2010**, 49, 6726.

SECTION I

*Graphene based semiconductors
in photocatalytic hydrogen and
oxygen generation*

2

Visible light photocatalytic hydrogen generation using dye-sensitized graphene oxide as photocatalyst^(*).

^(*) M. Latorre-Sánchez, C. Lavorato, M. Puche, V. Fornés, R. Molinari and H. Garcia. Chem. Eur. J. 2012, 18, 16774 – 16783.

2.1. Introduction

Although graphene (G) is a nanomaterial with high electron mobility and high conductivity, graphene oxide (GO), in which partial oxidation of the G sheets has occurred, can exhibit a behavior as semiconductor [1]. GO is readily prepared in large quantities through the oxidative exfoliation of graphite followed by sonication of the resulting oxidized graphite oxide [2]. The most generally employed method to perform graphite oxidation, the Hummers procedure [3], can be performed under different conditions and in this way GO with different degrees of oxidation, as determined by the percentage of carbon in the sample, can be obtained.

It has been recently reported that GO, either alone or in combination with TiO₂, can catalyze hydrogen generation from water upon UV irradiation [4]. The results obtained under these conditions suggest that the degree of oxidation of G-like sheets influences the photocatalytic activity [5]. Other recent reports have used GO in combination with other photocatalysts,

such as CdS and BiVO₄, to enhance the activity of this inorganic salt for visible-light water splitting, by either using a photoelectrochemical cell or applying the Z-scheme [6]. Because solar light contains only a small proportion (about 4%) of energy in the UV region, the use of G-derived materials to generate hydrogen from water by using sunlight as the primary energy resource would require the development of a system that is responsive to visible light [7].

Inspired by the Grätzel solar cells, in which metallic complexes or organic dyes are used as light harvesters to absorb visible light and inject electrons into the conduction band of TiO₂ or other metal oxide semiconductors [8], it is likely that the same methodology could also be applicable to introduce visible-light photocatalytic activity in GO. In this context, it has been found that Eosin Y in combination with platinum nanoparticles acts as a photocatalyst for visible-light photocatalytic hydrogen generation on GO [9]. Because the use of precious metals for hydrogen generation considerably increases the cost of the process, it is highly desirable to develop dye-GO photocatalysts that can operate without the need for platinum. Thus, the data currently available indicate that there is still a need for the development of GO semiconductors that can be applied for water splitting by using solar light in the absence of noble metals.

The results presented below further confirm the remarkable influence of the degree of GO oxidation on the photocatalytic activity as well as the possibility of using dyes as photosensitizers of G-like materials to reach high quantum yield efficiencies for visible-light hydrogen evolution from water in the absence of any expensive noble metal.

2.2 Experimental section

2.2.1 Photocatalytic hydrogen production tests

Two types of experiments using different setups were carried out depending on the irradiation source. For laser irradiation the second harmonic (532 nm) output of a Nd-YAG laser (7ns FWHP, 367 mW) was used. The photoreactor was a cylindrical Pyrex vessel (48 mL total volume) with an inlet and outlet bearing independent valves and equipped with a manometer to determine the pressure and a thermocouple to measure the temperature in the gas phase (see Figure 2.1). All the system was purged with an argon flow for at least 30 minutes before irradiation to ensure the absence of oxygen in the system. The photocatalytic solution (25 mL) containing 20 v/v % of methanol as sacrificial electron donor was continuously magnetically stirred during irradiation. All the experiments were carried out at the same laser energy and using optically matched solutions of the photocatalyst at the laser wavelength. The amounts used for the catalysts Th/GO, PY/GO, AO/GO, MB/GO, $\text{Ru}(\text{bipy})_3^{2+}/\text{GO}$ and $[\text{Ru}(\text{bipy})_3]^{2+}@\text{GO}$ were 1.13, 0.63, 1.08, 1.05, 1.43 and 0.55 mg, respectively, in 25 mL of photocatalytic solution.



Figure 2.1. Photograph of the system used in the tests with laser irradiation

The temperature varied at maximum 2 °C during irradiation. The percentage of hydrogen evolved in the photoreactor during the irradiation was determined by gas chromatography (GS-MOL 15 meters column ID 0.55 mm TCD from J&W Scientific) previously calibrated with standards and the moles of hydrogen generated were calculated taking into account the ideal gas law ($n=P*V/RT$).

The photocatalytic experiments using solar simulator were carried out with the output of a Thermo Oriel 911992 Solar Simulator having a AM 1.5G filter (1300 W/m^2) and placing a 335 ml photoreactor (285 ml of solution) 13 cm down the lamp (see Figure 4.2).

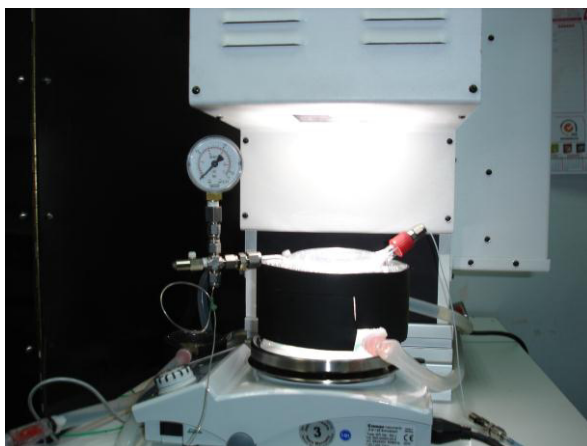


Figure 2.2. Photograph of the system used in the tests with solar simulator irradiation

2.2.2 Quantum yield calculation

The quantum yield (QY) for the hydrogen evolution using the second harmonic (532 nm) output of a Nd-YAG laser (7ns FWHP, 367 mW) was calculated using the following formula:

$$QY (\%) = \frac{\text{number of reacted electrons}}{\text{number of absorbed photons}} \times 100$$
$$\frac{2 \times \text{number of evolved } H_2 \text{ molecules}}{\text{number of absorbed photons}} \times 100$$

The absorbed photons by the catalyst were calculated measuring the power of the laser before (incident photons) and after our system containing 20% methanol aqueous solution with and without catalyst.

2.2.3 Preparation of graphene oxides (GOs)

GO1 (less oxidized GO) was synthesized from graphite flakes (Sigma-Aldrich) using a modified Hummers method [3]. A mixture of graphite

flakes (2 g) and NaNO_3 (1 g) was introduced in concentrate H_2SO_4 solution (46 mL, 18 M) and cooled to 0°C . While maintaining vigorous stirring, 6 g of KMnO_4 was added slowly in portions to keep the reaction temperature below 20°C . The reaction mixture was warmed up to 35°C and maintained at this temperature under stirring for 1 h. After this time, 92 ml of water was added slowly, producing an increase in temperature to 98°C and the resulting suspension was maintained at this temperature for 20 min. Then, the suspension was diluted to approximately 280 mL by adding water and treated with 9 ml H_2O_2 (35 %); upon treatment with the peroxide the suspension turned bright yellow. After air cooling, the suspension was filtered and washed with HCl (1:10, 37 %) solution and then with water. The remaining solid was suspended in water and sonicated. Then, the suspension was centrifugated at 400 rpm, the solid removed, and the diluted suspension was newly centrifugated at 15000 rpm for 4 h. The GO used in this work has a particle size corresponding to the solid obtained between the two centrifugations, after drying at 60°C .

GO2 (more oxidized GO) was prepared following a method described previously [15]. A mixture of concentrated $\text{H}_2\text{SO}_4/\text{H}_3\text{PO}_4$ (360:40 mL) was added to a mixture of graphite flakes (3 g) and KMnO_4 (18 g) producing an exothermic reaction that was controlled in an ice bath. The mixture was heated to 50°C and stirred for 24 h and then it was cooled to room temperature and poured onto 400 mL of ice with 30% H_2O_2 (3 ml). The suspension was filtered, washed with 1:10 HCl (37 %) solution and water and the resultant solid suspension was centrifugated and dried in the same manner as GO1.

The GO suspensions were prepared by exfoliation of the GO solids by sonication in Milli-Q water for 2 h with an ultrasound source (400 W) to give aqueous suspensions of GO sheets with a concentration of 500 mgL⁻¹.

2.2.4 Preparation of GO with dyes

In this study 5 types of cationic dyes were mixed with 500 mg/L of GO1 suspension, leading to 5 different dye/GO photocatalysts. The cationic dyes used were thionin acetate (Th A), pyronin Y (PY), acridine orange hydrochloride hydrate (AO), methylene blue (MB) and tris(bipyridine)ruthenium(II) dichloride hexahydrate ([Ru(bipy)₃]²⁺), all from Sigma-Aldrich. For all of them, preparation of the dye/GO1 suspension was made by dropwise addition of an aqueous solution of each dye (1 gL⁻¹) to a stirred suspension of GO1 (50 mL). Instantaneous precipitation due to the mix of the negatively charged GO1 sheets with the cationic dye molecules was observed. The addition of dye was continued until no further precipitation occurred (excess of dye). The resulting precipitated dye/GO solid is washed with Milli-Q water and recovered by centrifugation at 10000 rpm. These cycles of washing and centrifugation are repeated until the supernatant solution is colorless (typically 4 cycles). In the case of the anionic dye, cis-diisothiocyanato-bis(2,2'-bipyridyl-4,4'-dicarboxylate) ruthenium(II) bis(tetrabutylammonium) (N719, from Solaronix) and the neutral dye, copper (II) phthalocyanine (from Fluka), no precipitation of any solid was observed upon mixing the dye solutions with the GO suspension, so that just simple mixtures of GO suspension (500 mg/L) and dye solution (150 mg/L) in the appropriate reaction volume to achieve the same optical absorbance at 532 nm than the catalysts composed of cationic dye/GO were tested. The volumes used

were 2.63 mL and 4.7 mL of N719 and copper (II) phthalocyanine solutions, respectively and 1.6 mL of GO suspension for 25 mL of photocatalytic solution.

The preparation of the photocatalyst composed of $[\text{Ru}(\text{bipy})_3]^{2+}$ incorporated in the interlaminar space of GO1 ($[\text{Ru}(\text{bipy})_3]^{2+}@\text{GO}$) was carried out by heating 0.1 g of GO1 in 100 ml 0.0134 M of $[\text{Ru}(\text{bipy})_3]^{2+}$ at 60 °C during three days, leading to a cationic exchange of the dye. Then, the suspension was filtered and the solid obtained was washed and dried at 60 °C. $[\text{Ru}(\text{bipy})_3]^{2+}@\text{GO}$ aqueous suspension (330 mg/L) was prepared by sonicating this solid with an ultrasound source (400W) for 2 h in Milli-Q water.

2.2.5 Characterization techniques

TEM images were recorded by using a Philips CM300 FEG microscope operating at 100 kV. A set of TEM images of the dye/GO1 samples used as photocatalysts are presented in the Supporting Information. The chlorine content of the $[\text{Ru}(\text{bipy})_3]^{2+}@\text{GO1}$, $[\text{Ru}(\text{bipy})_3]^{2+}/\text{GO1}$, AO/GO1, PY/GO1, and MB/GO1 samples was determined by EDX analysis conducted by using an EDAX system (Oxford Instruments) attached to a JEOL JSM-5410 electronic microscope. The Raman measurements (RenishawinVia Raman Microscope) were carried out at RT with the $\lambda=514.5$ nm line of an Ar ion laser as an excitation source. X-ray diffraction (XRD) patterns were obtained by using a Philips X'Pert diffractometer and copper radiation ($\text{Cu}_{\text{K}\alpha}=1.541178 \text{ \AA}$). XPS analysis was performed by using a VG-Escalab 210 photoelectron spectrometer with a $\text{Mg}_{\text{K}\alpha}$ X-ray source. AFM images were recorded by using a Multimode Nanoscope 3A instrument operating in tapping mode and with a Si wafer

as the substrate. FTIR spectroscopy was conducted by using a Nicolet 8700 Thermo spectrometer. Solid-state ^{13}C NMR spectra were recorded at RT by using a Bruker AV400WB spectrometer with 908 pulse length of 5 ms and a recycle delay of 5 s. The samples were spinning at the magic angle at 10 kHz.

2.3 Results and discussion

2.3.1 Hydrogen generation using laser irradiation

Part of this study was performed by irradiating the samples with the second harmonic of a Nd/YAG laser, which has a monochromatic wavelength of $\lambda=532$ nm. This laser study with monochromatic visible radiation ensures that the observed hydrogen-generation activity is exclusively due to visible-region excitation. Our study is based on two GO materials obtained by chemical oxidation of graphite followed by ultrasound sonication. The difference between the two GO materials is the oxidative treatment, which results in two GO materials that differ by about 10% in their carbon and oxygen content. The degree of G oxidation can be reliably controlled by following the Hummers conditions (KMnO_4 and H_2O_2 at low temperature) and by using H_2SO_4 (lower degree of oxidation) or H_3PO_4 (higher degree of oxidation) as the Brønsted acid. Using the Hummers oxidation protocol with H_2SO_4 or H_3PO_4 guarantees reproducibility in the preparation of the two samples. In this way two GO samples with different degrees of oxidation can be prepared in a reproducible and reliable way with the purpose of testing the photocatalytic activity with visible light in combination with dyes. The characterization of the GO samples was in agreement with the reported data and was carried out by combustion elemental analyses to determine

the carbon content, by Fourier-transform infrared (FTIR) spectroscopy, solid-state ^{13}C NMR spectroscopy (see the Supporting Information), X-ray photoelectron spectroscopy (XPS), and Raman spectroscopy. The XPS and Raman spectra of GO1 (less oxidized GO) and GO2 (more oxidized GO) are shown in Figures 2.3 and 2.4 and are in accordance with the expected spectra for GO materials [10].

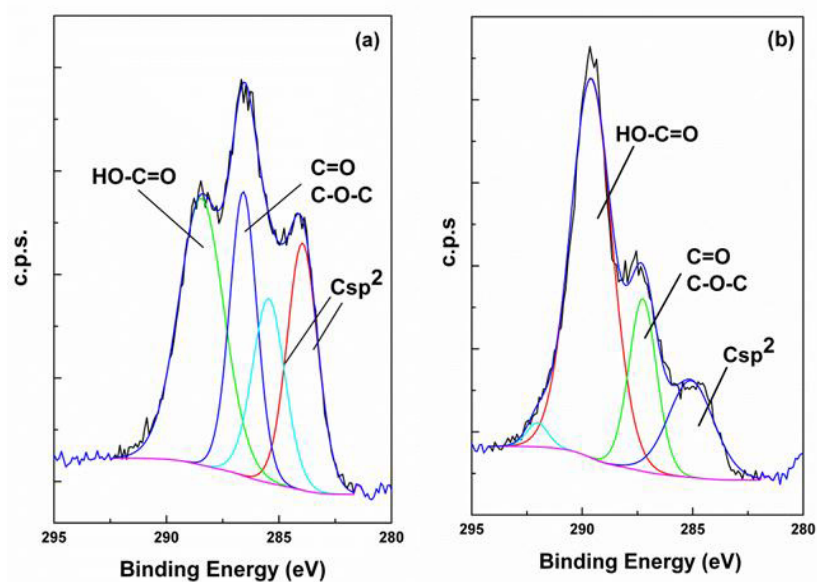


Figure 2.3. C1s XPS spectra of (a) GO1 and (b) GO2.

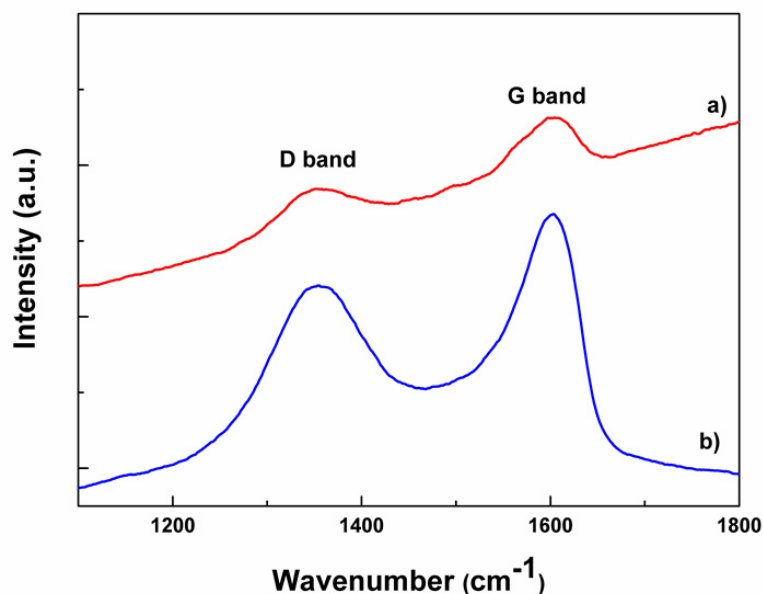


Figure 2.4. Raman spectra of GO1 (a) and GO2 (b) recorded at room temperature with the 514.5 nm line of an Ar ion laser as excitation source. The two characteristic peaks of G-derived materials have been indicated in the plot.

In particular, the XPS spectra reveal the presence of different types of sp^2 carbon atoms bonded to oxygen, whereas in the Raman spectra characteristic D and G bands are observed at 1345 and 1600 cm^{-1} , respectively. The surface atomic C/O ratio determined by XPS gives values of 2.02 for GO1 and 1.26 for GO2, indicating the lower degree of oxidation in GO1.

Transmission electron microscopy (TEM) images of these GO samples reveal the bidimensional morphology of the GO sheets, which have a length of a few micrometers (Figure 2.5). These images, together with atomic force microscopy (AFM) studies (Figure 2.6), indicate that the samples are mostly composed of single, double, and triple GO layers, accompanied by aggregates composed of a few layers of GO.

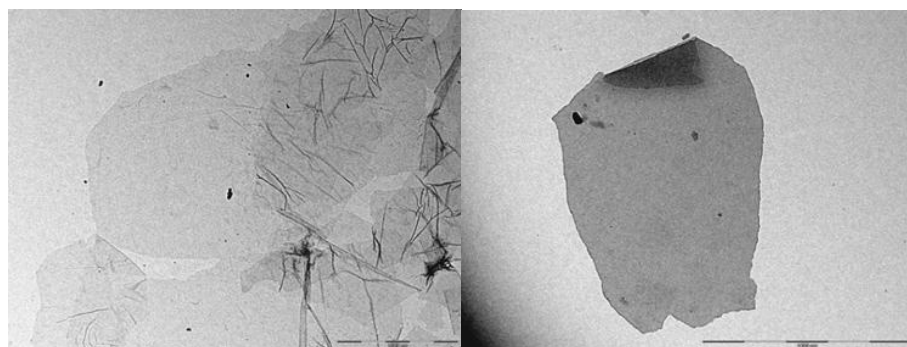


Figure 2.5. TEM images of GO1 sheets (scale bars: 1000 nm).

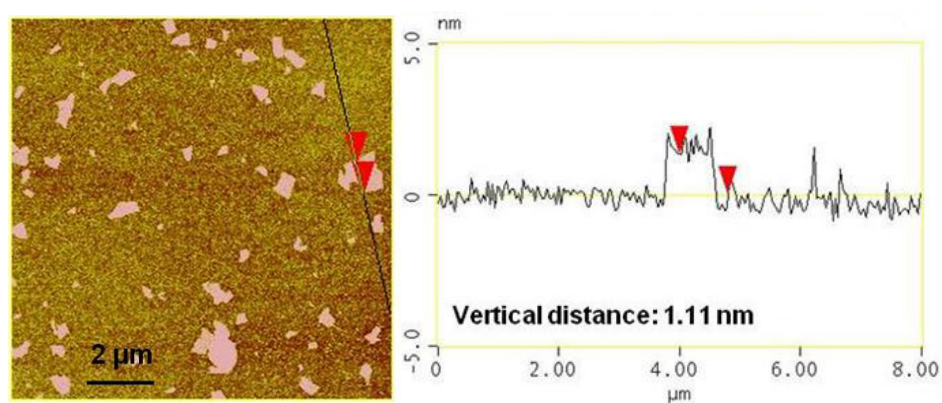


Figure 2.6. AFM topographic image of GO1 sheets and height profile of a single layer.

Both GO samples formed persistent colloidal suspensions in water. The zeta potentials of these colloids are -34 and -47 mV for GO1 and GO2, respectively. The negative value indicates that the GO sheets carry negative charges and the absolute voltage value indicates their high stability. The zeta potential measures the bias voltage necessary to initiate coalescence of the colloidal particles, and thus the higher the zeta potential, the higher the stability of the colloidal solution. Therefore, GO

suspensions are, in principle, appropriate to interact strongly with cationic dyes due to complementary Coulombic charges.

When the GO suspensions (optical absorbance 0.2) were irradiated by using a $\lambda=532$ nm laser in the presence of methanol as the sacrificial electron donor, evolution of hydrogen was observed (Figure 2.7). We selected monochromatic $\lambda=532$ nm to demonstrate the visible-light activity of the material. The use of a laser (367 mW) provides enough photon flux to conveniently measure H_2 evolution. Although both GO samples generate hydrogen, this preliminary study indicates that the less oxidized GO sample (GO1) was more efficient than the GO sample with higher oxygen content (GO2), and for this reason subsequent studies were based on the less oxidized GO1 sample. Precedents in the literature, in which three GO samples with differing degrees of oxidation were tested as photocatalysts, have reported similar results that show a remarkable influence of the oxygen content of GO on the photocatalytic activity [5].

Because an induction period was observed in the time–conversion plot, an increase in the hydrogen generation rate was observed 90 min after irradiation of the GO1 sample. We were intrigued by the possibility that this induction period could be related to some changes in the GO1 sample to produce irradiation-induced variation in the surface functional groups. Accordingly, we determined the presence in the gas phase of CO evolved during the photocatalytic hydrogen generation. The purpose was to determine whether the evolution of CO takes place prior to the increase in efficiency for hydrogen generation. It was observed, however, that the evolution of CO follows the same temporal profile as the hydrogen production, that is, an increase in the CO evolution rate also occurs after 90 min.

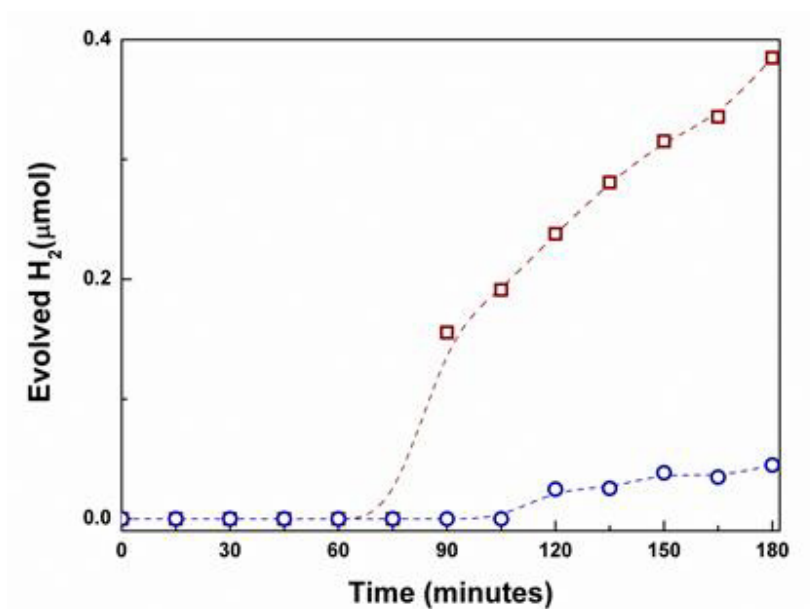
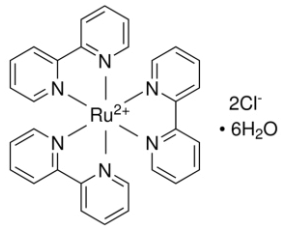
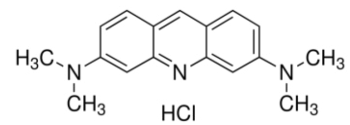
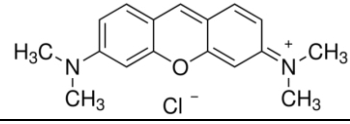
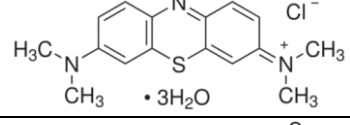
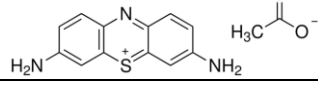
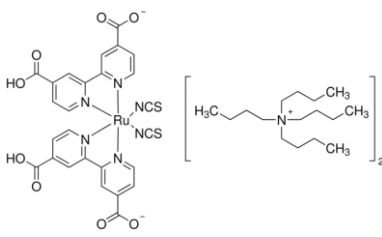
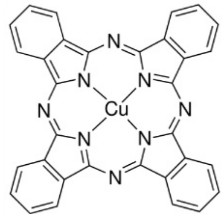


Figure 2.7. Amount of hydrogen evolved during the photocatalytic run using GO1 and GO2 as photocatalysts and methanol as sacrificial electron donor, under 532 nm laser irradiation. \blacksquare : GO1; \bullet : GO2.

2.3.2 Dyes as GO photosensitizers

Despite the previous comments about hydrogen generation on GO, it has to be noted that the efficiency of plain GO for hydrogen production under $\lambda=532$ nm irradiation was low and there was still much room for improvement. To increase the efficiency, we examined mixtures of GO1 with a series of dyes, the structures and abbreviations of which are shown in Table 2.1, which also indicates the percentage of dye in the catalyst as determined by combustion nitrogen chemical analysis.

Table 2.1. Names and structures of dyes tested as GO photosensitizers

Name	Structure	Loading [wt %]
Tris(bipyridine)ruthenium(II) dichloride hexahydrate ($[\text{Ru}(\text{bipy})_3]^{2+}$)		39($[\text{Ru}(\text{bipy})_3]^{2+}$ @GO 1) 11($[\text{Ru}(\text{bipy})_3]^{2+}$ /GO1)
Acridine Orange hydrochloride (AO)		21
Pyronin Y (PY)		18
Methylene blue (MB)		17
Thionin acetate (Th)		16
cis-(diisothiocyanato)-bis(2,2'-bipyridyl-4,4'-dicarboxylate) ruthenium(II) bis(tetrabutylammonium) (N719)		-
Copper phthalocyanine (CuPc)		-

The series of dyes under study included some tricyclic basic dyes in which the positive charge should promote association with GO1 through electrostatic attraction. This positive dye/ negative GO1 association was demonstrated in the case of methylene blue (MB) by stirring an aqueous solution of GO1 (0.05 mgmL^{-1}) with MB (0.5 mgmL^{-1}) for 1 h. During this period, a light precipitated evolved and the supernatant was removed by centrifugation of the colloidal solution. It was observed that a percentage of MB disappeared from the solution and was present in the GO1 residue. Chlorine analysis by EDX established that the percentage of anion in the GO1/dye samples for MB, AO, PY, and $[\text{Ru}(\text{bipy})_3]^{2+}$ is negligible, which indicates that ion metathesis with replacement of chloride by the negative charges of GO1 is the most likely adsorption mechanism for these dyes. In all cases the irradiation studies were performed at the same laser fluency and by using solutions of the same absorbance at $\lambda = 532 \text{ nm}$. Using solutions of different dyes with GO1 at the same optical density corrects for the influence of differences in the absorption coefficient of the dyes at the irradiation wavelength, which guarantees that the same number of $\lambda = 532 \text{ nm}$ photons is absorbed. This allows us to draw conclusions about the relative efficiency of hydrogen generation as a function of the structure of the dye. The profiles of hydrogen evolution as a function of the irradiation time are shown in Figure 2.8 (the difference between $[\text{Ru}(\text{bipy})_3]^{2+}@GO1$ and $[\text{Ru}(\text{bipy})_3]^{2+}/GO1$ is the presence of the complex in the intergallery space or adsorbed on the external surface, as discussed below.)

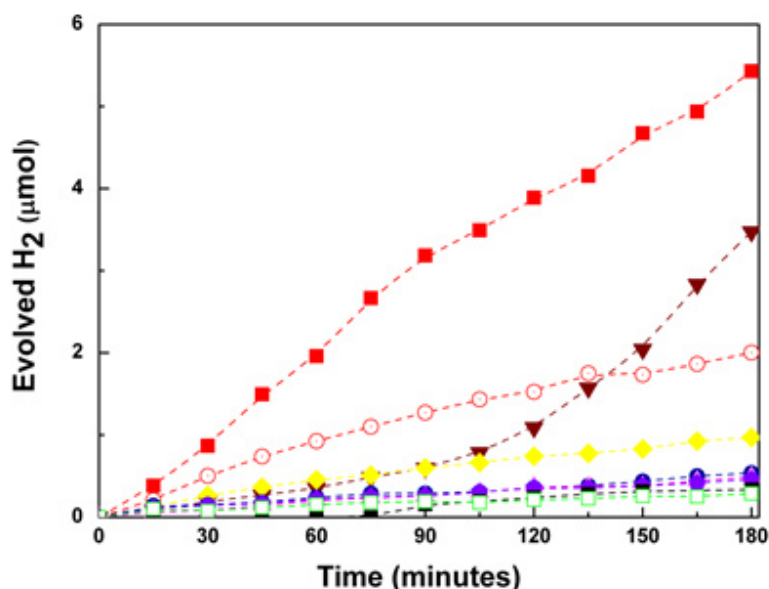
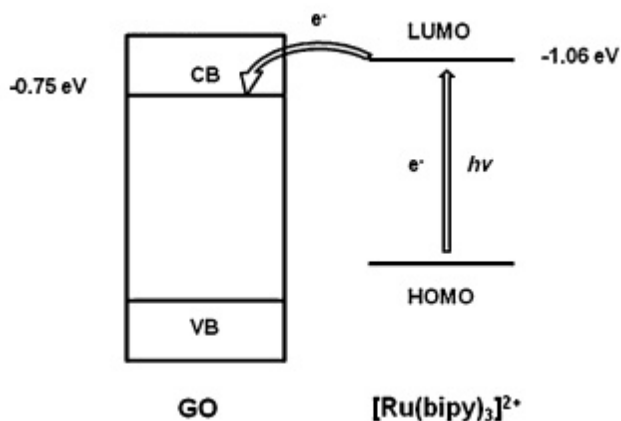


Figure 2.8. Amount of hydrogen evolved during the photocatalytic run using GO as photocatalyst with a series of dyes, methanol as sacrificial electron donor, under 532 nm laser irradiation. ■ : [Ru(bipy)₃]²⁺@GO ([Ru(bipy)₃]²⁺ incorporated in the interlayer space of few layers GO). ○ : [Ru(bipy)₃]²⁺/GO ([Ru(bipy)₃]²⁺ supported on GO). ▼: N719/GO. ◆ : AO/GO. ● : MB/GO. ▲ PY/GO. ◆ : Th/GO. □: CuPc/GO. ■ : GO.

As can be seen in Figure 2.8, there are a number of dyes that have a minor influence on the ability of GO to act as a photocatalyst for hydrogen generation. However, of this series of dyes, [Ru (bipy)₃]²⁺ deposited on GO1 sheets clearly enhances the efficiency for this process by increasing the amount of hydrogen at 180 min by a factor of five with respect to GO1 only. Control experiments under the same conditions using the dyes in the absence of GO1 did not lead to the observation of H₂ evolution. The result of the control experiments agree with literature data in which the use of noble metals[11] or metal oxides[12] in combination with dyes is required to observe some H₂ evolution. An interesting and unexpected result was

the behavior of the commercially available ruthenium complex with negative charges (N719), which is widely used as dye harvester in dye-sensitized solar cells.[13] In this case the temporal profile of hydrogen evolution shows an induction period in which the rate of hydrogen formation is lower than the cationic ruthenium complex $[\text{Ru}(\text{bipy})_3]^{2+}$ but then, after approximately 100 min, the efficiency of hydrogen generation increases notably to give a final amount of hydrogen at 3 h that is almost double the amount obtained by using cationic $[\text{Ru}(\text{bipy})_3]^{2+}$ deposited onto GO1 sheets as the photosensitizer. This temporal profile suggests that the initial dye is converted into a more active species or is relocated with respect to GO1. We also tested a neutral dye, CuPc, but in this case the photocatalytic activity of GO1 was not affected by the presence of the dye. The fact that $[\text{Ru}(\text{bipy})_3]^{2+}$ and N719 were the best performing dyes for visible-light photosensitization of GO1 is not totally unexpected in view of their good performance in photoinduced electron transfer. In fact, of the characteristics for a suitable choice of dye for visible-light H_2 generation, we have to consider a significant absorption band in the visible region and a long lifetime as well as suitable energy of the electronically excited state. The ruthenium polypyridyl complexes have all these characteristics. Concerning the photosensitization mechanism, it has been shown that changing the extent of oxidation GO varies the energy of the valence band (VB), but the energy of the conduction band (CB) as determined by impedance spectroscopy is fairly constant at -0.75 eV with respect to Ag/AgCl reference electrode.[5] Upon light excitation, $[\text{Ru}(\text{bipy})_3]^{2+}$ reaches the triplet excited state, which has an energy of -1.06 eV with respect to the same reference electrode [14].

Therefore, from a thermodynamic point of view, electron injection from the $[\text{Ru}(\text{bipy})_3]^{2+}$ LUMO into the CB of GO1 will be favorable (see Scheme 2.1). Although kinetic data on the electron injection rate is still not available, the high surface contact and orbital overlapping due to the accessibility of flat G suggest that this injection is fast.



Scheme 2.1. Schematic diagram showing the electron injection from the LUMO of $[\text{Ru}(\text{bipy})_3]^{2+}$ to the CB of GO1 (V vs. Ag/AgCl).

The most efficient system for hydrogen generation at $\lambda=532$ nm, in which the amount of hydrogen generated is also almost linear with respect to the irradiation time, was obtained when the $[\text{Ru}(\text{bipy})_3]^{2+}$ dye was located within the interlamellar space of aggregates of a few GO1 layers ($[\text{Ru}(\text{bipy})_3]^{2+}@GO1$). The linearity of the H_2 evolution over time in the presence of $[\text{Ru}(\text{bipy})_3]^{2+}@GO1$ and the fact that TEM imaging of the sample after 3 h of laser irradiation does not reveal the presence of metal nanoparticles indicates that the $[\text{Ru}(\text{bipy})_3]^{2+}@GO1$ sample is stable during the photocatalytic study. The superior activity of $[\text{Ru}(\text{bipy})_3]^{2+}@GO1$ is demonstrated when the hydrogen production is

considered per mass unit, giving a value of $3290 \text{ mmolh}^{-1}\text{g}^{-1}$, which is much higher than the productivity measured here for Au-doped TiO_2 under the same conditions ($<50 \text{ mmolh}^{-1}\text{g}^{-1}$). The low density of GO1 compared to titania is responsible for this remarkable value.

This new material was obtained by heating the ruthenium complex and the oxidized graphite at reflux, which leads to a cationic exchange of the complex. Incorporation of the $[\text{Ru}(\text{bipy})_3]^{2+}$ complex between the oxidized graphite layers was assessed by X-ray diffraction (XRD), which shows a shift in the position of the diffraction peak from a 2θ value of 11.5° , which corresponds to oxidized graphite,[15] to a smaller 2θ angle (6°) that according to the Bragg diffraction law corresponds to an interlamellar distance of 14.09 \AA . Calculations at the molecular mechanics level indicate that the diameter of octahedral $[\text{Ru}(\text{bipy})_3]^{2+}$ is about 13 \AA and considering the thickness of the GO1 layer the sum of both values agrees very well with the interlayer spacing determined for the $[\text{Ru}(\text{bipy})_3]^{2+}@\text{GO1}$ system. Transmission optical spectroscopy of $[\text{Ru}(\text{bipy})_3]^{2+}@\text{GO1}$ shows the characteristic peaks of the ruthenium complex at $\lambda=250, 260, \text{ and } 290 \text{ nm}$ and the broad structured visible band from $\lambda=390$ to 500 nm with a peak at $\lambda=460 \text{ nm}$ on top of a continuous absorption due to GO. Figures 2.9 and 2.10 show the corresponding XRD pattern and absorption spectra of $[\text{Ru}(\text{bipy})_3]^{2+}@\text{GO1}$ compared with the spectra of GO1 prepared under the same conditions. Because no significant differences are observed in the optical spectra due to $[\text{Ru}(\text{bipy})_3]^{2+}$ intercalation into the GO1 intergallery space in comparison to the situation in which this complex is deposited on the surface, it can be inferred that the same thermodynamic consideration indicated in Scheme 2.1 should also apply to $[\text{Ru}(\text{bipy})_3]^{2+}@\text{GO1}$. However, the kinetics of

the process may be even more favorable due to the increased contact between the metal complex and GO1.

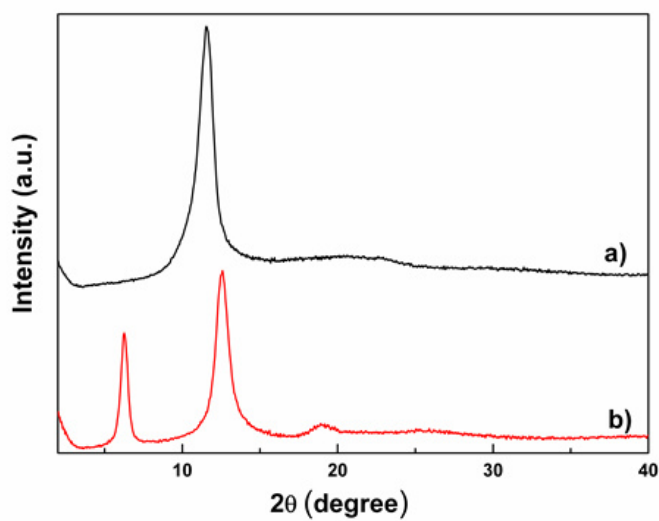


Figure 2.9. XRD patterns of a) GO and b) [Ru(bipy)₃]²⁺@GO photocatalysts.

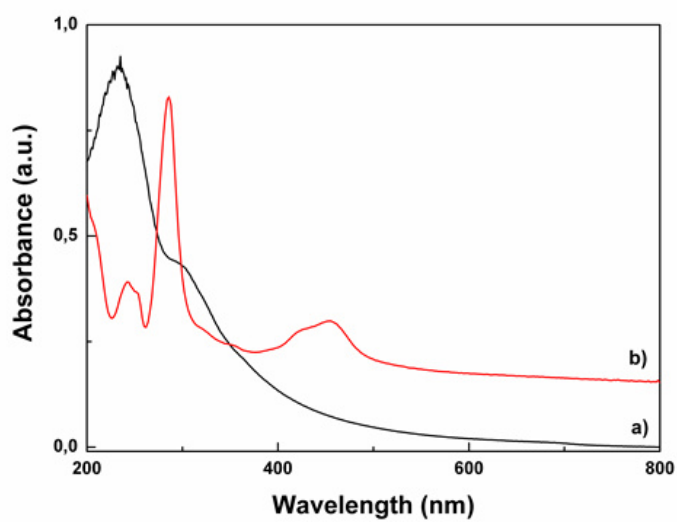


Figure 2.10. UV-Vis spectra of a) GO and b) [Ru(bipy)₃]²⁺@GO aqueous suspensions.

Optimization of the amount of $[\text{Ru}(\text{bipy})_3]^{2+}@\text{GO1}$ photocatalyst required for maximal hydrogen generation under $\lambda=532\text{ nm}$ irradiation shows that a very small amount of this material (0.02 gL^{-1}) is enough to achieve the highest activity. In fact, it was observed that higher weights of $[\text{Ru}(\text{bipy})_3]^{2+}@\text{GO1}$ can be even detrimental for hydrogen production, particularly at longer irradiation times (Figure 2.11).

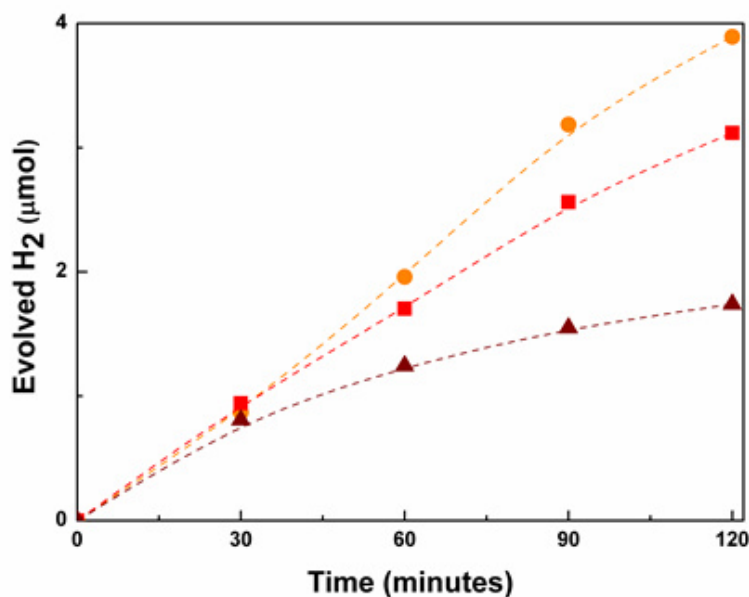


Figure 2.11. Amount of hydrogen evolved during the photocatalytic runs using different concentration of $[\text{Ru}(\text{bipy})_3]^{2+}@\text{GO}$ as photocatalysts under 532 nm laser irradiation. ● : 0.02 g/L . ■ : 0.12 g/L . ▲ : 0.46 g/L .

This could be due to triplet–triplet annihilation or some other kind of self-quenching that competes with the required electron transfer from the $[\text{Ru}(\text{bipy})_3]^{2+}$ triplet excited state to GO1. In previous studies of $[\text{Ru}(\text{bipy})_3]^{2+}$ covalently attached to single-wall carbon nanotubes, it has been observed, by using laser flash photolysis, a clear change in the nature of the

transients depending on the concentration of $[\text{Ru}(\text{bipy})_3]^{2+}$. [16] Moreover, recently it has been determined two different regimes in the quenching of $[\text{Ru}(\text{bipy})_3]^{2+}$ triplets by G in aqueous solution [17].

Moreover, tests to compare the hydrogen evolution with $[\text{Ru}(\text{bipy})_3]^{2+}@GO1$ in the presence of triethylamine or methanol as the sacrificial electron donor at free pH were carried out. The results shown in Figure 2.12 indicate that in this case methanol is a more appropriate sacrificial agent.

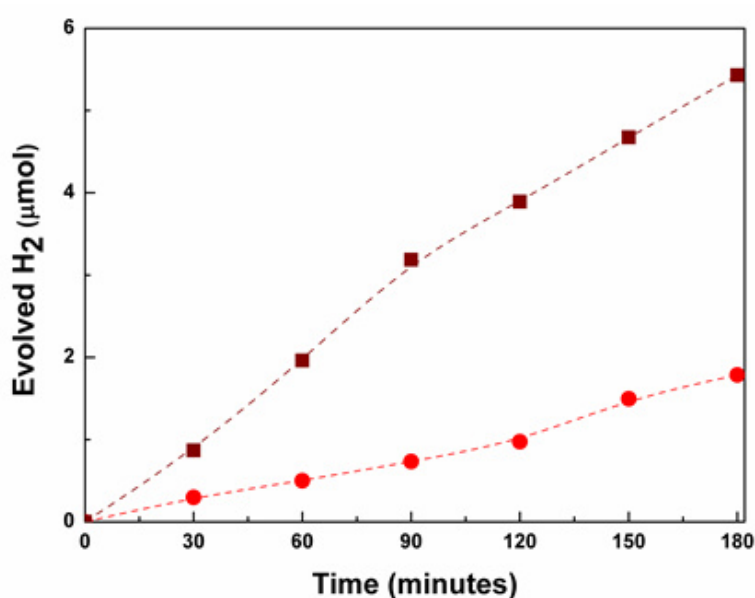


Figure 2.12. Amount of hydrogen evolved during the photocatalytic run using 0.02 g/L of $[\text{Ru}(\text{bipy})_3]^{2+}@GO$ as photocatalysts and 20 v/v% of methanol or triethylamine as sacrificial electron donor, under 532nm laser irradiation. ■ : Methanol. ● : Triethylamine.

The quantum yields for hydrogen evolution achieved by using $\lambda=532$ nm monochromatic light were 0.12 and 0.008% for $[\text{Ru}(\text{bipy})_3]^{2+}@GO1$ and

GO1, respectively. Therefore, further work is necessary in this area to find an optimal dye and its adequate deposition on GO1.

This strategy of dye intercalation inside the intergallery space of a few layers of G should also improve the efficiency of the other dyes shown in Table 2.1. To prove that intercalation is a valid strategy, we proceeded to prepare an analogous material in which MB was accommodated inside the interlayers of a few layers of GO1. It was observed that MB@GO1 improved the efficiency for H₂ generation by 1.5 times compared with MB/GO1, but it was still much less efficient than [Ru(bipy)₃]²⁺@GO1.

2.3.3 Photocatalytic hydrogen generation using solar simulator

In the previous section we provided compelling evidence for the visible-light activity of the dye/GO1 system for hydrogen generation in the presence of a sacrificial electron donor under monochromatic laser light. However, for any practical application the photocatalytic hydrogen production should operate with solar light. The sunlight spectrum has a continuous distribution of visible and infrared light accompanied by a small percentage of UV light. Therefore, it was of interest to determine the activity of the [Ru- (bipy)₃]²⁺@GO1 system in sunlight.

For the irradiation source in this study we used a solar simulator (1300 Wm⁻²) coupled with an AM 1.5G filter that takes into account the effect of atmosphere filtering the sunlight. Figure 2.13 shows the activity for hydrogen generation under these conditions and compares the activity of GO1 with that of [Ru (bipy)₃]²⁺@GO1.

As expected in view of previous laser studies, GO1 in the absence of dyes was not able to produce a detectable amount of hydrogen under these experimental conditions. This fact is not surprising in view of the temporal

profile of H₂ evolution by using laser irradiation (see Figure 2.7) in which a long induction period of 75 min was observed before H₂ detection. In the case of the less powerful solar simulator irradiation, the induction period observed in Figure 2.7 could correspond to a complete lack of activity over the entire period under study. In contrast, the [Ru-(bipy)₃]²⁺@GO1 photocatalyst was able to produce hydrogen under sunlight illumination (6 mmol g⁻¹ h⁻¹). Considering the spectrum of solar light, this photocatalytic activity should derive mostly from visible-light radiation. To confirm this, a cut-off filter was used to eliminate the UV wavelengths from the solar simulator light (λ > 400 nm). As shown in Figure 2.13, coincident temporal profiles were measured for the [Ru(bipy)₃]²⁺@GO1 system upon exposure to the full light output of the solar simulator or to the filtered light. These results indicate the minor proportion of UV light in the solar simulator output and confirm GO1 photosensitization by [Ru(bipy)₃]²⁺.

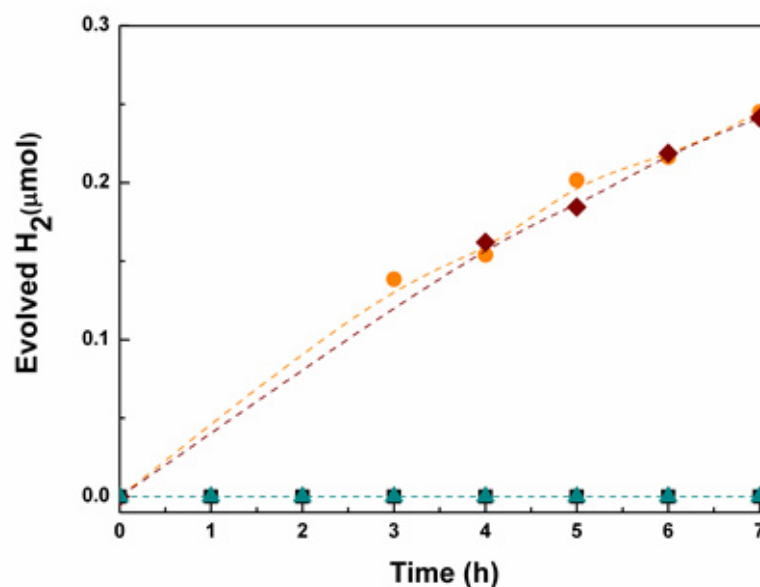


Figure 2.13. Amount of hydrogen evolved during the photocatalytic run using $[\text{Ru}(\text{bipy})_3]^{2+}@\text{GO}$ and GO as photocatalysts and methanol as sacrificial electron donor under solar simulator irradiation. ● : $[\text{Ru}(\text{bipy})_3]^{2+}@\text{GO}$, $\lambda > 400\text{nm}$. ◆ : $[\text{Ru}(\text{bipy})_3]^{2+}@\text{GO}$, solar light irradiation. ▲ : GO, $\lambda > 400\text{nm}$. ■ : GO, solar light irradiation. Catalyst concentration = 0.02 g/L.

2.3.4 Stability of the $[\text{Ru}(\text{bipy})_3]^{2+}@\text{GO}$ photocatalyst

One major point of concern in a photocatalyst is its stability under operation conditions. This issue is particularly important in the present case considering that GO can be photochemically reduced to G, which, in addition to changes in the energy bands, can agglomerate due to lower hydrophilicity to produce a precipitation of the suspension. In addition, in some photocatalytic systems based on dyes [18], it has been determined that the photochemical stability of the organic component is the limiting factor of the photochemical stability.

To address the stability of the $[\text{Ru}(\text{bipy})_3]^{2+}@\text{GO}$ system for hydrogen production we subjected a solution of $[\text{Ru}(\text{bipy})_3]^{2+}@\text{GO}$ catalyst to

long irradiation times under $\lambda = 532$ nm laser irradiation and determined the temporal profile of the hydrogen evolution and the absorbance of the solution.

The results are shown in Figure 2.14 and correspond to an aging test compared with the data obtained by using the solar simulator (Figure 2.13). As shown in Figure 2.14, the temporal profile of hydrogen evolution was not linear and exhibited a lower hydrogen generation rate at longer irradiation times than the fresh material, which indicates deactivation of the photocatalyst.

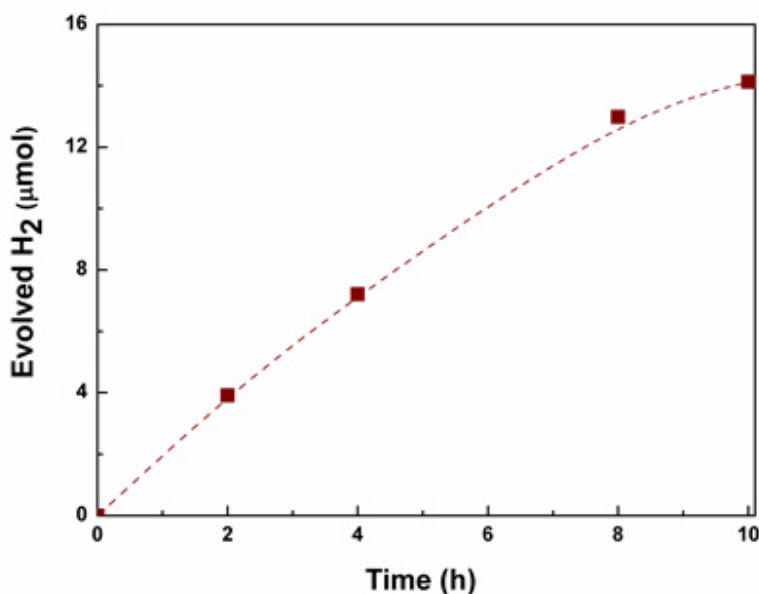


Figure 2.14. Amount of hydrogen evolved during the photocatalytic run using 0.02 g/L of $[\text{Ru}(\text{bipy})_3]^{2+}$ @GO as photocatalyst and methanol as sacrificial electron donor under 532 nm laser irradiation for 10 h.

The decomposition of the dye and the changes in the GO1 structure are the two most probable reasons for this decay in photocatalytic activity. Thus, as shown in Figure 2.15, the characteristic bands at $\lambda = 420$ and 460 nm

corresponding to the $[\text{Ru}(\text{bipy})_3]^{2+}$ dye disappear almost completely after laser irradiation for 10 h, this disappearance is accompanied by a decrease in the absorbance at $\lambda=532$ nm and the observation of some CO evolution from the solution. Considering that the system does not contain oxygen, the most likely origin of the CO is partial GO1 decomposition that occurs during the photocatalytic reaction. TEM images of either $[\text{Ru}(\text{bipy})_3]^{2+}/\text{GO1}$ or $[\text{Ru}(\text{bipy})_3]^{2+}@\text{GO1}$ do not show any indications of the presence of the ruthenium complex, which suggests that this dye is well dispersed on the GO1 support and that no metal nanoparticles are formed during the incorporation of the dye. In contrast, a TEM survey of the $[\text{Ru}(\text{bipy})_3]^{2+}@\text{GO1}$ sample after laser irradiation for 10 h, for which the UV/Vis spectrum shows the decomposition of $[\text{Ru}(\text{bipy})_3]^{2+}$ reveals the presence of metal nanoparticles with a broad size distribution from a few nanometers to almost 100 nm, which indicates that dye decomposition causes the formation of ruthenium nanoparticles. In addition, after 10 h of illumination it is possible to see some photocatalytic material suspended in the aqueous solution, probably due to a partial reduction of GO1 and the lower hydrophilicity of the resulting G.

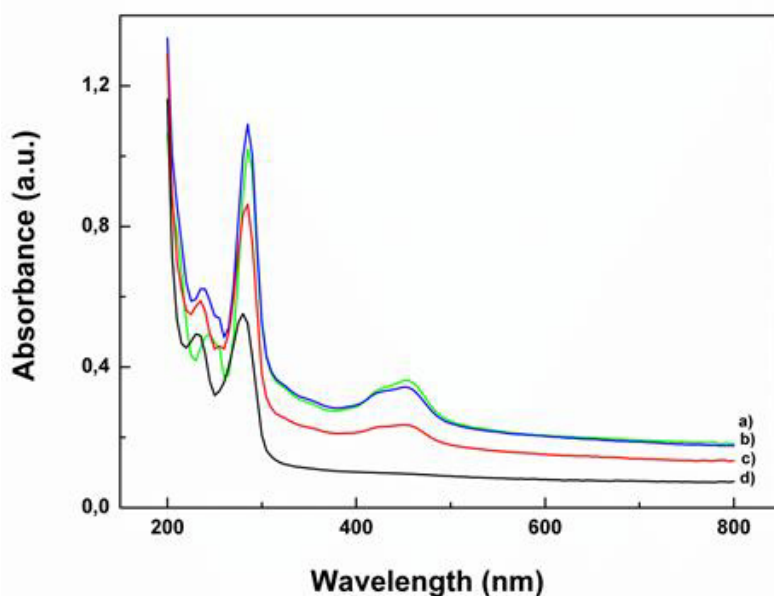


Figure 2.15. UV-visible spectra of [Ru(bipy)₃]²⁺@GO suspension after irradiation under 532 nm laser for a) 0 h. b) 2 h. c) 4 h. d) 10 h.

2.3.5 Oxygen evolution

Conventional semiconductors can catalyze the photocatalytic generation of hydrogen from water in the presence of a sacrificial electron donor, but they may also be able to generate oxygen in the presence of a sacrificial electron acceptor agent. The two most typical sacrificial electron acceptors that are widely employed for oxygen generation are Ag⁺ and Ce⁴⁺. Considering the formation of silver nanoparticles in the reduction of Ag⁺, it is frequently more convenient to use Ce⁴⁺ ions to test photocatalytic oxygen generation from water [19]. Herein we were interested in determining if the most efficient photocatalytic system for hydrogen generation is also able to generate oxygen from water in the presence of Ce⁴⁺ (0.01m [Ce(NH₄)₂(NO₃)₆]). Note that oxidation of water to oxygen

requires holes with oxidation potentials higher than 1.26 V, which may not be present in GO1. Besides thermodynamics considerations, oxygen generation is also a more complex process than hydrogen formation from a kinetic point of view. Herein, by using the $[\text{Ru}(\text{bipy})_3]^{2+}$ @GO1 system in the presence of Ce^{4+} we were unable to measure detectable amounts of oxygen in the reaction. In fact, even under these conditions we could only observe a residual production of hydrogen due to the incomplete quenching of all the photogenerated electrons by Ce^{4+} . Precedents in the literature by using GO samples in the absence of dyes under UV irradiation have also found that some GO samples are unable to generate oxygen from water [5]. In the present case it is likely that the positive holes in the system correspond to the oxidized form of the dye rather than to holes localized on the GO and this must reduce the oxidation power of these holes.

2.6 Conclusions

In this Chapter it was shown that the photocatalytic activity of GO for hydrogen generation from water/methanol mixtures under visible light can be implemented by the presence of dyes. Cationic and anionic dyes can produce this visible light photocatalytic activity in GO in the absence of any noble metal, such as Pt or Au. The most efficient material prepared herein has $[\text{Ru}(\text{bipy})_3]^{2+}$ dye molecules that are located in the intergallery space of incompletely delaminated GO, in which packages of several GO layers are still grouped and the dye is incorporated in the interlaminar spaces. This photocatalyst is two orders of magnitude more efficient than titania-based visible-light photocatalysts that contain Au, as measured under the same experimental conditions with a $\lambda=532$ nm laser as

excitation source. The same photocatalytic system is inactive for the generation of oxygen from water in the presence of Ce^{4+} as the sacrificial electron acceptor. The use of a solar simulator with or without a UV filter is sufficient to produce hydrogen from water/methanol solutions. However, the stability and durability of the photocatalytic system is unsatisfactory because the $[\text{Ru}(\text{bipy})_3]^{2+}$ dye is degraded during light irradiation and evolution of CO from GO is observed. Nevertheless, the present data open new opportunities for the preparation of optimized G materials with low dispersion that contain the appropriate loading of guest and number of layers to maximize the photoresponse and, in particular, the desired photocatalytic activity.

2.7 References

- [1] a) Y. Zhu, S. Murali, W. Cai, X. Li, J. W. Suk, J. R. Potts, R. S. Ruoff, *Adv. Mater.* **2010**, 22, 3906 – 3924; b) G. Eda, C. Mattevi, H. Yamaguchi, H. Kim, M. Chhowalla, *J. Phys. Chem. C* **2009**, 113, 15768 – 15771.
- [2] a) D. A. Dikin, S. Stankovich, E. J. Zimney, R. D. Piner, G. H. B. Dommett, G. Evmenenko, S. T. Nguyen, R. S. Ruoff, *Nature* **2007**, 448, 457 – 460; b) S. Park, R. S. Ruoff, *Nat. Nanotechnol.* **2009**, 4, 217 – 224.
- [3] W. S. Hummers, R. E. Offeman, *J. Am. Chem. Soc.* **1958**, 80, 1339 – 1339.
- [4] a) T.-F. Yeh, J.-M. Syu, C. Cheng, T.-H. Chang, H. Teng, *Adv. Funct. Mater.* **2010**, 20, 2255 – 2262; b) X.-Y. Zhang, H.-P. Li, X.-L. Cui, Y. Lin, *J. Mater. Chem.* **2011**, 21, 2801 – 2806.
- [5] T.-F. Yeh, F.-F. Chan, C.-T. Hsieh, H. Teng, *J. Phys. Chem. C* **2011**, 115, 22587 – 22597.

- [6] a) P. Gao, J. Liu, S. Lee, T. Zhang, D. D. Sun, *J. Mater. Chem.* **2011**, 21, 2292–2298; b) Y. H. Ng, A. Iwase, A. Kudo, R. Amal, *J. Phys. Chem. Lett.* **2010**, 1, 2607–2612; c) A. Iwase, Y. H. Ng, Y. Ishiguro, A. Kudo, R. Amal, *J. Am. Chem. Soc.* **2011**, 133, 11054–11057; d) Q. Li, B. Guo, J. Yu, J. Ran, B. Zhang, H. Yan, J. R. Gong, *J. Am. Chem. Soc.* **2011**, 133, 10878–10884.
- [7] a) J. Zhu, D. Chakarov, M. Zch, L. Zang, in *Nanostructured Materials for Photolytic Hydrogen Production*, Springer, Heidelberg, **2011**, pp. 441–486; b) M. A. Khan, S. I. Woo, O. B. Yang, *Int. J. Hydrogen Energy* **2008**, 33, 5345–5351.
- [8] B. O'Regan, M. Gratzel, *Nature* **1991**, 353, 737–740.
- [9] S. Min, G. Lu, *J. Phys. Chem. C* **2011**, 115, 13938–13945.
- [10] a) K. N. Kudin, B. Ozbas, H. C. Schniepp, R. K. Prud'homme, I. A. Aksay, R. Car, *Nano Lett.* **2007**, 7, 36–41; b) D. Yang, A. Velamakanni, G. L. Bozoklu, S. Park, M. Stoller, R. D. Piner, S. Stankovich, I. Jung, D. A. Field, C. A. Ventrice, Jr., R. S. Ruoff, *Carbon* **2009**, 47, 145–152.
- [11] Y.-J. Yuan, J.-Y. Zhang, Z.-T. Yu, J.-Y. Feng, W.-J. Luo, J.-H. Ye, Z.-G. Zou, *Inorg. Chem.* **2012**, 51, 4123–4133.
- [12] L. Li, L. Duan, F. Wen, C. Li, M. Wang, A. Hagfeldt, L. Sun, *Chem. Commun.* **2012**, 48, 988–990.
- [13] S. E. Koops, B. C. O'Regan, P. R. F. Barnes, J. R. Durrant, *J. Am. Chem. Soc.* **2009**, 131, 4808–4818.
- [14] A. Juris, V. Balzani, F. Barigelletti, S. Campagna, P. Belser, A. von Zelewsky, *Coord. Chem. Rev.* **1988**, 84, 85–277.
- [15] D. C. Marcano, D. V. Kosynkin, J. M. Berlin, A. Sinitskii, Z. Sun, A. Slesarev, L. B. Alemany, W. Lu, J. M. Tour, *ACS Nano* **2010**, 4, 4806–4814.

- [16] R. Martn, L. Jimenez, M. Alvaro, J. C. Scaiano, H. Garcia, *Chem. Eur. J.* **2010**, 16, 7282 –7292.
- [17] M. de Miguel, M. Alvaro, H. Garcia, *Langmuir* **2012**, 28, 2849 – 2857.
- [18] R. Abe, K. Sayama, H. Arakawa, *J. Photochem. Photobiol. A* **2004**, 166, 115 –122.
- [19] C. M. Gonzalez, Y. Liu, J. C. Scaiano, *J. Phys. Chem. C* **2009**, 113, 11861 – 11867.

3

N-doped graphene derived from biomass as visible light photocatalyst for hydrogen generation from water-methanol mixtures.^(*)

(*) C. Lavorato, A. Primo, R. Molinari and H. Garcia.
Accepted by Chemistry A European Journal

3.1 Introduction

In the context of solar fuels [1, 2] and, in particular, photocatalytic hydrogen production, [3-5] there is much current interest in the use of graphene (G)-based materials as catalysts and photocatalysts in replacement of metal oxide solids and TiO₂ [6-12].

The main two reasons for this interest are sustainability and flexibility in the modification and design of the photocatalyst. The use of carbon-based materials is considered sustainable since they can be derived from renewable biomass feedstocks. In contrast, there is a limited resource availability of titanium dioxide and other metal oxide semiconductors. On the other hand, due to the robustness of anatase and other crystalline phases, doping of TiO₂ has proven to be difficult and requiring harsh experimental conditions, mainly performed as a solid state reaction [13-15]. In contrast, G materials can be modified by covalent or not covalent

attachment of photoresponsive units or even by replacement of some carbon atoms in the G layers by other heteroatoms.[16-21]

Recently it has been reported that pyrolyzing chitosan, a natural nitrogen containing biopolymer, nitrogen-doped G and few-layers graphitic nanoplatelets are formed. [22] This distribution of N-doped G and nanoplatelets present in suspension after exfoliation of pyrolysed chitosan will be broadly denoted as (N)G in the sequel for simplicity. Transformation of chitosan, one of the main solid wastes from the fishing industry and widely available, [23] into (N)G constitutes a remarkable example of biomass valorization. In addition, chitosan has the advantage to act as a single source of carbon and nitrogen making straightforward the doping process.

The presence of nitrogen atoms on the G sheets modifies their electronic bands, becoming a semiconductor, rather than a conductor as all-carbon G.[24, 25] A recent theoretical DFT study[26] has shown that doping with nitrogen alters the electronic band structure of the G sheet depending on the percentage of substitution, becoming (N)G a semiconductor with a band gap that grows continuously from 0.1 to 0.7 eV for 2 % and 10 % of nitrogen doping, respectively. According to these calculations, it is anticipated that (N)G could exhibit a behavior as photocatalyst, although an experimental evidence for this prediction is still missing. In spite of the growing interest in the use of G type materials as photocatalysts for hydrogen generation, there are still no reports of the use of doped G as photocatalysts. The most widely reported use of G in photocatalysis is as promoter of the photocatalytic activity of metal oxide nanoparticles, particularly, as promoter of the activity of TiO_2 [8, 27]. Related to the work described in Chapter 2 is the seminal finding that graphene oxide

(GO), in the absence of any semiconductor, exhibits photocatalytic activity for hydrogen generation, and its activity depends on the degree of oxidation[3]. It was shown that organic dyes can expand the photocatalytic activity of GO into the visible region by acting as light harvesters groups and injecting electrons into the conduction band of the GO[4, 28-30].

Concerning with N-doped G, this material has been used as electrocatalyst for catalyzed oxygen reduction [17] and as support for cadmium sulfide nanoparticles[31]. It has also been reported that a polymeric graphitic carbon nitride, containing or not platinum, can act as photocatalyst for hydrogen generation with visible light (420-460 nm) from water-triethanolamine mixtures [32]. However what is missing is the direct use of (N)G as visible-light photocatalyst for hydrogen generation.

This Chapter reports chitosan pyrolysis to produce (N)G materials that were tested for their photocatalytic activity for hydrogen generation under monochromatic UV and visible light excitation. The photocatalytic activity using simulated Sunlight has also been determined. The optimization of photocatalytic activity depending on the preparation conditions for enhanced hydrogen generation from water-methanol mixtures is presented below. This study complements a recent report on the photocatalytic activity of P-doped G having supported Pt nanoparticles [33].

3.2 Experimental Section

3.2.1 Synthesis of (N)G

Chitosan spheres were obtained starting from an acid aqueous solution of chitosan (1 g chitosan in 25 mL of a 0.3M CH₃COOH aqueous solution) that was precipitated in the shape of millimetric spheres by adding drop

wise this solution into aqueous base (NaOH, 4 M). The spheres are removed by filtration and dried by a process that requires the gradual replacement of water by ethanol. The process consists in immersing the hydrogel beads in a sequence of ethanol/water baths of increasing alcohol concentration (10, 30, 50, 70, 90 and 100 vol%). Subsequently, ethanol was removed by supercritical CO₂ drying (above 73 bar pressure and 31 °C temperature) by using an E3000 critical point drying apparatus to yield aerogel beads. Pyrolysis of these chitosan beads were performed in an oven under Ar flow (1 ml x min⁻¹) heating at 200-280°C for 2 h, and then at temperatures between 200-900 °C for 2 h depending on the sample. Finally, (NG sheets were obtained by milling the graphitic beads and then dispersing the particles into an aqueous solution that was ultra-sonicated for 30 minutes by using Sonics Vibra Cell (700 W). Approximately 30 wt.% of the graphitic carbon residue obtained from chitosan pyrolysis becomes suspended in the aqueous phase after sonication. The remaining residue was decanted and the aqueous suspension centrifuged at 15,000 rpm before experiments.

3.2.2 Photocatalytic hydrogen production tests

Experiments were carried out by using two different irradiation sources, either the second harmonic output of a Nd-YAG laser (7s FWHP, 367 mW) at 355 and 532 nm, or a solar simulator (Wewport Oriel Instrumens, 1000W). The photoreactor was a cylindrical quartz vessel (56 mL total volume) with an inlet and outlet bearing independent gauges and a manometer to determine the pressure and a thermocouple to measure the temperature in the gas phase. To ensure the absence of oxygen in the system, all the system was purged with an argon flow for at least 30 min

before irradiation. The photocatalytic solution (30 mL) containing 30 v/v % of methanol as sacrificial electron donor was continuously magnetically stirred during irradiation. All the laser experiments were carried out at the same laser energy and using optically matched solutions of the photocatalyst at the laser wavelength. The catalysts amount used was 5.87, 3.53, 2.11, 3.68, 1.72 mg, for the chitosan pyrolysed at 200, 400, 600, 800, 900 °C, respectively, in 30 mL of photocatalytic solution. The temperature varied a maximum 2 °C during irradiation. The percentage of hydrogen evolved in the photoreactor during the irradiation was determined by gas chromatography using GS-MOL column of 15 meters and 0.55 mm ID with TCD from J&W Scientific previously calibrated with standards. The mol of hydrogen generated were calculated taking into account the ideal gas law ($n = PV/RT$).

3.2.3 General characterization

Transmission electron microscopy (TEM) images were made with a Philips CM300 FEG microscope operating at 100 kV. The Raman measurements (Renishaw inVia Raman Microscope) were carried out at room temperature with the 514.5 nm line of an Ar ion laser as an excitation source. XPS analyses were carried out on a VG Escalab 200R photoelectron spectrometer provided with MgK α 1 X-ray ($h\nu = 1254.6$ eV) 120 watts source and a hemispherical electron analyser. The samples were deposited as a thin film on double side adhesive tape and then mounted on a sample rod, placed in a pretreatment chamber and degassed under a residual pressure ca. 2×10^{-9} mbar for 1 h. The area under analysis was around 2.4 mm^2 and the pass energy of the analyser was set at 20 eV. Charging effects were corrected by calibrating spectra to the binding

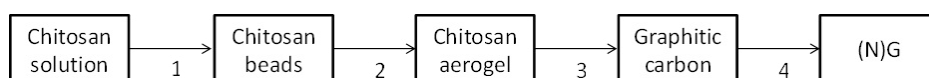
energy of C 1s peak at 284.9 eV. This reference gave BE values with an accuracy of ± 0.15 eV. Data processing was performed with the XPS peak software, the spectra were decomposed with the least squares fitting routine provided with this software using Gauss/Lorentz (90/10) lines and after subtracting a Shirley background. Atomic fractions were calculated using peak areas normalized on the basis of sensitivity factors. Atomic ratios were computed from the intensity ratios normalized by atomic sensitivity factors. Atomic force microscopy (AFM) images were obtained with a Multimode Nanoscope 3A equipment working in tapping mode, using a Si-wafer as substrate. Independent samples were cast and the thickness distribution of the individual (N)G flakes determined. The samples were submitted to 30 min sonication, followed by 15,000 rpm centrifugation before been analysed by AFM.

3.3. Results and Discussion

3.3.1. Preparation of (N)G

Preparation of (N)G was accomplished by pyrolysis under inert atmosphere of chitosan aerogel beads and exhaustive sonication in water, leading after the removal of the residues by centrifugation to persistent well-dispersed (N)G suspension without the need of surfactants or any other additives (Scheme 3.1). Approximately 30 wt.% of the pyrolysed chitosan carbon can be suspended as (N)G material after exhaustive sonication. Chitosan aerogel beads were prepared starting from acid aqueous solution of chitosan that was precipitated by drop wise addition of these solutions into basic aqueous solutions (step i in Scheme 3.1). The hydrogel beads were collected by filtration and converted into alcogels by gradual replacement of water by ethanol. Finally, chitosan beads were

submitted to supercritical CO₂ drying (ii in Scheme 3.1) as previously reported[34]. This procedure ensures the preparation of chitosan beads with a large porosity and surface area (523 m²/g) [35]. In contrast, it has been observed that sudden removal of water causes the collapse of the polymeric chitosan fibrils due to strong hydrogen bridging interactions, rendering materials with considerably smaller surface area[36-38]. Pyrolysis of these chitosan aerogels was performed in an oven under argon atmosphere (iii in Scheme 3.1). As it has been reported previously, the quality of the G depends on the pyrolysis temperature, decreasing the density of defects as the temperature increases[34]. This increase in the G quality can be assessed by X-ray photoelectron spectroscopy (XPS) and Raman spectroscopy of the pyrolyzed chitosan residue.



Scheme 3.1. Synthesis of (N)G. i) Formation of chitosan hydrogel by precipitation with NaOH in water; ii) Formation of chitosan aerogels by H₂O-to-EtOH exchange and supercritical CO₂ drying; iii) Pyrolysis of chitosan aerogels under inert atmosphere; iv) Exfoliation in water by ultrasound sonication and separation of the non suspended residue.

In XPS (Fig. 3.1), the peak corresponding to C_{1s} of the sample pyrolyzed at 900 °C can be adequately deconvoluted in two components with binding energies of 284.9 and 286.8 eV and relative proportions of 83 % and 13 %, respectively, attributable to graphenic sp² carbon and to sp² carbon atoms bonded to nitrogen, respectively.

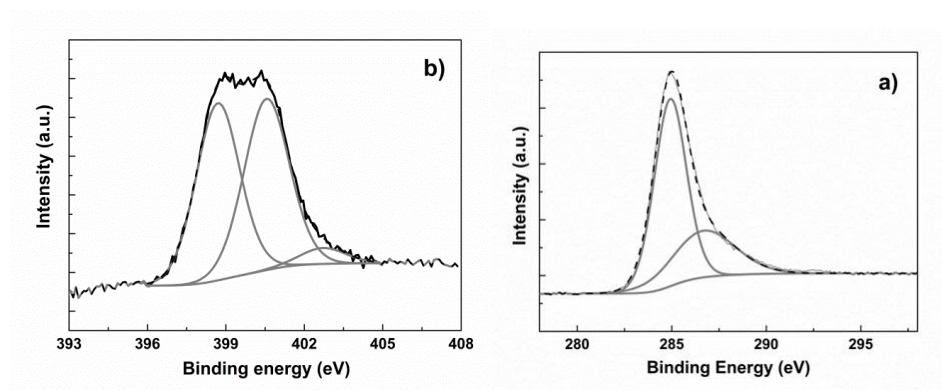


Figure 3.1. Experimental C1s and N1s peaks recorded in the XPS spectra of chitosan pyrolysed at 900 °C. a) C1s peak is deconvoluted into two components corresponding to graphenic C (284.9 eV) and sp² C bonded to N (286.8 eV). b) N1s peak is deconvoluted into three components corresponding to pyridine nitrogen (398.3 eV), pyridinium nitrogen of condensed polycycles (401.2 eV) and pyridine N-oxide (402.8 eV). The Shirley-type corrected baseline used in the fitting is also indicated.

We have also observed the presence of N_{1s} peak whose relative intensity decreases depending of the pyrolysis temperature. In fact, combustion chemical analysis shows the presence of nitrogen in a weight percentage of 16.2 % for the sample pyrolyzed at 600 °C, decreasing the N content along with the pyrolysis temperature. This decrease in the nitrogen content of the (N)G samples is reflected in XPS in the intensity of the N_{1s} peak and also in the proportion of the carbon atoms that are connected to nitrogen in the deconvolution of the C_{1s} peak. Table 3.1 summarizes analytical and relevant XPS data for the samples under study.

Table 3.1. Nomenclature of the (N)G samples used in this study and main analytical and photocatalytic activity data. Irradiation conditions: 30% of methanol as the sacrificial electron donor in water (30 ml), 355 nm laser irradiation (367 mW), room temperature, all photocatalysts exhibiting 0.2 absorbance at 355 nm.

Sample-pyrolysis temperature ^a	N content (wt %) ^b	XPS		H ₂ production	
		Percentage of graphenic C (%) ^c	r ₀ (μmol g ⁻¹ h ⁻¹) ^d	μmol (3 h) ^e	
(N)G-200	16.2	---	336.2	5.9	
(N)G-400	15.8	---	1497.6	15.9	
(N)G-600	15.1	24.4	2633.5	16.7	
(N)G-800	8.1	43.4	4999.1	55.2	
(N)G-900	5.4	83.0	16040.7	82.8	

^[a] The number after the dash corresponds to the pyrolysis temperature; ^[b] Determined by combustion chemical analysis; ^[c] Determined by deconvolution of the C_{1s} XPS peak; ^[d] Initial reaction rate; ^[e] Total production at 3 h irradiation.

In contrast to the information provided by XPS, the Raman spectra of all the series of (N)G samples were almost coincident (Figure 3.2), exhibiting the characteristic “G” and “D” peaks at 1580 and 1380 cm⁻¹, respectively. No significant shifts in the position of the “G” and “D” peaks as a function of the pyrolysis temperature was observed. In general, the presence of an intense “D” band of Raman spectra is associated to the presence of defects, characteristic of G samples with low crystallinity. However, it should be noted that in a related precedent describing the Raman spectra of N-doped G[39], observation of an intense “D” band, as recorded also in the present case, was attributed to the presence of N atoms in the G layers acting as defect sites [25].

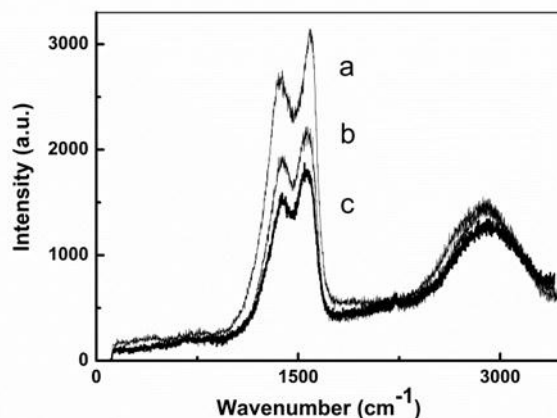


Figure 3.2. Raman spectra recorded for (N)G-900 (a), (N)G-800 (b) and (N)G-600 (c) recorded using 514 nm as excitation and at 2 mW power.

Imaging techniques provide firm evidence for the hexagonal arrangement of the (N)G samples and the monolayer morphology of (N)G accompanied by the presence of graphitic (N)G platelets after sonication. Thus, high resolution TEM images of the (N)G samples (Figure 3.3) shows that the atoms in the (N)G layers exhibit the typical expected hexagonal atomic structure. Selected area electron diffraction (see also Figure 3.3) shows the presence of diffraction patterns expected for well crystallized G layers. It has been possible to count for those graphitic platelets the number of layers by the periodic contrast changes of the image. As an example, Figure 3.3 also shows the contrast profile determined for a particular graphitic (N)G platelet, for which the individual layers can be counted. The morphology of the platelets correspond to layers about 2 μm in length as determined by TEM and SEM.

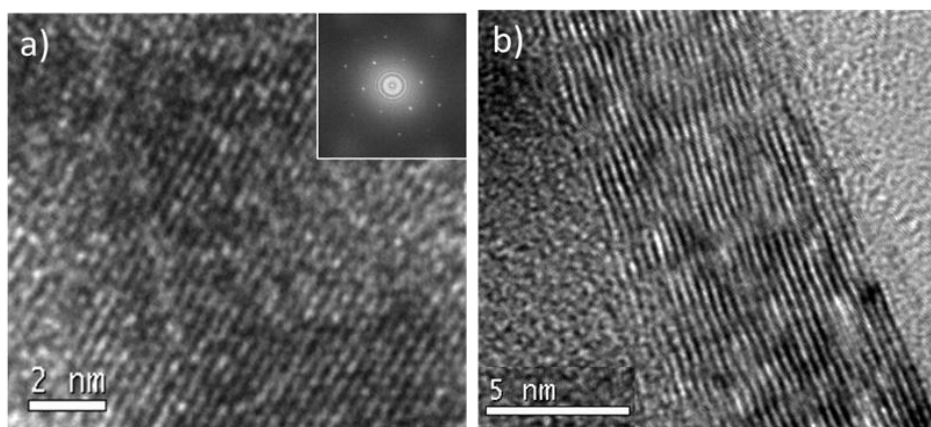


Figure 3.3. a) High-resolution TEM images of (N)G-900 sheets showing the alignment of the atoms. The inset shows the selected area electron diffraction obtained for this image. b) Cross-section of a (N)G-900 platelet in which the stacking of individual sheets can be seen.

The thickness of (N)G particles after sonication of the pyrolysed chitosan aerogel beads can be also determined by statistical analysis of the flake thickness by AFM. As an example, Fig. 3.4 shows AFM images obtained for a representative (N)G sample. The subnanometric vertical resolution of the AFM images shows that some of these particles have a thickness distribution between 1 and 5 nm that should correspond to single G or few-layers graphitic platelets, respectively.

Therefore, the above characterization data support the formation of N-doped G accompanied by graphitic platelets from natural chitosan as a single source of carbon and nitrogen atoms. Considering that chitosan comes from the main waste of fishery industry, the synthesis of N-doped G constitutes a remarkable example of biomass valorization.

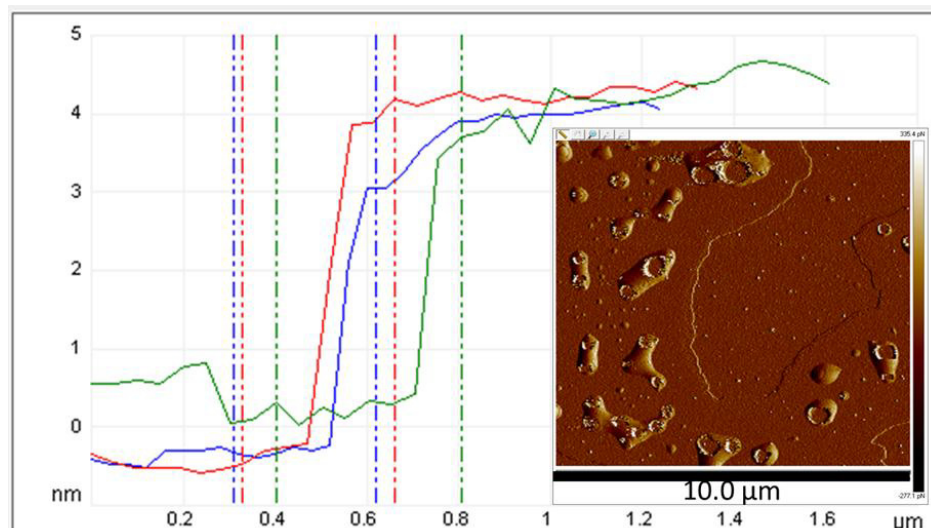


Figure 3.4. Vertical height of three different cross sections showing that the platelet shown in the inset is constituted by few layers G. The inset shows the morphology of the platelet and the presence on its surface of bubbles caused by solvent evaporation.

3.3.2. UV light photocatalytic activity

As indicated in the introduction, the main purpose of this study is to evaluate the photocatalytic activity of (N)Gs for hydrogen generation from water-methanol mixtures. It should be commented that related precedents in the literature [3, 6, 40] have shown that G is devoid of photocatalytic activity due to the conducting properties of this material. In contrast, GO can exhibit a behavior as semiconductor being able to generate hydrogen upon UV irradiation in water-methanol mixtures [3].

The UV-light photocatalytic activity depends on the degree of oxidation [41]. In the present case, was included in this study a sample of GO as a reference to compare its photocatalytic activity with those exhibited by (N)G samples under the same conditions. Fig. 3.5 shows the temporal profile of hydrogen evolution from water-methanol (3:1) mixture upon

355 nm irradiation of (N)G samples as a function of pyrolysis temperature in the range of 200 to 900 °C for optically matched solutions of (N)G at 355 nm. The exact photocatalysts weights are given in the experimental section. Control experiments using chitosan as photocatalyst failed to observe any H₂ generation.

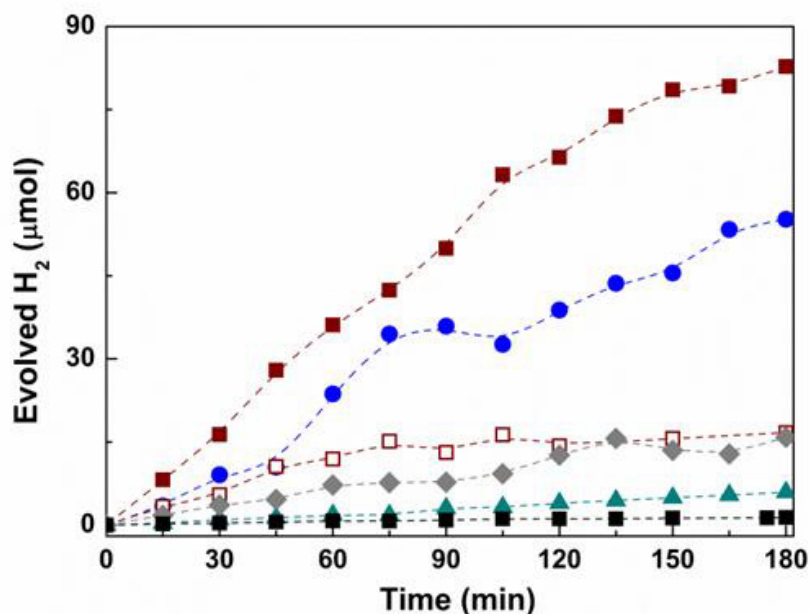
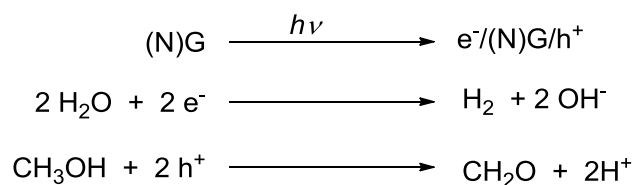


Figure 3.5. Hydrogen evolution upon 355 nm irradiation of water-methanol (3:1) mixtures in the presence of (N)G obtained from chitosan pyrolysis at different temperatures. The photocatalytic activity of GO as photocatalysts is also plotted. ■ : GO; ▲: 200°C; ◆ : 400°C ; □: 600°C; ● : 800°C; ■ : 900°C. Irradiation conditions: 30% of methanol as the sacrificial electron donor in water (30 ml), 355 nm laser irradiation (367mW), room temperature, all photocatalysts exhibiting 0.2 absorbance at 355 nm. For the exact photocatalyst weight for each material refer to the experimental section.

As it can be seen in the Figure, all (N)G samples exhibit photocatalytic activity that is not present in G. This photocatalytic activity is even higher

than GO taken as reference, increasing the amount of hydrogen evolved as the pyrolysis temperature increases. The most efficient sample at the same photon absorption being (N)G obtained by pyrolysis of chitosan aerogel beads at 900°C. For this sample, considering the all the N atoms present in the photocatalyst act as a kind of active center, a turnover number of 12.5 was estimated by dividing the final μmols of H_2 evolved by the μmols of N present in the (N)G. It is, however, very likely that the real turnover number is even higher considering that the three different populations of N atoms observed in XPS could exhibit different photocatalytic efficiency. If the comparison is made by weight of sample, the (N)G at 900 °C has to be considered even more efficient than the (N)G samples pyrolysed at lower temperatures, since less weight of (N)G 900 oC is required to reach higher H_2 generation. This trend can be rationalized considering that as the pyrolysis temperature increases, the crystallinity of the (N)G samples increases while N is still present and the decrease in the number of defects on the G-type structure appears to be the most important parameter governing the photocatalytic efficiency of the (N)G materials, rather than the total N percentage content that decreases with the pyrolysis temperature (see Table 3.1). Scheme 3.1 illustrates the proposed photocatalytic mechanism for hydrogen generation from water in the presence of methanol as sacrificial agent.



Scheme 3.1. Photocatalytic mechanism for hydrogen generation using methanol as sacrificial electron donor.

The photocatalytic experiments presented in Fig. 3.5 were carried out using solutions optically matched at the wavelength of the laser used for excitation (355 nm). After extensive laser irradiation, a significant decrease in the absorbance of the solution was observed. Fig. 6 illustrates these changes for the (N)G-900 sample that is the most efficient one. This decrease in absorbance could be related to a degradation of the (N)G sample upon extended irradiation. In fact, a prolonged experiment in which the experiment was performed for 10 h showed that the hydrogen evolution decreases gradually over the time tending eventually to a plateau (see inset B of Fig. 3.6). This would indicate that the photocatalytic efficiency of the materials could be limited by degradation of (N)G sample. This is the most likely reason why the slope of H₂ generation in the time-conversion plots decreases upon prolonged irradiation times.

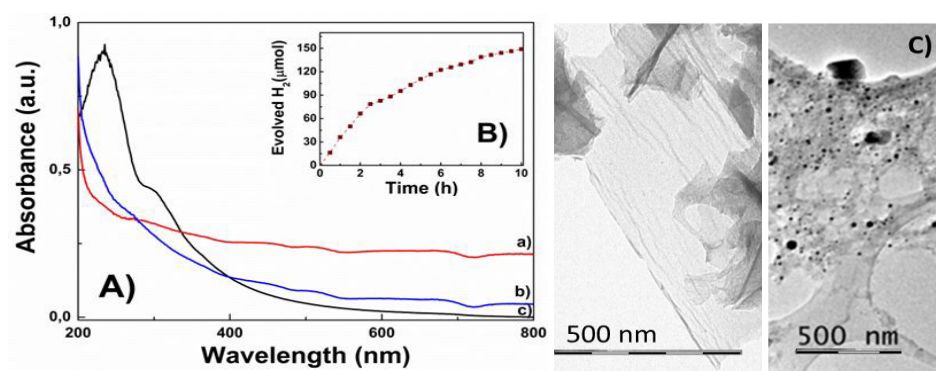


Figure 3.6. A) UV/Vis spectra of a (N)G-900 suspension before (a) and after irradiation with 355 nm laser for 10 h (b) compared to the spectrum of GO (c). Inset B): Hydrogen evolution in a photocatalytic run using (N)G-900 as photocatalyst (1.7 mg) and methanol (30%) as sacrificial electron donor in water (30 mL) under 355 nm laser irradiation at room temperature for 10 h; it is proposed that the decrease in the H₂ evolution rate is due to changes in the (N)G-900 photocatalytic activity. C) Representative TEM image of (N)G-900 before (left) and after 10 h laser irradiation (right).

TEM images of used (N)G photocatalyst having a residual activity (see Fig. 3.6C) shows a remarkable change in the morphology of the sample, with the appearance of dense particles. We propose that these changes in the 2D morphology of (N)G is responsible for the decrease in the H₂ evolution rate observed in the photocatalytic measurements. This issue of photocatalytic stability, certainly of large importance for G-based materials, requires independent studies to determine the reasons of this morphological change, possible ways to prolong the durability of the material and deeper characterization of the exhausted photocatalyst.

3.3.3. Visible light photocatalytic activity

As it can be seen in Fig. 3.6, GO is characterized by an intense absorption peak in the UV region with a residual absorption spanning in the visible range. Accordingly, it has been reported that GO exhibits photocatalytic activity only upon UV light irradiation and that GO has almost no response with visible light[42]. These results have been confirmed in the present study. In contrast, it is known that G has an almost constant absorption throughout the entire UV-visible region. We were interested in determining if the almost constant absorbance throughout all the wavelength range (“neutral absorption”) characteristic of G material allows the use of visible light for hydrogen evolution using (N)G photocatalyst. To address this important point we performed photocatalytic tests using monochromatic visible light at 532 nm. The results are presented in Fig. 3.7, as it can be seen there, almost no hydrogen was observed for GO in agreement with the reported lack of visible light photo activity [43]. Under the same conditions the (N)G-900 sample exhibited, in contrast, an activity that was almost coincident with

that monitored using 355 nm laser at the same intensity (compare the temporal profiles of hydrogen evolution for (N)G samples pyrolysed at 900 °C in Figs. 3.5 and 3.7). This similar photocatalytic activity for these two different wavelengths is in accordance with the same light absorption for both wavelengths characteristic of the neutral optical spectrum of (N)G and the use of similar light intensity for irradiation.

3.3.4. Power dependency and influence of (N)G amount on photocatalytic H₂ evolution

The mechanism of the photocatalytic hydrogen evolution and, in particular, the fact that the process using laser excitation is not predominantly monophotonic was assessed by performing a laser power dependency study of hydrogen evolution. The results are presented in the inset a) of Fig. 3.7. As it can be seen there, the hydrogen evolution does not follow a linear relationship with the laser power. In fact, a fitting of the experimental data indicates that hydrogen evolution under the conditions studied can be adequately fitted to a two-term polynomy $y = 4 \times 10^{-8} x + 3 \times 10^{-9} x^2$, where “y” is the volume of H₂ at 1 h and “x” is the laser power. This mathematical equation indicates the simultaneous occurrence of mono and biphotonic processes under the present experimental conditions. At low laser fluencies, the monophotonic term predominates, while at high powers the process is predominantly biphotonic. This would indicate that the hydrogen measured in the laser experiments arises mainly from two-photon absorption, a fact that can be rationalized in a simple way considering that the photocatalytic process is far more efficient when the two electrons involved in the formation of one H₂ molecule are provided in the same laser shot by simultaneous absorption of two photons.

We also determined the influence of the amount of (N)G on the hydrogen evolution. As it is observed in the inset b) of Fig. 3.7, the amount of hydrogen formed is almost constant with the amount of (N)G in the range of concentration between 0.03 and 0.12 $\text{g}\cdot\text{L}^{-1}$. This observation indicates that under our experimental conditions, most of the photons entering in the system are already absorbed even using the lowest amount of (N)G tested.

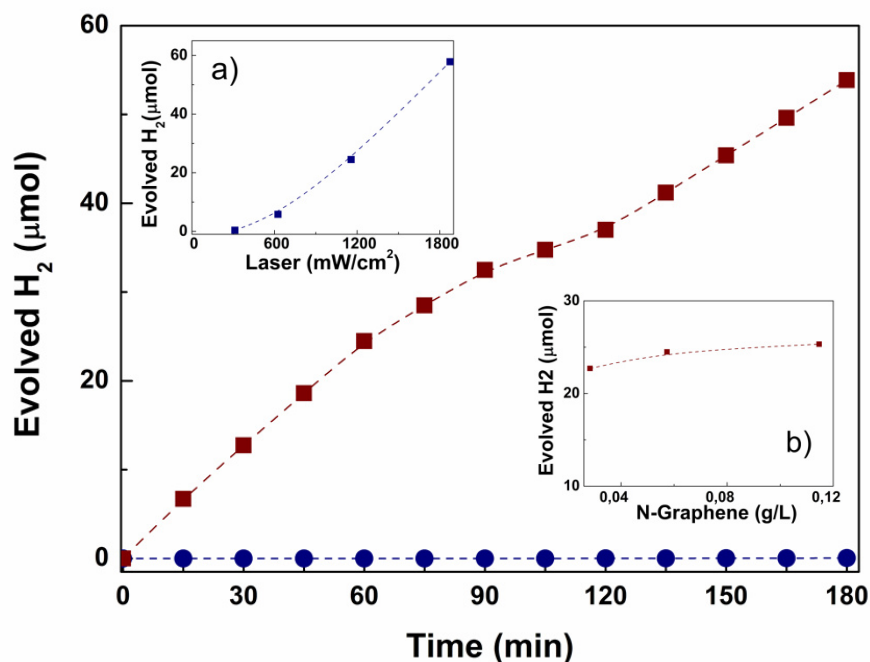


Figure 3.7. Hydrogen evolution using (N)G-900 and GO as photocatalysts. Reaction conditions: methanol (30%) as sacrificial electron donor in water (30 mL), under 532 nm laser irradiation, photocatalyst absorbance at 532 nm 0.2 absorbance: ● GO; ■ (N)G. Inset a): Hydrogen evolved in a photocatalytic run using (N)G as photocatalyst (0.057 g/L), methanol (30% v/v) as the sacrificial electron donor, under 532 nm laser irradiation at different laser powers. inset b): hydrogen evolved during photocatalytic runs with different concentrations (N)G (0.028g/L; 0.057 g/L; 0.115 g/L) as photocatalyst under 532 nm laser irradiation. Methanol (30% v/v) was used as sacrificial electron donor in water.

3.3.5. Failure of water oxidation

Water oxidation to form molecular oxygen is thermodynamically and kinetically more complex than hydrogen generation from water. Precedents in the literature have shown that GO as photocatalyst for water reduction in the presence of sacrificial electron acceptor is not capable to generate oxygen from water [3, 4]. In the present case, we also performed a test using silver nitrate as sacrificial electron acceptor to explore the possibility of photocatalytic water oxidation using (N)G as photocatalyst. We were, however, unable to observe the formation of oxygen, a fact that can be probably due to the low oxidation potential of photogenerated holes in (N)G. These experimental observation can be rationalized considering that the computational calculations predict a maximum bandgap for (N)G of 0.7 eV that would be insufficient for generation of H₂ and O₂ with the same material. Thus, the issue of a G-based photocatalyst for the overall water splitting still remains open.

3.3.6. Photocatalytic hydrogen generation by (N)G under simulated solar light irradiation

Previously, we have shown the photocatalytic hydrogen evolution using monochromatic laser irradiation either in the UV (355 nm) or in the visible (532 nm) region. In order to show the applicability of (N)G for hydrogen generation from water-methanol mixtures, we have also studied the photocatalytic activity of this material upon irradiation with simulated sun light. Due to the much lower power of the solar simulator compared to the lasers employed in the previously, the possibility to have biphotonic processes by simultaneous absorption of two photons should be negligible (see inset a in Fig. 3.7) for powers lower than 500 mW/cm², corresponding

to the solar simulator. For the sake of comparison, we have included in the study the activity of GO that is known to generate hydrogen under UV light irradiation, but not with visible light [3]. The results obtained for hydrogen generation using polychromatic simulated sun light are shown in Fig. 3.8. As it can be seen there, while GO under the same conditions does not evolve measurable amount of hydrogen, (N)G exhibits photocatalytic activity for hydrogen generation, in agreement with the photoresponse of this material under visible light excitation.

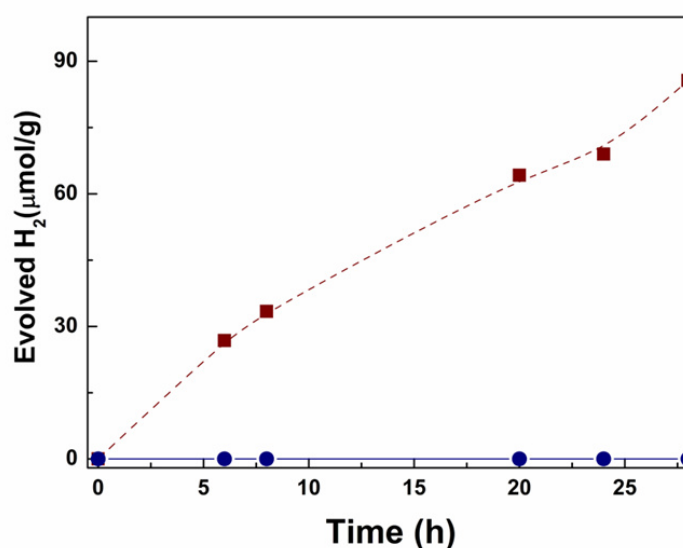


Figure 3.8. Hydrogen evolution in photocatalytic runs with (N)G and GO (0.1146 g/L) as photocatalyst in 30 mL of water/methanol (30 % v/v) mixtures under solar irradiation (1000 W). ■: (N)G; ●: GO.

3.4. Conclusion

In the present chapter it was shown that, in contrast with the behavior of G, (N)G behaves as a semiconductor and exhibits high efficiency for the photocatalytic generation of hydrogen from water- methanol mixtures with

similar efficiency using UV or visible light. This result sharply contrast also with the reported behavior of GO that is only active under UV light. This visible light photo response should arise from the neutral absorbance throughout all the UV-visible spectrum characteristic of G material. It was observed that the photocatalytic activity largely depends on the crystallinity of the sample and on the pyrolysis temperature, improving the efficiency along the increase in the crystallinity of (N)G. One point that deserves further study is how to increase the photostability of the material that tends to deactivate upon extended irradiation. Considering the wide range of doped Gs available, our study opens the way for exploring other doped G materials to search for optimal and durable G-based photocatalyst for hydrogen generation from water.

3.5 References

- [1] P. D. Tran, L. H. Wong, J. Barber, J. S. C. Loo, *ENERGY & ENVIRONMENTAL SCIENCE* **2012**, 5, 5902.
- [2] A. C. Ferrari, D. M. Basko, *Nat. Nanotechnol.* **2013**, 8, 235.
- [3] T. F. Yeh, J. M. Syu, C. Cheng, T. H. Chang, H. S. Teng, *Advanced Functional Materials* **2010**, 20, 2255.
- [4] M. Latorre-Sanchez, C. Lavorato, M. Puche, V. Fornes, R. Molinari, H. Garcia, *Chemistry-a European Journal* **2012**, 18, 16774.
- [5] T. Peng, K. Li, P. Zeng, Q. Zhang, X. Zhang, *J. Phys.Chem. C* **2012**, 116, 22720.
- [6] X. An, J. C. Yu, *RSC Adv.* **2011**, 1, 1426.
- [7] L. Han, P. Wang, S. Dong, *Nanoscale* **2012**, 4, 5814.
- [8] Y. Hau Ng, I. V. Lightcap, K. Goodwin, M. Matsumura, P. V. Kamat, *J. Phys. Chem. Lett.* **2010**, 1, 2222.

- [9] D. R. Dreyer, C. W. Bielawski, *Chemical Science* **2011**, 2, 1233.
- [10] D. W. Boukhvalov, D. R. Dreyer, C. W. Bielawski, Y.-W. Son, *ChemCatChem* **2012**, 4, 1844.
- [11] D. R. Dreyer, H.-P. Jia, A. D. Todd, J. Geng, C. W. Bielawski, *Organic & Biomolecular Chemistry* **2011**, 9, 7292.
- [12] H.-P. Jia, D. R. Dreyer, C. W. Bielawski, *Tetrahedron* **2011**, 67, 4431.
- [13] A. Zaleska, *Recent patents on engineering* **2008**, 2, 157.
- [14] M. Sathish, B. Viswanathan, R. P. Viswanath, C. S. Gopinath, *Chemistry of Materials* **2005**, 17, 6349.
- [15] Y. Cong, J. Zhang, F. Chen, M. Anpo, *J. Phys. Chem. C* **2007**, 111, 6976.
- [16] R. Ballesteros-Garrido, M. de Miguel, A. Doménech-Carbó, M. Álvaro, H. García, *Chem. Commun.* **2013**, 49, 3236.
- [17] L. Qu, Y. Liu, J. B. Baek, L. Dai, *ACS Nano* **2010**, 4, 1321.
- [18] J. Malig, P. Doz, N. Jux, D. Kiessling, J. J. Cid, P. Vázquez, T. Torres, D. M. Guldi, *Angew. Chem. Int. Ed.* **2011**, 50, 3561.
- [19] J. Malig, C. Romero-Nieto, N. Jux, D. M. Guldi, *Advanced Materials* **2012**, 24, 800.
- [20] R. D. Costa, J. Malig, W. Brenner, N. Jux, D. M. Guldi, *Adv. Mater.* **2013**, 25, 2600.
- [21] M. E. Ragoussi, J. Malig, G. Katsukis, B. Butz, E. Spiecker, G. de la Torre, T. Torres, D. M. Guldi, *Angewandte Chemie-International Edition* **2012**, 51, 6421.
- [22] A. Primo, P. Atienzar, E. Sanchez, J. M. Delgado, H. García, *Chem. Commun.* **2012**, 48, 9254.

- [23] M. Chandrasekaran, *Valorization of food processing by-products*, CRC Press USA, **2013**.
- [24] D. Usachov, O. Vilkov, A. Grüneis, D. Haberer, A. Fedorov, V. K. Adamchuk, A. B. Preobrajenski, P. Dudin, A. Barinov, M. Oehzelt, C. Laubschat, D. V. Vyalikh, *Nano Lett.* **2011**, *11*, 5401.
- [25] D. Wei, Y. Liu, Y. Wang, H. Zhang, L. Huang, G. Yu, *Nano Lett.* **2009**, *9*, 1752.
- [26] P. Rani, V. K. Jindal, *RSC Adv.* **2013**, *3*, 802.
- [27] S. Morales-Torres, L. M. Pastrana-Martinez, J. L. Figueiredo, J. L. Faria, A. M. Silva, *Environ Sci. Pollut. Res. Int.* **2012**, *19*, 3676.
- [28] S. X. Min, G. X. Lu, *Journal of Physical Chemistry C* **2011**, *115*, 13938.
- [29] Z. G. Mou, Y. P. Dong, S. J. Li, Y. K. Du, X. M. Wang, P. Yang, S. D. Wang, *International Journal of Hydrogen Energy* **2011**, *36*, 8885.
- [30] Q. Xiang, J. Yu, M. Jaroniec, *Nanoscale* **2011**, *3*, 3670.
- [31] L. Jia, D.-H. Wang, Y.-X. Huang, A.-W. Xu, H.-Q. Yu, *Physical Chemistry C* **2011**, *115*, 11466.
- [32] X. Wang, K. Maeda, A. Thomas, K. Takanahe, G. Xin, J. M. Carlsson, K. Domen, M. Antonietti, *Nature materials* **2009**, *8*, 76.
- [33] M. Latorre-Sánchez, A. Primo, H. García, *Angewandte Chemie International Edition* **2013**, n/a.
- [34] A. Primo, A. Forneli, A. Corma, H. García, *Chemsuschem* **2012**, *5*, 2207.
- [35] R. Valentin, K. Molvinger, F. Quignard, D. Brunel, *New J. Chem.* **2003**, *27*, 1690.
- [36] R. Bellamkonda, J. P. Ranieri, N. Bouche, P. Aebischer, *J. Biomed. Mater. Res.* **1995**, *29*, 663.

- [37] H. Trieu, S. Qutubuddin, *Polymer* **1995**, *36*, 2531.
- [38] G. P. Dillon, Z. Yu, A. Sridharan, J. P. Ranieri, R. V. Bellamkonda, *J. Biomater. Sci., Polym. Ed.* **1998**, *9*, 1049.
- [39] K. S. Kim, Y. Zhao, H. Jang, S. Y. Lee, J. M. Kim, K. S. Kim, J. H. Ahn, P. Kim, J. Y. Choi, B. H. Hong, *Nature* **2009**, *457*, 706.
- [40] G. Williams, B. Seger, P. V. Kamat, *ACS Nano* **2008**, *2*, 1487.
- [41] K. Krishnamoorthy, R. Mohan, S. J. Kim, *Appl. Phys. Lett.* **2011**, *98*, 244101.
- [42] X. Y. Zhang, H. P. Li, X. L. Cui, Y. Lin, *J. Mater. Chem.* **2010**, *20*, 2801.
- [43] I. V. Lightcap, T. H. Kosel, P. V. Kamat, *Nano Lett.* **2010**, *10*, 577.

4

Natural alginate as graphene precursor and template in the synthesis of nanoparticulate ceria-graphene water oxidation photocatalyst.^(*)

(*) C. Lavorato, A. Primo, R. Molinari and H. García.
Submitted to ACS Catalysis

4.1. Introduction

Semiconducting metal oxides, such as TiO₂, ZnO, and WO₃, exhibit photocatalytic activity whose efficiency depends on many factors related to their synthesis and to their textural properties [1, 2]. In particular, the morphology and the average size of the particles are key parameters that exert a strong influence on the photocatalytic performance of the materials[3, 4]. Besides the particle size, the surface functionality and hydrophobicity as well as the density of surface hydroxyl groups also play important roles on the photocatalytic activity. Surface area, particle size and density of hydroxyl groups are largely determined by the synthetic methodology used for the preparation of the material [5,6]. In this context, it has been [7,8,9,10] recently reported the use of biopolymers as templating agent for the synthesis of TiO₂ and CeO₂ nanoparticles (NPs) having a high photocatalytic activity for water splitting, either for reduction (TiO₂) or for oxidation (CeO₂). In material science the use of

templates for the synthesis of solids is a general methodology to gain control on the morphology and structure of the particles and the use of natural biopolymers as templates is an illustrative example of biomass wastes valorization. Continuing with the application of natural biopolymers as templates for the synthesis of photocatalysts having activity for water splitting, herein we show an original process that can effect simultaneously the generation of metal oxide NPs acting as photocatalyst as well as graphene acting as promoter in intimate contact with ceria NPs to improve their efficiency.

In the case of TiO_2 [1,12], it has been well documented that the intimate contact with G sheets can increase by a factor of two the photocatalytic activity inherent to TiO_2 [13], a fact that has been attributed to a more efficient charge separation originated by the migration of electrons from the TiO_2 conduction band to G (Scheme 4.1). It could be likely that an analogous process could also operate for other semiconductors and, similarly to TiO_2 , the photocatalytic activity of these other semiconductors could also be enhanced by adequate interfacial contact with G-based carbons. In the present work we have confirmed the validity of this concept by preparing highly crystalline ceria NPs embedded in a graphene matrix formed by pyrolysis under anaerobic conditions of the polymeric template employed in the synthesis. The results that will be described below show the potential use of natural biopolymers for the preparation of photocatalysts with enhanced performance with respect to the conventional hydrothermal synthesis of these metal oxides and represent a clear example of biomass valorization.

4.2. Experimental

4.2.1. Photocatalytic oxygen production tests

The photocatalytic solution (25 ml) containing water, 0.01 M of AgNO_3 as sacrificial electron acceptor and 20 mg of photocatalyst was continuously stirred magnetically during irradiation. The volume of oxygen evolved in the photoreactor during the irradiation was quantified by gas chromatography (GS-MOL 15 meters column ID 0.55 mm and TCD from J&W Scientific) previously calibrated with standards and the moles of oxygen generated were calculated taking into account the ideal gas law ($n = PV/RT$).

4.2.2. Synthesis of CeOx/graphene

1 g of alginic acid sodium salt was added in 100 mL of water and stirred for 2-3 h to obtain a good dispersed solution. Then, this solution was filtered. The alginic filtered solution was added drop by drop stirring slowly in two different aqueous solutions of $(\text{NH}_4)_2\text{Ce}(\text{NO}_3)_6$ having 55 g/L or 110 g/L. The samples were left overnight without stirring. Subsequently, the beads prepared were washed with water and finally were submitted to gradual exchange of water by ethanol. The beads were submitted to supercritical CO_2 and then calcined in Argon at 200°C for 2 h at 800 or 900°C . The obtained CeO_2/G samples were sonicated for at least 1 h before the photocatalytic tests.

4.2.3. Textural and analytical properties measurements

Raman spectra were recorded at ambient temperature with 514 nm laser excitation at 2 mW power by using a Renishaw In Via Raman

spectrometer equipped with a CCD detector. TEM images were recorded in a Philips CM300 FEG system with an operating voltage of 100 kV. XPS spectra were recorded on a SPECS spectrometer equipped with a Phoibos 150 9MCD detector using a nonmonochromatic X-ray source (Al and Mg) operating at 200 W. The samples were evacuated in the prechamber of the spectrometer at 1×10^{-9} mbar. The samples have been activated in situ in nitrogen flow at 450 °C for 3 h followed by evacuation at 10⁻⁸ mbar. Deconvolution and fitting of the experimental peaks was carried out after nonlinear Shirley-type background subtraction and peak correction by the transmission function of the spectrometer.

The Atomic Force Microscopic measurements were conducted using contact mode in air at ambient temperature using a Veeco AFM apparatus. Experimental tests were carried out for 4 h under UV irradiation using the 200 W xenon-doped mercury lamp (Hamamatsu Lightningcure LC8, 0.5 cm distance). The photoreactor was a cylindrical pyrex vessel (48 ml total volume) with an inlet and outlet that has a manometer and a thermocouple to determine in the gas phase the pressure and the temperature, respectively. To ensure the absence of oxygen all the system was purged with an argon flow for 30 min before irradiation.

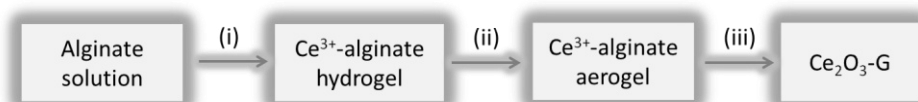
4.3. Results and discussion

In the present study we have prepared a series of CeO_x NPs embedded on a G based matrix. The two parameters that have been optimized during the synthesis are the temperature of the pyrolysis process and the weight percentage of the biopolymer in the material. The synthesis of the photocatalyst is summarized in Scheme 4.1. The process starts with the

precipitation of cerium alginate beads by dropping an aqueous alginate solution into an aqueous solution of cerium ammonium nitrate (i) in Scheme 4.1.

Scheme 4.1. Procedure for the synthesis of CeOx/G samples.

- i) Precipitation of Ce³⁺-containing alginate hydrogel with (NH₄)₂Ce(NO₃)₆;
- ii) drying by H₂O to EtOH exchange and CO₂ supercritical drying;
- iii) pyrolysis under Ar flow.



It is well known in the literature that alginate forms solid precipitates with Ca²⁺ as well as other di- and tripositive metal cations [14,15]. The hydrated cerium alginate beads were dried by gradual exchange of water by ethanol by stirring the cerium alginate beads consecutively in a series of five water-ethanol solutions of increasing percentage of ethanol from 20 wt % up to pure ethanol. Finally the resulting alcogel beads were submitted to supercritical CO₂ drying to form aerogels having large surface area up to 400 m²/g (step ii in Scheme 4.1) [7]. Previously, calcination in air of these cerium alginate aerogel beads producing the combustion of the natural alginate polymer has been reported [7]. This aerobic combustion leads to the complete removal of the organic material leaving CeO₂ particles. In the present case, in contrast, the cerium alginate beads were submitted to pyrolysis under inert atmosphere at temperatures in the range from 800 to 900 °C (step iii in Scheme 4.1). This thermal treatment leads, on one hand, to the formation of CeOx NPs, while the

oligosaccharide is decomposed forming graphitic carbons. In the literature, it was reported that pyrolysis of alginate beads without containing Ce^{3+} ions leads to the formation of graphitic carbon residues [16]. In the present case, the process undergone by alginate is similar to the one reported leading to graphitic residues, except that the sample also contains Ce^{3+} that evolves to CeO_x . In that way, this CeO_x/G composite having an intimate contact between the two components can have interesting photocatalytic properties derived from the combination of cerium oxide embedded in G based carbon.

The resulting four CeO_x/G materials were characterized by analytical, textural and spectroscopic techniques. Combustion chemical analysis shows that the samples contain different percentages of carbon related to the composition of the initial solution and to the pyrolysis temperature (Table 4.1).

Table 4.1. List of the CeO_x -G samples studied, details of preparation procedure and percentage of graphitic carbon content.

Samples	Carbon content (%)	Amount of $(\text{NH}_4)_2\text{Ce}(\text{NO}_3)_6$ (g)	Pyrolysis temperature ($^\circ\text{C}$)
$(\text{CeO}_x\text{-G})_A$	2.5	11	900
$(\text{CeO}_x\text{-G})_B$	5.19	11	800
$(\text{CeO}_x\text{-G})_C$	0.015	22	900
$(\text{CeO}_x\text{-G})_D$	0.56	22	800

TEM images of the materials show the presence of highly crystalline CeO_x NPs embedded inside the carbon matrix (Fig. 4.1). It was observed

that the CeO_x NPs presented well-defined triangular, cubic or hexagonal shapes with a narrow particle size distribution about 30 nm. With GIF (energy filtered imaging technique), we mapped the elemental distribution of Ce, O and C in a selected area of the microscopy image.

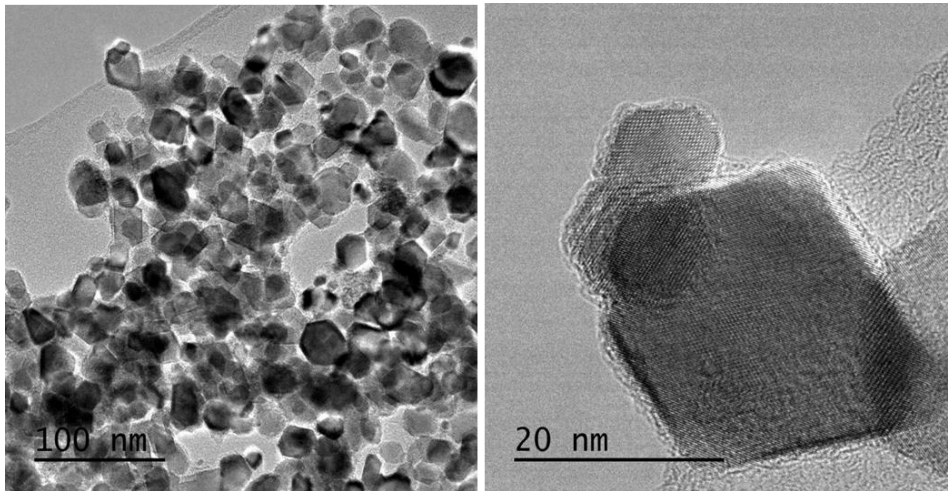


Figure 4.1. TEM (left) and high-resolution TEM (right) of (CeO_x-G)_A. The morphology of the CeO_x crystallites with defined geometrical shapes can be clearly observed.

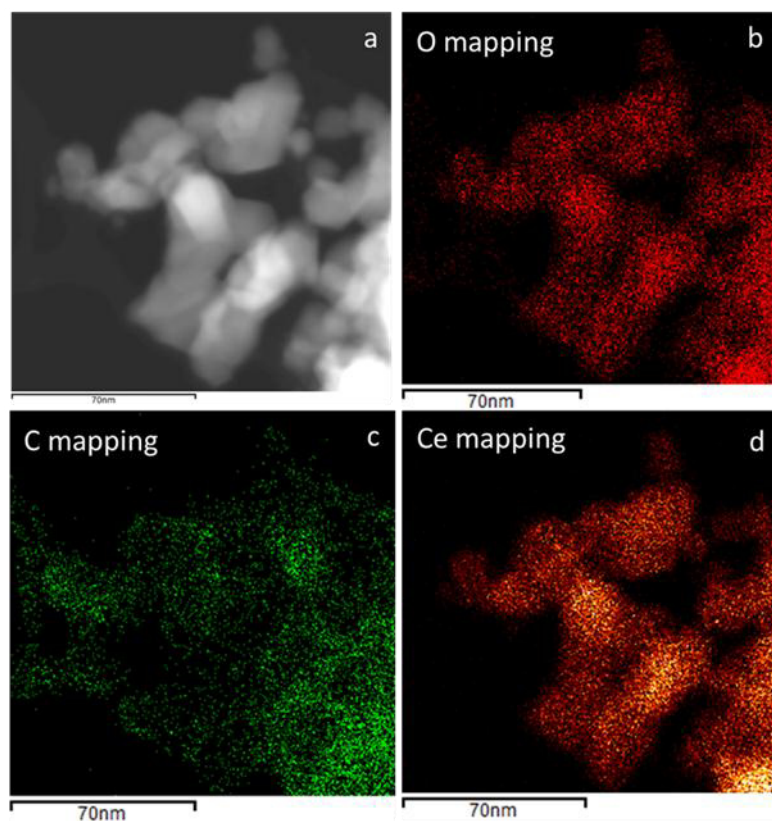


Figure 4.2. a) Zero-loss TEM image of $(\text{CeO}_x\text{-G})_A$ sample. b) c) d) GIF imaging show elemental distribution of oxygen, carbon and cerium respectively. Note the coincidence of O and Ce mapping images, while C is spread in a larger area covering CeO_x NPs.

It is evidenced that these regular NPs correspond to CeO_x NPs that are covered by a C matrix (Fig. 4.2). In agreement with reported TEM images of related samples obtained by alginate pyrolysis, TEM images show that the carbon material is constituted by imperfect stacking of graphenic layers that in the inner part of the wall have a sponge like morphology probably caused by the evolution of a large quantity of gases during the thermal treatment [16]. It has been already stated that this imperfect

stacking of the graphenic layers, also revealed by the broad XRD peak at 2θ 260, is suitable to perform exfoliation of the individual G layers reaching, in aqueous suspension, the state of single-layer or few-layers G [17]. Wide angle XRD also shows, on the other hand, the expected peaks for well crystallized CeOx materials. It should be commented that even though pyrolysis temperature is relatively high, the average particle size of CeOx NPs is small (5-20 nm), a fact that has been previously observed also for TiO₂ [8] and that has been attributed to the effect of the biopolymer and the materials derived from it during the thermal treatment, controlling the growth and agglomeration of the inorganic NPs.

Raman spectroscopy is a suitable technique to report on the nature of the carbonaceous materials [18] and CeOx nanoparticles [19-22]. In all cases, we have been able to monitor the characteristic G and D bands appearing at 1600 and 1346 cm⁻¹ that correspond to the peaks of graphenic carbon with defects on the G layers (Fig. 4.3).

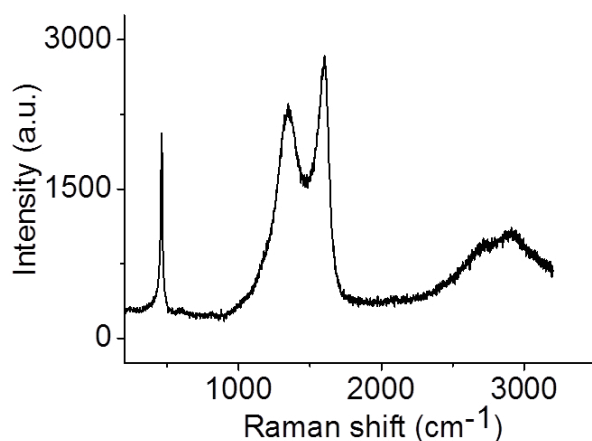


Figure 4.3. Raman spectrum of (CeOx-G)A recorded using 514 nm laser. The peaks corresponding to ceria and G have been marked in the plot.

Interestingly, it was observed that the width of the G peak decreases with the pyrolysis temperature increasing, suggesting that the crystallinity of the G component of the samples increases with the pyrolysis temperature. With regard to CeO_x NPs, the frequency at 462 cm⁻¹ is related to symmetrical stretching of the Ce-O₈ vibrational unit, corresponding to the triply degenerate F_{2g} mode of fluorite CeO₂ and the only one allowed in first order Raman scattering. XPS also reports on the composition of the series of samples and the oxidation state of the elements from the binding energy of these elements. In the present case, XPS of the series of CeO_x/G samples has allowed detection of the C1s peak (Fig. 4.4). Deconvolution of the experimental peak shows three components appearing at 285.0 eV, 286.5 eV and 288.8 eV corresponding the first one to sp² graphenic carbons and the second and third to carbon atoms bonded to oxygen. The relative proportion between these three peaks differs from one sample to the other, indicating that the crystallinity, reflected by the relative proportion of graphenic carbons, depends on the percentage of ceria and pyrolysis temperature.

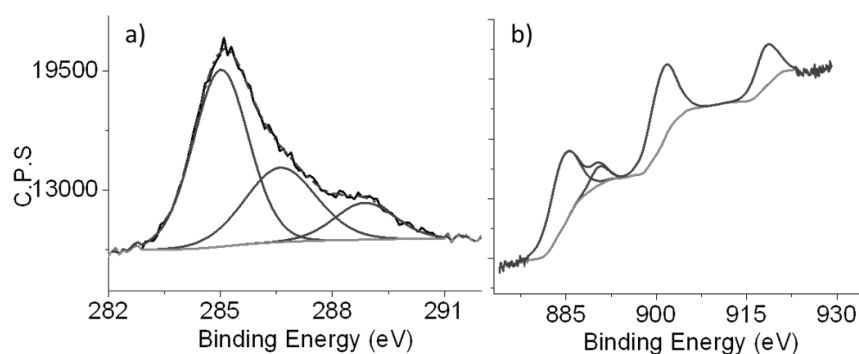


Figure 4.4. a) C1s peak and the best fitting considering two major components corresponding to graphenic sp^2 C and C bonded to oxygen.
 b) Ce 3d peaks showing the predominant presence of +III (peaks at 885.6 eV and 901.8 eV) vs +IV (peak at 918.6 eV) in the $(\text{CeOx-G})_A$ sample.

Interestingly, analysis of the 3d peak of Ce reveals a large proportion of Ce (+III) with respect to Ce (+IV) (Fig. 4.4). This fact is not totally unexpected considering that pyrolysis is carried out under reductive conditions required for graphitization of alginate. In a related precedent pyrolyzing a hybrid Ni, Mn-hydroxalcalite with graphene oxide (GO), the reduction of Ni (+II) to Ni (0) has been observed and these reductive conditions will be also responsible in the present case of the predominant presence of Ce (+III) over Ce (+IV) [23].

Concerning the predominant percentage of Ce (+III) with respect to Ce (+IV) in the CeOx/G composites and its potential influence on the behavior as semiconductor it is worth commenting that CeO₂ constituted by micrometric particles is an insulator oxide and not semiconductor material [24]. By decreasing the particle size from micrometers in the nanometric domain, it has been observed that the presence of oxygen vacancies in the lattice and the increasing confusion between +IV and +III

oxidation states is responsible for this behavior as semiconductor [25]. Thus, in the present case, the nanometric size of CeO_x and the presence of +III and +IV oxidation states are adequate traits for observation of the photocatalytic activity of ceria derived from the semiconducting properties. Nevertheless, the fact that the stoichiometry is far from CeO₂ in our samples, is the reason why we prefer to denote our samples as CeO_x.

4.3.1. Photocatalytic activity

The purpose of this study is to prepare novel photocatalysts in which the metal oxide NPs are in intimate contact with G layers to assess whether or not these materials exhibit enhanced photocatalytic activity for oxygen generation from water using Ag⁺ as sacrificial electron acceptor. Aimed at this purpose, we have included in our study commercial ceria NPs and carried out the photocatalytic tests using a xenon lamp emitting UV and visible radiation. Prior to their photocatalytic evaluation, the samples were submitted to sonication for periods longer than 1 h. This sonication has been found to be crucial to produce exfoliation of the graphenic layers leading to mono- or few-layers G. This process of exfoliation can be conveniently followed by AFM microscopy where the number of layers in the exfoliation material can be determined. In particular, AFM images (Figure 4.5) show micrometric domains of G layers in agreement with the effect of the sonication producing exfoliation of the as-synthesized G materials.

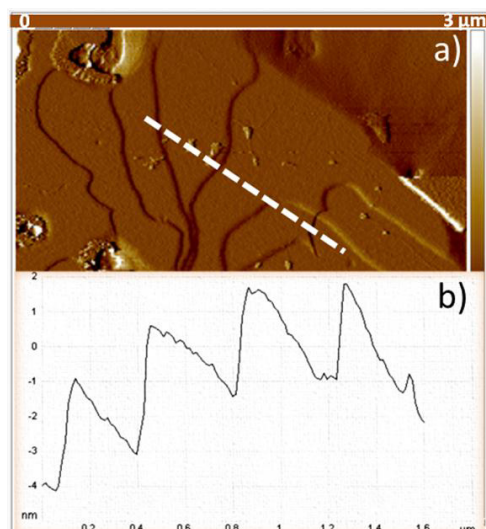


Figure 4.5. a) AFM image taken for the $(\text{CeO}_x\text{-G})_A$ sample after 1 h sonication in which the presence large micrometric G sheets can be observed and b) shows the vertical height along the lines shown in panel A.

4.3.2. Oxygen generation by photocatalytic water oxidation

As it can be seen (Fig. 4.6), all the ceria samples exhibit photocatalytic activity for water oxidation, but the percentage of G and the pyrolysis temperature determine the different photocatalytic activity of the resulting samples. When the G percentage is low, the photocatalytic activity of the resulting sample is comparable to that of commercial CeO_2 . However, when the G percentage is higher, the photocatalytic activity of the CeO_x/G composite, measured as initial reaction rate or by total amount of oxygen evolved at final time, is significantly higher than that of the CeO_2 as control. We have also observed a strong influence of the pyrolysis temperature on the photocatalytic activity, the optimal material of the series being the one in which the pyrolysis temperature was performed at 900 °C. In the case of TiO_2 , it has also been found that the optimal G percentage was in the range between 1 and 5 wt% and also in this case the

preparation conditions influence the improvement of the photocatalytic activity [11,12]. In the present case, the most efficient composite for photocatalytic oxygen generation in the presence of Ag^+ was determined when the percentage of carbon was 2.5 wt %. The results obtained (Fig. 4.6) are in line with those previously found for TiO_2 [26], but in this case they refer to the oxygen evolution by water oxidation, thus, complementing the results reported for the photocatalytic water reduction using TiO_2 as metal oxide semiconductor. Following the rationalization accepted for TiO_2/G composites and illustrated in Scheme 4.1 [11, 12], the most reasonable justification to understand the influence of G on the photocatalytic activity of CeO_x is that due to the intimate contact between the two components, photoinduced charge separation is enhanced for CeO_x/G with respect to CeO_x .

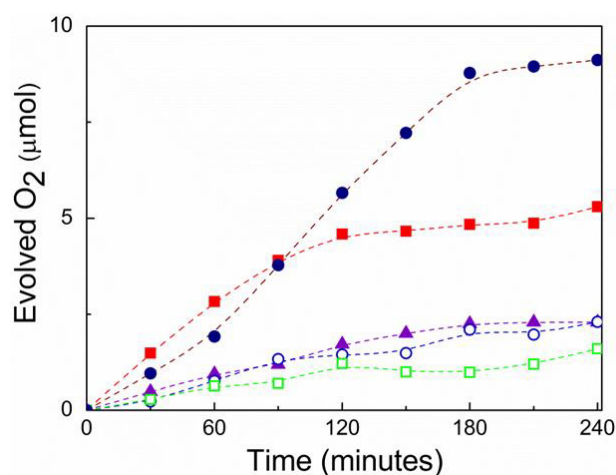


Figure 4.6. Oxygen evolved in the photocatalytic water oxidation using different CeO_x -G samples as photocatalysts and CeO_2 from Aldrich as reference, ● : $(\text{CeO}_2/\text{G})_A$, ■ : $(\text{CeO}_2/\text{G})_B$, ○ : $(\text{CeO}_2/\text{G})_C$, □ : $(\text{CeO}_2/\text{G})_D$, ▲ : CeO_2 from Sigma Aldrich. Irradiation conditions: 0.1 M AgNO_3 as sacrificial electron acceptor, 25 mL of water, 20 mg of catalyst, Xe lamp (150 W).

After light absorption by CeOx semiconductor and promotion of an electron to the CeOx conduction band (CB), some of these electrons would be transferred to G. Migration of the electrons from CeOx to G will prolong the lifetime of charge separations and will increase the probability of the photocatalytic event. In support of this proposal, it should be recalled that the CB energy of CeO₂ NPs is very close to that of TiO₂ anatase [27], for which this e⁻ migration from the semiconductor CB to G is widely accepted [28, 29]. It is also worth to comment that abundant precedents in the literature have shown that while G-based materials acting as photocatalysts are able to reduce water to H₂, none of these materials are able to oxidize water to oxygen [30-32]. Thus, it seems that the positive h⁺ should not migrate to G since otherwise, these h⁺ will not be able to effect H₂O oxidation.

When putting the values of O₂ evolution obtained (Fig. 4.6) into context, it should be considered that the samples do not contain noble metal or other co-catalyst and also that oxygen generation is thermodynamically and kinetically less favorable than hydrogen formation [33, 34]. Therefore, the data shown (Fig. 6) are among the most active photocatalysts for oxygen generation from water in the presence of sacrificial electron acceptors under UV irradiation.

4.4. Conclusions

In the present chapter it was shown that CeOx NP embedded on a graphitic carbon matrix can be prepared in a single step by pyrolysis of cerium alginate conveniently dried. These samples can be adequately exfoliated by sonication and the resulting CeOx/G suspension behave as enhanced photocatalyst for water oxidation using Ag⁺ ions as sacrificial

electron acceptor. Depending on the preparation conditions, the photocatalytic activity varies considerably by around one order of magnitude, the best conditions were found for the material in where the composition is 2.5 wt% of G that has been obtained by pyrolysis at 900 °C. This optimized material performed three times better than commercial CeO₂ NPs. This work illustrates the advantages of using a natural biopolymer as template in the preparation of photocatalysts. These biopolymers can not only control the particle size and surface functional groups, but also can provide graphitic residue precursors of G to enhance the photocatalytic activity.

4.5 References

- [1] Daghrir, R., Drogui, P., Robert, D., *Ind. Eng. Chem. Res.* **2013**, *52*, 3581-3599.
- [2] Subramanian, V., Wolf, E. E., Kamat, P. V., *Langmuir* **2003**, *19*, 469-474.
- [3] Xu, H., Wang, W., Zhu, W., *J. Phys. Chem. B* **2006**, *110*, 13829-13834.
- [4] Jiang, X., Wang, T., *Environ. Sci. Technol.* **2007**, *41*, 4441-4446.
- [5] Andersson, M., Österlund, L., Ljungström, S., Palmqvist, A., *J. Phys. Chem. B* **2002**, *106*, 10674-10679.
- [6] Peng, T., Zhao, D., Dai, K., Shi, W., Hirao, K., *J. Phys. Chem. B* **2005**, *109*, 4947-4952.
- [7] Primo, A., Marino, T., Corma, A., Molinari, R., García, H., *J. Am. Chem. Soc* **2011**, *133*, 6930-6933.
- [8] Buaki-Sogo, M., Serra, M., Primo, A., Alvaro, M., García, H., *Chemcatchem* **2013**, *5*, 513-518.

-
- [9] Luo, Q., Bao, L., Wang, D., Li, X., An, J., *J. Phys. Chem. C* **2012**, *116*, 25806-25815.
- [10] Liu, X., Gao, Y., Cao, C., Luo, H., Wang, W., *Langmuir* **2010**, *26*, 7671-7674.
- [11] Zhang, Y., Tang, Z. R., Fu, X., Xu, Y. J., *ACS Nano* **2010**, *4*, 7303-7314.
- [12] Williams, G., Seger, B., Kamat, P. V., *ACS Nano* **2008**, *2*, 1487-1491.
- [13] Linsebigler, A. L., Lu, G., Yates, J. T., *Chem. Rev.* **1995**, *95*, 735-758.
- [14] Ouwerx, C., Velings, N., Mestdagh, M. M., Axelos, M. A. V., *Polym. gels netw.* **1998**, *6*, 393-408.
- [15] Wang, Z. Y., Zhang, Q. Z., Konno, M., Saito, S., *Biopolymers* **1993**, *33*, 703-711.
- [16] Primo, A., Forneli, A., Corma, A., Garcia, H., *Chemsuschem* **2012**, *5*, 2207-2214.
- [17] Primo, A., Atienzar, P., E., S., Delgado, J. M., García, H., *Chem. Commun.* **2012**, *48*, 9254-9256.
- [18] Ferrari, A. C., Basko, D. M., *Nat. Nanotechnol.* **2013**, *8*, 235-246.
- [19] Inguanta, R., Piazza, S., Sunseri, C., *Nanotechnology* **2007**, *18*, 485605
- [20] Martínez-Arias, A., Gamarra, D., Fernández-García, M., Wang, X. Q., Hanson, J. C., Rodriguez, J. A., *J. Catal.* **2006**, *240*, 1-7.
- [21] Shan, W., Feng, Z., Li, Z., Zhang, J., Shen, W., Li, C., *J. Catal.* **2004**, *228*, 206-217.

- [22] Ferreira, A. C., Ferraria, A. M., Botelho do Rego, A. M., Gonçalves, A. P., Girao, A. V., Correia, R., Gasche, T. A., Branco, J. B., *J. Mol. Catal. A-Chem* **2010**, *320*, 47-55.
- [23] Abellán, G., Latorre-Sánchez, M., Fornés, V., Ribera, A., García, H., *Chem. Commun.* **2012**, *48*, 11416-11418.
- [24] Skorodumova, N. V., Ahuja, R., Simak, S. I., Abrikosov, I. A., Johansson, B., Lundqvist, B. I., *Phys. Rev. B* **2001**, *64*, 1151081-1151089.
- [25] Abad, A., Concepción, P., Corma, A., García, H., *Angew. Chem. Int. Ed.* **2005**, *44*, 4066-4069.
- [26] Gomes Silva, C., Juárez, R., Marino, T., Molinari, R., García, H., *J. Am. Chem. Soc* **2011**, *133*, 595-602.
- [27] Corma, A., Atienzar, P., García, H., Chane-Ching, J., *Nat. Mat.* **2004**, *3*, 394-397.
- [28] Zhang, J., Zhu, Z., Tang, Y., Fenq, X., *J. Mater. Chem. A* **2013**, *1*, 3752-3756.
- [29] Zhang, H., Lv, X., Li, Y., Wang, Y., Li, J., *ACS Nano* **2010**, *4*, 380-386.
- [30] Hau Ng, Y., Iwase, A., Kudo, A., Amal, R., *J. Phys. Chem. Lett.* **2010**, *1*, 2607-2612.
- [31] Zhang, X. Y., Li, H. P., Cui, X. L., Lin, Y., *J. Mater. Chem.* **2010**, *20*, 2801-2806.
- [32] Iwase, A., Hau Ng, Y., Ishiguro, Y., Kudo, A., Amal, R., *J. Am. Chem. Soc* **2011**, *133*, 11054-11057.
- [33] Graetzel, M., *Acc. Chem. Res.* **1981**, *14*, 376-384.
- [34] Hoganson, W., Babcock, G. T., *Science* **1997**, *277*, 1953-1956.

5

Preparation of Graphene Quantum Dots from Pyrolyzed Alginate^(*)

(*) P. Atienzar, A. Primo, C. Lavorato, R. Molinari and H. García.
Langmuir 2013, 29, 6141–6146.

5.1 Introduction

Graphene (G) being one atom thick layer of extended sp^2 carbons represents the limit of the thinnest possible 2D conductive surface [1,2], exhibiting very fast electron mobility and high charge carrier density [3]. One of the most convenient procedures for the preparation of G suspensions consists in the deep oxidation of graphite flakes followed by exfoliation of the resulting graphite oxide by sonication in the appropriate solvent and reconstitution of G by reduction of the dispersed graphene oxide (GO) [4–6]. While this methodology enjoys high reproducibility and can produce highly concentrated aqueous suspensions of GO (about 0.1 mg L^{-1}), the materials present in the suspensions are typically constituted by micrometric sheets of nanometric thickness. Because of the remarkable properties derived from 2D confinement at the nanoscale caused by the effect of the edges, G quantum dots (GQDs) exhibit new properties such as emission and their behavior as spin qubit with collective spin states [7,8]. Recent reviews have summarized the unique properties of

GQDs [9–14]. It is, therefore, very important to develop reliable and efficient procedures for the preparation of GQDs to exploit their unique properties arising from confinement. Unfortunately, graphite oxidation and exfoliation is not a suitable procedure to obtain GQDs, since it fails to provide nanometric sheets that have a large tendency to undergo complete oxidation to CO₂ and other alternative procedures have to be implemented. For this reason GQDs have to be prepared in alternative ways, such as for instance by acid-catalyzed microwave pyrolysis of carbon precursors [15]. Because of their size, GQDs form persistent dispersions in different solvents and may have large biomedical application due to the possibility to cross cellular membranes [16]. Also, GQDs have attracted considerable attention as emerging fluorescent dots for bioimaging, sensing [17], pollutant removal [18], and even in photovoltaic devices [19]. GQDs also hold promise in catalysis due to their large surface area and accessibility of the active sites [20]. In the present chapter is reported an innovative and efficient preparation of GQDs of tunable dimensions and describe the unique photophysical properties GQD suspensions.

5.2 Experimental section

5.2.1 Synthesis of graphene [G] quantum dots

Alginate sodium salt beads from brown algae (commercially available from Sigma) were pyrolyzed in argon atmosphere using the following oven program: 200 °C during 2 h for annealing and then heating at 10 °C/min up to 900 °C for 6 h. This multilayer graphitic powder is stirred magnetically in water or acetonitrile in a quartz cuvette and exposed to the pulses from the second harmonic of a Nd:YAG laser (50–130 mJ pulse⁻¹). The suspension becomes increasing black as the time of the laser ablation

increases. After the treatment, the supernatant was collected by decantation and characterized by UV–vis optical spectroscopy using a Cary 5G spectrophotometer. Raman spectra were recorded after solvent evaporation by casting a drop of the suspension on a glass substrate. XRD patterns of the pyrolyzed alginate beads were recorded by milling the beads and compressing the powder in the corresponding sample holder. XRD patterns were recorded on a Philips Cubix Pro using Cu K α radiation at 45 kV and 40 mA in the 2 θ range from 5° to 70°.

5.2.2 Textural and analytical properties measurements

Raman spectra were recorded at ambient temperature with 514 nm laser excitation by using a Renishaw In Via Raman spectrometer equipped with a CCD detector.

TEM images were recorded in a Philips CM300 FEG system with an operating voltage of 100 kV. XPS spectra were recorded on a SPECS spectrometer equipped with a Phoibos 150 9MCD detector using a nonmonochromatic X-ray source (Al and Mg) operating at 200 W. The samples were evacuated in the prechamber of the spectrometer at 1×10^{-9} mbar. Some of the samples have been activated in situ in nitrogen flow at 450 °C for 3 h followed by evacuation at 10^{-8} mbar. The measured intensity ratio of components was obtained from the area of the corresponding peaks after nonlinear Shirley-type background subtraction and corrected by the transmission function of the spectrometer. The atomic force microscopic measurements were conducted using contact mode in air at ambient temperature using a Veeco AFM apparatus. Laser ablation was carried out using a second-harmonic output of Nd:YAG laser from Spectra Physics operating a 1 Hz. The pyrolyzed alginate beads were

placed in a septum-capped $1 \times 1 \text{ cm}^2$ quartz cuvette that was magnetically stirred while ablated. After the required time, an aliquot of the suspension (100 μL) was filtered and analyzed by optical spectroscopy. Emission and excitation spectra were recorded in a PTI spectrofluorimeter having Czerny Turner monochromators. Transient spectra were recorded using a Luzchem laser flash photolysis apparatus. The experiment was controlled by a computer that controlled data acquisition and provided data storage capability. The samples were submitted to N_2 purging at least 15 min before the experiments.

5.3 Results and discussion

Recently was reported that pyrolysis of natural chitosan can form G films on various supports [21]. On the basis of this finding, we performed the pyrolysis of millimetric alginate beads at 900 °C to form graphitic carbon residues. XRD patterns of these alginate-derived carbons show that pyrolyzed alginate beads have a tendency to form graphitic carbons, although the broadness of the peak at 23° indicates low crystallinity and loose z-stacking compared to graphite (Figure 5.1). Similar observations that pyrolysis of alginate form graphitic carbons have been already reported in the literature [22].

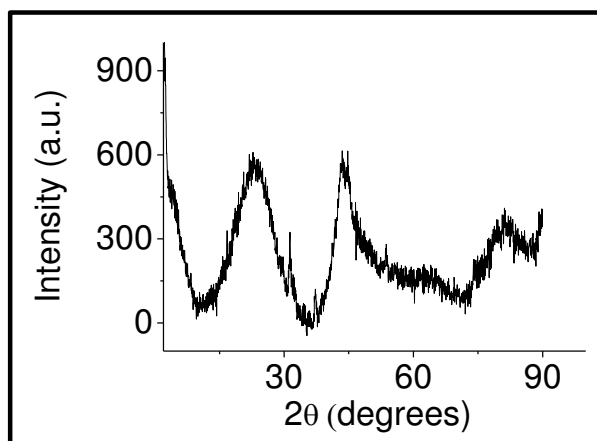


Figure 5.1 XRD pattern of the alginate derived carbon obtained by pyrolysis at 900°C

When carbon residues from alginate were submitted to ablation in a solvent using 532 nm laser pulses, an increasing darkening of the liquid phase is observed. Figure 5.2 shows the increasing intensity of the optical UV–vis absorption spectra of acetonitrile upon 532 nm laser ablation of the alginate derived carbon in contact with this solvent, suggesting that some carbon residue is detached from the submillimetric solid carbon beads, becoming suspended in the liquid phase. We noticed that the region 200–300 nm (not shown in Figure 5.2) contain some fine structure in the optical spectra that could correspond to the liberation of small condensed polycyclic aromatic compounds during laser ablation. The 300–800 nm show an increasing absorption intensity of the liquid phase upon prolonging the laser treatment, indicating that the extent of graphitic debris in the solution increases over the time.

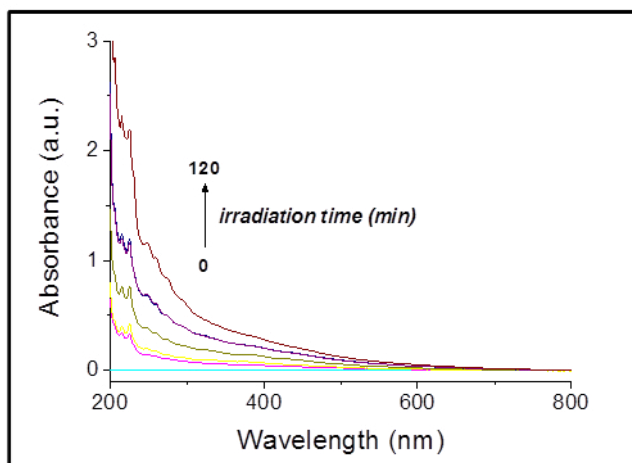


Figure 5.2. UV-Vis spectra of acetonitrile in contact with alginate-derived carbon beads that has been ablated with 532 nm nanosecond laser pulses for an increasing time (0, 30, 60, 90 and 120 min).

In related precedents it has been reported that λ_{\max} depends on the size of the GQD. The fact that Figure 5.2 does not show these variations suggests that in the present case there is a polydispersity in the size distribution that does not allow to discriminate the average size by optical spectroscopy [9]. The presence of G dispersed in acetonitrile was confirmed by Raman spectroscopy of the residue resulting after removing acetonitrile by evaporation where the presence of the two peaks corresponding to the G and D bands of graphene at 1600 and 1360 cm^{-1} was observed (Figure 5.3a). The large intensity of the D band observed in Figure 5.3a could be related to the presence of defects associated with the small particle size and the relative large contribution of functional groups in the periphery of the particles. XP spectroscopy can monitor the energy of the core electrons of the elements present in the carbon residue. The XP spectra of the material resulting after laser ablation are also compatible with the presence of G in the acetonitrile dispersion, showing the C 1s peak

characteristic of G (Figure 5.3b). Deconvolution of the experimental C 1s peak suggests the presence of two components at 284.8 and 287.4 eV binding energies that are compatible with the assignment to graphitic and carboxylic carbons, respectively. The large proportion of carboxylic carbons (~15%) in comparison with other G samples suggests the small dimension of the G residue, being compatible with a large ratio between periphery and internal carbons as observed in microscopy.

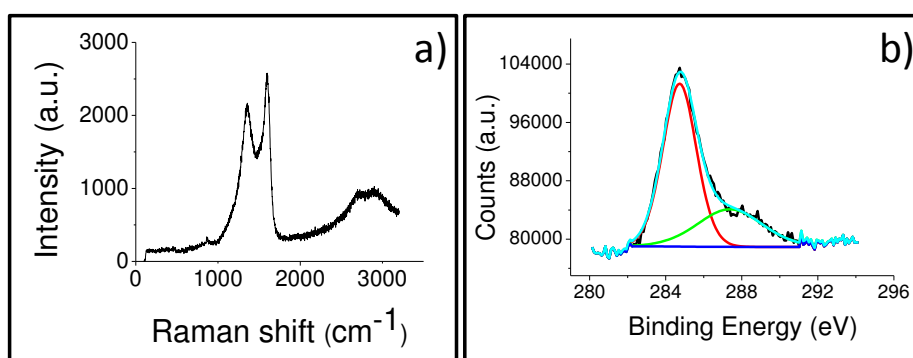


Figure 5.3. a) Raman spectra and b) C 1s XPS peak of the alginate derived carbon after pyrolysis at 900 °C. Note in Raman spectra the presence of characteristic 2D band at about 2500 cm^{-1} that is characteristic of highly crystalline G samples. The experimental C1s peak has been fitted to two components of binding energies of 284.8 and 287.4 eV, respectively.

AFM and TEM images of the carbon residue present in acetonitrile after laser ablation were crucial to show the presence of GQD flakes with small dimensions. The average number of layers of the GQD and the dimensions of the flakes decrease along the number of laser pulses, suggesting that the initial suspended graphitic debris of small dimensions is undergoing further exfoliation in acetonitrile. While the nanoparticles present at initial stages of the ablation process can be better considered as graphitic

quantum dots, the decrease in the number of layers upon increasing the number of laser shots leads to few-layers GQDs. In fact, the graphitic debris present at shorter laser ablation treatments exhibits a larger dispersion in sizes and number of layers, while as the ablation time increases the colloidal particles tend to be GQDs of narrower particle size. Figure 5.4 shows illustrative AFM images of the type of material present in acetonitrile solution by ablation of the alginate-derived carbons as a function of the photolysis time.

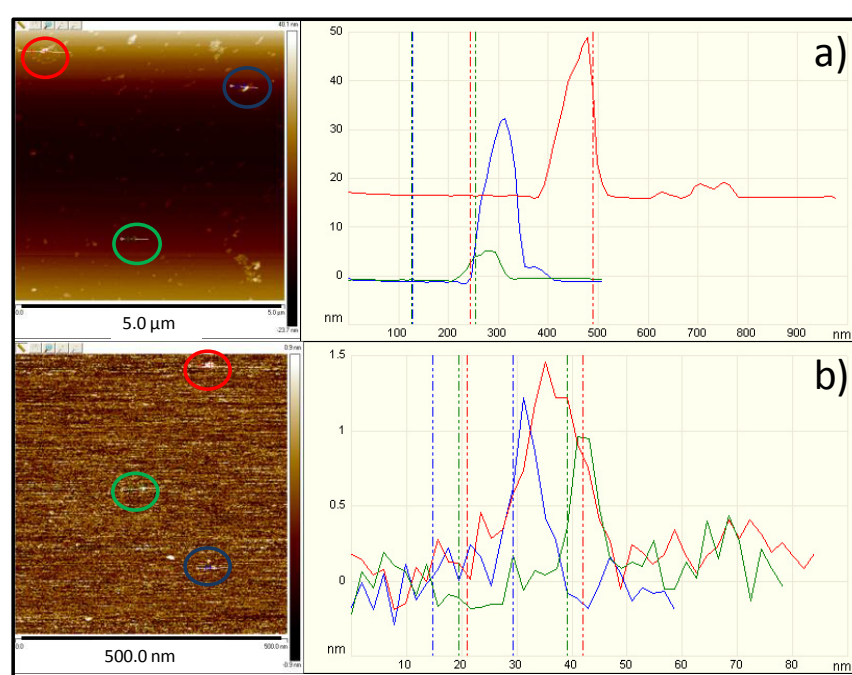


Figure 5.4. AFM images (left) and corresponding height profile (right) measured for the GQD flakes present in acetonitrile suspension after 5 min (a) and 40 min (b) ablation time. The circles indicate the particles that have been monitored and each particle has been identified by the same color in the left and right side.

Thus, graphitic debris at 5 min of laser exposure consisted in particles of about 100 nm length and from 5 to 30 nm thickness, corresponding to

multilayer G flakes. At 40 min ablation, acetonitrile contained mostly GQDs of 10–20 nm length with 1–1.5 nm depth on average corresponding to single or few layer GQDs. A rough estimation of an apparent quantum yield of GQD formation based on the 60 min irradiation at 10 Hz assuming the complete exfoliation of 1.5 mg of precursor indicates that each pulse forms about 1010 GQD considering an average 20 nm size. Electron diffraction of the material present in acetonitrile shows the polycrystalline nature of the sample indicating that the suspended carbon residue corresponds to small particles of well-defined G layers (Figure 5.5a). TEM image shows the expected morphology for the GQD material present in acetonitrile (Figure 5.5b). The information provided in Figure 5.5 is crucial to firmly support that the carbon debris present in the liquid phase after laser ablation is crystalline and has the structure of G, although its dimensions are small.

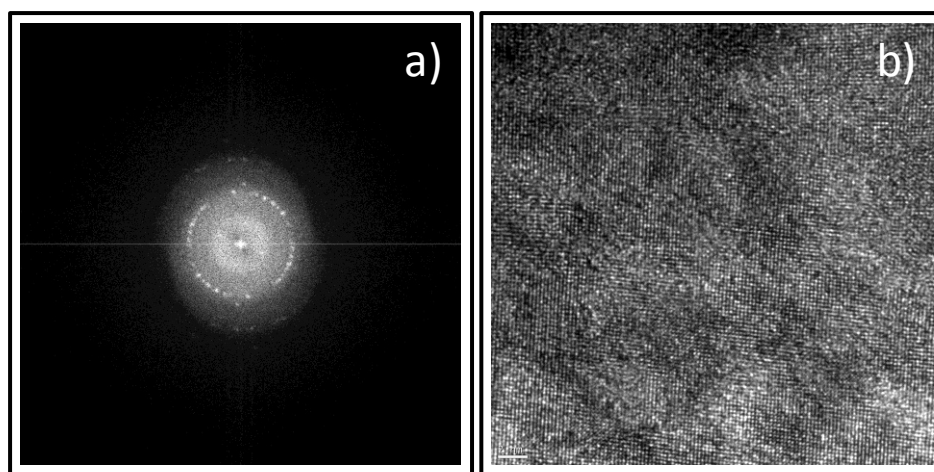


Figure 5.5. Electron diffraction (a) and high resolution TEM image (b) of the GQD dissolved in acetonitrile after 532 nm laser ablation for 40 min.

The same behavior commented for acetonitrile was also observed when the laser ablation was performed using water and ethanol as solvents, indicating that the procedure appears general for the preparation of persistent dispersions of GQDs in a liquid phase. Moreover, no influence of the suspension temperature was observed, and identical results in terms of variation of the optical spectrum were observed when the laser ablation was carried out at 60 °C.

On the basis of the reported formation of G by pyrolysis of alginate [22], the graphitic nature of the alginate-derived carbon residues, and the previous reports on the literature about graphite exfoliation by laser ablation [23], we propose that, in the present case, laser ablation is causing exfoliation of graphitic debris from submillimetric pyrolyzed alginate beads in the form of small GQDs that become easily suspended in the liquid phase. Considering that alginate is a biomass waste, the present finding constitutes a remarkable example of biomass valorization by transforming this waste into a material of high added value.

It has been reported that GQDs can exhibit blue emission [24–26], although the intensity of the emission increases upon surface passivation by appropriate functionalization with poly(ethylene glycol) or suitable groups [27,28]. In the present case, we have observed that the GQDs prepared by laser ablation from pyrolyzed alginate also emit. Since the emission intensity in water can be somewhat lower due to some quenching, acetonitrile was selected to determine the photoluminescence properties of GQDs prepared here. In contrast, G sheets obtained by sonication of pyrolyzed alginate beads do not exhibit any emission even in acetonitrile. The key features of the emission are that (i) the emission maximum depends, particularly for larger GQD particles, on the excitation

wavelength and (ii) there is a notable influence of the size and ablation time on the emission that increases in intensity as the GQD size decreases. The first feature can be interpreted as indicating a large inhomogeneity in the GQD samples that at initial times would be constituted by a range of graphitic debris, each particular quantum dot being excited preferentially at a particular wavelength. The second property, i.e., the increase of photoluminescence intensity with the ablation time, can be related to the decrease in the average size of the GQD, since photoluminescence is an intrinsic property of small G sheets. Figure 5.6 illustrates these two emission features that are indicative of the quantum confinement of the exciton, the most emissive GQD sample being the one obtained at the longest ablation time that exhibits a fluorescence peak at 430 nm after excitation at 350 nm.

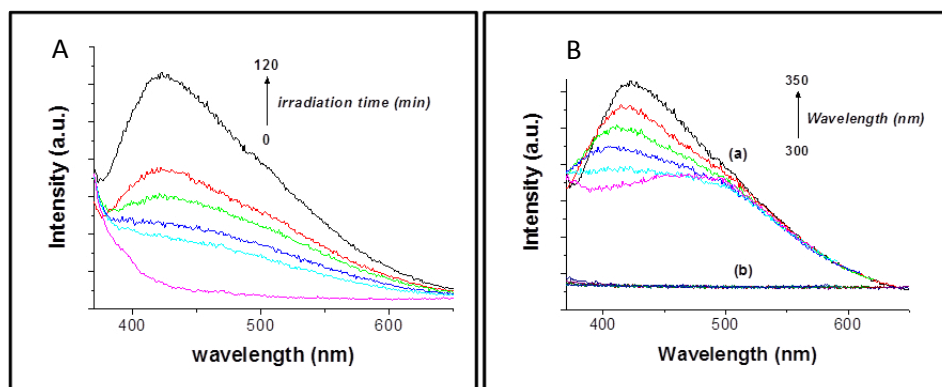


Figure 5.6. A) Fluorescence spectra of acetonitrile solutions of GQDs after excitation at 350 nm obtained from pyrolysed alginate upon increasing the laser exposure for 0, 5, 10, 20, 40 and 120 min. B) Fluorescence spectra of an acetonitrile solution of GQD after irradiation for 120 min as a function of the excitation wavelength from 300 to 350 nm every 10 nm.

Worth noting is that some of the samples whose photoluminescence is shown in Figure 5.6 are the same than those whose absorption spectra are presented in Figure 5.2. Excitation spectra of the emission monitoring at wavelengths in the range of 390–510 nm for the GQD sample prepared at the longest ablation time are shown in Figure 5.7. As can be seen there, the excitation spectra vary with the emission wavelength, indicating that photoluminescence peaks arise from different emitting species. It is worth noting that Figures 5.2 and 5.6 can be used to follow in a simple way the progress of the formation of GQDs from pyrolyzed alginate beads and the decrease in the particle size. Typically, the emission intensity in GQDs should change with the average particle size. The fact that no much variation in the position of the λ_{em} is observed as a function of the time could be again related to the polydispersity of the GQDs. Nevertheless, we performed the corresponding excitation spectra at different emission wavelengths for samples after the longest ablation time. Figure 5.7 presents these spectra. A clear red-shift in the position of λ_{ex} as a function of the emission wavelength provides support to the distribution of the particle size observed by imaging techniques.

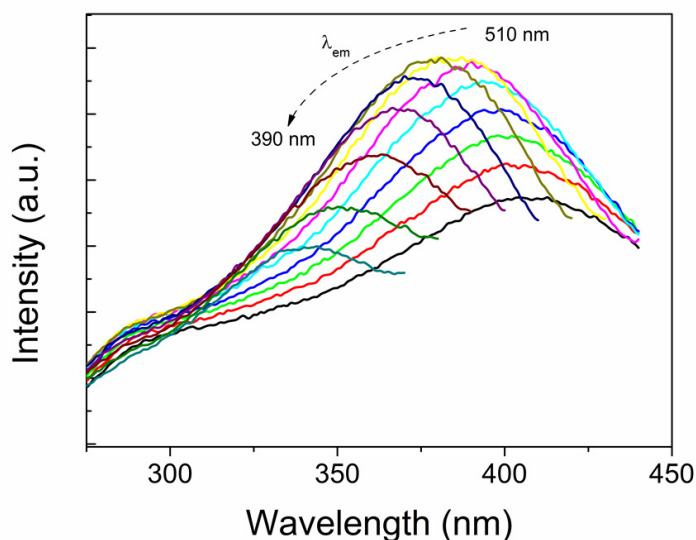


Figure 5.7. Excitation spectra monitoring different emission wavelengths (indicated in the plot) recorded for an acetonitrile solution of GQDs obtained after 120 min ablation time.

To gain understanding on the photophysics of the GQDs prepared in the present study, the samples were also studied by transient absorption spectroscopy. 532 nm excitation of a GQD solution in acetonitrile allows the detection of a transient spectrum characterized by a continuous absorption in the entire monitored wavelength range (Figure 5.8). The temporal profile of the signals was coincident at all wavelengths, suggesting that these spectra correspond to a single species (inset of Figure 5.8). The signal decay shows two regimes, one of them decaying faster in less than 1 μ s, followed by a slower decay taking place in tens of microseconds. The relative contribution of these two regimes can be estimated from the relative intensity of the signals immediately after the laser pulse and after 1 μ s as 80 and 20%, respectively.

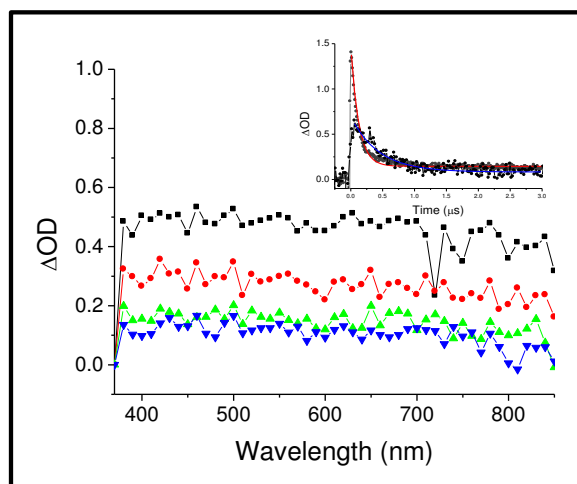


Figure 5.8. Transient spectra recorded at 0.21 (■), 0.61 (●), 1.01 (▲) and 1.41 μ s (▼) after 532 nm laser excitation of an Ar-purged acetonitrile solution of GQD. The inset shows the signal decay monitored at 500 nm of a Ar purged solution.

On the basis of the precedents reported in the literature about this continuous transient absorption [29], we attribute this species to a charge separation state with the generation of electrons in the upper conduction band and positive holes in the occupied molecular orbitals of the highest energies. In support of this assignment, the signal intensity grows upon addition of methanol and decreases upon oxygen quenching. The temporal profile would be indicative of, at least, two main deactivation mechanisms, probably by recombination of geminate electrons and holes (fast decay) or annihilation after migration of the charges away from the initial point of charge separation and subsequent recombination after random walk. It should be, however, commented that controls submitting to transient spectroscopy analogous suspensions of G sheets obtained by exfoliation of pyrolyzed alginate beads also exhibit similar transient spectra, although lacking the shortest component of the signal and reaching lower intensity. Therefore, it seems that these microsecond

transients attributable to charge separation are not specific of GQDs and should not be responsible for the emission that could probably arise from much shorter lived species. In fact, the emission lifetime of the GQDs (estimated by fitting the temporal profile to a single-exponential decay) varies somewhat depending on the monitored emission wavelength in the range of 390–510 nm, being relatively independent of the ablation time (see inset of Figure 5.9). This emission varies in the range of 5–10 ns that should overlap, but it does not coincide, with the shortest regime observed in laser flash photolysis. Thus, although the system is very complex due to the polydispersity of the sample, it is clear that emissive species can only be present in the first microsecond after the laser pulse.

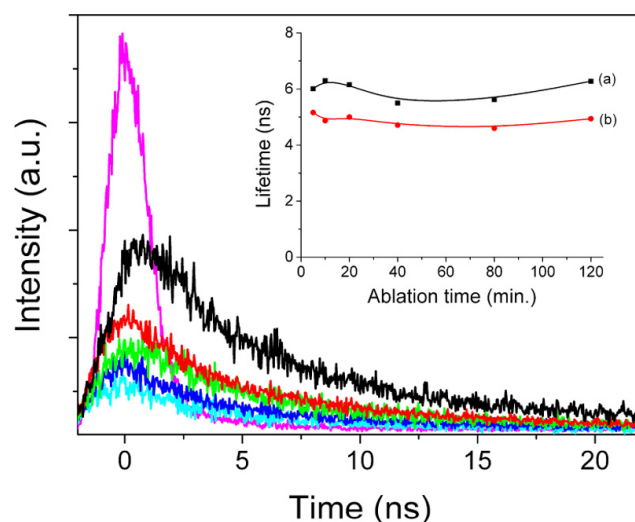


Figure 5.9. Temporal profile of the emission monitored at 500 nm upon 350 nm excitation for a series of GQDs. The profiles correspond (from top to bottom) to the samples obtained after 5 (cyan), 10 (blue) 20 (green), 40 (red), and 120 min (black) laser ablation treatment. The shortest pink plot corresponds to the profile of the lamp. The decrease in emission intensity should be attributed to the shift in the λ_{exc} excitation wavelength as observed in Figure 5.6. Inset: emission lifetime estimated from the best fitting to a monoexponential decay of the emission signal monitored at 500 (a) or 430 (b) nm.

5.4 Conclusions

In summary, due to the loose packing of the graphitic carbon material resulting upon pyrolysis of alginate particles, as indicated by the broad XRD peaks, laser ablation in acetonitrile, water, or other solvents results in the leaching of small carbon debris from the solid to the solution. The process can be followed by different spectroscopic and imaging techniques that show that the amount of leached carbon debris increases upon laser exposure and that the morphology of these residues tends to GQDs by reducing the dimensions of the sheets and by increasing exfoliation. The resulting GQDs exhibit photoluminescence as a function of the ablation time, increasing in intensity as the ablation time increases. Thus, this study shows a convenient protocol to obtain GQDs from pyrolyzed alginate allowing a certain control on the size and properties of these nanoparticles.

5.5 References

- [1] Geim, A. K.; Novoselov, K. S. The rise of graphene. *Nat. Mater.* **2007**, 6, 183–191.
- [2] Novoselov, K. S.; Geim, A. K.; Morozov, S. V.; Jiang, D.; Zhang, Y.; Dubonos, S. V.; Grigorieva, I. V.; Firsov, A. A. Electric field effect in atomically thin carbon films. *Science*, **2004**, 306, 666–669.
- [3] Bolotin, K. I.; Sikes, K. J.; Jiang, Z.; Klima, M.; Fudenberg, G.; Hone, J.; Kim, P.; Stormer, H. L. Ultrahigh electron mobility in suspended graphene. *Solid State Commun.* **2008**, 146, 351–355.
- [4] Park, S.; Ruoff, R. S. Chemical methods for the production of graphenes. *Nat. Nanotechnol.* **2009**, 4, 217–224.

-
- [5] Stankovich, S.; Dikin, D. A.; Piner, R. D.; Kohlhaas, K. A.; Kleinhammes, A.; Jia, Y.; Wu, Y.; Nguyen, S. T.; Ruoff, R. S. Synthesis of graphene-based nanosheets via chemical reduction of exfoliated graphite oxide. *Carbon*, **2007**, 45, 1558–1565.
- [6] Zhu, Y. W.; Murali, S.; Cai, W. W.; Li, X. S.; Suk, J. W.; Potts, J. R.; Ruoff, R. S. Graphene and graphene oxide: Synthesis, properties, and applications. *Adv. Mater.* **2010**, 22, 3906–3924.
- [7] Ponomarenko, L. A.; Schedin, F.; Katsnelson, M. I.; Yang, R.; Hill, E. W.; Novoselov, K. S.; Geim, A. K. Chaotic Dirac billiard in graphene quantum dots. *Science*, **2008**, 320, 356–358.
- [8] Trauzettel, B.; Bulaev, D. V.; Loss, D.; Burkard, G. Spin qubits in graphene quantum dots. *Nat. Phys.* **2007**, 3, 192–196.
- [9] Baker, S. N.; Baker, G. A. Luminescent carbon nanodots: Emergent nanolights. *Angew. Chem., Int. Ed.* 2010, 49 (38), 6726–6744.
- [10] Cao, L.; Meziani, M. J.; Sahu, S.; Sun, Y. P. Photoluminescence properties of graphene versus other carbon nanomaterials. *Acc. Chem. Res.* **2013**, 46 (1), 171–180.
- [11] Jiang, H. J. Chemical preparation of graphene-based nanomaterials and their applications in chemical and biological sensors. *Small* **2011**, 7 (17), 2413–2427.
- [12] Recher, P.; Trauzettel, B. Quantum dots and spin qubits in graphene. *Nanotechnology* **2010**, 21 (30).
- [13] Rozhkov, A. V.; Giavaras, G.; Bliokh, Y. P.; Freilikher, V.; Nori, F. Electronic properties of mesoscopic graphene structures: Charge confinement and control of spin and charge transport. *Phys. Rep.* **2011**, 503 (2–3), 77–114.

- [14] Sheng, W. D.; Korkusinski, M.; Guclu, A. D.; Zielinski, M.; Potasz, P.; Kadantsev, E. S.; Voznyy, O.; Hawrylak, P. Electronic and optical properties of semiconductor and graphene quantum dots. *Front. Phys.* **2012**, 7 (3), 328–352.
- [15] Liu, S.; Wang, L.; Tian, J.; Zhai, J.; Luo, Y.; Lu, W.; Sun, X. Acid-driven, microwave-assisted production of photoluminescent carbon nitride dots from N,N-dimethylformamide. *RSC Adv.* **2011**, 1 (6), 951–953.
- [16] Markovic, Z. M.; Ristic, B. Z.; Arsić, K. M.; Klisić, D. G.; Harhaji-Trajković, L. M.; Todorović-Marković, B. M.; Kepić, D. P.; Kravić-Stević, T. K.; Jovanović, S. P.; Milenković, M. M.; Milivojević, D. D.; Bumbasirević, V. Z.; Dramićanin, M. D.; Trajković, V. S. Graphene quantum dots as autophagy-inducing photodynamic agents. *Biomaterials* **2012**, 33, 7084–7092.
- [17] Lu, W.; Qin, X.; Liu, S.; Chang, G.; Zhang, Y.; Luo, Y.; Asiri, A. M.; Al-Youbi, A. O.; Sun, X. Economical, green synthesis of fluorescent carbon nanoparticles and their use as probes for sensitive and selective detection of mercury(II) ions. *Anal. Chem.* **2012**, 84 (12), 5351–5357.
- [18] Liu, S.; Tian, J.; Wang, L.; Zhang, Y.; Luo, Y.; Asiri, A. M.; Al-Youbi, A. O.; Sun, X. A novel acid-driven, microwave-assisted, one-pot strategy toward rapid production of graphitic N-doped carbon nanoparticles-decorated carbon flakes from N,N-dimethylformamide and their application in removal of dye from water. *RSC Adv.* **2012**, 2 (11), 4632–4635.

- [19] Shen, J.; Zhu, Y.; Yang, X.; Li, C. Graphene quantum dots: emergent nanolights for bioimaging, sensors, catalysis and photovoltaic devices. *Chem. Commun.* **2012**, 48, 3686–3699.
- [20] Liu, S.; Tian, J.; Wang, L.; Luo, Y.; Sun, X. A general strategy for the production of photoluminescent carbon nitride dots from organic amines and their application as novel peroxidase-like catalysts for colorimetric detection of H₂O₂ and glucose. *RSC Adv.* **2012**, 2 (2), 411–413.
- [21] Primo, A.; Atienzar, P.; Sánchez, E.; Delgado, J. M.; García, H. From biomass wastes to large-area, high-quality, N-doped graphene: catalyst-free carbonization of chitosan coatings on arbitrary substrates. *Chem. Commun.* **2012**, 48, 9254–9256.
- [22] Primo, A.; Forneli, A.; Corma, A.; García, H. From biomass wastes to highly efficient CO₂ adsorbents: Graphitisation of chitosan and alginate biopolymers. *ChemSusChem* **2012**, 5, 2207–2214.
- [23] Qian, M.; Zhou, Y. S.; Gao, Y.; Feng, T.; Sun, Z.; Jiang, L.; Lu, Y. F. Production of few-layer graphene through liquid-phase pulsed laser exfoliation of highly ordered pyrolytic graphite. *Appl. Surf. Sci.* **2012**, 258, 9092–9095.
- [24] Shen, J. H.; Zhu, Y. H.; Chen, C.; Yang, X. L.; Li, C. Z. One-pot green synthesis of optically pH-sensitive carbon dots with upconversion luminescence. *Chem. Commun.* **2010**, 47, 2580–2582.
- [25] Silva, A. M.; Pires, M. S.; Freire, V. N.; Albuquerque, E. L.; Azevedo, D. L.; Caetano, E. W. S. Graphene nanoflakes: Thermal stability, infrared signatures, and potential applications in the field of spintronics and optical nanodevice. *J. Phys. Chem. C* **2011**, 114, 17472–17485.

- [26] Wang, Q. L.; Zheng, H. Z.; Long, Y. J.; Zhang, L. Y.; Gao, M.; Bai, W. J. Microwave–hydrothermal synthesis of fluorescent carbon dots from graphite oxide. *Carbon* **2012**, 49, 3134–3140.
- [27] Shen, J. H.; Zhu, Y. H.; Yang, X. L.; Zong, J.; Zhang, J. M.; Li, C. Z. One-pot hydrothermal synthesis of graphene quantum dots surfacepassivated by polyethylene glycol and their photoelectric conversion under near-infrared light. *New J. Chem.* **2012**, 36, 97–101.
- [28] Tang, L. B.; Ji, R. B.; Cao, X. K.; Lin, J. Y.; Jiang, H. X.; Li, X. M.; Teng, K. S.; Luk, C. M.; Zeng, S. J.; Hao, J. H.; Lau, S. P. Deep ultraviolet photoluminescence of water-soluble self-passivated graphene quantum dots. *ACS Nano* **2012**, 6, 5102–5110.
- [29] de Miguel, M.; Álvaro, M.; García, H. Graphene as a quencher of electronic excited states of photochemical probes. *Langmuir* **2012**, 28, 2849–2857.

SECTION II

*Titanium based semiconductors in
photocatalytic hydrogenation of organics
also in membrane reactors*

6

Overview on photocatalytic reduction of organics^(*)

^(*)Part of this Chapter was published as: R. Molinari, P. Argurio, C. Lavorato. Review on reduction and partial oxidation of organics in photocatalytic (membrane) reactors. *Current Organic Chemistry*, 2013, 17, 21, 2516 – 2537.

6.1. Introduction

Reduction and oxidation processes play an important role in the production of a wide range of chemicals and precursors in the synthesis of organic compounds with high added value such as drugs, vitamins, fragrances, *etc.* Traditional industrial processes for making chemicals are considered today unsustainable in terms of resources and environmental impact, since in many cases, they use toxic and hazardous substances as catalysts or solvents [1-4]. Thus, considering the environmental pollution on a global scale, the development of totally new, environmentally friendly, clean chemical technologies and processes has become the most important challenge facing chemical scientists in the field of green chemistry [5].

Use of light, particularly visible light, as driving force for chemical reactions has attracted much attention of organic chemists. On the basis of this, the application of photocatalytic reactions to organic synthesis has

attracted high interests to develop, in perspective, environmentally benign synthetic processes [6].

Heterogeneous photocatalysis, based on the use of a semiconductor (the photocatalyst), is a discipline that includes a large variety of reactions: partial or total oxidations, dehydrogenation, hydrogenation (e.g. hydrogen transfer), metal deposition, water detoxification, gaseous pollutant removal, bactericidal action *etc.* [7]. The main difference compared to conventional catalysis is the photonic activation mode of the catalyst, which replace the thermal activation. Indeed the electronic structure of a semiconductor is characterized by a conduction band (CB) and a valence band (VB) separated by a band gap of energy (E_g). When semiconductors are excited by photons with energy equal to or higher than their band gap energy level, valence electrons are promoted from VB to CB. Electrons and holes migrate to the surface of the semiconductor and, respectively, reduce and oxidize the adsorbed substrate.

Because of the highly unselective reactions involved in the photocatalytic processes, these ones have been widely studied in environment remediation, in which organic and inorganic pollutants in liquid and gas phases are totally degraded to innocuous substances. However, in last years some studies have been carried out on the application of photocatalysis in reaction of synthesis such as selective reduction and oxidation. These studies demonstrated that high selectivity could be obtained in photo-oxidation and photo-reduction processes in comparison to conventional methods by appropriately selecting or modifying some photocatalytic parameters, as the semiconductor surface or the excitation wavelength. In this framework, the photocatalytic oxidation of organic compounds has been largely studied because the most common

semiconductors have VB edges more positive than oxidation potentials of most organic functional groups [6]. Instead, photocatalytic reductions are less frequently found, because the reducing power of a CB electron is significantly lower than the oxidizing power of a VB hole [8, 9].

Despite the photocatalytic process offers interesting advantages, its use in the industry is still limited for three different reasons [10]: i) recombination of photo-generated electron/hole pairs; ii) fast backward reaction; iii) difficulty to employ visible light that limits the effectiveness of utilization of solar energy.

In order to solve the above mentioned problems, continuous efforts have been made to promote the photocatalytic activity and enhance the visible light response. Adding electron donors or electron scavengers, able to react irreversibly with the photo-generated VB holes or CB electron, respectively, the photocatalytic electron/hole separation can be enhanced resulting in higher quantum efficiency. Electron donors or electron scavengers can be oxidized by VB holes or reduced by CB electrons, respectively; the remaining strong reducing CB electrons or strong oxidizing VB holes can reduce/oxidize the substrate. Noble metals, including Pt, Au, Pd, Rh, Ni, Cu and Ag, have been reported to be very effective for enhancement of TiO₂ photocatalysis (noble metal doping or metal ion doping). Photo-excited electrons can be transferred from CB of TiO₂ to metal particles deposited on the surface of TiO₂, while photo-generated VB holes remain on the TiO₂. This behaviour greatly reduces the possibility of electron-hole recombination, resulting in efficient separation and stronger photocatalytic reactions [11-16]. Besides, the metal reduce the band gap energy of the photocatalyst, thus shifting the radiation absorption towards higher wavelengths, permitting to use visible

light [17-21]. The same effect can be also obtained by doping the catalyst with anions, such as N, F, C, S and B [22-28]. Other ways to overcome previous limitations consist in dye sensitization, composite semiconductors, metal ion-implantation *etc.*

The use of a photocatalytic system allows to obtain the following advantages, making the photocatalytic process very attractive in view of development of a “green” process: i) the reactions can be carried out under mild conditions running them closer to room temperature and pressure; ii) it avoids the use of environmentally and unhealthy dangerous heavy metal catalysts and strong chemical oxidant/reducing agents by using safer photocatalysts (TiO_2 is the most used); iii) it uses mild oxidants (molecular oxygen, in some cases from the air); iv) it requests very few auxiliary additives; v) it does not produce harmful chemicals; vi) it can be applied to a wide range of substrates in liquid, solid and gaseous phase; vii) it offers a good alternative to the energy-intensive conventional treatments methods with the possibility to use renewable solar energy; viii) it can be combined with other physical and chemical technologies (e.g. membrane separations).

Photocatalytic membrane reactors (PMRs) represent a technology of great scientific interest because they improve the potentialities of classical photoreactors (PR) and those of membrane processes with a synergy of both technologies (e.g.: chemical reactions and separation processes are obtained in one step) thus minimizing environmental and economical impacts [29, 30]. The membrane allows not only the recovery of the catalyst, immobilizing it on/in the membrane or using membrane to maintain it in suspension, but also the selective separation of molecules present in the reaction environment to obtain a selective separation of the

products and minimizing the formation of by-products thus improving the selectivity. Higher energy efficiency, modularity and easy scale up are some other advantages of PMRs with respect to convectional PRs. One of the first examples in the application of a membrane (porous sol-gel derived (SGD) alumina) as a micro-organized medium to control the photochemical selectivity of organic transformations thanks to surface adsorption and confinement within the pores, was reported by Schultz and Anderson in 1999 [31].

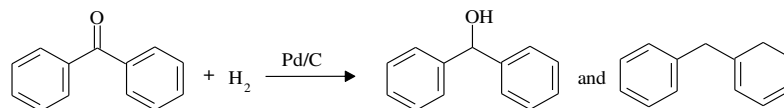
In this Chapter the most recent advances in the photocatalytic reduction of organics for selective conversions are discussed. Some first applications of PMRs in organic syntheses, reported in literature, are also described.

6.2. Hydrogenation

6.2.1. Catalytic hydrogenation and transfer hydrogenation

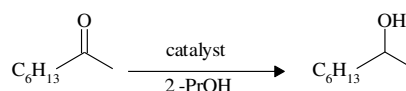
Hydrogenation is extensively used in many industrial processes such as purification of waste water through selective hydrogenation of acetylene and butadiene [32], production of liquid fuels, e.g. by hydrogenation of intermediates from biomass [33, 34], hydrogenation of ketones to their corresponding alcohols intermediates in the pharmaceutical industry [35], *etc.*

The hydrogenation reaction needs high activation energy that can be lowered using catalysts, as metals, e.g. platinum, palladium and nickel, that are among the most widely used catalysts [32]. The mechanism of this reaction consists of addition of hydrogen atoms to an organic molecule which causes the reduction of a functional group (Scheme 6.1). The simplest source of two hydrogen atoms is molecular hydrogen (H_2).



Scheme 6.1. Catalytic hydrogenation of benzophenone to benzhydrol and by-product.

However, molecular hydrogen is a gas of low molecular weight and therefore has high diffusivity, it is easily ignited and presents considerable hazards, particularly on the large scale use. Hydrogen atoms can be also transferred from a donor molecule (e.g. EtOH or other alcohols) to an acceptor substrate (e.g. ketone) as showed in Scheme 6.2.



Scheme 6.2. Transfer hydrogenation of 2-octanone to 2-octanol using propanol as hydrogen source.

This reaction is a transfer hydrogenation in which the use of hydrogen donors obviates these difficulties. Indeed no gas containment and pressure vessels are required, simple stirring and heating of solutions is usually all that is necessary [36]. Transfer hydrogenation compared to hydrogenation reaction is safer and allows optimizing the costs associated with molecular hydrogen storing and transporting.

Salts and complexes of Pd, Pt, Ru, Ir, Rh, Fe, Ni, and Co are used as homogeneous catalysts for the transfer hydrogenation of organic substrates. Among them Rh, Ru, and Pd were found to be the most active catalysts for this reaction. A problem associated with homogeneous catalysts has been the difficulty of their recovery from reaction environment. Metals as Ni, Rh, Ru, Pt, Ir, Os, and Co, are widely used as

catalysts for heterogeneous transfer hydrogenation. The most active catalysts are based on palladium metal. In a study of relative catalytic activity for the transfer hydrogenation of 2-methylbuta-1,3-diene using 2-methylhydroquinone as the hydrogen donor, decreasing activity was observed in the order Pd > Rh > Ni > Pt [36, 37].

Hydrogen donors largely used for homogeneous catalysis are alcohols, hydroaromatics, cyclic ethers, and occasionally formic and ascorbic acids. For heterogeneous catalysis, widely used electron donors are hydrazine, formic acid and formates, phosphinic acid and phosphinates, indoline, and cyclohexene [36]. A correct choice of solvent is an important factor in transfer hydrogenation. Solvent may promote catalytic activity by displacing other strongly bound species or may compete with substrates and hydrogen-donor molecules for sites on the catalyst surface. Instead, strong bond between hydrogen donor and transition metal may show no catalytic activity [38]. However, high operational temperatures (100-200 °C) and the use of expensive catalysts are usually required for transfer hydrogenation [38-40].

6.2.2. Photocatalytic transfer hydrogenation

Photocatalytic transfer hydrogenation represents a technology of great scientific interest because reactions can occur under mild experimental conditions by using light as energy source and employing cheaper photocatalysts. As a consequence, this type of hydrogenation reactions will become safer and more attractive on both economical and environmental point of view. The most widely used catalyst for photocatalytic transfer hydrogenation under UV-light is titanium dioxide. Methanol, ethanol and 2-propanol were used as both hydrogen donors and

hole scavengers in the photocatalytic reductions of aromatic ketones, using TiO_2 as catalyst [35, 41]. Alcohols are used in large excess (e.g. as solvent) to shift the reaction to the desired product, because during the transfer hydrogenation alcohols are oxidized to ketones or aldehydes that can compete with the substrate. The reaction is radical type with formation of radical intermediates obtained by abstracting a hydrogen atom from the α position to the hydroxyl group of individual alcohols [42, 43]. The use of formic acid instead of alcohols as hole scavenger and hydrogen donor, allows to make the reaction irreversible producing H_2 and CO_2 as oxidation products [44, 45].

The general mechanism of photocatalytic transfer hydrogenation is described by several steps as shown below [46].



Illumination of semiconducting TiO_2 particles by the supra-band gap irradiation causes the formation of charge carriers. The positive holes (h^+) are generated in the valence band and the negative electrons (e^-) in the conduction band of semiconductor (step 1). Using TiO_2 as semiconductor, Kohtani *et al.* [46] reported that some CB electrons and VB holes are subsequently trapped at the deep defect Ti site and Ti-OH sites respectively (steps 2 and 3). The adsorbed substrate can be reduced by CB

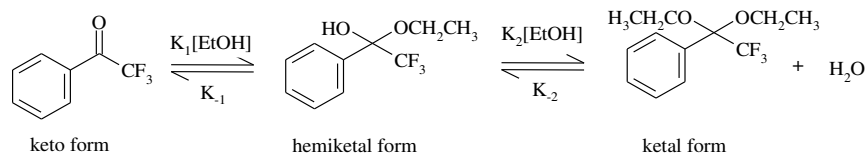
electrons or electrons trapped at the $\text{Ti}_{\text{dt}}^{3+}$ sites (steps 4 and 5). Electron donors are oxidized by VB holes enhancing photocatalytic electron/hole separation (step 6) avoiding the e^-/h^+ recombination (steps 7 and 8).

In the photocatalytic reductions the removal of O_2 from the reaction mixture blowing argon before the reaction is required to improve reaction rate and selectivity because O_2 behaves as a competitive scavenger of the electron (e_{cb}) on the photocatalyst surface and it is converted to reactive oxygen radical (O_2^\bullet).

6.2.3. Photocatalytic hydrogenation of ketones

The reduction of benzophenone to benzhydrol (hydroxydiphenyl methane, $(\text{C}_6\text{H}_5)_2\text{CHOH}$) has been receiving much attention because its derivatives are important intermediates in the pharmaceutical industry [47]. Main products obtained by benzhydrol are: antihistamines, antihypertensive agents and antiallergenic agents. Other applications of benzhydrol are in the synthesis of agrochemicals (e.g. hexachlorophene and dichlorophen), as a fixative in perfumery and as a terminating group in polymerization reactions [35].

The conventional route to produce alcohols is the catalytic reduction of the corresponding ketones. The reduction of $=\text{C}=\text{O}$ and multiple bonds using hydrogen gas flow and metal catalysts is widely reported. The most used common hydrogen donor are alcohols that can react with ketones to produce the corresponding alcohol (Scheme 6.2). Therefore, in acidic conditions or when the carbonyl carbon became more electrophilic for the influence of the electronegative group as $-\text{CF}_3$, ketones react with alcohol to give ketals as by-product (Scheme 6.3) [46].



Scheme 6.3. Equilibrium between 2,2,2-trifluoroacetophenone (TFAP), Hemiketal, and Ketal Species in Ethanol.

Kohtani *et al.* [46], reported the mechanism of ketal formation that involves equilibrium protonation:

- 1) ketone is attacked by alcohol producing neutral hemiketal (or hemiacetal);
- 2) the hemiketal further undergoes protonation and loss of water to give an oxocarbenium ion which is attacked by another mole of alcohol producing ketal.

Homogeneous catalysts as Ru, Ir, have been reported to be effective for ketones reduction, despite these catalysts are difficult to be recovered [48-51]. Instead, heterogeneous noble metal catalysts as Pd, Pt, Ru and Au can be recovered and reused [52-56]. Recently Shimura *et al.* [57] reported the use of Ni-loaded CeO_2 as catalyst for the transfer hydrogenation of aliphatic and aromatic ketones by 2-propanol to the corresponding alcohols without base as co-catalyst. This catalyst was prepared by H_2 -reduction of NiO-loaded CeO_2 with low catalyst loading (1–3 mol%). Authors reported that ketones were reduced to the corresponding alcohols after 24 h at 80 °C with excellent yields (70–98%). Ni- CeO_2 is especially effective for the reaction of aliphatic ketones and it was reused 5 times for hydrogenation of 2-octanone without lack of its catalytic activity.

Photochemical [58] and photocatalytic reduction [59] represent alternative routes and green methods to synthesize benzhydrol avoiding dangerous conditions and expensive catalysts. In particular, photocatalytic reduction

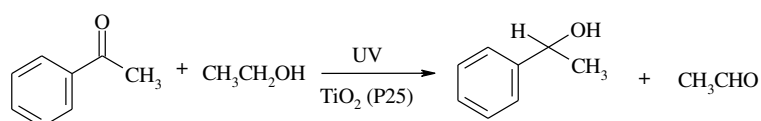
is a recent matter of study in comparison to the photochemical route which has been investigated since long time.

Photosensitive molecules that absorb in the range of UV-light as acetophenone (absorption spectrum in ethanol with maximum absorption at wavelengths 241 nm and 279 nm [46]) or benzophenone can be reduced without the catalyst in alcoholic solution for the effect of UV-light (photochemical reaction). The mechanism of this reaction is unselective and the amount of the desired product is usually very low [60]. For instance, Escobar *et al.* [35] reported 93% of benzophenone conversion by using isopropanol in N₂ atmosphere under UV light irradiation in 45 minutes. The main problem of this reduction method is the lack of selectivity to the desired product; indeed, the main product was benzopinacol (90%) instead of benzhydrol.

Comparing photochemical and photocatalytic reactions, the presence of the catalyst increases selectivity and yield towards the desired product because the absorption of light on the semiconductor generates the separation of the electron–hole couple. Electrons and holes that migrate to the surface of the semiconductor can, respectively, reduce ketones and oxidize electron donor allowing the transfer of hydrogen from alcohol to ketone [46].

To achieve suitable system productivity, various semiconductors and electron donor have been tested. In 1989 Shiragami *et al.* [59], studying the photocatalytic reduction of several aromatic ketones, obtained 47% yield to benzhydrol using acetonitrile as solvent, triethylamine as electron donor and cadmium sulphide as catalyst. Recently, Escobar *et al.* [35] reported high conversion and high yield to benzhydrol (70%) by using 2 g L⁻¹ of TiO₂ in an excess of isopropanol as electron donor.

In the absence of molecular oxygen, and using alcohol as solvent, Kohtani *et al.* [41] studied the photocatalytic activity of polycrystalline P25 TiO₂ powder to hydrogenate aromatic ketones into corresponding secondary alcohols. The reactions were tested by using methanol, ethanol, and propan-2-ol as the solvent and hole scavenger. The authors reported that the hydrogenation of acetophenone proceeded almost quantitatively in ethanol (97% yield). The formation of acetaldehyde, produced by the oxidation of ethanol, was simultaneously observed during the irradiation. The overall reaction is illustrated in Scheme 6.4. They also found that most of the reaction rate depends on the reduction potential (E_{red}) of substrates.



Scheme 6.4. TiO₂-Photocatalyzed hydrogenation of acetophenone.

During the photocatalytic hydrogenation of aromatic ketones, when TiO₂ is irradiated with UV light under deaerated conditions, in the presence of a sacrificial hole scavenger, the photocatalyst powder color changed into blue-gray [41]. The blue-gray species were assigned to the CB and surface trapped electrons (Ti³⁺) accumulated on the TiO₂ surface induced by the UV irradiation. The adsorption of ketones on TiO₂ surface and their solubility in the solvent is an important parameter for the efficiency of the photocatalytic transfer hydrogenation. The adsorption of acetophenone on TiO₂ in ethanol solution follows the Langmuir equation [46]:

$$n = (n_{\text{max}} K_{\text{ad}} C_{\text{APO}}) / (1 + K_{\text{ad}} C_{\text{APO}}) \quad (9)$$

where n is the molar amount of adsorption on the TiO_2 powder in mol g^{-1} , n_{max} is the maximum adsorption in mol g^{-1} , K_{ad} is the adsorption constant in L mol^{-1} , and C_{AP0} is the concentration of acetophenone (AP) at equilibrium. The density of adsorption sites for acetophenone on P25 TiO_2 with a powder specific surface area of ca. $50 \text{ m}^2 \text{ g}^{-1}$, is estimated to be ca. $10^{-7} \text{ mol m}^{-2}$. The value of K_{ad} for acetophenone in ethanol is smaller than in water due to the satisfying solubility in ethanol. Probably the lone pair electrons on the carbonyl oxygen of aromatic ketones should interact with Ti sites on TiO_2 surface. As reported for other carbonyl compounds [61, 62], instead, ethanol strongly interact with hydroxyl groups on TiO_2 surface through hydrogen bonds. Rekoske and Barteau [62] also reported that adsorption of acetaldehyde (produced by ethanol oxidation) on rutile and anatase TiO_2 involves a strong interaction between the carbonyl oxygen atom and the surface cation (Ti^{4+}) sites. Kohotani *et al.* [46] reported that the ketal form produced by trifluoroacetophenone (TFAP) cannot interact with the surface Ti^{4+} sites on TiO_2 because of the lack of the carbonyl group.

6.2.4. Photocatalytic hydrogenation of ketones with visible light

Solar light contains only a small amount (about 4%) of energy in the UV region. Therefore, the use of visible light, as the driving force for chemical reactions has attracted much attention of organic chemists [63, 64]. Besides, high-energy UV-light often induces undesired by-products due to the excessive energy input in thereactng environment (i.e. high production of reducing and/or oxidizing agents), which can be limited by using visible light as energy source [1].

Some dyes having visible light sensitivity can be used in photocatalytic systems as suitable materials to catch most of the energy available from sun light. Under visible light illumination, the excited dyes can inject electrons into the conduction band of semiconductors to initiate the photocatalytic reactions [1, 65].

This process of electron transfer between photosensitizer/semiconductor and reactant is often difficult because it can be limited by their oxidation/reduction potential. An alternative solution is the introduction of a co-catalyst (such as an organometallic complex) that is used as electro mediator between photosensitizer/semiconductor and reactant (Fig. (6.1)).

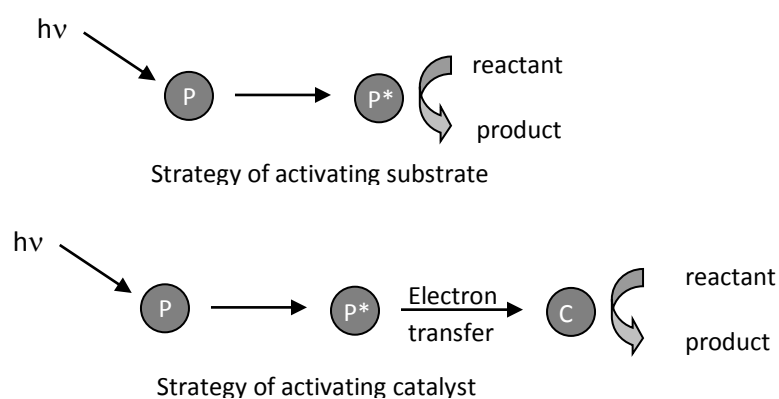


Figure 6.1. Schematic illustration of the strategy of activating a reactant or catalyst with a photo-excited electron-transfer process. P = photosensitizer/semiconductor; P* = the excited state of photosensitizer/semiconductor; C = catalyst.

Li *et al.* [1] evidenced that this strategy to activate a catalyst has the following advantages: i) facilitates the charge separation process in space; ii) reduces the energy barrier of reactants by multistep electron-transfer; iii) improves the selectivity of reactions with complexes as active sites; and iv) design rationally the reactions according to the well-known

research on organometallic chemistry. High selectivity values on visible light photocatalytic hydrogenation of various ketones were obtained using CdS nanoparticles as semiconductor for their good visible light response ability. Four types of iridium-based complexes **1-4** and $[\text{Cp}^*\text{Rh}(\text{bpy})(\text{H}_2\text{O})]^{2+}$ (Fig. (6.2)), where Cp^* is the excited state catalyst-photosensitizer, were used as co-catalysts supported on CdS by a photo-reduction method. $[\text{Cp}^*\text{Rh}(\text{bpy})(\text{H}_2\text{O})]^{2+}$ showed very poor activity to accept electron by CdS under visible light irradiation for photocatalytic reduction of cyclohexanone in water as solvent and lactic acid as hydrogen donor. Only iridium complexes **1** and **2**, reported in Fig. (6.2), were able to reduce cyclohexanone with TON 541 and 251, respectively, as catalyst with iridium-based complexes [1].

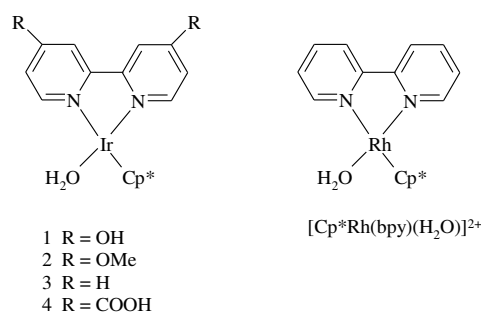


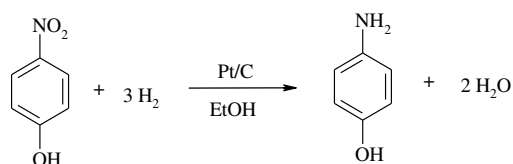
Figure 6.2. Structure of four types of iridium-based complexes and $[\text{Cp}^*\text{Rh}(\text{bpy})(\text{H}_2\text{O})]^{2+}$ used as co-catalysts and supported on CdS.

6.2.5. Photocatalytic hydrogenation of nitrocompounds

Nitrocompounds, toxic for the environment, are widely generated as by-products in pharmaceutical and agrochemical industry. The reduction of nitro aromatic to amino aromatic compounds, important intermediates for the production of dyes, pharmaceuticals and organic light-emitting diodes, has received much attention recently [44, 66]. Among various amino

compounds, 4-aminophenol (4-AP) is a vital precursor for the production of different medicines like paracetamol, phenacetin, acetanilide, *etc.* [6].

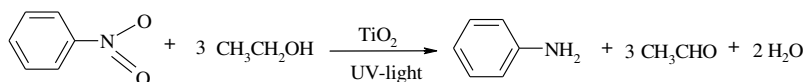
Various methods are used to produce amino compounds, such as homogeneous, heterogeneous hydrogenation, and transfer hydrogenation. Vaidya *et al.* [67] reported the catalytic hydrogenation of p-nitrophenol to p-aminophenol (Scheme 6.5) conducted in a batch-slurry reactor by using several heterogeneous metal catalysts. The results indicated that the catalytic activity for hydrogenation reactions followed the order Pt > Pd > Ni > Rh > Ru. The highest catalytic activity was observed for platinum catalyst (1% Pt/C), instead ruthenium catalyst had the lowest activity (only 10% conversion in 5 h). The hydrogenation rate and the catalytic activity were improved increasing the solvent polarity.



Scheme 6.5. Hydrogenation of p-nitrophenol to p-aminophenol.

To avoid the use of molecular hydrogen, the transfer hydrogenation of p-nitrophenol to p-aminophenol with nanoparticles nickel catalyst supported on silica-alumina using hydrazine hydrate as hydrogen donor was investigated [68]. Authors reported that this catalyst was very efficient for this reaction. It was found a total conversion of the substrate in only 69 seconds instead of 260 seconds for commercial Raney nickel. However, such process creates environmental toxic metal oxide sludge. In this last decade green methods as photocatalytic transfer hydrogenation have been developed for photocatalytic reduction of a nitro group to an amino group

by several steps. Flores *et al.* [8] reported and proposed a photocatalytic redox pathway of nitrobenzene in the presence of ethanol using titanium dioxide as semiconductor in deoxygenated conditions (Scheme 6.6).



Scheme 6.6. Photocatalyzed hydrogenation of nitrobenzene to aniline in presence of ethanol.

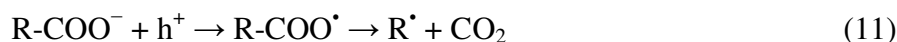
Aniline, acetaldehyde and water were the main products of the photocatalytic transfer hydrogenation of nitrobenzene after 24 h of UV-light irradiation. This photocatalytic reaction occurred because the reduction potential of nitrobenzene (-0.5 V *versus* SCE) is higher than TiO₂ (-0.85 V *versus* SCE) and the oxidation potential of ethanol is lower (+1.25 V *versus* SCE) than TiO₂ (+3.0 V *versus* SCE) [8, 69].

Brezova *et al.* [42] studied the influence of solvent (methanol, ethanol, 1-propanol, 2-propanol, 1-butanol, i-butanol) and various parameters, such as viscosity, polarity, polarisability, and polarity/polarisability on photo-reduction rate of 4-nitrophenol to 4-aminophenol by using titanium dioxide as the catalyst. Authors reported that the ability of solvent to stabilize the produced charged intermediate species, plays an important role in TiO₂ photosensitized reduction of 4-nitrophenol in alcohol solvents.

Recently Imamura *et al.* [44] studied photocatalytic reduction of nitrobenzenes and aminonitrobenzenes (m-NBS) to aminobenzenes and diaminobenzenes, respectively. These reactions were conducted in aqueous suspensions of titanium(IV) oxide (TiO₂) as catalyst and formic acid or oxalic acid as electron donors employing deaerated and aerated

conditions under UV light. Authors reported high yield (99%) of m-aminobenzensulfonic acid (m-ABS) after 60 minutes of photoirradiation also employing an artificial air condition ($O_2:N_2 = 1:4$). Despite the presence of O_2 must be avoided, because it competes with the substrate and can be reduced to oxygen radical causing oxidation of substrates, in this case re-oxidation of the amino group of m-ABS did not occur even in the presence of O_2 . Probably formic acid was efficient as hole scavenger preventing the oxidation of m-NBS and the re-oxidation of m-ABS. Moreover, m-NBS is more reducible than O_2 and it was reduced at its place. Finely, possible repulsion of the reduced functional group (ammonium group, $-NH_3^+$) from the protonated, positively charged TiO_2 surface in acidic suspensions, avoided the re-oxidation of m-ABS.

Formic acid (FA) and oxalic acid (OA) are “green” sacrificial reagents because they are easily oxidized and converted into carbon dioxide (CO_2), which is separated from the solvent under acidic conditions. The photocatalytic effect in the presence of formic acid can be attributed to the photo-Kolbe reaction, originally evidenced by Kraeutler *et al.* [70] in the presence of various carboxylic acids:



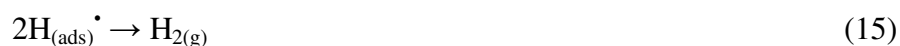
Whebe *et al.* [45] reported a similar mechanism for formic acid:



where formate ions can trap the photo-generated holes with the formation of formate radical that spontaneously decomposes to H^\bullet and CO_2 .

Sato *et al.* [71], reported, the gas-phase photodecomposition of formic acid into $H_2 + CO_2$ over a Pt/TiO_2 catalyst [72] in which the photo-

generated electrons are partly transferred to Pt particles. The negatively charged metal particles reduce protons into hydrogen:



Atomic hydrogen can recombine and desorb as H_2 or participate in the organic compound reduction reaction, adsorbed on photocatalyst.

To improve the photocatalytic activity of TiO_2 Wang *et al.* [73] reported the preparation of N-doped TiO_2 by a modified sol-gel method using urea as nitrogen source. This new catalyst showed higher photocatalytic activity compared to pure TiO_2 for the reduction of aromatic nitro compounds to the corresponding amines obtaining high values of yield (from 90% to 99%) in very short time (from 7 to 19 minutes). Wu *et al.* [74], reported high efficient photocatalytic reduction of 4-nitroaniline (4-NA) to p-phenylenediamine (PPD) over microcrystalline $\text{SrBi}_2\text{Nb}_2\text{O}_9$ using ammonium oxalate as electron donor. It was found that its photocatalytic activity was higher than the P25 commercial TiO_2 (Evonik) sample. 4-NA was completely reduced to PPD after 40 min of UV light irradiation at 254 nm using $\text{SrBi}_2\text{Nb}_2\text{O}_9$ as catalyst.

6.2.6. Photocatalytic hydrogenation of nitrocompounds with visible light

As before mentioned, photocatalysis for transformation of organics using visible light irradiation is one of most important developing fields for future application. In this case, the targeted catalyst should have a stable excited triplet state, redox potential, and visible light absorption [6]. Based on that, organic dyes that have redox propriety (Fig. (6.3)) and visible light absorption can be screened to be used in photocatalysis.

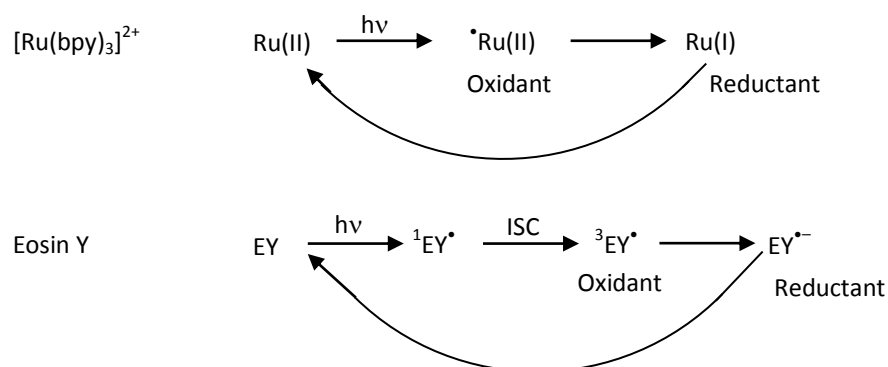


Figure 6.3. Comparable photoredox cycles of $[\text{Ru}(\text{bpy})_3]^{2+}$ and Eosin Y.

Recently, dye sensitized TiO_2 and transition metal nanoparticles were used for visible light photo-reduction of nitro derivatives [75]. Various nitrobenzenes were reduced to anilines using Ru-sensitized TiO_2 photocatalysts by using LEDs or sunlight as irradiation source. The very simple preparation method of dye sensitized TiO_2 , which consists only in the mixing of components, makes it easy to be applied in organic synthesis.

The problem, generally associated with the use of dyes, is their poor stability in the reaction medium; on the contrary, they may be destroyed during reactions at different conditions. For the reduction of 4-nitrophenol (4-NP) to 4-aminophenol (4-AP) by using NaBH_4 as electron donor, Gazi *et al.* [6] reported the study of several dyes as: Alizarin S Red, Bromophenol Blue, Bromopyrogallol Red, Rhodamine B, Methylene Blue, Rose Bengal and Eosin Y, that have absorption band in the visible region. Among them Methylene Blue (MB), and Rose Bengal (RB) in homogeneous as well as heterogeneous form were found to be stable in the

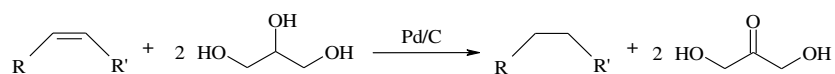
reaction medium, while Eosin Y (EY) was stable only absorbed on the resin (Seralite) surface (heterogeneous form). Despite they have absorption band in the visible region, Rose Bengal on resin (RRB) was not able to photoreduce 4-NP to 4-AP, while Methylene Blue on resin (RMB) showed low photocatalytic activity in the reduction of 4-NP (17% of conversion in 50 min irradiation). Instead, the best result in terms of conversion (60% in 50 min) was obtained by using Eosin Y on resin (REY) as catalyst. Authors reported a probable mechanism of photocatalytic reduction process that involves some crucial steps such as [6]: i) substrate adsorption on the catalyst surface; ii) electron transfer from borohydride/borate to the catalyst and its excitation to its triplet state; iii) electron transfer from catalyst to the adsorbed 4-nitrophenolate; iv) hydrogen atom transfer from $\text{BH}_4/\text{solvent}$ to the 4-nitrophenolate and formation of 4-aminophenol; v) desorption of products from the surface of the catalyst.

6.2.7. Photocatalytic hydrogenation of unsaturated compounds

Hydrogenation of double C=C bond is extensively used for many applications as purification of waste water, production of gas and liquid fuels, or intermediates in industrial processes (e.g. nylon production) [76, 77], *etc.*

The partial hydrogenation of benzene to cyclohexene is a chemical reaction of industrial interest because it can be used to synthesize several compounds, from which the main is nylon production [78]. Among various hydrogenation catalysts that are able to hydrogenate benzene, ruthenium and Pt based catalysts showed high activity for this reaction [79].

Wolfson *et al.* [80, 81] reported the possibility of using glycerol as both solvent and hydrogen donor for transfer hydrogenation of various unsaturated organic molecules (Scheme 7). Glycerol is a green solvent, biodegradable, and recyclable liquid that is the main by-product from the conversion of oils and fats [82]. Especially reduction of cyclohexene over Pd/C was tested obtaining 69% of conversion after 5 h of reaction at 70 °C. The use of glycerol as a solvent facilitated: the solubility of reactants and catalysts, product separation and transition metal complex recycling. Therefore, during these reactions, glycerol was dehydrogenated to dihydroxyacetone that is used in sunless tanning compounds and as intermediate for organic synthesis.



Scheme 6.7. Transfer-hydrogenation of olefins using glycerol as solvent and hydrogen donor.

Concerning the photocatalytic approach to reduce multiple C-C bond Anpo *et al.* [83] studied the photocatalytic reduction of alkenes in water with H₂ flow by using Pt-loaded and unloaded TiO₂ as catalysts to enhance the reaction:



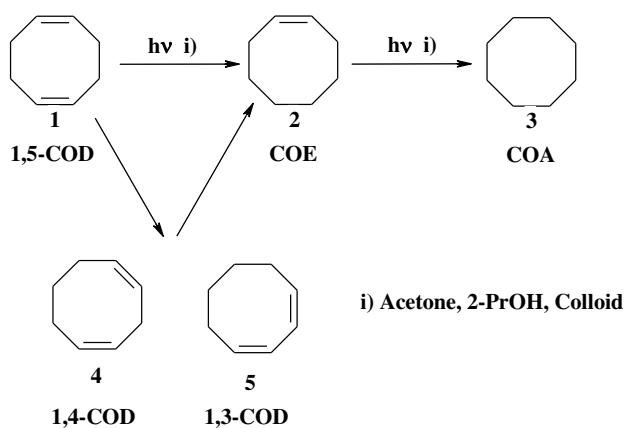
Subsequently photocatalytic transfer hydrogenation of cyclohexane, using water as hydrogen source and ethanol as electron donor, in absence of hydrogen gas flow, was carried out by Khan *et al.* [84]. In this case a very low yield of cyclohexane (7-8%) was obtained in aqueous ethanol solutions (80:20 ethanol-water) with K[Ru(H-EDTA)Cl]·2H₂O and Pt/CdS/RuO₂ as semiconductor.

Other catalysts studied for photocatalytic transfer hydrogenation of diolefins have been metal carbonyl cluster catalysts [85-87]. Yanagawa *et al.* [87] reported the photo-assisted selective hydrogenation of limonene by hydrogen transfer from 2-propanol over a Rh carbonyl cluster catalyst $[\text{Rh}_6(\text{CO})_{16}]$ in the presence of a small amount of acetone under UV-light. In this work all the hydrogen formed by the dehydrogenation of 2-propanol was very efficiently added to unsaturated compounds, in fact, H_2 was not found in the gas phase during this process. Akioka *et al.* [88] applied this process to the photocatalytic transfer hydrogenation of norbornadiene and quadricyclane.

6.2.8. Photocatalytic partial hydrogenation of unsaturated compounds

Hanaoka *et al.* [86] reported the effect of additive and of rhodium colloid catalyst ($\text{Rh}_4(\text{CO})_{12}$) for selective photocatalytic transfer hydrogenation of 1,5-cyclooctadiene (1,5-COD) to cyclooctene (COE). Colloid catalysts are considered as heterogeneous catalysts without support. Rhodium colloid particles were prepared with an irradiation method that consists of stirring a solution with $\text{Rh}_4(\text{CO})_{12}$ in 2-propanol and acetone for 32 minutes, under UV-VIS light. This solution was stable for several days in absence of a polymer stabilizer [85]. During this preparation, after a short period under UV irradiation, $\text{Rh}_4(\text{CO})_{12}$ absorption band in the range between 350 to 700 nm was enhanced. Authors attributed the new absorption spectrum to a scattering band caused by highly dispersed colloidal metal. Indeed, TEM analysis showed small particles divided in: primary particles with size of 2 nm and secondary particles with 20 nm of diameter formed by aggregation of primary particles. Photocatalytic transfer hydrogenation of 2-propanol to 1,5-cyclooctadiene (Scheme 6.8) using colloidal rhodium

catalyst in presence of acetone, showed high selectivity to cyclooctene (86%) with a ratio of hydrogenation rate $R=(\text{cyclooctadiene to cyclooctene}/\text{cyclooctene to cyclooctane})$ equal to 4.8.



Scheme 6.8. Reaction path of photocatalytic transfer hydrogenation of 1,5-COD (elaborated from [86]).

To improve the selectivity Hanaoka *et al.* [86] added transition metal salts as: $\text{Fe}(\text{NO}_3)_3 \cdot 9 \text{H}_2\text{O}$, $\text{Cu}(\text{NO}_3)_2 \cdot 2.5 \text{H}_2\text{O}$, $\text{Ni}(\text{NO}_3)_2 \cdot 6 \text{H}_2\text{O}$ to colloidal rhodium catalyst. Transmission electron spectroscopy showed a good dispersion and separation between colloidal particles while aggregated secondary particles were not observed in the solution containing rhodium and iron. Results in terms of selectivity and hydrogenation rate are showed in Table 6.1.

Table 6.1. Additive effect by salts of transition light metals on the photocatalytic transfer hydrogenation of 1,5-COD (Reaction condition: $\text{Rh}_4(\text{CO})_{12}$ 3mg, 2-propanol 32 ml, acetone 8 ml, 20 °C, under N_2) (*).

Additive	R=(COD to COE/COE to COA)	Max selectivity of COE (%)
none	5.5	86
$\text{Fe}(\text{NO}_3)_3 \cdot 9 \text{H}_2\text{O}$	1.1	94
$\text{Cu}(\text{NO}_3)_2 \cdot 2.5\text{H}_2\text{O}$	9.0	89
$\text{Ni}(\text{NO}_3)_2 \cdot 6 \text{H}_2\text{O}$	1.3	91

(*) COD = cyclooctadiene; COE = cyclooctene; COA = cyclooctane

In particular, addition of $\text{Fe}(\text{NO}_3)_3 \cdot 9 \text{H}_2\text{O}$, enhances the selectivity to 94% after 6 h of irradiation and the hydrogenation rate for both steps (COD to COE, and COE to COA), while, hydrogenation rate of COE to COA decreased at lower amount of Fe salt added in the solution. Authors proposed the reaction mechanism for photocatalytic transfer hydrogenation of 1,5-COD as follows: i) photo excitation of acetone extracted an hydrogen atom from 2-propanol; ii) transfer of the hydrogen atom to rhodium colloid; iii) desorption of hydrogen species as H_2 or hydrogen atoms transferred to olefin adsorbed on the colloid surface reducing it.

Reaction rate, selectivity and particle size of the colloid are influenced by modification of colloid surface for additive effect. Iron cationic particles are present in solution as Fe^{3+} , they are attracted and adsorbed on the surface of rhodium colloidal particles that are negatively charged thus changing their surface charge. This causes electrostatic repulsion among particles preventing aggregation of colloids. Furthermore, the affinity of rhodium particles for the substrate is influenced by addition of iron salts as

additive. The affinity of 1,5-COD towards the catalyst surface is stronger than COE; the access of COE to the catalyst surface is blocked by the strongly adsorbed 1,5-COD through a competitive adsorption, preventing the transfer hydrogenation of COE under existence of 1,5-COD. Consequently, the reduction of COE began only after 6 h when 1,5-COD were almost consumed.

6.3. Studies on photo-conversions in PMRs

6.3.1. Outline on photocatalytic membrane reactors

In traditional slurry photoreactors the recovery of the unsupported catalyst from the reaction environment is one of the key challenges in view of large scale applications. Photocatalytic membrane reactors (PMRs), which are hybrid systems where photocatalysis is coupled with a membrane separation, are a very promising approach to overcome this limitation.

A membrane process is a physical separation technique which does not involve a phase change and allows to operate in continuous mode, e.g. in pollutants removal from waters [89,90]. In a PMR system, the appropriate choice of the membrane and membrane module configuration is mainly determined by the type of photocatalytic reaction, indeed, the membrane can assume many roles as catalyst recovery, separation of the products, rejection of the substrate, *etc.* When the photocatalytic process is used as a synthetic pathway, the main objective can be the selective separation of the product, e.g. minimizing its successive oxidation, which lead to undesirable by-products.

PMRs allow to operate in continuous systems in which the reaction of interest and the selective separation of the product(s) simultaneously occurs, resulting competitive with other separation technologies in terms

of material recovery, energy costs, reduction of the environmental impact, and selective removal of the components.

Different systems combining photocatalysis with pressure-driven membrane techniques, such as nanofiltration (NF) and ultrafiltration (UF) for the degradation of organic pollutants are reported in literature [91-93]. One of the main drawbacks of these systems is the membrane fouling. Coupling of photocatalysis and membrane distillation (MD) could avoid this problem, and an almost complete retention of total organic carbon (TOC) content is reported [94-96]. Self cleaning properties can be generated on a membrane by coating its surface with TiO_2 particles [97,98]. Also dialysis membranes were successfully coupled with a photoreactor in order to mineralize organic compounds contained in artificial turbid waters [99]. Recently, it has been demonstrated that the integration of heterogeneous photocatalysis with the pervaporation operation is a very promising method to improve the detoxification efficiency of water streams containing organic pollutants at low concentration [100].

These works evidence that PMRs have been widely studied in water purification by complete oxidation of organic pollutants. Despite the great potentiality of the photocatalytic process and the important advantages that can be achieved by its coupling with a membrane separation system, the research in the field of photocatalytic organic syntheses in PMRs in reduction of organic compounds is still at a nascent stage. The first studies on photo-conversions in PMRs, can open the way to future applications of PMRs in organic synthesis.

6.3.2. Partial hydrogenation in PMRs

The literature search on this very specific and interdisciplinary research theme did not provide any result. However, as an example, in the following some photocatalytic reductions of CO₂ in membrane reactors are reported.

The depletion of fossil fuels and the global warming would require the development of carbon dioxide capture and/or converting it into useful chemicals to solve both problems [101-103]. Use of various semiconductor catalysts in a heterogeneous system is one of promising research studies focusing on the photocatalytic reduction of CO₂ to form marketable products such as methane, methanol, formic acid and ethanol, all of high interest [104-106]. Many processes for catalytic CO₂ conversion require high-temperature and/or pressure conditions. On the contrary, photocatalytic processes occur under relatively mild conditions with lower energy input, especially where the reaction is activated by solar energy [107].

The photo-reduction of CO₂ by water involves the generation of two important species as H• (hydrogen atom) and •CO₂⁻ (carbon dioxide anion radical) produced by electron transfer from the conduction band according to the following reactions:



These radicals can then combine to form other substances as carbon monoxide, formic acid, formaldehyde, methanol and methane [107, 108].

Cao *et al.*, reported the use of functionalized carbon nanoparticles with gold or platinum coating as photocatalysts for the reduction of CO₂ to produce formic acid. The estimated quantum yield to formic was found to

be around 0.3% after irradiation with visible light (425-720 nm) for 5 h. Other photoproducts such as methanol were also found. The authors reported that the quantum yield obtained using this new catalyst under visible light was higher than using suspended TiO₂ nanoparticles (Degussa P25) as photocatalysts under UV light irradiation (through a 350 nm cut-off filter) [109].

To improve the efficiency of CO₂ reduction, separation of the photocatalyst from the solution, which normally contains many species, was carried out by immobilizing it in a Nafion membrane. Premkumar *et al.* [110] reported the preparation of metal phthalocyanines (MPCs) adsorbed into a Nafion membrane for the photocatalytic reduction of CO₂. The membrane (1 cm²) was pretreated by boiling it in concentrated HNO₃ and following washed with distilled water. Then MPC-adsorbed Nafion membrane was obtained by immersing the membrane in a solution containing a known concentration of CoPC or ZnPC in DMF. The authors reported that CoPC and ZnPC were adsorbed irreversibly on the membrane (Nf/CoPC and Nf/ZnPC) and they found that the acidic nature of the membrane accelerated the CO₂ reduction process operating in aqueous solution of triethanolamine (TEA) and HClO₄ under visible light. Noble metals such as silver, gold, copper, platinum, and palladium, typically, were deposited onto a TiO₂ surface to improve its photocatalytic activity under visible light [111]. However, it is widely reported that colloidal particles can aggregate easier in suspension reducing the active surface area and compromising the behavior of the photoreaction due to severe light scattering effect of the aggregates [112]. Several strategies have been attempted to avoid this problem such as introduced TiO₂ in zeolite cavities for subsequent platinum coating, or the preparation of TiO₂

nanoparticle films (≈ 15 nm) on a glass substrate via the sol–gel method, followed by the photodeposition of silver nanoparticles (35 – 60 nm) [113,114]. However, to increase the crystallinity of the nanoparticles, high-temperature calcination is required which caused significant agglomeration of the nanoparticles and negatively affected their photocatalytic activities [115]. Pathak *et al.* [116] reported the preparation of silver doped TiO₂ nanoparticles homogeneously dispersed in Nafion membrane used as photocatalyst for the reduction of CO₂ to methanol. The procedure for the preparation of TiO₂ in nanoscale cavities of Nafion membrane [117] consists of dipping cleaned Nafion-117 membrane films (Du Pont Co.) in a solution of Ti(OC₃H₇)₄ in isopropanol (0.5 M) for 48 h. After several wash with isopropanol and acetone, to form TiO₂ nanoparticles in the membrane structure, the films were immersed in boiling water for the hydrolysis of Ti(OC₃H₇)₄. Finally, TiO₂ nanoparticles entrenched in Nafion membrane films were coated with silver metal via photolysis. The silver coating resulted in significant improvements of the photocatalytic conversion of CO₂ to methanol as the main reduction product. These films showed high chemical and photochemical stability, and they were found reusable in repeated photocatalytic reactions.

Nishimura *et al.* [118, 119], reported a novel approach to improve performance of CO₂ reduction over TiO₂ semiconductor under UV light by using a membrane reactor composed by a gas separation membrane and TiO₂ film. Whereas, molecular diameters of some products such as CO and CH₄ are little larger than CO₂ and water vapor (diameters CO: 0.38 nm, CH₄: 0.38 nm, CO₂: 0.33 nm, water vapor: 0.28 nm), membrane gas separation was possible. The silica or alumina membranes used for this study were prepared by sol–gel and dip-coating methods. The gas

separation was obtained through both molecular sieving diffusion and the so called Knudsen diffusion mechanisms, which can separate the gases even if the pore size of silica layer is larger than the molecular diameter of gas to be separated. Electron probe micro-analyzer (EPMA) images of TiO₂ film prepared under several rising speed (RS) conditions showed a large amount of crystallized TiO₂ coated on the gas separation membrane. RS equal to 1.1 mm/s was the optimum coating condition since the best CO₂ conversion performance as well as the nearly best CO₂ permeation performance was obtained under this condition.

Photocatalytic reduction experiments [119], were performed in a photocatalytic membrane reactor, which consisted of one gas separation membrane with a TiO₂ film, one quartz glass tube and four UV lamps (365nm) located symmetrically at 20 mm from the surface of gas separation membrane. During the experiments of photocatalytic reduction CO₂ was flowed for 15 minutes through the reactor, and after, the valves located at inlet and outlet, were closed. Then, water was injected and vaporized into the reactor at 353K and the irradiation by the UV lamp was started. Photocatalytic tests in the membrane reactor were performed in the same experimental condition of batch type but a gas circulation by means a tube pump was used to feed the reactant.

The experiment by batch type and gas circulation type was carried out in two times, from 0 h to 216 h and from 216 h to 408 h, respectively (Fig (6.4)).

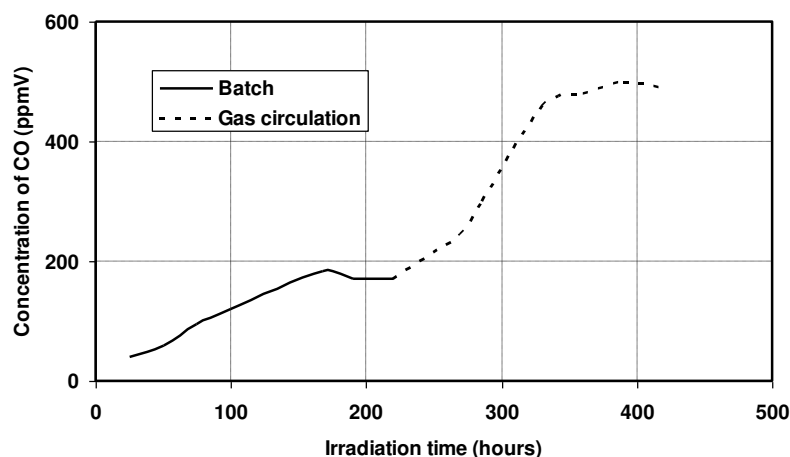


Figure 6.4. CO Concentration change in the batch and membrane reactor under UV light irradiation (adapted from [119]).

Obtained results evidenced that the highest value of CO concentration (183 ppmV) was obtained after 168 h of UV irradiation in the batch reactor, after the CO concentration started decreasing slightly. This behavior is caused by re-oxidation of the product. When a gas circulation in the membrane reactor began, the concentration of CO started to increase again, obtaining the highest value of CO concentration equal to 502 ppmV after 384 h. This behavior demonstrates that using the membrane reactor with gas circulation, steady state reaction and re-oxidation of CO were prevented and then the CO production rate improved.

6.4. Conclusions

The literature survey reported in the present Chapter points out that the selective reduction of organics with the aid of light energy over photocatalysts is a promising technology for the production of many chemicals. Suitable design of the catalytic system (choice of the

photocatalyst, photocatalyst design, combination of photocatalysts, use of an electron acceptor, *etc.*) allows to minimize secondary reactions, thus increasing yield and selectivity. By combination of the excellent catalytic performance, the mild reaction conditions, the green nature of catalyst and the ability to use visible-light energy, the photocatalytic method is expected to provide an energy-efficient and environmentally benign route for organic synthesis. Even if the utilization of visible light is in principle highly advisable, from a practical point of view it results to be appealing only if it is accompanied with a sufficiently high yield of the desired products. Integration of the photocatalysis with a membrane process in the Photocatalytic Membrane Reactors (PMRs), thanks to the synergy of both technologies (e.g.: chemical reactions and separation processes are obtained in one step) can generate a powerful technology to produce chemicals using environmental friendly processes, although much studies are still needed before taking advantage of their potentiality at industrial level. On the basis of this, there are no doubt that photocatalysis coupled to membranes is a promising research area in organic synthesis.

6.5 References

- [1] Li, J.; Yang, J.; Wen, F.; Li, C. A visible-light-driven transfer hydrogenation on CdS nanoparticles combined with iridium complexes. *Chem. Commun.*, **2011**, *47*, 7080-7082.
- [2] Molinari, R.; Caruso, A.; Palmisano, L. In *Comprehensive Membrane Science and Engineering*; Drioli E. and Giorno L., Eds; Elsevier Science B.V.: Oxford, **2010**; Vol. 3, pp. 165-193.

- [3] Palmisano, G.; Augugliaro, V.; Pagliaro, M.; Palmisano, L. Photocatalysis: a promising route for 21st century organic chemistry. *Chem. Commun.*, **2007**, 33, 3425-3437.
- [4] Herrmann, J.M.; Duchamp, C.; Karkmaz, M.; Thu Hoai, B.; Lachheb, H.; Puzenat, E.; Guillard, C. Environmental green chemistry as defined by photocatalysis. *J. Hazard. Mater.*, **2007**, 146, 624-629.
- [5] Anpo, M. Utilization of TiO₂ photocatalysts in green chemistry. *Pure Appl. Chem.*, **2000**, 72, 1265-1270.
- [6] Gazi, S.; Ananthakrishnan, R. Metal-free-photocatalytic reduction of 4-nitrophenol by resin-supported dye under the visible irradiation. *Appl. Catal. B-Environ.*, **2011**, 105, 317-325.
- [7] Herrmann J.-M. Heterogeneous photocatalysis: state of the art and present applications. *Top. Catal.*, **2005**, 34, 49-65.
- [8] Flores, S.O.; Rios-Bernij, O.; Valenzuela, M.A.; Cordova, I.; Gomez, R., and Gutierrez, R. Photocatalytic reduction of nitrobenzene over titanium dioxide: by-product identification and possible pathways. *Top. Catal.*, **2007**, 44, 507-511.
- [9] Palmisano, G.; García-López, E.; Marci, G.; Loddo, V.; Yurdakal, S.; Augugliaro, V.; Palmisano, L. Advances in selective conversions by heterogeneous photocatalysis. *Chem. Commun.*, **2010**, 46, 7074-7089.
- [10] Ni, M.; Leung, M. K. H.; Leung, D. Y. C.; Sumathy, K. A review and recent developments in photocatalytic water-splitting using TiO₂ for hydrogen production. *Renew. Sust. Energ. Rev.*, **2007**, 11, 401-425.

- [11] Colmenares, J. C.; Aramendía, M. A.; Marinas, A.; Marinas, J. M.; Urbano, F. J. Synthesis, characterization and photocatalytic activity of different metal-doped titania systems. *Appl. Catal. A-Gen.*, **2006**, *306*, 120–127.
- [12] Mizukoshi, Y.; Makise, Y.; Shuto, T.; Hu, J.; Tominaga, A.; Shironita, S.; Tanabeet S. Immobilization of noble metal nanoparticles on the surface of TiO₂ by the sonochemical method: Photocatalytic production of hydrogen from an aqueous solution of ethanol. *Ultrason. Sonochem.*, **2007**, *14*, 387–392.
- [13] Wang, C.-T. Photocatalytic activity of nanoparticle gold/iron oxide aerogels for azo dye degradation. *Non-Cryst. Solids*, **2007**, *353*, 1126–1133.
- [14] Araña, J.; Peña Alonso, A.; Doña Rodríguez, J.M.; Herrera Melián, J.A.; González Díaz, O.; Pérez Peña, J. Comparative study of MTBE photocatalytic degradation with TiO₂ and Cu-TiO₂. *Appl. Catal. B-Environ.*, **2008**, *78*, 355–363.
- [15] Chen, C.; Wang, Z.; Ruan, S.; Zou, B.; Zhao, M.; Wu, F. Photocatalytic degradation of C.I. Acid Orange 52 in the presence of Zn-doped TiO₂ prepared by a stearic acid gel method. *Dyes Pigm.*, **2008**, *77*, 204–209.
- [16] Wu, G.; Chen, T.; Su, W.; Zhou, G.; Zong, X.; Lei, Z.; Li, C. H₂ production with ultra-low CO selectivity via photocatalytic reforming of methanol on Au/TiO₂ catalyst. *Int. J. Hydrogen Energy*, **2008**, *33*, 1243–1251.
- [17] Kudo, A.; Sekizawa, M. Photocatalytic H₂ evolution under visible light irradiation on Ni-doped ZnS photocatalyst. *Chem. Commun.*, **2000**, *15*, 1371–1372.

- [18] Egerton, T. A.; Mattinson, J. A. The influence of platinum on UV and 'visible' photocatalysis by rutile and Degussa P25. *J. Photochem. Photobiol. A*, **2008**, *194*, 283–289.
- [19] Ge, L. Novel visible-light-driven Pt/BiVO₄ photocatalyst for efficient degradation of methyl orange. *J. Mol. Catal. A-Chem.*, **2008**, *282*, 62–66.
- [20] Qi, B.; Yu, Y.; He, X.Q.; Wu, L.Z.; Duan, X.F.; Zhi, J.F. Series of transition metal-doped TiO₂ transparent aqueous sols with visible-light response. *Mater. Chem. Phys.*, **2012**, *135*, 549-553.
- [21] Khakpash, N.; Simchi, A.; Jafari, T. Adsorption and solar light activity of transition-metal doped TiO₂ nanoparticles as semiconductor photocatalyst. *J. Mater. Sci.-Mater. El.*, **2012**, *23*, 659-667.
- [22] Ling, Q.; Sun, J.; Zhou, Q. Preparation and characterization of visible-light-driven titania photocatalyst co-doped with boron and nitrogen. *Appl. Surf. Sci.*, **2008**, *254*, 3236–3241.
- [23] Sun, H.; Bai, Y.; Jin, W.; Xu, N. Visible-light-driven TiO₂ catalysts doped with low-concentration nitrogen species. *Sol. Energy Mater. Sol. Cells*, **2008**, *92*, 76–83.
- [24] Peng, F.; Cai, L.; Yu, H.; Wang, H.; Yang, J. Synthesis and characterization of substitutional and interstitial nitrogen-doped titanium dioxides with visible light photocatalytic activity. *J. Solid State Chem.*, **2008**, *181*, 130–136.
- [25] Carvalho Collazzo, G.; Foletto, E.L.; Jahn, S.L.; Villetti, M.A. Degradation of Direct Black 38 dye under visible light and sunlight irradiation by N-doped anatase TiO₂ as photocatalyst. *J. Environ. Manage.*, **2012**, *98*, 107-111.

- [26] Wong, M.S.; Hsu, S.W.; Rao, K.K.; Kumar, C. P. Influence of crystallinity and carbon content on visible light photocatalysis of carbon doped titania thin films. *J. Mol. Catal. A-Chem.*, **2008**, 279, 20–26.
- [27] Xu, J.; Ao, Y.; Fu, D.; Yuan, C. Low-temperature preparation of F-doped TiO₂ film and its photocatalytic activity under solar light. *Appl. Surf. Sci.*, **2008**, 254, 3033–3038.
- [28] Li, L.; Yang, Y.; Liu, X.; Fan, R.; Shi, Y.; Li, S.; Zhang, L.; Fan, X.; Tang, P.; Xu, R.; Zhang, W.; Wang, Y.; Ma, L. A direct synthesis of B-doped TiO₂ and its photocatalytic performance on degradation of RhB. *Appl. Surf. Sci.*, **2013**, 265, 36–40.
- [29] Molinari, R.; Caruso, A.; Argurio, P.; Poerio, T. Degradation of the drugs Gemfibrozil and Tamoxifen in pressurized and de-pressurized membrane photoreactors using suspended polycrystalline TiO₂ as catalyst. *J. Membrane Sci.*, **2008**, 319, 54–63.
- [30] Molinari, R.; Caruso, A.; Poerio, T. Direct benzene conversion to phenol in a hybrid photocatalytic membrane reactor. *Catal. Today*, **2009**, 144, 81–86.
- [31] Schultz, F.S.; Anderson, M.A. Effects of surface adsorption and confinement on the photochemical selectivity of previtamin D₃ adsorbed within porous sol-gel derived alumina. *J. Am. Chem. Soc.*, **1999**, 121, 4933–4940.
- [32] Rylander, P.N. *Ullmann's Encyclopedia of Industrial Chemistry*, 6th ed.; Wiley-VCH, Verlag GmbH & Co. KGaA: Weinheim, Germany, **2003**.

- [33] Chang, N.; Aldrett, S.; Holtzapple, M. T.; Davison, R. R.. Kinetic studies of ketone hydrogenation over Raney nickel catalyst. *Chem. Eng. Sci.*, **2000**, *55*, 5721-5732.
- [34] Yan Z.; L. Lin.; S. Liu. Synthesis of γ -Valerolactone by Hydrogenation of Biomass-derived Levulinic Acid over Ru/C Catalyst. *Energ. Fuels*, **2009**, *23*, 3853–3858.
- [35] Escobar, E.A.; Zapata, M. Á. V.; Hernández, S.A.; Flores Valle, S. O.; Berny, O. R.; Ángeles, V. J. G.; Reyes, I. C. Photocatalytic Reduction of Benzophenone on TiO₂: Effect of Preparation Method and Reaction Conditions. *J. Mex. Chem. Soc.*, **2010**, *54*, 133-138.
- [36] Johnstone, R.A.W.; Wilby, A.H. Heterogeneous Catalytic Transfer Hydrogenation and Its Relation to Other Methods for Reduction of Organic Compounds. *Chem. Rev.*, **1985**, *85*, 129-170.
- [37] Anderson, J. R. *Structure of Metallic Catalysts*; Academic Press: New York, **1975**.
- [38] Masters, C.; Kiffen, A. A.; Visser, J. P. Transfer Hydrogenation in the Presence of a Homogeneous Rhodium Catalyst. *J. Am. Chem. Soc.*, **1976**, *98*, 1357–1364.
- [39] Nishiguchi, T; Fukuzumi, K. Transfer-hydrogenation and transfer-hydrogenolysis. III. Hydrogen transfer from dioxane to olefins catalyzed by chlorotris(triphenylphosphine)rhodium(I). *J. Am. Chem. Soc.*, **1974**, *96*, 1893–1897.
- [40] Nishiguchi, T; Fukuzumi, K. ; Fukuzumi, K. Hydrogen transfer from dioxane to an olefin catalyzed by chlorotris(triphenylphosphine)rhodium(I). *J. Am. Chem. Soc.*, **1972**, *94*, 8916–8917.

- [41] Kohtani, S.; Yoshioka, E.; Saito, K.; Kudo, A.; Miyabe, H. Photocatalytic hydrogenation of acetophenone derivatives and diaryl ketones on polycrystalline titanium dioxide. *Catal. Commun.*, **2010**, *11*, 1049–1053.
- [42] Brezova, V.; Blazkova, A.; Surina, I.; Havlinova, B. Solvent effect on the photocatalytic reduction of 4-nitrophenol in titanium dioxide suspensions. *J. Photoch. Photobio. A*, **1997**, *107*, 233-237.
- [43] Kaise, M.; Nagai, H.; Tokuhashi, K.; Kondo, S.; Nimura, S.; Kikuchi, O. Electron Spin Resonance Studies of Photocatalytic Interface Reactions of Suspended M/TiO₂ (M = Pt, Pd, Ir, Rh, Os, or Ru) with Alcohol and Acetic Acid in Aqueous Media. *Langmuir*, **1994**, *10*, 1345-147.
- [44] Imamura, K.; Iwasaki, S.; Maeda, T.; Hashimoto, K.; Ohtani, B.; Kominami, H. Photocatalytic reduction of nitrobenzenes to aminobenzenes in aqueous suspensions of titanium(IV) oxide in the presence of hole scavengers under deaerated and aerated conditions. *Phys. Chem. Chem. Phys.*, **2011**, *13*, 5114–5119.
- [45] Wehbe, N.; Jaafar, M.; Guillard, C.; Herrmann, J.-M.; Miachon, S.; Puzenat, E.; Guilhaume, N. Comparative study of photocatalytic and non-photocatalytic reduction of nitrates in water. *Appl. Catal. A-Gen.*, **2009**, *368*, 1–8.
- [46] Kohtani, S.; Yoshioka, E.; Saito, K.; Kudo, A.; Miyabe, H. Adsorptive and Kinetic Properties on Photocatalytic Hydrogenation of Aromatic Ketones upon UV Irradiated Polycrystalline Titanium Dioxide: Differences between Acetophenone and Its Trifluoromethylated Derivative. *J. Phys. Chem. C*, **2012**, *116*, 17705–17713.

- [47] Meltzer, P.C.; Liang, A. Y.; Madras B. K. 2-Carbomethoxy-3-(diarylmethoxy)-1rH,5rH-tropane Analogs: Synthesis and Inhibition of Binding at the Dopamine Transporter and Comparison with Piperazines of the GBR Series *J. Med. Chem.*, **1996**, *39*, 371-379.
- [48] Gladiali, S.; Alberico, E. Asymmetric transfer hydrogenation: chiral ligands and applications. *Chem. Soc. Rev.*, **2006**, *35*, 226-236.
- [49] Ikariya, T.; Blacker, A. J.; Asymmetric Transfer Hydrogenation of Ketones with Bifunctional Transition Metal-Based Molecular Catalysts. *Acc. Chem. Res.*, **2007**, *40*, 1300–1308.
- [50] Zhao, M.; Yu, Z; Yan, S.; Li, Y. Room-temperature Ru(II)-catalyzed transfer hydrogenation of ketones and aldehydes in air. *Tetrahedron Lett.*, **2009**, *50*, 4624–4628.
- [51] Malacea, R., Poli, R.; Manoury, E. Asymmetric hydrosilylation, transfer hydrogenation and hydrogenation of ketones catalyzed by iridium complexes. *Coord. Chem. Rev.*, **2010**, *254*, 729–752.
- [52] Yu, J. Q.; Wu, H. C.; Ramarao, C.; Spencer, J. B.; Ley, S. V. Transfer hydrogenation using recyclable polyurea-encapsulated palladium: efficient and chemoselective reduction of aryl ketones. *Chem. Commun.*, **2003**, 678–679.
- [53] Alonso, F.; Riente, P.; Reinoso, F. R.; Martinez, J. R.; Escribano, A. S.; Yus, M. Platinum nanoparticles supported on titania as an efficient hydrogen-transfer catalyst. *J. Catal.*, **2008**, *260*, 113–118.
- [54] Alonso, F.; Riente, P.; Reinoso, F. R.; Martinez, J. R.; Escribano, A. S.; Yus, M. A Highly Reusable Carbon-Supported Platinum Catalyst for the Hydrogen-Transfer Reduction of Ketones. *Chem.Cat.Chem*, **2009**, *1*, 75–77.

- [55] Baruwati, B.; Polshettiwar, V.; Varma, R. S. Magnetically recoverable supported ruthenium catalyst for hydrogenation of alkynes and transfer hydrogenation of carbonyl compounds. *Tetrahedron Lett.*, **2009**, *50*, 1215–1218.
- [56] He, L.; Ni, J.; Wang, L. C.; Yu, F. J.; Cao, Y.; He, H. Y.; Fan, K. N. Aqueous Room-Temperature Gold-Catalyzed Chemoselective Transfer Hydrogenation of Aldehydes. *Chem.–Eur. J.*, **2009**, *15*, 11833–11836.
- [57] Shimura, K.; Shimizu, K. Transfer hydrogenation of ketones by ceria-supported Ni catalysts. *Green Chem.*, **2012**, *14*, 2983–2985.
- [58] Bachmann, W. E.. The Photochemical Reduction of Ketones to Hydrols. *J. Am. Chem. Soc.*, **1933**, *55*, 391–395.
- [59] Shiragami, T.; Pac, C. Yanagida S. Nonmetallised CdS-catalysed photoreduction of aromatic ketones to alcohols and/or pinacols. *J. Chem. Soc., Chem. Commun.*, **1989**, *13*, 831–832.
- [60] Hanley, L. Flash Photolysis of Benzophenone.
http://www.chem.uic.edu/chem343/Manuals/MainLabs/Flash_Benzophenone_F12.pdf.
- [61] Henderson, M. A. Acetone Chemistry on Oxidized and Reduced TiO₂(110) *J. Phys. Chem. B.* **2004**, *108*, 18932–18941.
- [62] Rekoske, J. E.; Barteau, M. A. Competition between Acetaldehyde and Crotonaldehyde during Adsorption and Reaction on Anatase and Rutile Titanium Dioxide. *Langmuir*, **1999**, *15*, 2061–2070.
- [63] Yoon, T. P.; Ischay, M. A.; Du, J. Visible light photocatalysis as a greener approach to photochemical synthesis *Nat. Chem.*, **2010**, *2*, 527–532.

- [64] Zeitler, K. Photoredox Catalysis with Visible Light. *Angew. Chem.*, **2009**, *48*, 9785 – 9789.
- [65] Latorre-Sanchez, M.; Lavorato, C.; Puche, M.; Fornes, V.; Molinari, R.; Garcia, H. Visible-Light Photocatalytic Hydrogen Generation by Using Dye-Sensitized Graphene Oxide as a Photocatalyst. *Chem-Eur. J.*, **2012**, *18*, 16774-16783.
- [66] Wang, X.; Pehkonen, S.O.; Ray, A. K. Photocatalytic reduction of Hg(II) on two commercial TiO₂ catalysts. *Electrochim. Acta*, **2004**, *49*, 1435-1444.
- [67] Vaidya, M. J.; Kulkarni, S. M.; Chaudhari, R. V. Synthesis of p-Aminophenol by Catalytic Hydrogenation of p-Nitrophenol. *Org. Process Res. Dev.*, **2003**, *7*, 202-208.
- [68] El Maksod, I. H. A.; Hegazy, E. Z.; Kenawy, Sayed., H. T.; S. Saleh S. An environmentally benign, highly efficient catalytic reduction of p-nitrophenol using a nano-sized nickel catalyst supported on silica-alumina.. *Adv. Synth. Catal.*, **2010**, *352*, 1169–1178.
- [69] Tada, H.; Ishida, T.; Takao, A.; Ito, S. Drastic enhancement of TiO₂-photocatalyzed reduction of nitrobenzene by loading Ag clusters. *Langmuir*, **2004**, *20*, 7898-7900.
- [70] Kraeutler, B.; Bard, A.J. Heterogeneous photocatalytic decomposition of saturated carboxylic acids on titanium dioxide powder. Decarboxylative route to alkanes. *J. Am. Chem. Soc.* **1978**, *100*, 5985-5992.
- [71] Sato, S. Photo-Kolbe Reaction at Gas-Solid Interfaces. *J. Phys. Chem.* **1983**, *87*, 3531-3537.

- [72] Ranjit, K.T.; Varadarajan, T.K.; Viswanathan, B. Photocatalytic reduction of nitrite and nitrate ions on Ru/TiO₂ catalysts. *J. Photoch. Photobio. A*, **1995**, *89*, 67-68.
- [73] Wang, H.; Yan, J.; Chang, W.; Zhang, Z. Practical synthesis of aromatic amines by photocatalytic reduction of aromatic nitro compounds on nanoparticles N-doped TiO₂. *Catal. Commun.*, **2009**, *10*, 989–994.
- [74] Wu, W; Liang, S.; Chen, Y.; Shen, L.; Zheng, H.; Wu, L. High efficient photocatalytic reduction of 4-nitroaniline to p-phenylenediamine over microcrystalline SrBi₂Nb₂O₉. *Catal. Commun.*, **2012**, *17*, 39–42.
- [75] Földner, S.; Mild, R.; Siegmund, H. I.; Schroeder, J. A.; Gruber, M.; König, B. Green-light photocatalytic reduction using dye-sensitized TiO₂ and transition metal nanoparticles. *Green Chem.*, **2010**, *12*, 400-406.
- [76] Faita Rodrigues, M. F.; Gomez Cobo, A. J. Influence of the support nature and morphology on the performance of ruthenium catalysts for partial hydrogenation of benzene in liquid phase. *Catal. Today*, **2010**, *149*, 321–325.
- [77] Amoa, K. Catalytic Hydrogenation of Maleic Acid at Moderate Pressures. *J. Chem. Educ.*, **2007**, *84*, 1948.
- [78] Sato, K.; Aoki M.; Noyori, R. A green rote to adipic acid: direct oxidation of cyclohexene with 30 percent hydrogen peroxide, *Science*, **1998**, *281*, 1646.
- [79] Rylander, P.N. *Hydrogenation Methods*, Academic Press: London, **1985**.

- [80] Wolfson, A.; Tavor, D.; Dlugy, C.; Shotland, Y. Employing glycerol in transfer hydrogenation dehydrogenation reactions. US Patent 61/137239, **2008**.
- [81] Wolfson, A.; Dlugy, C.; Shotland, Y.; Tavor, D. Glycerol as solvent and hydrogen donor in transfer hydrogenation-dehydrogenation reactions. *Tetrahedron Lett.*, **2009**, *50*, 5951-5953.
- [82] Tavor, D.; Popov, S.; Dlugy, C.; Wolfson, A. Catalytic transfer-hydrogenations of olefins in glycerol. *Org. Commun.*, **2010**, *3*, 70-75.
- [83] Anpo, M.; Aikawa, N.; Kubokawa, Y. Photocatalytic hydrogenation of alkynes and alkenes with water over titanium dioxide. Platinum loading effect on the primary processes. *J. Phys. Chem.*, **1984**, *88*, 3998-4000.
- [84] Khan, M.M.T.; Rao, N.N. Photocatalytic hydrogenation of cyclohexene through H₂O as source of H₂ by Pt/CdS/RuO₂ semiconductor particulate system catalised by K[Ru(H-EDTA)Cl]₂H₂O. *J. Mol. Catal.*, **1990**, *58*, 323-329.
- [85] Hanaoka, T.; Kubota, Y.; Takeuchi, K.; Matsuzaki, T.; Sugi, Y. Colloidal rhodium catalyzed photo transfer hydrogenation of 1,5-cyclooctadiene. *J. Mol. Catal. A*, **1995**, *98*, 157-160.
- [86] Hanaoka, T.; Matsuzaki, T.; Sugi, Y. Selective photocatalytic transfer-hydrogenation to 1,5-cyclooctadiene with light transition metal modified rhodium colloid catalyst. *J. Mol. Catal. A*, **1999**, *149*, 161-167.
- [87] Yanagawa, A.; Hatae, T.; Yada, S.; Sugimori, A.; Takagi, Y. Photo-assisted hydrogen transfer from alcohol to limonene catalyzed by [Rh₆(CO)₁₆]. *Chem. Lett.*, **1999**, *9*, 899-900.

- [88] Akioka, T.; Inoue, Y.; Yanagawa, A.; Hiyamizu, M.; Takagi, Y.; Sugimori, A. A comparative study on photocatalytic hydrogen transfer and catalytic hydrogenation of norbornadiene and quadricyclane catalyzed by $[\text{Rh}_6(\text{CO})_{16}]$. *J. Mol. Catal. A*, **2003**, *202*, 31–39.
- [89] Molinari, R.; Argurio, P.; Romeo, L. Studies on interactions between membranes (RO and NF) and pollutants (SiO_2 , NO_3^- , Mn^{++} and humic acid) in water. *Desalination*, **2001**, *138*, 270-281.
- [90] Molinari, R.; Argurio, P.; Pirillo, F. Comparison between stagnant sandwich and supported liquid membranes in copper(II) removal from aqueous solutions: Flux, stability and model elaboration. *J. Membrane Sci.*, **2005**, *256*, 158-168.
- [91] Molinari, R.; Argurio, P.; Poerio, T.; Bonaddio, F. Photo assisted fenton in a batch and a membrane reactor for degradation of drugs in water. *Sep. Sci. Technol.*, **2007**, *42*, 1597-1611.
- [92] Molinari, R.; Palmisano, L.; Drioli, E.; Schiavello M. Studies on various reactor configurations for coupling photocatalysis and membrane processes in water purification. *J. Membrane Sci.*, **2002**, *206*, 399-415.
- [93] Molinari, R.; Borgese, M.; Drioli, E.; Palmisano, L.; Schiavello M. Hybrid processes coupling photocatalysis and membranes for degradation of organic pollutants in water. *Catal. Today*, **2002**, *75*, 77-85.
- [94] Mozia, S.; Tomaszewska, M.; Morawski, A.W. A new photocatalytic membrane reactor (PMR) for removal of azo-dye Acid Red 18 from water. *Appl. Catal. B-Environ.*, **2005**, *59*, 131-137.

- [95] Mozia, S.; Morawski A.W. Hybridization of photocatalysis and membrane distillation for purification of wastewater. *Catal. Today*, **2006**, *118*, 181-188.
- [96] Mozia, S.; Tomaszewska, M.; Morawski, A.W. Photocatalytic membrane reactor (PMR) coupling photocatalysis and membrane distillation—Effectiveness of removal of three azo dyes from water. *Catal. Today*, **2007**, *129*, 3-8.
- [97] Madaeni, S.S.; Ghaemi, N. Characterization of self-cleaning RO membranes coated with TiO₂ particles under UV irradiation. *J. Membrane Sci.*, **2007**, *303*, 221-233.
- [98] Kim, S.H.; Kwak, S.-Y.; Sohn, B.-H.; Park, T.H. Design of TiO₂ nanoparticle self-assembled aromatic polyamide thin-film-composite (TFC) membrane as an approach to solve biofouling problem, *J. Membrane Sci.*, **2003**, *211*, 157-165.
- [99] Azrague, K.; Aimar, P.; Benoit-Marquié, F.; Maurette, M.T. A new combination of a membrane and a photocatalytic reactor for the depollution of turbid water. *Appl. Catal. B-Environ.*, **2007**, *72*, 197-204.
- [100] Camera-Roda, G.; Santarelli, F. Intensification of Water Detoxification by Integrating Photocatalysis and Pervaporation. *J. Sol. Energ. Eng.*, **2007**, *129*, 68-73.
- [101] Olah, G.A.; Goeppert, A.; Surya Prakash G.K. Chemical recycling of carbon dioxide to methanol and dimethyl ether: from greenhouse gas to renewable, environmentally carbon neutral fuels and synthetic hydrocarbons. *J. Org. Chem.*, **2009**, *74*, 487-498.
- [102] Benson, S.; Cook P. In: *IPCC Special Report on Carbon Dioxide Capture and Storage*; Metz, B.; Davidson, O.; de Coninck, H.; Loos,

- M.; Meyer, L. Eds; Cambridge University Press: New York, **2005**; pp.197-276.
- [103] Asi, M.A.; He, C.; Su, M.; Xia, D.; Lin, L.; Deng, H.; Xiong, Y.; Qiu, R.; Li, X.-Z. Photocatalytic reduction of CO₂ to hydrocarbons using AgBr/TiO₂ nanocomposites under visible light. *Catal. Today*, **2011**, *175*, 256–263.
- [104] Ashley, M.; Magiera, C.; Ramidi, P.; Blackburn, G.; Scott, T.G.; Gupta, R.; Wilson, K.; Ghosh, A.; Biswas, A. Nanomaterials and processes for carbon capture and conversion into useful by-products for a sustainable energy future. *Greenhouse gases: science and technology*, **2012**, *2*, 419-444.
- [105] Pan, P.W.; Chen, Y.W. Photocatalytic reduction of carbon dioxide on NiO/InTaO₄ under visible light irradiation. *Catal. Commun.*, **2007**, *8*, 1546-1549.
- [106] Zhang, Q.H.; Han, W.D.; Hong, Y.J.; Yu, J.G. Photocatalytic reduction of CO₂ with H₂O on Pt-loaded TiO₂ catalyst. *Catal. Today*, **2009**, *148*, 335-340.
- [107] Usubharatana, P.; McMartin, D.; Veawab, A.; Tontiwachwuthikul, P. Photocatalytic process for CO₂ emission reduction from industrial flue gas streams. *Ind. Eng. Chem. Res.*, **2006**, *45*, 2558-2568.
- [108] Aliwi, S.M.; Aljubori, K.F. Photoreduction of CO₂ by metal sulphide semiconductors in the presence of H₂S. *Sol. Energ. Mat. Sol. C.*, **1989**, *18*, 223-229.
- [109] Cao, L.; Sahu, S.; Anilkumar, P.; Bunker, C.E.; Xu, J.; Shiral Fernando, K.A.; Wang, P.; Gulians, E.A.; Tackett, K.N. Sun. Y.-P. Carbon nanoparticles as visible-light photocatalysts for efficient CO₂ conversion and beyond. *J. Am. Chem. Soc.*, **2011**, *133*, 4754–4757.

- [110] Premkumar, J.R.; Ramaraj, R. Photoreduction of carbon dioxide by metal phthalocyanine adsorbed Nafion membrane. *Chem. Commun.*, **1997**, 343-344.
- [111] Haick, H.; Paz, Y. Long-range effects of noble metals on the photocatalytic properties of titanium dioxide. *J. Phys. Chem. B*, **2003**, *107*, 2319-2326.
- [112] Egerton, T.A.; Tooley, I.R. Effect of changes in TiO₂ dispersion on its measured photocatalytic activity. *J. Phys. Chem. B*, **2004**, *108*, 5066-5072.
- [113] Anpo, M.; Yamashita, H.; Ichihashi, Y.; Fujii, Y.; Honda, M. Photocatalytic reduction of CO₂ with H₂O on titanium oxides anchored within micropores of zeolites: effects of the structure of the active sites and the addition of Pt. *J. Phys. Chem. B*, **1997**, *101*, 2632-2636.
- [114] Stathatos, E.; Lianos, P.; Falaras P.; Siokou, A. Photocatalytically deposited silver nanoparticles on mesoporous TiO₂ films. *Langmuir*, **2000**, *16*, 2398-2400.
- [115] Ohka, Y.; Tatsuma, T.; Fujii, T.; Naoi, K.; Niwa, C.; Kubota, Y.; Fujishima, A. Multicolour photochromism of TiO₂ films loaded with silver nanoparticles. *Nat. Mater.*, **2003**, *2*, 29-31.
- [116] Pathak, P.; Meziani, M.J.; Castillo, L.; Sun, Y.-P. Metal-coated nanoscale TiO₂ catalysts for enhanced CO₂ photoreduction. *Green Chem.*, **2005**, *7*, 667-670.
- [117] Liu, P.; Bandara, J.; Lin, Y.; Elgin, D.; Allard, L. F.; Sun, Y.-P. Formation of nanocrystalline titanium dioxide in perfluorinated ionomer membrane. *Langmuir*, **2002**, *18*, 10398-10401.

- [118] Nishimura, A.; Okano, Y. Hirota, M.; Hu, E. Effect of Preparation Condition of TiO₂ Film and Experimental Condition on CO₂ Reduction Performance of TiO₂ Photocatalyst Membrane Reactor. *International Journal of Photoenergy*, **2011**,
- [119] Nishimura, A; Komatsu, N.; Mitsui, G.; Hirota, M.; Hu, E. CO₂ reforming into fuel using TiO₂ photocatalyst and gas separation membrane. *Catalysis Today*, **2009**, 148, 341, 349.
- [120] Camera-Roda, G.; Santarelli, F.; Augugliaro, V.; Loddo, V.; Palmisano, G.; Palmisano, L.; Yurkadal, S. Photocatalytic process intensification by coupling with pervaporation. *Catal. Today*, **2011**, 161, 209-213.
- [121] Augugliaro, V.; Camera-Roda, G.; Loddo, V.; Palmisano, G.; Palmisano, L.; Parrino, F.; Puma, M.A. Synthesis of vanillin in water by TiO₂ photocatalysis. *Appl. Catal. B-Environ.*, **2011**, 111–112, 555–561.
- [122] Noubigh, A.; Mgaidi, A.; Abderrabba, M.; Provost, E.; Fürst, W. Effect of salts on the solubility of phenolic compounds: experimental measurements and modelling. *J. Sci. Food. Agr.*, **2007**, 87, 783-788.
- [123] Noubigh, A.; Abderrabba, M.; Provost, E. Temperature and salt addition effects on the solubility behaviour of some phenolic compounds in water. *J. Chem. Thermodyn.*, **2007**, 39, 297-303.

7

TiO₂ and Pd/TiO₂ as photocatalysts for hydrogenation of acetophenone in ethanol and aqueous solution under UV and visible light in batch and membrane reactors.

7.1 Introduction

The reduction of carbonyl compounds in the corresponding alcohols is an important transformation in organic synthesis [1]. Acetophenone has been used as a model substrate for hydrogenation of aromatic ketones in many studies [2,3]. The reduction product, phenylethanol, is used as a building block for the synthesis of bioactive compounds such as agrochemicals, pharmaceuticals, and natural products [4]. Moreover, phenylethanol is a high-value aroma compound with a rose-like odor that is used widely in flavor and fragrance compositions. For most applications natural flavors are preferred, but, due to limited natural resources of phenylethanol more production of this compound is essential [5].

Homogeneous (e.g. Ru, Ir) and heterogeneous catalysts (e.g. Pd, Pt, Ru and Au) have been reported to be effective for ketones reduction [6,14].

Recently Shimura et al. [1] reported the use of Ni-loaded CeO₂ as catalyst for the transfer hydrogenation of aliphatic and aromatic ketones to the corresponding alcohols by using 2-propanol without base as co-catalyst.

Since long time photochemical reactions [15], and more recently photocatalytic reductions [16] represent alternative routes and more sustainable methods to synthesize organic compounds with mild conditions and cheaper catalysts.

The most widely used photocatalyst for different applications, such as purification of waste water, photocatalytic oxidation and, more recently for reduction, is titanium dioxide (TiO₂).

Largely used as electron and hydrogen donor for photocatalytic reductions are alcohols. These donors are used in large excess (e.g. as solvent) to shift the reaction to the desired product, because during the transfer hydrogenation alcohols are oxidized to ketones or aldehydes that can compete with the substrate. On the contrary, the use of formic acid as electron and hydrogen donor, avoids the above problem because it is converted into carbon dioxide (CO₂) and hydrogen (H₂) making the reaction irreversible, and limits the formation of by products in the reactive environment [19-20]. Moreover, using formic acid in photocatalytic reactions (one of the major pollutants present in pharmaceutical wastewater) a simultaneous decomposition of pollutants and photocatalytic reduction of organics can take place.

Kohtani et al. [17] reported the photocatalytic activity of polycrystalline P25 TiO₂ powder to hydrogenate acetophenone and others aromatic ketones using methanol, ethanol, and propan-2-ol as solvent and electron donor under UV light. Escobar et al., reported photocatalytic transfer

hydrogenation of ketones using titanium dioxide as photocatalyst and 2-propanol as hydrogen donor [18].

Until now there are still not evidence in the use of formic acid as electron donor in the photocatalytic hydrogenation of ketones, while the use of a mixture of pollutants (oxalic acid, formic acid and formaldehyde) as electron donor was reported to enhance photocatalytic hydrogen generation [21]. Only recently Imamura et al. [19] studied photocatalytic reduction of nitrobenzenes and aminonitrobenzenes (m-NBS) in aqueous suspensions of titanium(IV) oxide as catalyst and formic acid or oxalic acid as electron donor employing deaerated and aerated conditions under UV light. Authors reported that formic acid was efficient as hole scavenger preventing the oxidation of m-NBS and the re-oxidation of m-ABS also under aerated condition. In view to make a cheaper and very green process, the best solvent is water; in addition the use of pollutants as electron donor for photocatalytic hydrogenation of organics makes this reaction more sustainable if it can be conducted under visible light.

Solar light contains only a small amount (about 4%) of energy in the UV region. For practical application, the use of visible light, as the driving force for chemical reactions has attracted much attention of organic chemists [22,23]. Moreover, high-energy UV-light often induces undesired by-products due to the excessive energy input in the reactive environment, which can be limited by using visible light as energy source, a field that is developing only in the last years [24].

The main problems of using titanium dioxide, cheap and widely available photocatalyst, are the electron/hole recombination and the spectrum of absorbance mainly in the UV region. However, noble metals, including Pt, Au, Pd, Rh, Ni, Cu and Ag have been reported to be very effective for

enhancement of TiO₂ photocatalytic activity decreasing the possibility of electron-hole recombination and reducing the band gap energy of the photocatalyst, thus shifting the radiation absorption towards higher wavelengths, permitting to use visible light. Recently, Li et al [24] reported the selective hydrogenation of various ketones under visible light by using four types of iridium-based complexes as co-catalysts supported on CdS nanoparticles as semiconductor. Very recently Ke et al. reported the selective reduction of various organic compounds using semiconductors loaded with gold nanoparticles [25].

In view of large scale applications photocatalytic membrane reactors combine the advantage of classical photoreactors and those of membrane processes with a synergy of both technologies. The membrane allows not only the recovery of the catalyst, immobilizing it on the membrane or using membrane to maintain the catalyst in suspension, but also the selective separation of the desired product from the reaction mixture permitting to obtain improvements of yield and selectivity limiting side catalytic reactions.

Despite the great potentiality of the photocatalytic processes and the important advantages that can be achieved by its coupling with a membrane separation system, there are still not evidence of their use in photocatalytic reduction of ketones.

In the present chapter the hydrogenation of acetophenone was investigated using commercial and palladium doped titanium dioxide in ethanol or water as solvent in photocatalytic batch and membrane reactors.

In particular, using ethanol as solvent and electron donor in batch reactor, different aspects have been investigated: (i) photochemical and photocatalytic hydrogenation of acetophenone, (ii) TiO₂ concentration,

(iii) UV and visible light activity of titanium dioxide doped with palladium, (iv) different intensity and distribution of irradiation source, (v) mixture of water ethanol (1:1) as solvent and electron donor.

Photocatalytic tests on hydrogenation of acetophenone using water as solvent and formic acid as electron donor were conducted in batch and membrane reactors. In particular tests were performed initially in a batch reactor optimizing the operative conditions such as (i) acetophenone, (ii) catalyst and (iii) formic acid concentrations, (iv) addition of methanol in aqueous solution, (v) pH. Subsequently in membrane reactors in which we tested (i) different substrate addition mode, (ii) visible light activity of palladium doped TiO₂ compared with commercial titanium dioxide under UV and visible light, (iii) formic acid and triethyl amine as electron donor, (iv) and different flow rates in order to study the influence of these parameters on phenylethanol production.

The results presented below open a new way for green photocatalytic reduction of ketones in water, under visible light, using a pollutant as electron donor obtaining an efficient extraction of the product from the aqueous phase during the photocatalytic tests by using a photocatalytic continuous membrane reactor.

7.2 Experimental section

7.2.1 Apparatus and Methods

Preliminary experimental tests on photocatalytic hydrogenation of acetophenone, using ethanol or water as solvent, were conducted in the batch reactor reported in Figure 7.1. The system consists of a cylindrical pyrex glass reactor with a volume of 500 mL with an immersed mercury lamp (medium pressure Hg lamp, 125 W, Helios Italquartz). The reactor is

equipped with 3 outputs in its top section for sampling the suspension, for blowing argon and for its degassing. In the photocatalytic reductions the removal of O_2 from the reaction mixture, blowing argon before the reaction, is required to improve the reaction rates and selectivity because O_2 behaves as a competitive scavenger of the electron (e_{cb}) on the photocatalyst surface and is converted to reactive oxygen radical (O_2^\bullet). The UV lamp was positioned axially inside the reactor and the circulation of distilled water, in the pyrex glass jacket surrounding it, allowed to maintain the system at a temperature of $32^\circ C$. The solution is subjected to agitation using a magnetic stirrer.

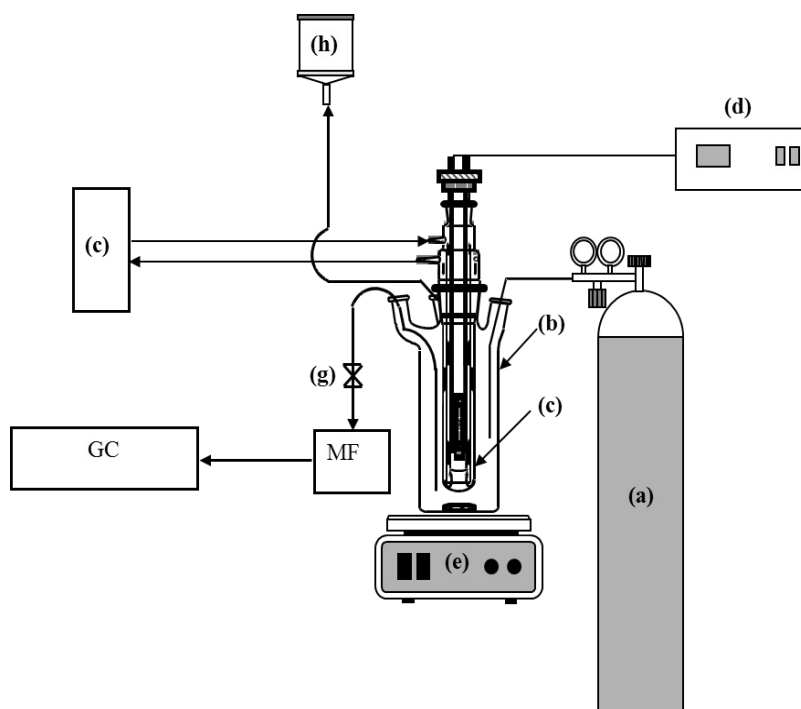


Figure 7.1. Scheme of the batch photoreactor: (a) argon cylinder; (b) photoreactor; (c) medium pressure Hg lamp with cooling jacket; (d) power supply; (e) magnetic stirrer; (f) thermostatic bath with cooling water; (g) sampling valve; (h) degassing system; (MF) samples microfiltration; (GC) gas chromatographic analyses.

Photocatalytic tests were carried out using different irradiation sources, for UV irradiation was used the immersed lamp previous described with the emission spectrum showed in Figure 7.2, while part of this study was performed by irradiating the reactive solution with a LED immersed lamp which has the emission spectrum from 400 to 800 nm, see Figure 7.3. This study with LED radiation ensures that the hydrogenation of acetophenone is exclusively due to visible-region excitation.

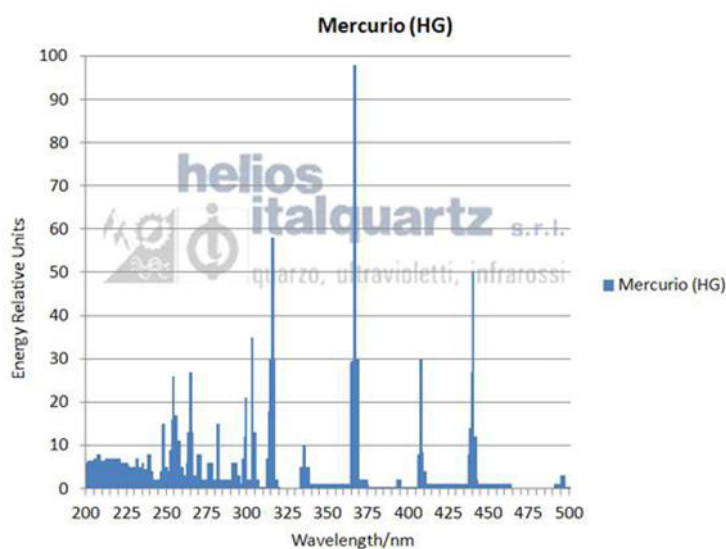


Figure 7.2. Emission spectrum of UV lamp.

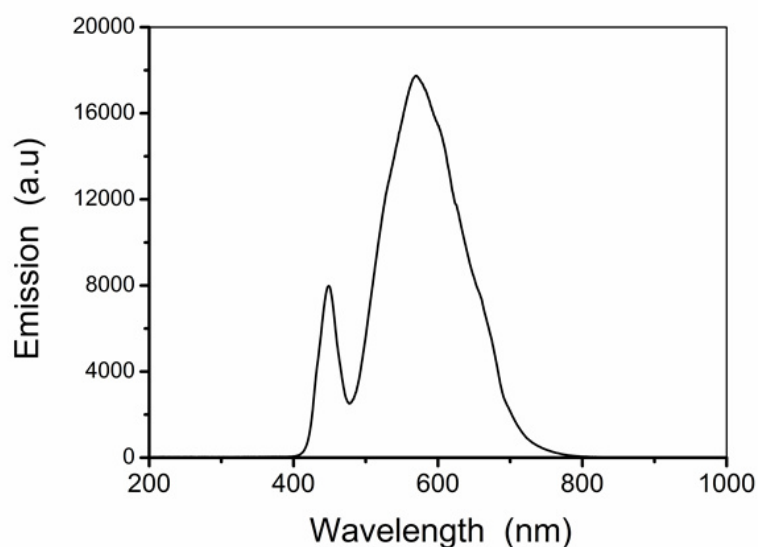


Figure 7.3. Spectrum of emission of LED immersed lamp.

Samples were taken from the solution each hour during all photocatalytic tests to identify concentrations of species involved in the chemical reaction. Each test was stopped after 7 hours. The samples were filtered through a hydrophobic membrane made of polypropylene (GH-Polypro, Pall Corporation, pore size 0.2 μm) to remove the catalyst before the analysis. When the photocatalytic tests were conducted in water, all samples were diluted with 50% of ethanol before to be filtered in order to avoid the adsorption of the reactant and the products on the membrane.

The photocatalytic tests conducted in batch photoreactor with ethanol as solvent were carried out using the following operative conditions: 50 mmol of acetophenone (5,84 mL) as substrate (on the basis of the amount used by Kohtany et al. [17]), an appropriate amount of TiO_2 and Pd/TiO_2 as photocatalysts; while, tests employing water as solvent were carried out using the following operative conditions: different concentrations of

acetophenone as substrate, different amount of TiO_2 and Pd/TiO_2 as photocatalysts and formic acid as hydrogen source and electron donor.

Experimental tests on photocatalytic hydrogenation of acetophenone in water solution in membrane photoreactors were performed in the systems schematized in Figures 7.4 and 7.5. Both photoreactors were made by coupling the membrane contactor module with the batch photocatalytic reactor previously mentioned (Figure 7.1) by means of a peristaltic pump that withdraws the solution from the photocatalytic zone to the separation zone. The solution comes back in the photoreactor by gravity. The permeation module, immersed in a thermostatic bath, is constituted by two compartment cells (each one with a volume of 130 mL) separated by a flat sheet of polypropylene membrane with an exposed membrane surface area of 28.3 cm^2 . The first compartment contains the aqueous phase coming from the photoreactor where the reaction was carried out, while the second one contains an organic stripping solution (heptane or acetophenone) mechanically stirred by a motor. Samples were withdrawn from the organic phases and analyzed each hour.

The photocatalytic tests conducted in membrane photoreactors were carried out using the following operative conditions: 1.5 g/L of titanium dioxide and Pd/TiO_2 as photocatalyst, 1.9 M of formic acid used as hydrogen and electron donor, pH 7.5, and water as solvent for a total volume of 724 mL. Acetophenone as substrate was added with different addition mode:

- 0.019 moles of acetophenone added with a syringe pump in the aqueous phase (Figure 7.5);
- 0.019 moles of substrate added in 130 mL of heptane used as organic phase (Figure 7.4);

- 130 mL of acetophenone used as both organic extracting phase and substrate reservoir (Figure 7.4).

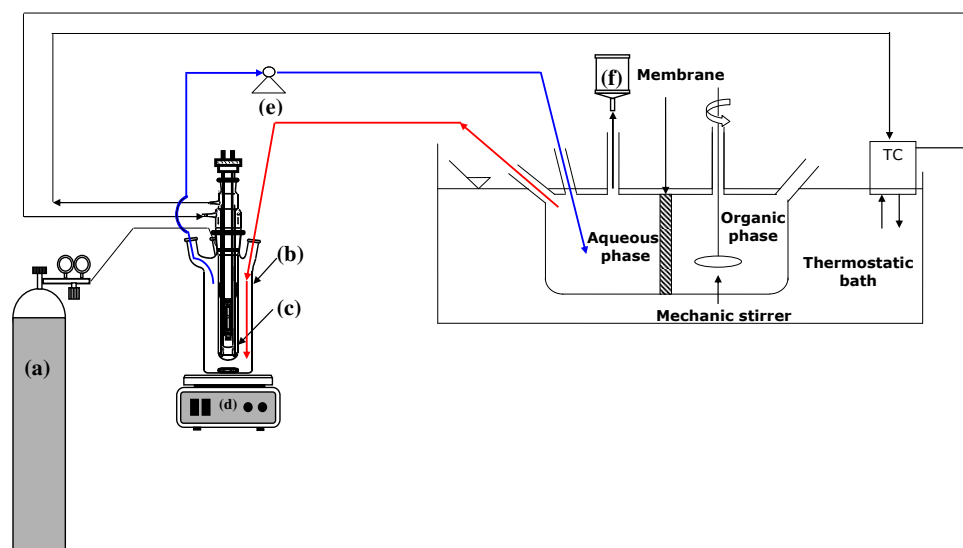


Figure 7.4. Scheme of the membrane photoreactor: (a) argon cylinder; (b) photoreactor; (c) medium pressure Hg lamp with cooling jacket; (d) magnetic stirrer; (e) peristaltic pump; (f) degassing system; (TC) temperature controller.

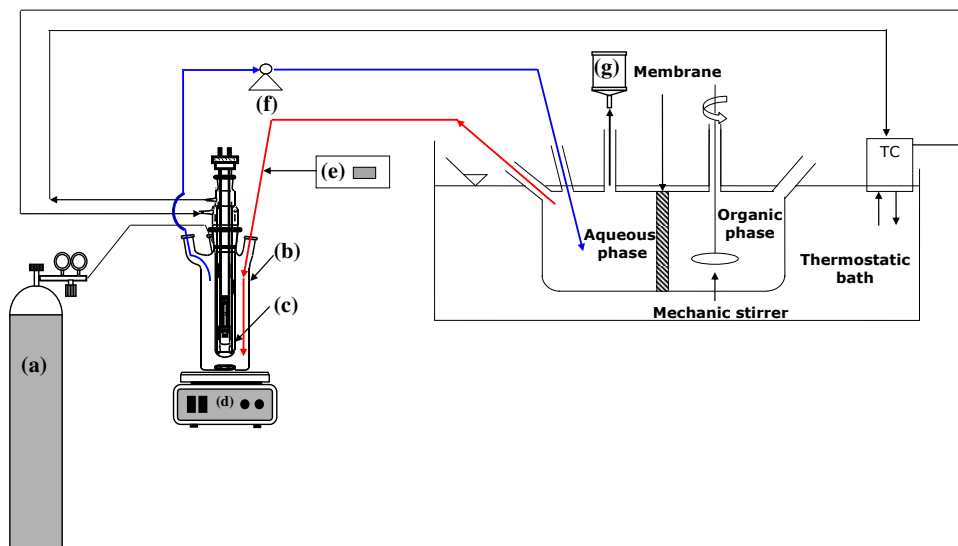


Figure 7.5. Scheme of the membrane photoreactor with syringe pump: (a) argon cylinder; (b) photoreactor; (c) medium pressure Hg lamp with cooling jacket; (d) magnetic stirrer; (e) syringe pump for substrate feed; (f) peristaltic pump; (g) degassing system; (TC) temperature controller.

Detection of possible reaction products was performed by a Gas Chromatograph, Agilent model 6890N equipped with a FID detector and a capillary column SupelcowaxTM 10 (Fused silica, 10 m x 0.1mm x 0.1 μ m film thickness). After separating the peaks of interest acetophenone and phenylethanol calibrations were carried out preparing and injecting three times different standards solutions.

The experimental tests were repeated three times to ensure that are ripetibile. The results of the experimental tests have been elaborated using the following parameters:

$$\text{Acetophenone conversion} = \frac{\text{moles reacted of acetophenone}}{\text{initial moles of acetophenone}} \times 100$$

$$\text{Selectivity to phenylethanol} = \frac{\text{moles of phenylethanol produced}}{\text{moles of reacted acetophenone}} \times 100$$

$$Q\% = \frac{\text{moles of phenylethanol extracted}}{\text{moles of phenylethanol tot.}} \times 100$$

$$\text{Productivity to phenylethanol} = \frac{\text{mg of phenylethanol tot.}}{\text{g of catalyst x hour}}$$

$$\text{Productivity to phenylethanol in organic phase} = \frac{\text{mg of phenylethanol extracted in org. phase}}{\text{g of catalyst x hour}}$$

Materials:

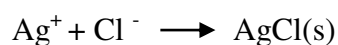
Titanium dioxide P25 (TiO₂) from Degussa was used as photocatalyst; Palladium(II) chloride, (PdCl₂, 99% purity) from Aldrich, was used to synthesize Pd/TiO₂; Ethanol absolute (C₂H₆O₂, 99.8% purity) from Panreac, was used as solvent and electron and hydrogen donors; Formic acid (CH₂O₂ 99% purity) from Carlo Erba reagents, was used as electron donors; Acetophenone Reagent Plus (C₈H₈O, 99% purity) from Sigma Aldrich, was used as substrate; n-Heptane analytical reagent A.R. (C₇H₁₆, 95% purity) from LAB-SCAN Analytical Sciences, was used as organic phase; sodium hydroxide, pellets, (NaOH 97+% purity), from Aldrich, was used to change the pH of the aqueous solution; Silver nitrate (AgNO₃) from Sigma Aldrich, was used for the argentometric method.

7.2.2 Synthesis of Pd/TiO₂

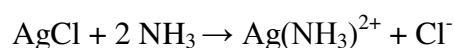
Pd/TiO₂ was synthesized by deposition-precipitation method. This preparation started with the dispersion of TiO₂ (4 g) in 40 mL of water in which 250 μL of ammonia (NH₃) were added to raise the pH to 10. The required amount of Pd (PdCl₂ acidic solution 0.056 M) was added drop wise to the basic TiO₂ solution under vigorous stirring for 2 hours. The pH was monitored and maintained between 9 and 10 by adding ammonia. This mixture was stirred for 30 min, after the solid was washed with water in order to remove chloride ions and ammonia, in particular small quantities of chloride ions can alter the properties of the catalyst because they can have a promoting or poisoning effect. These alterations in the activity of the catalyst are often caused by simple physical blocking of some adsorption sites.

The presence of chloride ions and ammonia in washing water were detected with the argentometric method and measuring the pH, respectively.

Argentometric method consists in the addition of silver nitrate solution (0.01M) in the aqueous solution containing chloride ions that reacts with silver ion forming a white precipitate, by the following reaction:



The presence of ammonia prevents the precipitation of chloride ions because the AgCl(s) can react with NH₃ and then solubilize, as shown in the following reaction:



The addition of nitric acid to the basic solution avoids the above problem because it allows to destroy the complex formed obtaining again the precipitation of AgCl(s).

Finally, the resulting catalyst was reduced chemically by adding 0.0711 g of NaBH₄ to Pd/TiO₂ suspended in 58.8 mL of distilled water under vigorous stirring at room temperature. Then the sample was dried at 100 °C for 24 h. The overall Pd/TiO₂ synthesis is schematized in Figure 7.6.

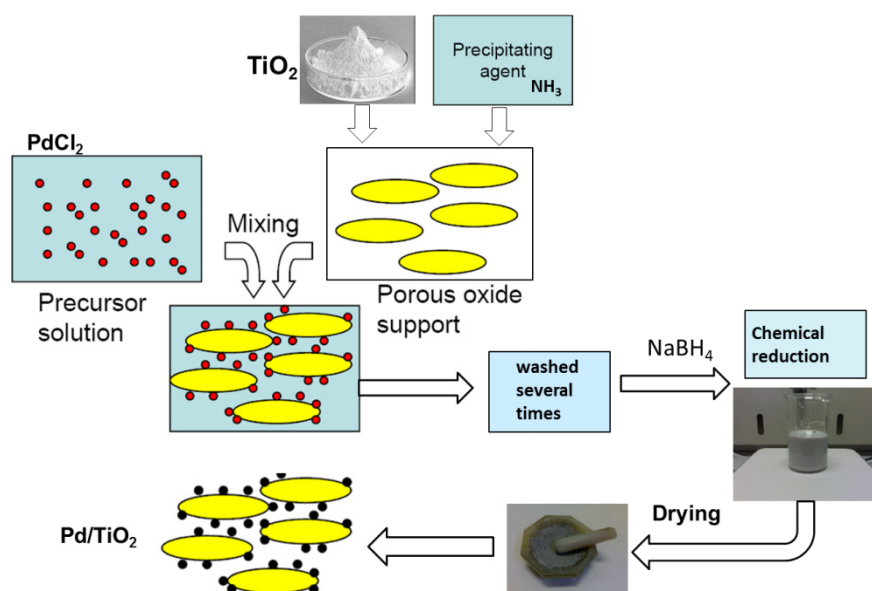


Figure 7.6. Schematization of Pd/TiO₂ synthesis.

The resulting Pd/TiO₂ sample was characterized by X-ray photoelectron spectroscopy (XPS) analysis that was performed using a VG-Escalab 210 photoelectron spectrometer with an Mg K α X-ray resource.

7.3. Results and discussion

7.3.1. Pd/TiO₂ characterization

The characterization of Pd/TiO₂ sample was carried out by X-ray photoelectron spectroscopy (XPS).

The XPS analysis showed that there are Ti, O, C and Pd elements on all the surface of the Pd/TiO₂ samples. The Ti element results from the TiO₂. The O element is assigned to TiO₂ and CO. The C element is assigned to the C pollution in the instrument.

The high resolution XPS of Ti 2p spectra are shown in Figure 7.7. All Ti 2p spectra of photocatalysts are usually characterized by a main doublet composed of two peaks. For TiO₂, the Eb (Ti 2p_{3/2}) is 460.24 eV and Eb (Ti 2p_{1/2}) is 466.018 eV, respectively, the binding energy difference, $E_b = E_b(\text{Ti } 2p_{1/2}) - E_b(\text{Ti } 2p_{3/2})$ is 5.7 eV, as reported in the literature [27]

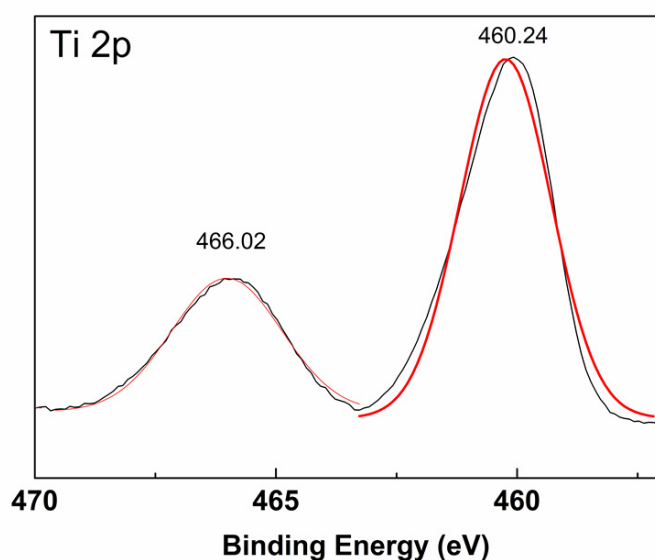


Figure 7.7. XPS (Ti2p) spectra of TiO₂

The percentage of Pd loaded on the TiO₂ surface correspond to 0.65%. The Pd (3d) peaks of Pd/TiO₂ are presented in Figure 7.8. The peaks at 347.5.0 eV (Pd 3d 5/2) and 342.86 eV (Pd 3d 3/2) are assigned to PdO.

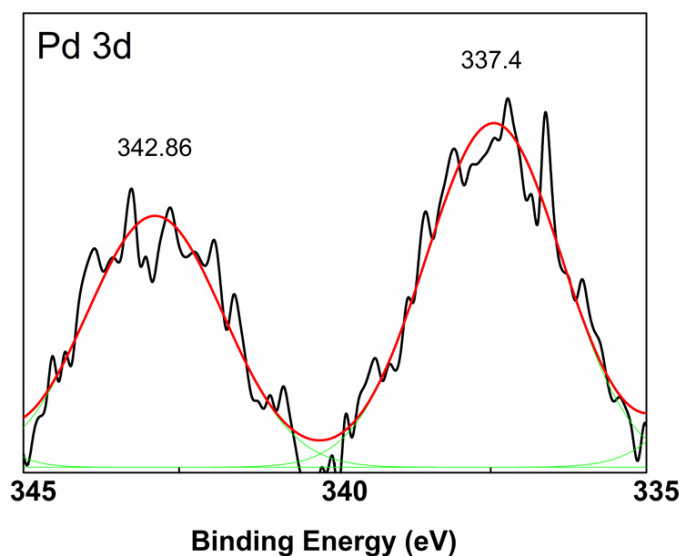


Figure 7.8. XPS (Pd3d) spectra of Pd/TiO₂

7.3.2 Photocatalytic hydrogenation of acetophenone in ethanol in batch reactor

Experimental tests on photocatalytic hydrogenation of acetophenone, conducted in batch reactor, using ethanol as solvent and electron and hydrogen donor, were carried out in order to investigate different aspects: photochemical and photocatalytic hydrogenation of acetophenone, different TiO₂ concentration, type of catalyst, different intensity and distribution of irradiation source, addition of 50% of water.

7.3.2.1 Amount of titanium dioxide

In order to optimize the operative conditions for photocatalytic hydrogenation of acetophenone in batch reactor in ethanol, tests with different amounts of titanium dioxide as photocatalyst were carried out.

In particular, the following amounts were considered:

- 0.1 g/L;
- 0.8 g/L;
- 1.5 g/L;
- 3.0 g/L;

The results show that increasing the amount of the catalyst acetophenone conversion decreases while the selectivity to phenylethanol increases (Figures 7.9 and 7.10).

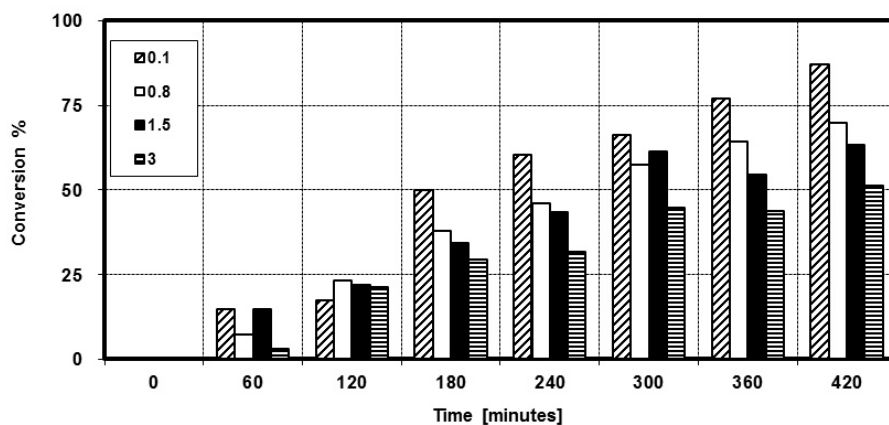


Figure 7.9. Comparison of acetophenone conversion vs. time using different amount of catalyst: 0.1 g/L, 0.8 g/L, 1.5 g/L, 3 g/L. Operative conditions: 500 mL ethanol, 50 mmol acetophenone, 32 °C, t=7h.

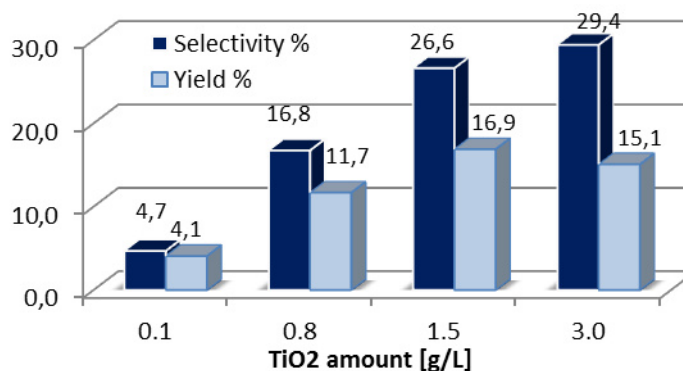


Figure 7.10. Comparison of selectivity and yield % using different amount of catalyst: 0.1 g/L, 0.8 g/L, 1.5 g/L, 3 g/L. Operative conditions: 500 mL ethanol, 50 mmol acetophenone, 32 °C, and 7h.

The yield has a maximum value for the amount of TiO₂ equal to 1.5 g/L (Figure 7.10). This trend can be explained considering that increasing the catalyst amount upper than a critical value a screening effect (increase in opacity and light scattering) of excess of particles occurs, which leads to a decreased passage of radiation through the suspension.

The selectivity to phenylethanol was enhanced increasing the photocatalyst concentration. On the contrary the acetophenone conversion value decreases using higher amount of TiO₂, this trend can be explained considering that the decreased passage of the radiation limits the reactivity of the system. This behavior could indicate a system reactive also without the catalyst. In fact, acetophenone is a photosensitive molecule that can absorb UV light (photolysis).

7.3.2.2 Acetophenone photolysis

The blank test without the catalyst in ethanol solution was carried out to confirm the possibility of photochemical reaction and to study the effect of UV-light irradiation on acetophenone. In Figure 7.11, it can be observed

that acetophenone conversion without photocatalyst is higher than by using 1.5g/L of TiO₂ (94% and 63.5% respectively). Despite this, phenylethanol production is very lower in the photochemical reaction (without the catalyst) than in the photocatalytic reaction (with the catalyst), obtaining a phenylethanol concentration of 4 and 20 mmol/L, respectively.

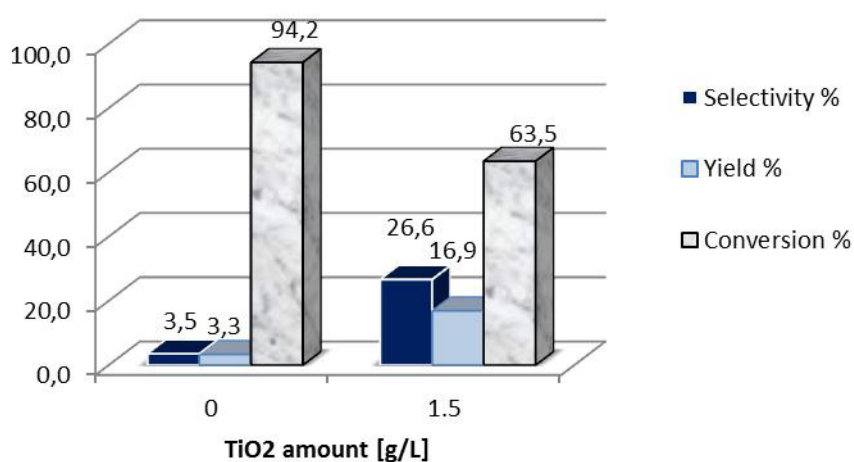
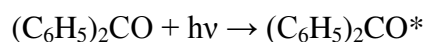
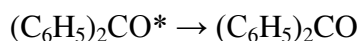


Figure 7.11. Comparison of acetophenone conversion, selectivity and phenylethanol yield % using 1.5 g/L of TiO₂ and without catalyst. Operative conditions: 500 mL ethanol, 50 mmol acetophenone, 32 °C, t=7h.

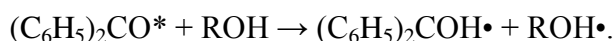
Obtained results confirm acetophenone photolysis. The mechanism of acetophenone photolysis is probably similar to that described for benzophenone ((C₆H₅)₂CO) [28]: when the substrate absorbs a UV/Visible photon, it is excited to its first electronic state:



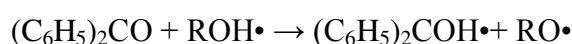
The excited benzophenone ($(\text{C}_6\text{H}_5)_2\text{CO}^*$) can then undergo intersystem crossing to the triplet state that can either i) slowly phosphoresce back down to the ground state



or, in the presence of isopropanol, ii) a proton is abstracted from the alcohol to form a protonated ketyl radical:



The $\text{ROH}\cdot$ radical can interact with the ground state of benzophenone to generate even more protonated ketyl radicals:



These intermediates start typical radical chain reactions.

This mechanism explains the very low selectivity (3.5%) and yield to phenylethanol (3.3%) despite the high acetophenone conversion value (Figure 6) due to unselective radical reactions resulting in predominant by-product formation.

In comparison to the test carried out with TiO_2 , the presence of the catalyst allows to obtain higher selectivity towards the desired product (26.6%) and higher yield (16.9%), because the semiconductor absorbs light then shields acetophenone from light radiation by limiting the radical reactions. As reported in Figure 7.10, the selectivity improves with the catalyst amount, because the contribution of photochemical reaction decreases by increasing the screen effect.

Furthermore electrons and holes that migrate on the surface of the semiconductor can, respectively, reduce acetophenone and oxidize ethanol to allow the transfer of the hydrogen from ethanol to acetophenone to produce phenylethanol. The photocatalytic transfer hydrogenation mechanism is the following:

TiO₂ absorbs light with separation of the electron–hole couple



Holes that migrate to the surface of the semiconductor can oxidize the ethanol adsorbed on photocatalyst with formation of acetaldehyde and H⁺



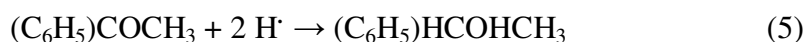
Electrons can reduce H⁺ to atomic hydrogen [20]



Atomic hydrogen can both recombine and desorb



or reacts with a substrate such as acetophenone (5).



7.3.2.3 Pd/TiO₂ photocatalytic activity

Experiments conducted in ethanol using Pd/TiO₂ were carried out in order to study the effect of the presence of Pd on TiO₂. It has been largely reported that noble metals are very effective for enhancing TiO₂ photocatalytic activity reducing the electron/hole recombination [29]. Furthermore Pd is the most widely used catalyst in transfer hydrogenation reactions. Figure 6 shows that acetophenone conversion with TiO₂ and Pd/TiO₂ were 63.5% and 96.2%, respectively. As expected acetophenone conversion increases using Pd/TiO₂ because noble metals reduce the possibility of electron-hole recombination, resulting in a stronger photocatalytic activity (7.12).

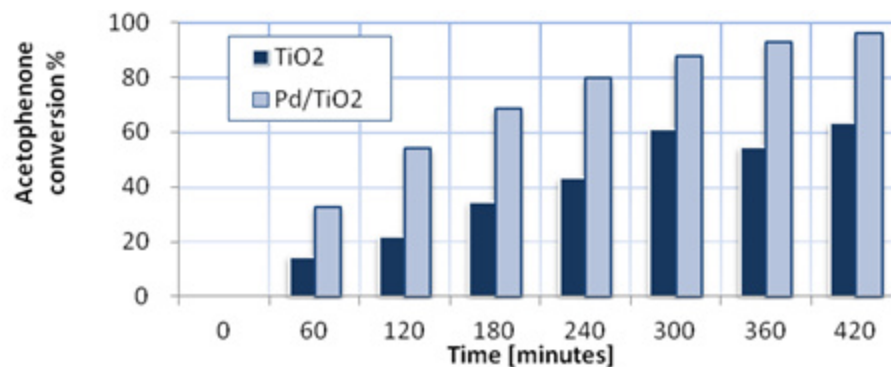


Figure 7.12. Comparison of acetophenone conversion vs. time using TiO₂ and Pd/TiO₂ as catalyst. Operative conditions: 500 mL ethanol, 50 mmol acetophenone, 1.5 g/L of photocatalyst, 32 °C, t=7h.

The values of selectivity and yield to phenylethanol significantly decrease using Pd/TiO₂ as catalyst as showed in Figure 7.13, due to the higher system activity.

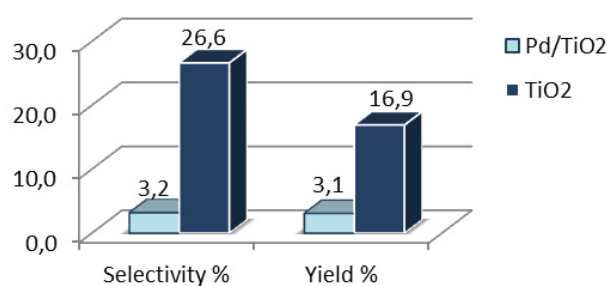


Figure 7.13. Comparison of selectivity and phenylethanol yield % using TiO₂ and Pd/TiO₂ as catalyst Operative conditions: 500 mL ethanol, 50 mmol acetophenone, 1.5 g/L of photocatalyst, 32 °C, t=7h.

Moreover a higher production of acetaldehyde from ethanol, almost three times more, using Pd/TiO₂ in comparison to the test carried out with TiO₂ alone, was observed (Figure 7.14).

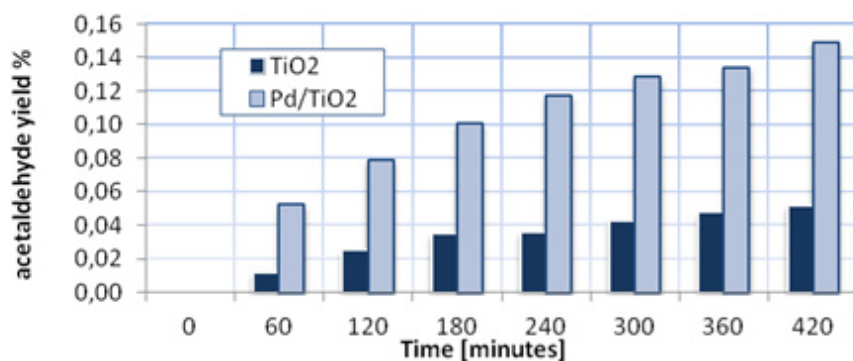
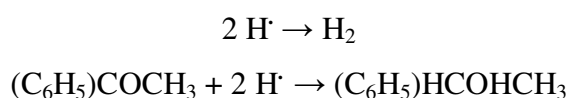


Figure 7.14. Comparison of acetaldehyde yield% vs. time using TiO₂ and Pd/TiO₂ as catalyst. Operative conditions: 500 mL ethanol, 50 mmol acetophenone, 1.5 g/L of photocatalyst, 32 °C, t=7h.

This phenomenon can be explained by considering the photocatalytic transfer hydrogenation mechanism described in the previous paragraph. As reported, electrons can reduce H⁺ to atomic hydrogen (3) that can either recombine and desorb generating hydrogen (4) or react with acetophenone (5) reducing it.

The higher production of acetaldehyde observed during the test conducted using Pd/TiO₂ indicate a significant atomic hydrogen production that reacted both with itself (4) and with acetophenone (5):



In fact, during the catalytic tests with Pd/TiO₂ an evolution of gas, from the reaction environment, was observed, and the possibility to produce H₂ using this catalyst was experimentally confirmed.

7.3.2.4 Influence of the intensity and distribution of irradiation source.

Tests conducted using two medium pressure Hg lamps, 125 W, Helios Italquartz, with different intensity of light irradiation ($I_A=35 \text{ mW/cm}^2$, used in the previous tests; $I_B=55 \text{ mW/cm}^2$) and different intensity distribution of the light irradiation ($W_B < W_A$, W = wide of intensity of the irradiation source, I = intensity of irradiation source) along the height of the reactor from the magnetic stirrer (figure 7.15) were carried out in order to know the influence of these parameters on the photocatalytic transfer hydrogenation of acetophenone using both TiO_2 and Pd/TiO_2 catalyst.

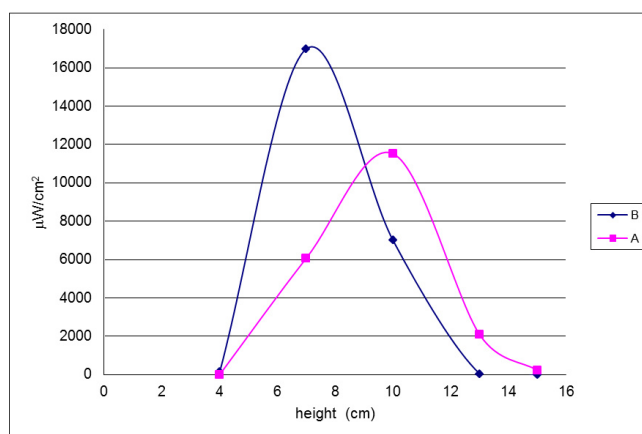


Figure 7.15. Comparison of the intensity distribution of the light of two Hg lamps in aqueous solution without catalyst.

The results showed that the acetophenone conversion and yield% to phenylethanol are greater using lamp “A” (35 mW/cm^2) than “B” (55 mW/cm^2), during the tests conducted with both catalyst (Figures 7.16 and 7.17).

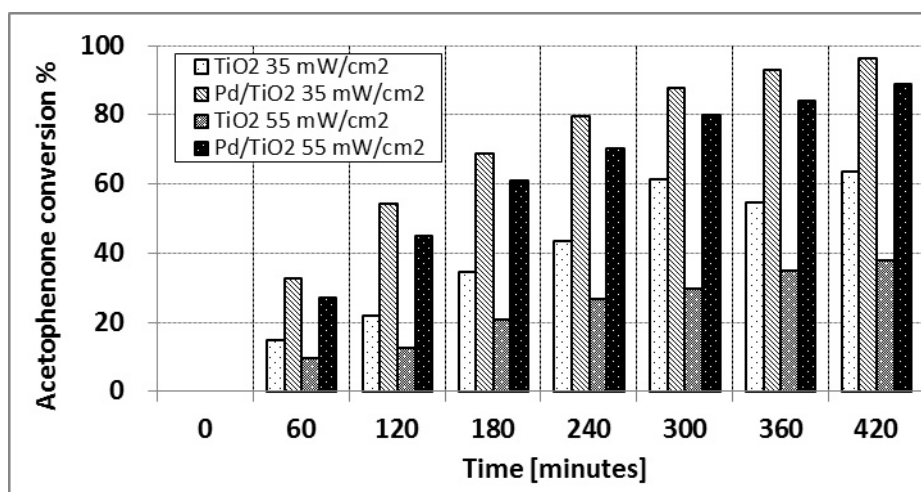


Figure 7.16. Comparison of acetophenone conversion vs. time using TiO₂ and Pd/TiO₂ as catalyst changing the intensity distribution of the light. Operative conditions: 500 mL ethanol, 50 mmol acetophenone, 1.5 g/L of photocatalyst, 32 °C, t=7h.

Contrarily the value of selectivity% increases using TiO₂ as catalyst with lamp “B” (Figure 7.17).

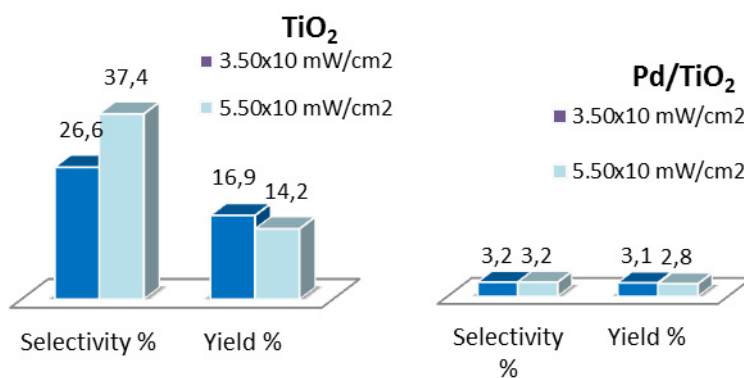


Figure 7.17. Comparison of selectivity and yield to phenylethanol % using TiO₂ Pd/TiO₂ as catalyst changing intensity and distribution light of the Hg Lamp. Operative conditions: 500 mL ethanol, 50 mmol acetophenone, 1.5 g/L of photocatalyst, 32 °C, t=7h.

Best results in terms of acetophenone conversion and yield to phenylethanol were obtained during tests conducted with the lamp at lower irradiation intensity (A). Probably, this behavior is due to the wider distribution of the light irradiation, despite the lower light intensity, of lamp “A” than “B”. This trend can be explained considering that at high light intensities the effect of the intensity of light irradiation on the reaction rate is almost negligible. Konstantinou et al., and Coleman et al., reported that at high light intensities ($I > 25 \text{ mW/cm}^2$) the rate becomes independent of the light intensity because increases both the separation and the recombination of electron–hole pairs [30,31].

7.3.2.5 Influence of solvent

Khan et al., studied photocatalytic hydrogenation of cyclohexene in aqueous ethanolic solution (80:20). Thus, in order to study the influence of the solvent on the photocatalytic transfer hydrogenation of the acetophenone, tests in ethanol and water (50:50) were carried out [32].

The results showed lower conversion, yield and selectivity during tests conducted in water/ethanol solution than ethanol (Figures 7.18 and 7.19).

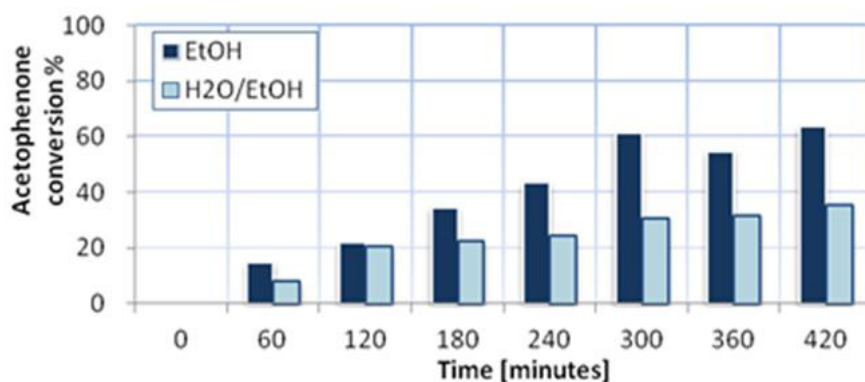


Figure 7.18. Comparison of acetophenone conversion% in ethanol and ethanol/water solution. Operative conditions: V=500 mL, 50 mmol acetophenone, 1.5 g/L of photocatalyst, 32 °C, t=7h.

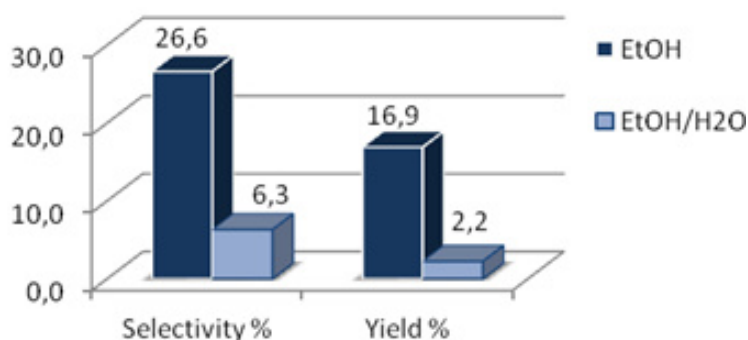


Figure 7.19. Comparison of selectivity and yield% in ethanol and ethanol/water solution. Operative conditions: V=500 mL, 50 mmol acetophenone, 1.5 g/L of photocatalyst, 32 °C, t=7h.

Acetophenone conversion in aqueous solution is about half compared to those obtained in ethanol, therefore almost all hydrogen used to reduce acetophenone is from ethanol, not from water.

Moreover, acetophenone is very slightly soluble in water, thus, the solubilization of the substrate in aqueous/ethanolic solution is more difficult than in pure ethanol. As a consequence, acetophenone adsorption on the photocatalyst dissolved in the liquid phase was lower in the aqueous solution causing low selectivity and yield (Figure 7.19).

7.3.3 Photocatalytic hydrogenation of acetophenone in aqueous solution in batch reactor

Despite the previous comments and in view to make a cheaper and very green process, the best solvent is water. For this reason, part of our study on photocatalytic transfer hydrogenation of acetophenone is carried out by

using water as solvent and formic acid as electron donor that is converted into carbon dioxide (CO₂) and hydrogen (H₂) making the reaction irreversible. Moreover, formic acid is one of the major pollutants present in pharmaceutical wastewater, therefore using it as electron and hydrogen donors, the decomposition of pollutants and photocatalytic reduction of organics can take place simultaneously.

Preliminary experimental tests are performed in batch reactor to optimize the reaction parameters such as acetophenone, catalyst and formic acid concentrations, addition of methanol and pH, in order to determine the best operative conditions that can be applied in membrane photoreactors.

7.3.3.1 Different substrate concentrations

Acetophenone is very slightly soluble in water (5.5 g/L). Then tests with different concentration of acetophenone, up and below the solubility limit, were carried out in order to know the influence of this parameter on the reaction under study. The comparison between photocatalytic hydrogenation of acetophenone using different concentration of the substrate (0.099 M or 0.026 M) indicates that, decreasing the amount of the substrate in the reaction environment, yield, selectivity and conversion increase (Figure 7.21).

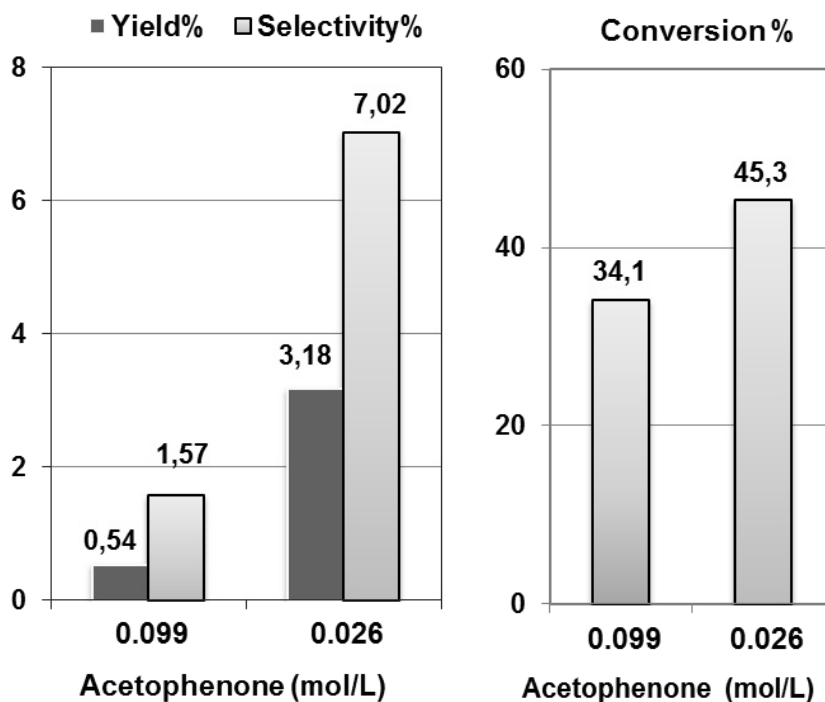


Figure 7.21. Comparison of phenylethanol yield %, selectivity % and acetophenone conversion % by using acetophenone 0.099 M and 0.026 M. Operative conditions: water (462.53 mL), formic acid (37.47 mL), TiO_2 (1.5 g/L), 32 °C, $t=7\text{h}$.

7.3.3.2 Addition of methanol in the solution

To improve the solubility of acetophenone in water a test adding 10% of methanol in the aqueous reacting phase (constituted by water, formic acid and NaOH at pH=4) was carried out. The results showed that by adding methanol the yield value did not change, while the conversion of acetophenone improved because the system was more reactive; as a consequence a decrease of selectivity was observed (Table 7.1). The results obtained indicate that the presence of methanol does not influence positively the reaction under study, for this reason subsequently tests were performed without methanol.

Table 7.1. Comparison of acetophenone conversion, selectivity and phenylethanol yield % by using aqueous solution or 10%MeOH aqueous solution. Operative conditions: formic acid (37.47 mL), acetophenone (0.026 M), TiO₂ (1.5 g/L), 32 °C, t=7h.

	Yield %	Selectivity %	Conversion %
Aqueous solution	3.18	7.02	45.31
10%MeOH aqueous solution	3.16	4.96	63.74

7.3.3.3 Tests at different pH

Photocatalytic tests on hydrogenation of acetophenone were carried out in water using 1.97 mol/L of formic acid by adding sodium hydroxide to obtain different acidic, basic and neutral pH in a range from 3 to 11 in order to study the influence of this parameter on phenylethanol yield and selectivity and acetophenone conversion. At acidic pH the selectivity value increases due to the repulsion of phenylethanol and TiO₂ that are both positive charged (Figure 7.22). At basic pH, conversion of acetophenone increases (Figure 7.23) but decreases the selectivity. The best yield was obtained during the reaction conducted at pH 7.5.

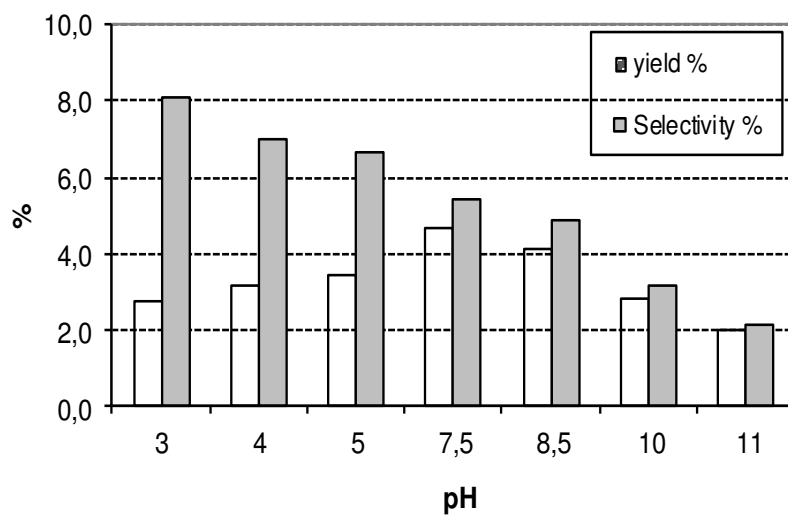


Figure 7.22. Comparison of selectivity and phenylethanol yield % at different pH. Operative conditions: water (462.53 mL), formic acid (37.47 mL), acetophenone (0.026 M), TiO₂ (1.5 g/L), 32 °C, t=7h.

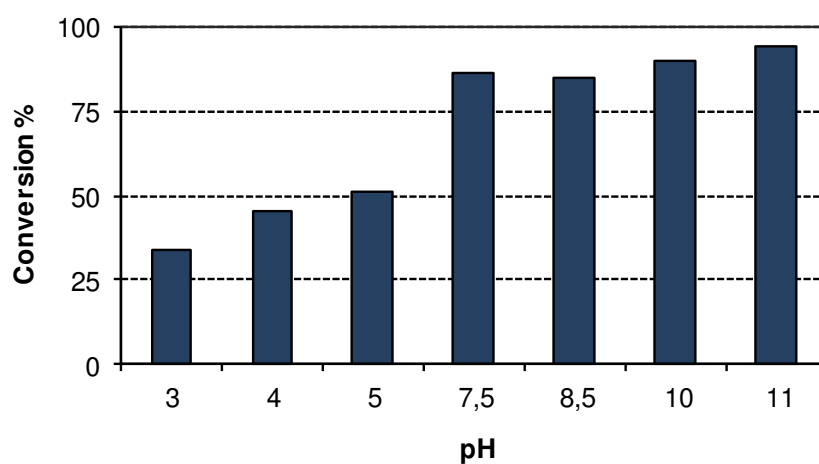


Figure 7.23. Comparison of acetophenone conversion % at different pH. Operative conditions: water (462.53mL), formic acid (37.47mL), acetophenone (0.026M), TiO₂ (1.5 g/L), 32°C, t=7h.

7.3.3.4 Amount of titanium dioxide

For practical application the use of optimized amount of photocatalyst is preferable to avoid an useless excess of catalyst and to ensure a total absorption of efficient photons. Therefore, tests with different amounts of titanium dioxide as catalyst were carried out in order to study the influence of this parameter on the reaction under study. In particular, the following concentrations were considered:

- 1 g/L;
- 1.5 g/L;
- 2.0 g/L.

The results show that increasing the amount of the catalyst, acetophenone conversion increases very slightly. The yield and selectivity have a maximum value for the amount of catalyst equal to 1.5 g/L (Figure 7.24).

The best result of yield obtained by using 1.5 g/L of TiO₂, is due to the fact that the reaction rate does not increase linearly with respect to the photocatalyst amount, but, above a certain value becomes independent of the mass of photocatalyst. This limit depends on the geometry and on the working conditions of the photoreactor, and corresponds to the maximum amount of TiO₂ in which all the particles are totally illuminated. For higher quantities of catalyst, a screening effect of excess particles occurs, which masks part of the photosensitive surface. These limits for titania in slurry batch photoreactors are reported to be in the range from 0.2 to 2.5 g/L [33]. In this case the maximum correspond to 1.5 g/L of TiO₂.

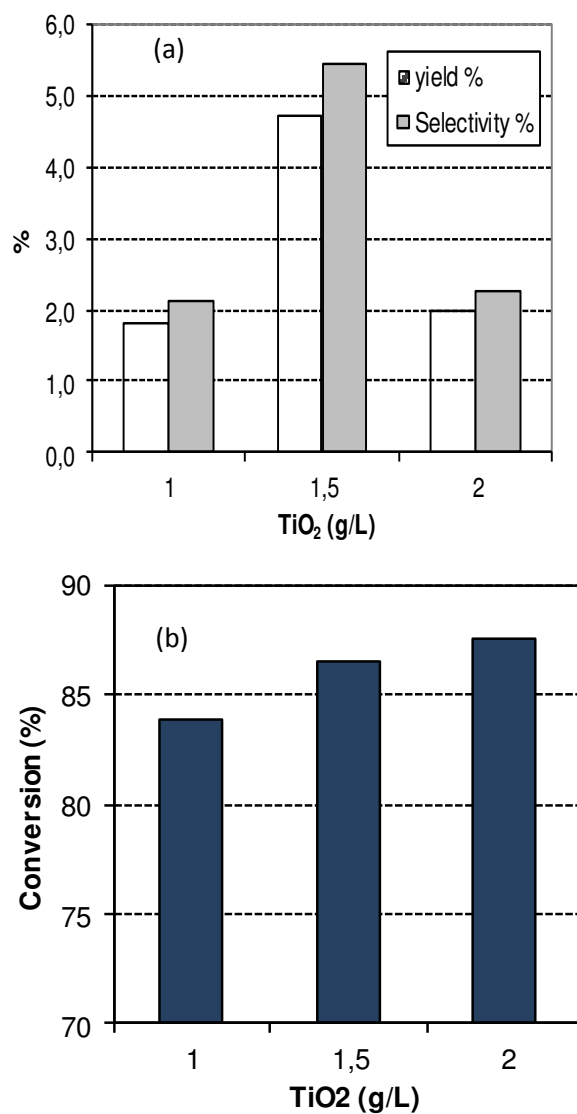


Figure 7.24. Comparison of (a) phenylethanol yield % and selectivity %, (b) acetophenone conversion % by using different concentration of TiO₂. Operative conditions: water (462.53 mL), formic acid (37.47 mL), acetophenone (0.026 M), pH = 7.5, 32 °C, t=7h.

7.3.3.5 Amount of formic acid

Photocatalytic hydrogenation of acetophenone was performed also changing the amount of formic acid in the aqueous solution maintaining pH 7.5. As expected, at lower concentration of formic acid the conversion of the substrate decreases (Figure 7.25). The best yield and selectivity values are obtained using HCOOH 1.9 M, increasing the concentration of formic acid decreases the selectivity probably due to an increase of the reactivity in the system.

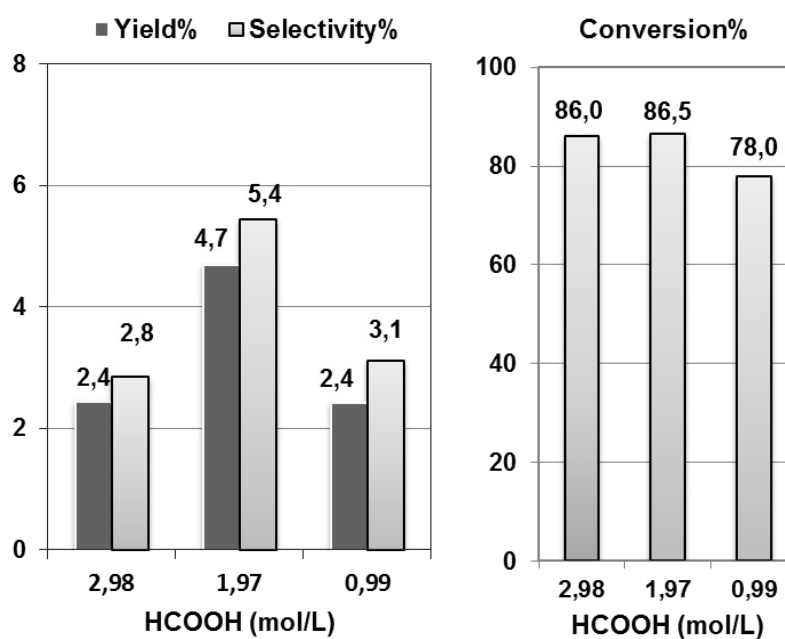


Figure 7.25. Comparison of (a) phenylethanol yield %, (b) selectivity % and (c) acetophenone conversion % by using different concentration of HCOOH. Operative conditions: water (462.53 mL), TiO₂ (1.5 g/L), acetophenone (0.026 M), pH = 7.5, 32 °C, t=7h.

7.3.4 Photocatalytic hydrogenation of acetophenone in aqueous solution in membrane reactors

Acetophenone reduction by using water as solvent was also performed in photocatalytic membrane reactors. Photocatalytic processes in membrane reactors allow chemical reaction and separation process to be obtained in one step.

According to the results obtained during tests conducted in batch photoreactor, photocatalytic tests were conducted in membrane photoreactors, using the following operative conditions: 1.5 g/L of titanium dioxide and Pd/TiO₂ as photocatalysts, 1.9 M of formic acid used as hydrogen and electron donor, pH 7.5, and water as solvent for a total volume of 724 mL.

Photocatalytic hydrogenation of acetophenone tests were performed using different substrate feeding mode in order to improve the phenyl ethanol yield and extraction, as previous described in paragraph 7.2.1

7.3.4.1 Substrate feeding with a syringe pump

Since, acetophenone is slowly soluble in water (5.5 g/L), to limit the solubility problems and to improve the reaction rate this substrate was fed drop wise with a syringe pump in the aqueous phase. The total amount of acetophenone 2.2 mL corresponding to 18.82 mmoles, was fed very slowly, 0.37 mL/h in 724 mL of aqueous solution, for 6 h in order to allow to the substrate the time to react during the last hour, all tests were stopped after 7 h. In this way the amount of acetophenone added drop by drop inside the photocatalytic batch reactor is much lower than the solubility limit of this compound.

For the extraction of the product was used heptane as organic phase that is a solvent already used for extraction of acetophenone and phenyl ethanol [4]. During the photocatalytic tests, acetophenone drop going inside the photocatalytic batch reactor was partially reduced to phenylethanol and both were stripped in the organic phase. This substrate feed is necessary to avoid the total extraction of acetophenone in the organic phase during the photocatalytic test before to be hydrogenated to phenyl ethanol because the affinity of acetophenone for heptane is higher than for water that is polar. The affinity of acetophenone for heptane is higher than that of phenylethanol for this solvent because of its minor polarity. In fact Mihal et al. [4] reported an extraction of phenylethanol ten times more than that of acetophenone, in contrast, with our system, we obtained results that show a ratio of the partition coefficients in heptane between acetophenone and phenylethanol, measured at the end of this reaction after 7 h, (2.74:1) much lower than reported [4], by using the same organic solvent (13.3:1). This behavior is due to the drop wise substrate alimentation that allows acetophenone reduction before being extract in the organic phase. 10.32% of phenylethanol extraction was obtained at the end of the reaction.

Photocatalytic hydrogenation tests on acetophenone were carried out in batch and membrane reactor system under the same experimental condition to compare the phenylethanol generation, productivity, selectivity, yield, Q % and acetophenone conversion% (Table 7.2 and Figure 7.26). In this case the batch photoreactor used for this test is the same of membrane photoreactor described in Figure 7.4, but without membrane. We put a flask at the place of the membrane reactor to obtain the same volume in both system (724 mL) with the same external recirculation and flow rate equal to 166 mL/min and feeding the substrate

with the same syringe pump previously described. This modification was made in order to check that the different trend between these two systems is due to the presence of the membrane.

Table 7.2. Comparison of phenylethanol produced and productivity in organic phase, in both organic and aqueous phase, selectivity% and yield % by using membrane and batch photoreactors. Operative conditions: formic acid 1.97 M (54.47 mL), water (670 mL), 2.2 mL of acetophenone (18.82 mmoles) fed with a syringe pump (0.37 mL/h for 6 h), flow rate =166 mL/min, TiO₂ (1.5 g/L), 32 °C, t=7h.

Type of reactor	PheEtOH produced (μmol)	PheEtOH produced in organic phase (μmol)	Productivity (mg x g ⁻¹ h ⁻¹)	Q%	Selectivity%	Yield%
PMR	236.34	24.39	3.80	10.32%	1.5	1.25
Batch R.	184.23	NA*	2.96	NA*	1.3	0.98

*NA=not applicable

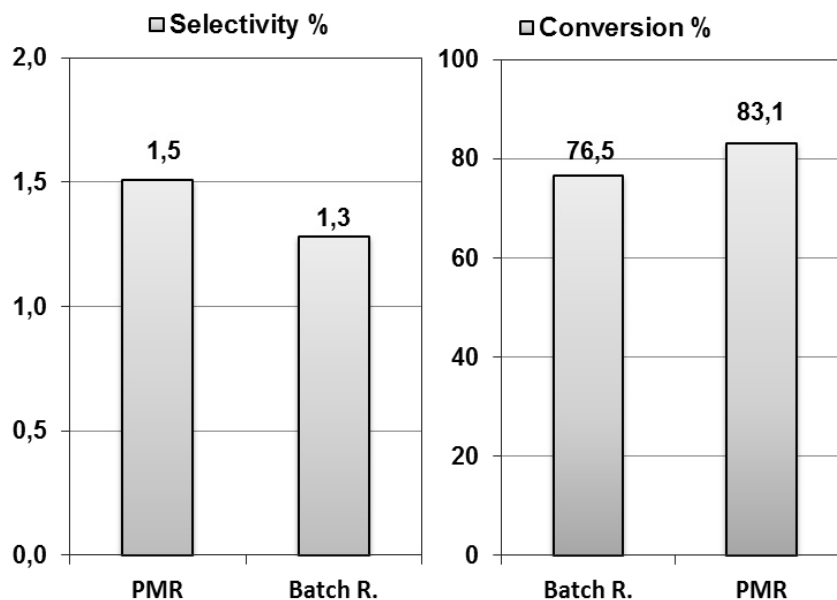


Figure 7.26. Comparison of selectivity % and acetophenone conversion % by using batch and membrane reactors. Operative conditions: formic acid (37.47 mL), water (670 mL), 2.2 mL of acetophenone (18.82 mmol) fed with a syringe pump (0.37 mL/h for 6 h), flow rate =166 mL/min, TiO₂ (1.5 g/L), 32 °C, t=7h.

As expected the results show that using a membrane reactor (PMR) the phenylethanol generation, yield%, conversion%, productivity improves. This behaviour is due to the stripping of phenylethanol in the organic phase that shift reaction forward to the product. Moreover, the extraction of phenylethanol from the reactive phase allows avoiding subsequent reduction reaction of the extracted product enhancing the selectivity value.

7.3.4.2 Acetophenone in heptane

In order to know the behaviour of a different substrate addition mode, the same amount of acetophenone used in the previous systems, 2.2 mL of acetophenone (18.82 mmol) was added directly in the organic phase

constituted by heptane before starting the photocatalytic reaction. With this system the substrate in the organic phase should permeate through the membrane in very small drops making a micro emulsion thus improving its solubility in water. As illustrated in Figure 7.27, acetophenone permeates across the hydrophobic membrane and reacts in the aqueous reactive phase. The phenylethanol produced, permeates back across the membrane and dissolves in heptane, where it is protected by subsequent reduction.

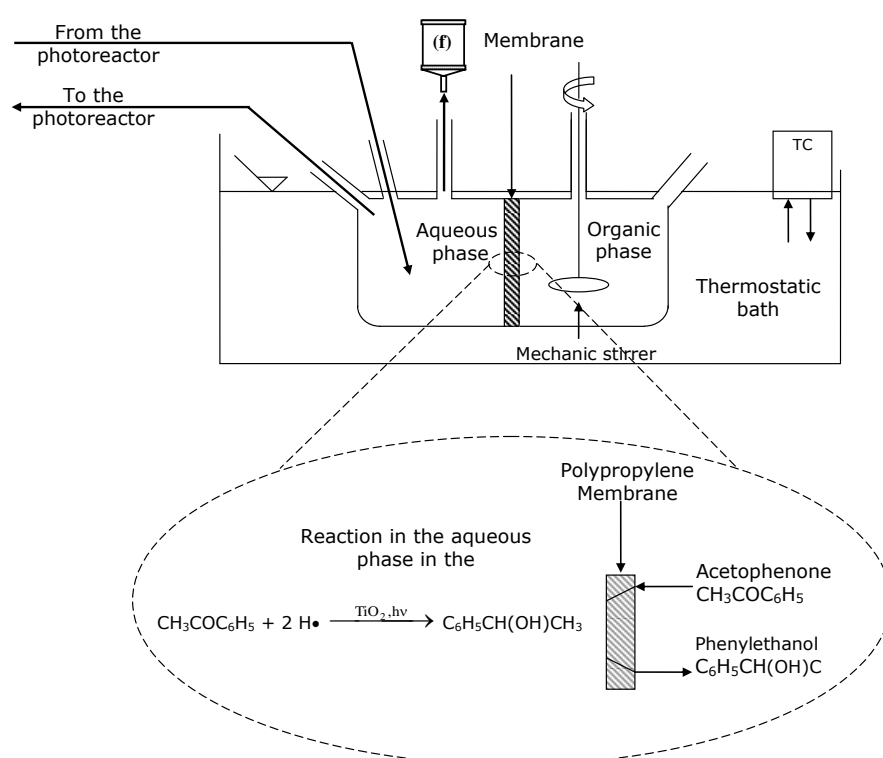


Figure 7.27. Scheme of reaction mechanism in photocatalytic membrane reactor.

The results show that the amount of phenylethanol produced using this system is almost the middle than that generated adding acetophenone with

a syringe pump and lower than obtained in the test conducted in the batch reactor (Table 7.3). This behaviour is due to the difficulty for acetophenone to pass from the organic phase to the aqueous phase because its higher affinity for heptane than water as solvent. In fact, the amount of acetophenone found in the aqueous phase at the end of the reaction in this case was about half than that found using the syringe pump to feed the substrate, 0.79 and 1.59 mmol, respectively. Moreover, heptane is volatile also at room temperature preventing its use for longer irradiation time in view of a system that works continuously.

Table 7.3. Comparison of phenylethanol produced and productivity in organic phase, in both organic and aqueous phase and Q % by using membrane and batch photoreactors with different substrate feeding mode. Operative conditions: formic acid (54.47 mL), water (670 mL), flow rate =166 mL/min, TiO₂ (1.5 g/L), 32 °C, t=7 h.

Substrate feeding mode	PheEtOH (μmol) total	Q%	Productivity (mg x g ⁻¹ h ⁻¹)	Productivity in the organic phase (mg x g ⁻¹ h ⁻¹)
Batch reactor - syringe pump	184.23	NA*	2.96	NA*
PMR Syringe pump	236.34	10.32%	3.80	0.39
PMR AcPhe in heptane	126.97	13.75%	2.04	0.28

*NA=not applicable

7.3.4.3 Acetophenone as organic phase

To avoid the observed problem we added in the membrane reactor 130 mL of acetophenone as organic phase for feeding the substrate by its permeability across the membrane and to extract the product at the same time using only one type of solvent. Thus acetophenone phase acted as

both extracting phase and substrate reservoir avoiding using other solvents.

Comparing three different substrate addition mode and two different organic phase (heptane and acetophenone) the results show that the extraction of phenylethanol increases by using acetophenone as organic phase compared to heptane (Table 7.4 and Figure 7.28) by indicating an higher affinity of phenylethanol for acetophenone than the other extractor.

Table 7.4. Comparison of phenylethanol produced and productivity in organic phase and in both organic and aqueous phase and Q % by using membrane and batch photoreactors with different substrate feeding mode. Operative conditions: formic acid (54.47 mL), water (670 mL), flow rate =166 mL/min, TiO₂ (1.5 g/L), 32 °C, t=7 h.

Substrate feeding mode	PheEtOH (μmol) total	Productivity ($\text{mg} \times \text{g}^{-1}\text{h}^{-1}$) tot	Productivity ($\text{mg} \times \text{g}^{-1}\text{h}^{-1}$) organic phase
Batch reactor-syringe pump	184.23	2.96	NA*
PMR Syringe pump	236.34	3.80	0.39
PMR AcPhe in heptane	126.97	2.04	0.28
PMR AcPhe as organic phase	276.20	4.44	0.97

*NA=not applicable

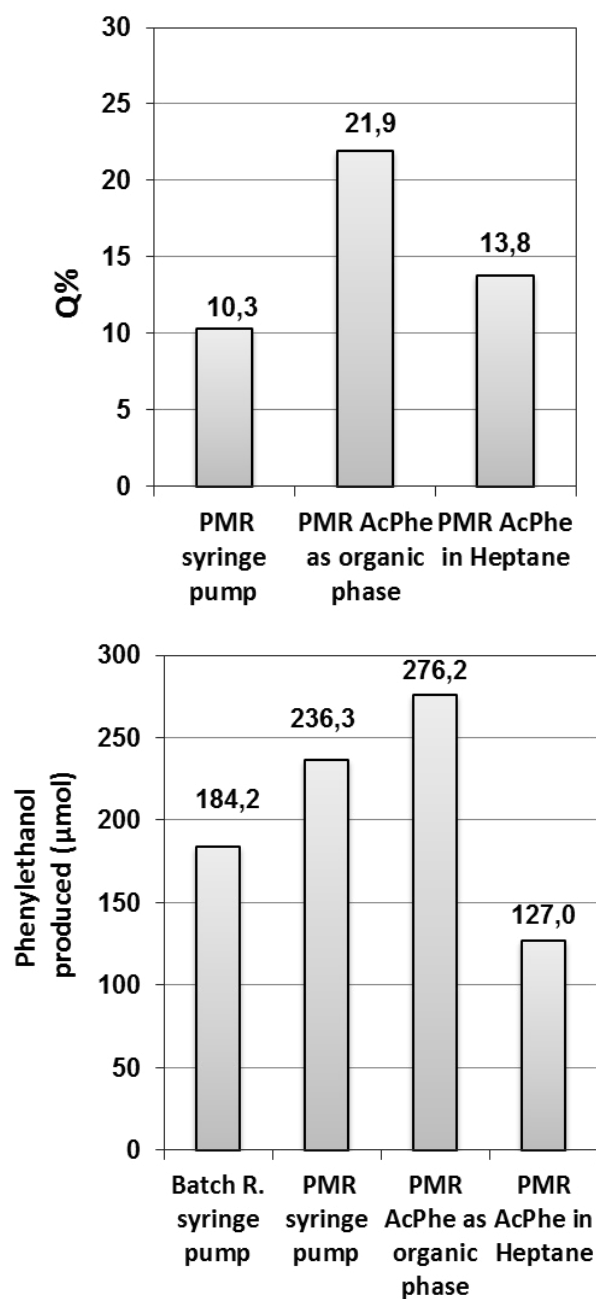


Figure 7.28. Comparison of Q% and phenylethanol generation by using membrane reactors with different substrate feeding mode: with a syringe pump, adding acetophenone in heptane and using acetophenone as organic phase.

Increasing the Q% also the phenylethanol production increases because the reaction is shifted towards the product (Figure 7.28). Figure 7.29 shows a higher and linearly increase of phenyl ethanol in the organic phase when acetophenone is used as both substrate and extractor. The most efficient system for the photocatalytic hydrogenation of acetophenone was found to be the membrane reactor in which the acetophenone was used as both substrate and organic phase.

Furthermore, with the previous systems which use heptane as solvent in both cases the final organic phase is constituted by mainly three components (acetophenone, phenylethanol and heptane) in contrast with the last system in which the final organic phase is constituted by mainly two component (acetophenone and phenylethanol). This makes easier the subsequent recovery of the desired product. Moreover acetophenone is less volatile than heptane (boiling point 202 °C and 98-99 °C, respectively), thus allowing the use of different temperatures and performing the reaction at longer irradiation time in view of a system that could work continuously. By using this system future works can be directed in the separation of the desired product from the organic phase by using a three-phases membrane reactor adding a third cell with an aqueous stripping solution.

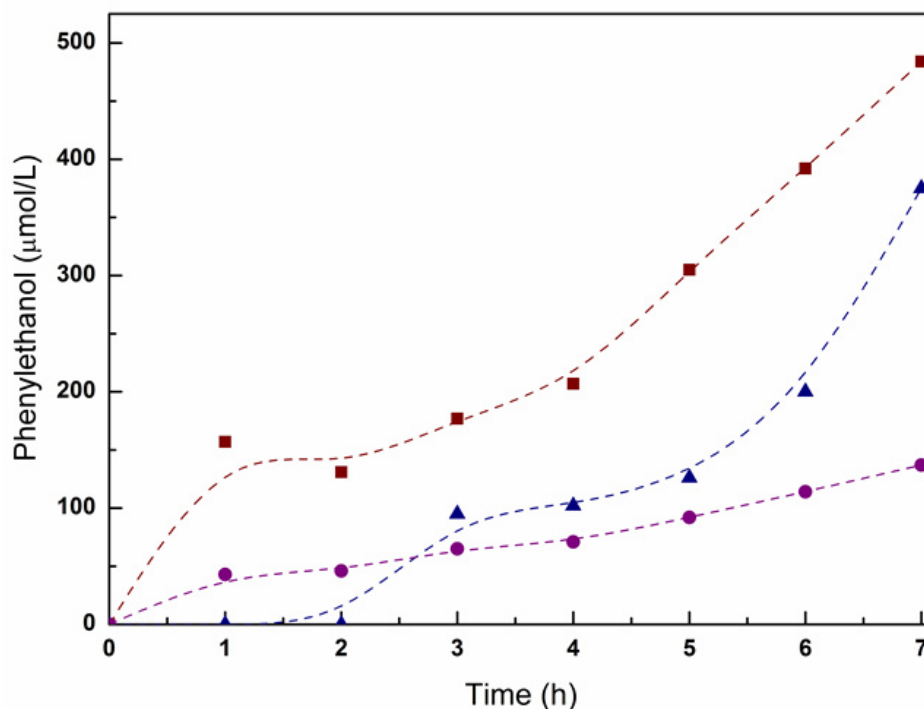


Figure 7.29. Phenylethanol concentration in the organic phase vs. time by using membrane reactors with different substrate feeding mode; ▲: with a syringe pump, ●: adding acetophenone in heptane, ■: using acetophenone as organic phase.

7.3.4.4 Formic acid / triethylamine

In order to increase the photocatalytic activity of titanium dioxide used as semiconductor we added in the aqueous solution triethylamine (TEA) instead of NaOH as base in order to obtain the operative pH at 7.5 (optimized during the previous tests). Triethylamine is an electron donor usually used in photocatalysis and used also in catalysis with formic acid (FA).

As expected, the results show that the amount of phenylethanol produced increases by adding TEA in the photocatalytic solution (Table 7.5). While the extraction percentage of the desired product decreases by using formic

acid/triethylamine as electron donor as showed in Figure 7.30. This behavior can be explained by the higher affinity of acetophenone and phenylethanol for FA/TEA/water solution (1:4:9.4) that FA/water (1:13) because TEA is less polar than water for the presence of three ethylic groups. Indeed, in this case the substrate permeates through the membrane more than in the previous tests by using FA/water/NaOH. The amount of acetophenone in the aqueous phase increased almost six times more than using only formic acid as electron donor. Despite of the increased production of phenylethanol, the main problem of adding TEA is the decreasing in phenylethanol extraction % in the organic phase that was almost the middle than that obtained by using FA without TEA. In fact the productivity in the organic phase was lower using FA/TEA than FA. (Table 7.5).

Table 7.5. Comparison of phenylethanol produced, productivity in organic phase and in both organic and aqueous phase and Q % by using formic acid (FA) and FA/TEA. Operative conditions: formic acid (54.47 mL), water, flow rate =166 mL/min, TiO₂ (1.5 g/L), 32 °C, t=7 h.

Electron donors	PheEtOH (μmol)	Productivity ($\text{mg} \times \text{g}^{-1}\text{h}^{-1}$) tot	Productivity ($\text{mg} \times \text{g}^{-1}\text{h}^{-1}$) organic phase
Formic acid	276.20	4.44	0.97
Formic acid/TEA	324.50	5.21	0.66

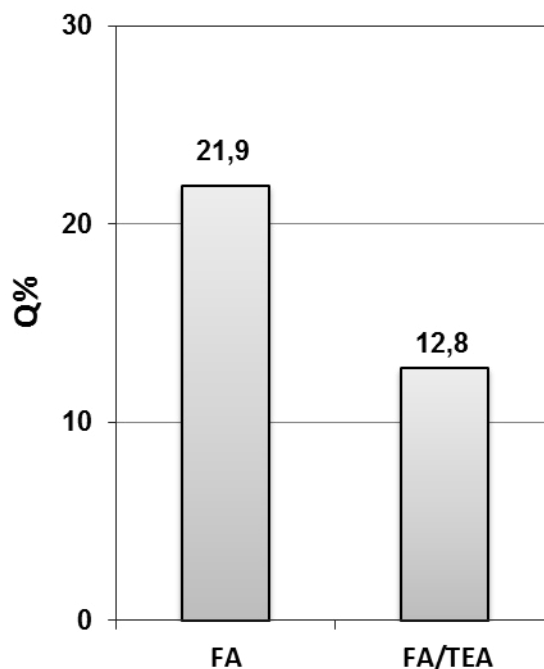


Figure 7.30. Comparison of phenylethanol produced and Q% by using FA or FA/TEA.

To solve the problem of the extraction of the desired product in the organic phase we increased the recirculation flow from 166 ml/min to 255 ml/min. As showed in Table 7.6 the extraction percentage of phenylethanol increases very slightly while decreases slightly the amount of desired product.

In conclusion, in view of a system that works continuously it is very important a good extraction of the desired product, moreover, the phenylethanol produced did not increase so much to justify the use of two electron donors. For this reason subsequent studies were conducted in the PMR by using formic acid alone as electron donor making this a more sustainable process avoiding also the increase of the reaction by-products because FA alone is decomposed in CO_2 and H_2 .

Table 7.6. Comparison of phenylethanol produced, productivity in organic phase and in both organic and aqueous phase and Q % by using FA/TEA changing the flux rate : 160 mL/min and 255 mL/min. Operative conditions: formic acid (54.47 mL), water, flow rate =166 mL/min, TiO₂ (1.5 g/L), 32 °C, t=7h.

Different flow rates (mL/min)	PheEtOH (μmol) total	Q%	Productivity (mg x g ⁻¹ h ⁻¹) tot	Productivity (mg x g ⁻¹ h ⁻¹) organic phase
166	324.50	12.75%	5.21	0.66
255	316.61	13.26	5.08	0.67

7.3.4.5 Visible light activity

In the previous tests were optimized the system and the operative condition for photocatalytic hydrogen generation under UV light.

Solar light contains only 5% of UV, therefore for any practical application this system should operate also with visible light. Commercial semiconductors as TiO₂ that is one of most efficient, stable and largely available photocatalyst, has the defect of working mostly using the UV light, indeed it absorbs only 5% of visible light [34]. Noble metals, as Pd, have been reported to be very effective for enhancement of TiO₂ photocatalysis reducing the possibility of electron-hole recombination and shifting the radiation absorption towards higher wavelengths, permitting the use of visible light. To increase the efficiency of TiO₂ under visible light we synthesized titanium dioxide doped with palladium. Both catalysts (TiO₂ alone and Pd/ TiO₂) were irradiated with the LED lamp which emission spectrum is reported in Figure 7.3 ($\lambda > 400\text{nm}$).

As expected TiO_2 was not active under visible light irradiation, while doping the commercial catalyst with palladium the concentration of phenylethanol in the organic phase increased linearly during the photocatalytic test (Figure 7.31).

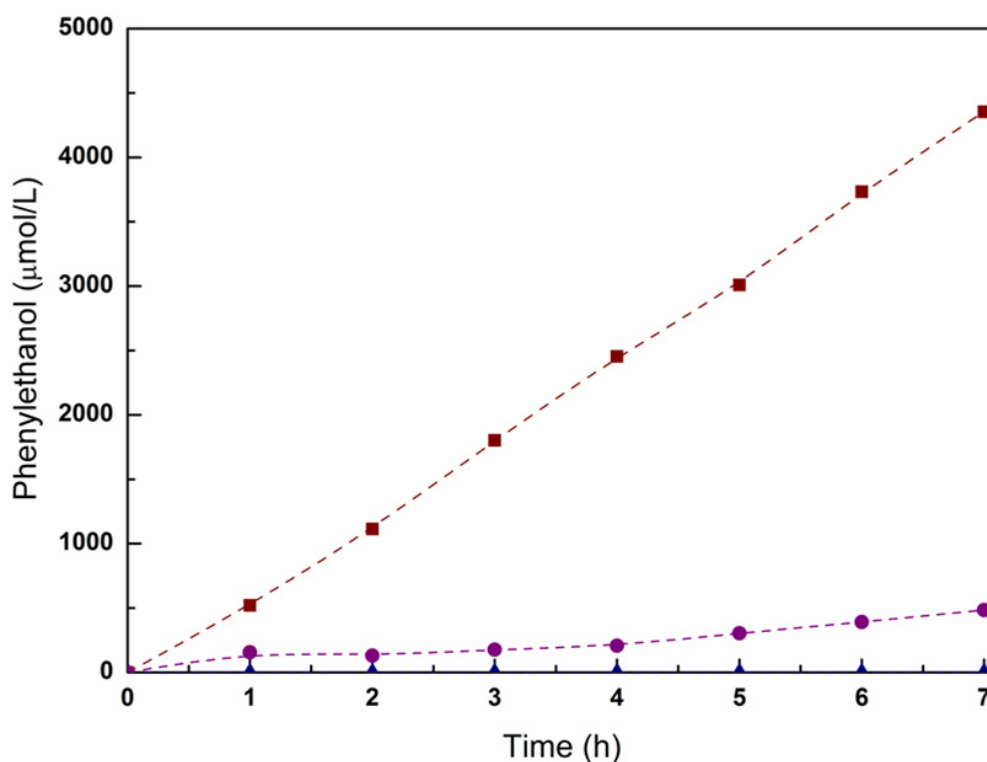


Figure 7.31. Phenylethanol extraction in the organic phase vs. time by using: TiO_2 (\blacktriangle) and Pd/TiO_2 (\blacksquare) under visible light and TiO_2 under UV (\bullet) light.

The highest activity of this modified photocatalyst was determined comparing the phenylethanol production by using Pd/TiO_2 photocatalyst that was higher than the amount of desired product obtained in all the previous tests conducted under UV light. Figure 7.32 and Table 7.7 shows an activity of Pd/TiO_2 under visible light five times higher than TiO_2

under UV light for the photocatalytic hydrogenation of acetophenone conducted in the same PMR system.

Table 7.7. Comparison of phenylethanol produced and productivity in organic phase and in both organic and aqueous phase and Q % by using membrane photoreactors with Pd/TiO₂ and TiO₂ under UV and visible light. Operative conditions: formic acid (54.47 mL), water (670 mL), flow rate =166 mL/min, TiO₂ (1.5 g/L), 32 °C, t=7 h.

Catalyst	λ	PheEtOH (μmol) total	PheEtOH (μmol) in organic phase	Productivity ($\text{mg} \times \text{g}^{-1} \times \text{h}^{-1}$) tot	Productivity $\text{mg}/\text{g} \times \text{h}$ in organic phase	Q%
Pd/TiO ₂	>400nm	1370.9	544.1	22.0	8.7	39.7%
TiO ₂	>400nm	ND	ND	ND	ND	ND
TiO ₂	UV	276.2	60.5	4.4	0.97	21.9%

ND: not detectable

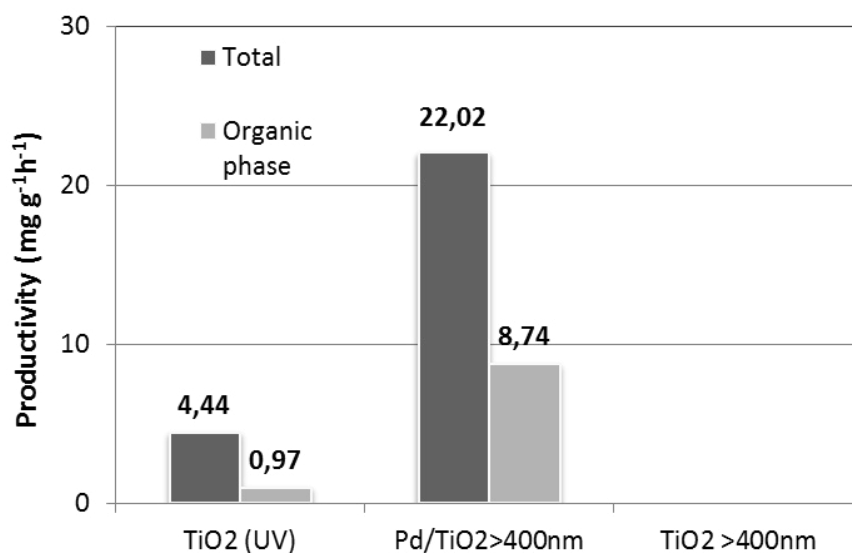


Figure 7.31. Comparison of productivity in organic and in both phases by using TiO₂ under UV and visible light and Pd/TiO₂ under visible light.

7.4 Conclusions

The results on the photocatalytic transfer hydrogenation of acetophenone dissolved in ethanol in batch reactor, presented in this Chapter, showed that phenylethanol yield had a maximum value at 1.5 g/L of catalyst (16.9%), increasing the catalyst amount the yield decreases, probably because a screening effect from the excess particles occurs, which leads to a decreased passage of radiation through the suspension. Instead, the highest acetophenone conversion (96.2%), accompanied by low yield and selectivity, was obtained by using Pd/TiO₂ as photocatalyst indicating a highly reactive system. The results found in water/ethanol solution (50/50 v/v) showed acetophenone conversion, yield (2.2%) and selectivity (6.3%) lower than in ethanol.

Using water as solvent and formic acid as electron donor, the results obtained on the photocatalytic transfer hydrogenation of acetophenone conducted in batch photoreactor indicated that the addition of methanol does not influence positively the reaction under study. The best result in terms of yield was achieved by using 1.5 g/L of TiO₂, as it was obtained in the tests with ethanol. At acidic pH the selectivity increased due to the repulsion of phenylethanol and TiO₂ that are both positive charged, thus avoiding successive hydrogenation. On the contrary, at basic pH the selectivity decreased, while the conversion of acetophenone increased. Summarizing, the best value of yield (4.7%) was obtained at pH 7.5 using 1.5 g/L of TiO₂ as photocatalyst and formic acid 1.9 M.

By comparison of the results obtained in the preliminary batch tests, it can be observed that the yield obtained using water as solvent with 7.5% of formic acid (1.9 M), in the better operative conditions, is double than that obtained using water with 50% of ethanol as both hydrogen and electron

donors, but, is not higher than that using 100% of ethanol. Despite this, the use of formic acid as electron donor in water as solvent is more convenient because it can be completely converted into CO₂ and H₂ during the photocatalytic transfer hydrogenation, thus avoiding the presence of hole scavenger and its oxidation by-products in final effluent coming from the photoreactor. On the contrary ethanol is partially oxidized to acetaldehyde that becomes another chemical, with the un-reacted EtOH, in the reacting environment. Considering this aspect, and the affinity of phenylethanol for ethanol higher than that for water, the recovery of the desired product, present in traces in ethanol at the end of the reaction, results more difficult by using ethanol than formic acid in water.

The use of a membrane reactor system for photocatalytic hydrogenation of acetophenone in water solution with formic acid as hydrogen and electron donors was found to improve phenylethanol production, yield%, conversion%, and productivity with respect to the use of batch reactor with the same substrate addition mode. The most efficient system for photocatalytic hydrogenation of acetophenone in terms of productivity (4.44 mg g⁻¹h⁻¹) and amount of phenylethanol produced (276.20 μmol), with Q% equal to 21.91%, was found to be the membrane reactor in which acetophenone was used as both organic phase and substrate reservoir. Commercial TiO₂ was not active under visible light but its photocatalytic activity was implemented by the presence of palladium. The amount of phenylethanol produced (1371 μmol) and the productivity (22.02 mg g⁻¹h⁻¹) by using Pd/TiO₂ photocatalyst under visible light were found to be five times higher than that obtained by using TiO₂ under UV light.

The results of the present study, using TiO₂ doped with palladium as photocatalyst, for photocatalytic hydrogenation of acetophenone in water

solution using a pollutant such as formic acid as electron donor, under visible light in membrane reactors, gave interesting results for application purposes allowing using a green system for the reduction of acetophenone.

7.5 References

- [1] Shimura, K.; Shimizu, K. Transfer hydrogenation of ketones by ceria-supported Ni catalysts. *Green Chem.*, **2012**, 14, 2983-2985.
- [2] Kohtani S., E. Yoshioka, K. Saito, A. Kudo, H. Miyab. Photocatalytic hydrogenation of acetophenone derivatives and diaryl ketones on polycrystalline titanium dioxide. *Catalysis Communications*, **2010**, 11, 1049–1053.
- [3] Rissom S., J. Beliczey, G. Giffels, U. Kragl and C. Wandrey. Asymmetric reduction of acetophenone in membrane reactors: comparison of oxazaborolidine and alcohol dehydrogenase catalysed processes. *Tetrahedron: Asymmetry*, **1999**, 10, 923–92.
- [4] Mihal M., Marko J., Annus J. and Stefuca V. *J. Chem Technol Biotechnol* 2012; 87: 1017–1026
- [5] Adler P., Hugen T., Wiewiora M. Kunz B. *Enzyme and Microbial Technology*, 48, 3, **2011**, 285–292.
- [6] Gladiali, S.; Alberico, E. Asymmetric transfer hydrogenation: chiral ligands and applications. *Chem. Soc. Rev.*, **2006**, 35, 226-236.
- [7] Ikariya, T.; Blacker, A. J.; Asymmetric Transfer Hydrogenation of Ketones with Bifunctional Transition Metal-Based Molecular Catalysts. *Acc. Chem. Res.*, **2007**, 40, 1300–1308.
- [8] Zhao, M.; Yu, Z; Yan, S.; Li, Y. Room-temperature Ru(II)-catalyzed transfer hydrogenation of ketones and aldehydes in air. *Tetrahedron Lett.*, **2009**, 50, 4624–4628.

- [9] Malacea, R.; Poli, R.; Manoury, E. Asymmetric hydrosilylation, transfer hydrogenation and hydrogenation of ketones catalyzed by iridium complexes. *Coord. Chem. Rev.*, **2010**, 254, 729–752.
- [10] Yu, J. Q.; Wu, H. C.; Ramarao, C.; Spencer, J. B.; Ley, S. V. Transfer hydrogenation using recyclable polyurea-encapsulated palladium: efficient and chemoselective reduction of aryl ketones. *Chem. Commun.*, **2003**, 678–679.
- [11] Alonso, F.; Riente, P.; Reinoso, F. R.; Martinez, J. R.; Escribano, A. S.; Yus, M. Platinum nanoparticles supported on titania as an efficient hydrogen-transfer catalyst. *J. Catal.*, **2008**, 260, 113–118.
- [12] Alonso, F.; Riente, P.; Reinoso, F. R.; Martinez, J. R.; Escribano, A. S.; Yus, M. A Highly Reusable Carbon-Supported Platinum Catalyst for the Hydrogen-Transfer Reduction of Ketones. *Chem. Cat. Chem.*, **2009**, 1, 75–77.
- [13] Baruwati, B.; Polshettiwar, V.; Varma, R. S. Magnetically recoverable supported ruthenium catalyst for hydrogenation of alkynes and transfer hydrogenation of carbonyl compounds. *Tetrahedron Lett.*, **2009**, 50, 1215–1218.
- [14] He, L.; Ni, J.; Wang, L. C.; Yu, F. J.; Cao, Y.; He, H. Y.; Fan, K. N. Aqueous Room-Temperature Gold-Catalyzed Chemoselective Transfer Hydrogenation of Aldehydes. *Chem. Eur. J.*, **2009**, 15, 11833–11836.
- [15] Bachmann, W. E.. The Photochemical Reduction of Ketones to Hydrols. *J. Am. Chem. Soc.*, **1933**, 55, 391–395.
- [16] Shiragami, T.; Pac, C. Yanagida S. Nonmetallised CdS-catalysed photoreduction of aromatic ketones to alcohols and/or pinacols. *J. Chem. Soc., Chem. Commun.*, **1989**, 13, 831-832.

- [17] Kohtani, S.; Yoshioka, E.; Saito, K.; Kudo, A.; Miyab., H. Photocatalytic hydrogenation of acetophenone derivatives and diaryl ketones on polycrystalline titanium dioxide. *Catal. Commun.*, **2010**, *11*, 1049–1053.
- [18] Escobar E.A., M. Á. V. Zapata, S.A. Hernández, S. O. Flores Valle, O. R. Berny, V. J. G. Ángeles, I. C. Reyes. Photocatalytic Reduction of Benzophenone on TiO₂: Effect of Preparation Method and Reaction Conditions. *J. Mex. Chem. Soc.*, **2010**, *54*, 3, 133-138.
- [19] Imamura, K.; Iwasaki, S.; Maeda, T.; Hashimoto, K.; Ohtani, B.; Kominami, H. Photocatalytic reduction of nitrobenzenes to aminobenzenes in aqueous suspensions of titanium(IV) oxide in the presence of hole scavengers under deaerated and aerated conditions. *Phys. Chem. Chem. Phys.*, **2011**, *13*, 5114–5119.
- [20] Wehbe, N.; Jaafar, M.; Guillard, C.; Herrmann, J.-M.; Miachon, S.; Puzenat, E.; Guilhaume, N. Comparative study of photocatalytic and non-photocatalytic reduction of nitrates in water. *Appl. Catal. A-Gen.*, **2009**, *368*, 1–8.
- [21] Li Y, Lu G, Li S. Photocatalytic production of hydrogen in single component and mixture systems of electron donors and monitoring adsorption of donors by in situ infrared spectroscopy. *Chemosphere*. **2003**, *52*, 5, 843-50.
- [22] Yoon, T. P.; Ischay, M. A.; Du, J. Visible light photocatalysis as a greener approach to photochemical synthesis *Nat. Chem.*, **2010**, *2*, 527–532.
- [23] Zeitler, K. Photoredox Catalysis with Visible Light. *Angew. Chem.*, **2009**, *48*, 9785 – 9789.

- [24] Li, J.; Yang, J.; Wen, F.; Li, C. A visible-light-driven transfer hydrogenation on CdS nanoparticles combined with iridium complexes. *Chem. Commun.*, **2011**, 47, 7080-7082.
- [25] Ke X., Zhang X., Zhao J., Sarina S., Barry J., and Zhu H. Selective reductions using visible light photocatalysts of supported gold nanoparticles. *Green Chem.*, **2013**, 15, 236-244
- [26] Molinari R., A. Caruso, L. Palmisano. Membrane operation. Innovative Separations and Transformations. Enrico Drioli and Lidietta Giorno. *WILEY-VCH Verlag GmbH and Co. KGaA, Weinheim*, **2009**.
- [27] J.G. Yu, X.J. Zhao, Q.N. Zhao, J.C. Du, XPS of study of TiO₂ photocatalytic thin film prepared by the sol-gel method, *Chin. J. Mater. Res.* **2000**, 14, 203-209.
- [28] Atkins, P; Physical Chemistry, 5th Ed., Freeman, New York: **1994**, 597-600.
- [29] Sakthivel S., M.V. Shankar, M. Palanichamy, B. Arabindoo, D.W. Bahnemanna, V. Murugesanb Enhancement of photocatalytic activity by metal deposition: characterisation and photonic efficiency of Pt, Au and Pd deposited on TiO₂ catalyst. *Water Research.* **2004**, 38, 3001-3008.
- [30] H. M. Coleman, M. I. Abdullah, B. R. Eggins, F. L. Palmer. Photocatalytic degradation of 17 β -oestradiol, oestriol and 17 β -ethinyloestradiol in water monitored using fluorescence spectroscopy. *Applied Catalysis B: Environmental.* **2005**, 55 23-30.
- [31] I. K. Konstantinou, T. A. Albanis TiO₂-assisted photocatalytic degradation of azo dyes in aqueous solution: kinetic and mechanistic

- investigations A review. *Applied Catalysis B: Environmental*. **2004**, 49, 1–14.
- [32] Khan M.M.T. and Rao N.N. Photocatalytic hydrogenation of cyclohexene through H_2O as source of H_2 by Pt/CdS/RuO₂ semiconductor particulate system catalised by $\text{K}[\text{Ru}(\text{H-EDTA})\text{Cl}]_2\text{H}_2\text{O}$. *Journal of Molecular Catalysis*. **1990**, 58, 323-329.
- [33] J.-M. Herrmann. Heterogeneous photocatalysis: state of the art and present applications. *Topics in Catalysis* Vol. 34, Nos. 1–4, 2005.
- [34] Magesh G., B. Viswanathan, R.P. Viswanath and T.K. Varadarajan. **2007**. *Photo/Electrochemistry & Photobiology in the Environment, Energy and Fuel*. Editors: Satoshi Kaneco, B. Viswanathan and Hideyuki Katsumata. Cap. 11 Photocatalytic routes for chemicals.

Conclusions

According to the proposed objectives and considering the results obtained in the overall work, the following conclusions have been reached.

During the first part of the present thesis, modification of graphene lattice, by inserting heteroatoms, or adding semiconductors or changing the layers size, improving the activity of the prepared materials, in different applications, were achieved.

Graphene was oxidized to Graphene Oxide (GO) and its photocatalytic activity for hydrogen generation from water/methanol mixtures with visible light was implemented by the presence of dyes affecting visible light photocatalytic activity of GO in the absence of any noble metal. The most efficient material prepared is the one in which the $[\text{Ru}(\text{bipy})_3]^{2+}$ dye molecules are located in the intergallery space of incompletely delaminated GO. This photocatalyst is two orders of magnitude more efficient than a titania based photocatalyst containing Au measured under the same experimental conditions using a 532 nm laser as excitation light. $[\text{Ru}(\text{bipy})_3]^{2+}$ @GO was able to generate hydrogen from water/methanol solutions under solar simulated light with or without UV filter

Doping graphene with nitrogen((N)G) by pyrolysis of chitosan, behaves as a semiconductor and exhibits high efficiency for the photocatalytic generation of hydrogen from water- methanol mixtures with similar efficiency using UV or visible light. The photocatalytic activity largely depends on the crystallinity of the sample and on the pyrolysis temperature, improving the efficiency along the increase in the crystallinity of (N)G. The most efficient system for hydrogen generation at

355 nm was obtained by pyrolysis of chitosan at 900°C, this photocatalyst was able to produce hydrogen also under sunlight illumination.

Starting from a natural biopolymer, CeO_x NP embedded on a graphitic carbon matrix were prepared in a single step by pyrolysis of cerium alginate conveniently dried. These samples were adequately exfoliated by sonication and the resulting CeO_x/G suspension behave as enhanced photocatalyst for water oxidation using Ag⁺ ions as sacrificial electron acceptor. Depending on the preparation conditions, the photocatalytic activity varies considerably by around one order of magnitude, the best conditions were found for the material in which the composition is 2.5 wt% of G that has been obtained by pyrolysis at 900 °C. This optimized material performed three times better photocatalytic activity than commercial CeO₂ NPs. This work illustrates the advantages of using a natural biopolymer as template in the preparation of photocatalysts. These biopolymers cannot only control the particle size and surface functional groups, but also can provide graphitic residue precursors of G to enhance the photocatalytic activity.

Alginate, a natural biopolymer, was used as precursor of graphitic carbon that was submitted to laser exposure obtaining Graphene Quantum Dots (GQDs) by reducing the dimensions of the sheets and by increasing exfoliation. The resulting GQDs exhibit photoluminescence as a function of the ablation time, increasing in intensity as the ablation time increases. In this way a convenient protocol to obtain GQDs from pyrolyzed alginate allowing a certain control on the size and properties of these nanoparticles was obtained. Considering that alginate is a biomass waste, the present finding constitutes a remarkable example of biomass valorization by transforming this waste into a material of high added value.

During the second part of the present thesis the photocatalytic hydrogenation of acetophenone by using titanium based semiconductors in batch and membrane reactors under UV and visible light was achieved.

The use of a membrane reactor system for photocatalytic hydrogenation of acetophenone in water solution with formic acid as hydrogen and electron donors was found to improve phenylethanol production, yield%, conversion%, and productivity with respect to the use of batch reactor with the same substrate addition mode. The most efficient system for photocatalytic hydrogenation of acetophenone in terms of productivity ($4.44 \text{ mg g}^{-1}\text{h}^{-1}$) and amount of phenylethanol produced ($276.20 \text{ }\mu\text{mol}$), with Q% equal to 21.91%, was found to be the membrane reactor in which acetophenone was used as both organic phase and substrate reservoir. Commercial TiO_2 was not active under visible light but its photocatalytic activity was implemented by the presence of palladium. The amount of phenylethanol produced ($1371 \text{ }\mu\text{mol}$) and the productivity ($22.02 \text{ mg g}^{-1}\text{h}^{-1}$) by using Pd/TiO_2 photocatalyst under visible light were found to be five times higher than that obtained by using TiO_2 under UV light. The results of the present study, using TiO_2 doped with palladium as photocatalyst, for photocatalytic hydrogenation of acetophenone in water solution using a pollutant such as formic acid as electron donor, under visible light in membrane reactors gave interesting results for application purposes allowing to use a green system for the reduction of acetophenone.

In conclusion, during this doctoral thesis the proposed objectives, also in relation to the strategic sector of the Regional Innovation Pole of Calabria Region concerning technologies for the sustainable management of environmental resources, have been achieved. Indeed, the obtained results

include: i) use of biomass waste, which is widely available and sustainable resource, as building block for the synthesis of the majority of the prepared catalysts, obtaining a biomass valorization by transforming this waste into a material of high added value; ii) use of a “green” process which is the photocatalysis that allowed to perform reactions under mild experimental conditions (room temperature and atmospheric pressure). Moreover, the results showed an enhancement of photocatalytic activity of various photocatalysts, obtaining to overcome one of the main limit of the photocatalysis, achieving the use of visible light as driving force for chemical reactions (e.g. hydrogen production and hydrogenation reactions) allowing in the future the use of sunlight, a clean, renewable and low cost energy source, as an alternative to energy intensive conventional treatment methods; iii) industrial application, for photocatalytic reduction of organic compounds avoiding the direct addition of hydrogen thus limiting the costs associated with its storage and transport making the hydrogenation reactions interesting for economic, safety and environmental purposes; iv) photocatalytic reactions performed using formic acid (one of the major pollutants present in pharmaceutical wastewater), as electron and hydrogen donor, with simultaneous decomposition of pollutants and photocatalytic reduction of organics; v) improvement of efficiency of the photocatalytic process and the possibility to allow chemical reactions and separation processes in one step using membrane reactors for photocatalytic hydrogenation of acetophenone, which in turn results in lower processing cost and minimum environmental impact.

Appendix

Scientific activity carried out during the PhD course

Publications:

1. Molinari R., Lavorato C., Poerio T. Performance of vanadium based catalyst in a membrane contactor for the benzene hydroxylation to phenol. *Applied Catalysis A: General*, 2012, Vol. 417-418, pp. 87-92
2. Latorre-Sánchez M., Lavorato C., Puche M., Fornés V., Molinari R. and Garcia H. Visible light photocatalytic hydrogen generation using dye-sensitized graphene oxide as photocatalyst. *Chem. Eur. J.* 2012, 18, 16774 – 16783.
3. Atienzar P., Primo A., Lavorato C., Molinari R. and García H. Preparation of Graphene Quantum Dots from Pyrolyzed Alginate. *Langmuir* 2013, 29, 6141–6146.
4. Molinari R., Argurio P., Lavorato C. Review on reduction and partial oxidation of organics in photocatalytic (membrane) reactors. *Current Organic Chemistry*, 2013, 17, 21 , 2516 – 2537.

5. Lavorato C., Primo A., Molinari R. and Garcia H. N-doped graphene derived from biomass as visible light photocatalyst for hydrogen generation from water-methanol mixtures. Accepted by Chem. Eur. J.
6. Lavorato C., Primo A., Molinari R. and García H. Natural alginate as graphene precursor and template in the synthesis of nanoparticulate ceria-graphene water oxidation photocatalyst. Submitted to ACS Catalysis.

Presentations to Scientific Conferences:

National Conferences:

- R. Molinari, C. Lavorato, P. Argurio. Preliminary study to use a membrane reactor in photocatalytic transfer hydrogenation of organic compounds. Convegno Congiunto della Sezioni Calabria e Sicilia della Società Chimica Italiana, Messina, 1-2 December 2011. (**oral presentation**)
- R. Molinari, P. Argurio, C. Lavorato. Membrane reactors and advanced/hybrid membrane process in green chemistry applications. Chimica e tecnologie per la salvaguardia ambientale e lo sviluppo sostenibile. 14 November 2013, Palermo. (**oral presentation**)

International Conferences:

- C. Lavorato, M. Latorre-Sánchez, M. Puche, V. Fornés, R. Molinari and H. Garcia. Visible light photocatalytic hydrogen generation using dye-sensitized graphene oxide as photocatalyst. 5th International Symposium on Carbon for Catalysis - Carbocat-V, Bressanone/Brixen (Italy), 28-30 June 2012. (**Oral presentation**).
- M.Latorre-Sánchez, C. Lavorato, V.Fornés, R.Molinari, H. García. Visible or Solar Light Photocatalytic Hydrogen Generation from Water Using Graphene Oxide. 7th European meeting on solar chemistry and photocatalysis: environmental applications (SPEA7), Porto, Portugal, 17-20 June 2012. (**Poster presentation**)
- C. Lavorato, A. Primo, R. Molinari and H. Garcia. N-doped graphene from mesoporous chitosan as photocatalyst for hydrogen generation. 5th Czech-Italian-Spanish Conference on Molecular Sieves and Catalysis, 16- 19 June, 2013 Segovia, Spain. (**Oral presentation**)

Presentations to Schools:

- C. Lavorato. Photocatalytic transfer hydrogenation of organic compounds in a membrane reactor. Forum PhD Students • GRICU PhD NATIONAL SCHOOL 2011, Mathematical Methods for Chemical Engineering /Nanotechnologies. Santa Margherita di Pula (CA), 26 september-october 2011. (**Oral presentation**)

Participation to Schools and Seminars:

- GRICU PhD NATIONAL SCHOOL 2011, Mathematical Methods for Chemical Engineering /Nanotechnologies. Santa Margherita di Pula (CA), 26 september-october 2011
- Tribo-Electric Charging of Powders (Prof. Mojtaba Ghadiri)
- Solar Fuels: Opportunities for Research (Prof. Siglinda Perathoner)
- Halogen Bonded Systems: From Separation Phenomena to Liquid Crystals (Prof. Giuseppe Resnati)
- “Novel Photocatalysts for Solar-Light Hydrogen Generation from Water” prof. Hermenegildo Garcia, 23 April 2012.
- “Benzene – Faraday, Kekulé, and Loschmidt” Prof. Heinz Roth, 23 April 2012.
- “Importance of proton coupled electron transfer in nanoparticle synthesis” Prof. J.C. Tito Scaiano, 23 April 2012.
- "Relation of Bone Implants to Bone Histology, Physiology, Calcium and Phosphate Metabolism", Prof. Selçuk ÖZCAN, 11 June 2013 (15.30 – 17.30).
- "A Ph.D. Thesis Study: Preparation of Hydroxyapatite/Silk Protein Thin Film Implant Surfaces, Investigation of their Microstructural Properties and Model Protein Interactions", Prof. Selçuk ÖZCAN, 13 June 2013 (11.30 – 12.30)
- “Creazione d'impresa”, Dott. Giuseppe Rossi, 11 June 2013 (11.30 -13.30) and 13 June 2013 (15.30 -17.30).
- Seminars made by researchers and PhD students of prof.Gracia research group (ITQ, UPV, Valencia, Spain) for a total of 36h.

Courses attended:

- Strumentazione ed analisi dei dati (Prof. Francesco Paolo Di Maio)
- Writing technical English (Prof. John Broughton)
- Fondamenti chimici delle operazioni a Membrane (prof.Drioli)

Acknowledgements

I thank the European Commission, the European Social Fund and Regione Calabria for financial support of my PhD fellowship.

I am grateful to the supervisors of my PhD thesis, Prof. Ch.mo Raffaele Molinari, Prof. Ch.mo Hermenegildo García and Ing. PhD Pietro Argurio, for the continuous support of my Ph.D study and research, for their patience, and immense knowledge, for giving me the opportunity to join in their research groups and to make available all the tools and techniques that have enabled the development of all the work that the final result is this thesis.

I am grateful for the help and support of all kind people around me:

I thank all other professors, colleagues, technical staff, all people that worked with me and in general all my friends at Università della Calabria and at the Universitat Politècnica de València for their kindness, help, support and assistance; I thank my family, and all my friends in all the world for the encouragement, support, assistance, help and kindness.